Universidade do Porto
Faculdade de Engenharia
FEUP

MICROMIXING IN CHEMICAL REACTORS

Test Reactions

Ph.D. Dissertation
in
Biological and Chemical Engineering

by

Maria Isabel da Silva Nunes

Departamento de Engenharia Química
Faculdade de Engenharia
Universidade do Porto

October 2007

To Lara and Quim

"Problems worthy of attack prove their worth by fighting back."

Paul Erdos (1913-1996)

Acknowledgements

I appreciate the support of Professor José Carlos Brito Lopes and Professor Madalena Maria Gomes de Queiroz Dias by the supervision of this work. They were not only mentors but also good friends.

I wish to thank Professor Alírio E. Rodrigues, Director of the LSRE, where this work was carried out. I also wish to thank Professor John R. Bourne and to Professor Lúcia Santos for numerous and productive discussions.

To my friends Vera and Vi a special thanks.

My gratitude to all colleagues in the LSRE that made this work possible with their help and support, specially: António Martins, Paulo Laranjeira and Ricardo Jorge Santos and also to the following colleagues from DAO - Universidade de Aveiro: Ana Paula Gomes, Arlindo Matos, Carlos Borrego, José Figueiredo and Luís Tarelho.

To my daughter, brother, parents and husband who deserve special credit for their affection and support.

Financial support for this work was in part provided by the research project FCT/POCTI71999/EQU/34151 for which the author is grateful. The author acknowledges her Ph.D. scholarship awarded by FCT, PRAXIS XXI/BD/9296/96.

Abstract

The azo coupling between 1-naphthol and diazotized sulfanilic acid and simultaneous azo coupling of 1- and 2-naphthol with diazotized sulfanilic acid have been widely used to study the influence of mixing on the product distribution of fast chemical reactions with fluid of low viscosities. The aim of this work is to study the influence of viscosity on the kinetics of those test reactions, for their subsequent application in the micromixing assessment studies in two reactors: NETmix® static mixer and mixing chamber of a RIM (Reaction Injection Molding) machine.

The kinetics studies were performed in both aqueous non-viscous and viscous media. The results obtained in the first study allowed clarifying some controversy found in the literature around the rate constants and the absorption spectrum of one product. For the second study it was necessary to choose a water-soluble additive to raise the solution viscosity, ensuring at the same time that no other properties were changed (e.g., Newtonian behavior, inertness, pH). Several polymeric and non-polymeric thickeners were studied, and a polyurethane solution was found to be a good choice. The rate constants for aqueous viscous medium can not be directly correlated with those in aqueous non-viscous medium maybe due to chemical interferences of the additive or to mixing limitations in the mixing chamber of the stopped-flow equipment used. For this equipment a methodology was developed for the mathematical treatment of kinetic data and the stopped-flow dead time and stoppage time determination, which corrects for the concentration gradients within the optical cell. This method also allows the simultaneous determination of rate constant.

The results obtained for the mixing characterization study in the NETmix® static mixer using the azo coupling of 1-naphthol in aqueous solution showed that the Reynolds number has a great influence on the mixing degree, and that this influence is more relevant for $Re < 200$. For higher values of Re the mixer behaves as a perfectly mixed reactor.

In the RIM machine the test reaction was the simultaneous coupling of 1- and 2-naphthol in the viscous medium. The increase of Reynolds number enhances the mixing intensity inside the mixing chamber, where a transition regime was identified ($100 < Re \leq 125$), from segregated to mixing state.

Resumo

O acoplamento azo entre o 1-naftol e o ácido sulfanílico diazotizado e o simultâneo acoplamento azo do 1- e 2-naftol com o ácido sulfanílico diazotizado têm sido muito usados para estudar a influência da mistura na distribuição produtos de reacções químicas rápidas, com fluidos de baixa viscosidade. O objectivo deste trabalho é estudar a influência da viscosidade na cinética destas reacções teste, para a sua posterior aplicação em estudos de caracterização da micromistura em dois reactores: misturador estático NETmix® e câmara the mistura de uma máquina de RIM (*Reaction Injection Molding*).

Os estudos cinéticos foram levados a cabo em meios aquoso não-viscoso e viscoso. Os resultados obtidos no primeiro estudo permitiram clarificar alguma controvérsia encontrada na literatura à cerca das constantes cinéticas e no espectro de absorvância de um produto. Para segundo estudo foi necessário escolher um aditivo, solúvel em água, para aumentar a viscosidade da solução, assegurando simultaneamente que outras propriedades permaneciam inalteradas (por exemplo, comportamento Newtoniano, inerte, pH). Foram estudados alguns espessantes poliméricos e não poliméricos e uma solução de poliuretano foi seleccionada como sendo uma boa escolha. As constantes cinéticas em meio aquoso viscoso não podem ser directamente correlacionadas com as em meio aquoso não-viscoso, talvez devido a interferências químicas do aditivo ou a limitações de mistura na câmara de mistura to equipamento *stopped-flow* usado. Para este equipamento, foi desenvolvida uma metodologia para o tratamento matemático dos dados cinéticos e para a determinação do tempo morto e do tempo de paragem, o qual corrige os gradientes de concentração dentro da célula óptica. Este método também permite a determinação simultânea da constante cinética.

Os resultados obtidos no estudo de caracterização da mistura no misturador estático NETmix®, usando a reacção de acoplamento azo do 1-naftol em solução aquosa, mostraram que o número de Reynolds tem uma grande influência no grau de mistura e que esta é mais relevante para $\mathrm{Re} < 200$. O misturador comporta-se como um reactor de mistura perfeita para valores mais elevados de Re.

O simultâneo acoplamento do 1- e 2-naftol em meio viscoso foi a reacção teste usada na máquina de RIM. O aumento do número de Reynolds melhora a intensidade da mistura no interior da câmara de mistura, onde foi indentificado um regime de transição ($100 < \mathrm{Re} \leq 125$), do estado de segregação para o de mistura.

Table of Contents

Page

List of Figures

Page

List of Tables

Page

Notation

Roman Letters

A	reagent A	
a	average minimum distance between the ions	
A_1	1-naphthol	
A_2	2-naphthol	
Abs	absorbance	[-]
Abs_0	absorbance at the mixing point	[-]
B	diazotized sulfanilic acid	
c	concentration	[mol·m^{-3}]
C	reagent C	
$\langle c_A \rangle_{op}$	concentration of reagent A at the observation point	[mol·m^{-3}]
D^2	deviation	[-]
d	injector diameter	[m]
D	diameter of mixing chamber of RIM machine	[m]
d_i	channel diameter of NETmix® network	[m]
D_j	chamber diameter of NETmix® network	[m]
Da	Damkhöer number	[-]
$E(\Theta)$	dimensionless residence time distribution function	[s^{-1}]
E_a	activation energy	[J·mol^{-1}]
F	mass flow rate	[mol·s^{-1}]
Fr	Froude number	[-]
H	height of mixing chamber of RIM machine	[m]
$H(t)$	Heaviside function	
I	ionic strength	[mol·m^{-3}]
k	rate constant	[m^3·mol·s^{-1}]
K	equilibrium constant	
k_0	frequency factor of Arrhenius law	[m^3·mol·s^{-1}]
k_{1o}	rate constant of the reaction $A_1 + B \rightarrow o - R$	[m^3·mol·s^{-1}]

k_{1p}	rate constant of the reaction $A_1 + B \rightarrow p-R$	[$m^3 \cdot mol \cdot s^{-1}$]
k_{2o}	rate constant of the reaction $o-R+B \rightarrow S$	[$m^3 \cdot mol \cdot s^{-1}$]
k_{2p}	rate constant of the reaction $p-R+B \rightarrow S$	[$m^3 \cdot mol \cdot s^{-1}$]
k_3	rate constant of the reaction $A_2 + B \rightarrow Q$	[$m^3 \cdot mol \cdot s^{-1}$]
k_{app}	apparent rate constant	[s^{-1}]
k_I	rate constant at ionic strengths I	[$m^3 \cdot mol \cdot s^{-1}$]
$k_{I=0}$	rate constants at ionic strength zero	[$m^3 \cdot mol \cdot s^{-1}$]
k_{mix}	mixing rate constant	[$m^3 \cdot mol^{-1} \cdot s^{-1}$]
k_{obs}	observed rate constant	[$m^3 \cdot mol^{-1} \cdot s^{-1}$]
k_{real}	real rate constant	[$m^3 \cdot mol^{-1} \cdot s^{-1}$]
L^0	oblique distance between two chamber centers	[m]
l_i	channel length	[m]
ℓ_{oc}	optical cell length	[m]
N	number of moles	[mol]
n	global order of reaction	
n_x	number of rows	
n_y	number of columns	
Q	1-[(4'-sulfophenyl)azo]-2-naphthol	
q	volumetric flow rate	[$m^3 \cdot s^{-1}$]
r	reagents ratio	[-]
R	generic reaction product or $R = o-R + p-R$	
r_i	rate of the reagent i	[$mol \cdot m^{-3} \cdot s^{-1}$]
R_M	momentum ratio	[-]
$o-R$	2-[(4'-sulfophenyl)azo]-1-naphthol	
$p-R$	4-[(4'-sulfophenyl)azo]-1-naphthol	
Re	Reynolds number	[-]
S	2,4-bis[(4'-sulfophenyl)azo]-1-naphthol	
T	temperature	[K] or [ºC]
t	time	[s]
t_0	stoppage time	[s]
$t_{1/2}$	half-life time	[s]

t_{mc}	residence time in the mixing chamber	[s]
t_{mixing}	characteristic mixing time	[s]
t_{op}	residence time up to the observation point	[s]
t_{reaction}	characteristic reaction time	[s]
ϑ	solution velocity	[m·s^{-1}]
V	volume	[m^3]
$V_{channels}$	volume of channels	[m^3]
ϑ_{inj}	superficial velocity at injector	[m·s^{-1}]
V_{inj}	volume injected on the mixing system	[m^3]
V_{mc}	volume of the mixing chamber	[m^3]
V_{NETmix}	volume of the NETmix®	[m^3]
ϑ_{oc}	solution velocity in the optical cell	[m·s^{-1}]
V_{oc}	volume of the optical cell	[m^3]
V_{op}	volume between T-mixer and observation point	[m^3]
x	space coordinate	
X_{Al}	yield of reagent A_l	[-]
X_Q	product yield (extended test system)	[-]
X_S	product yield (simplified test system)	[-]
X_S'	product yield (extended test system)	[-]
y	space coordinate	
z	axial coordinate	[m]
Z_C	charge on the reactive forms 1-naphtholate	
Z_D	charge on the reactive forms diazonium ion	
z_{oc}	axial coordinate in the optical cell	[m]
z_{op}	axial coordinate in the observation point	[m]

Greek letters

α	geometric parameter	[m]
β	geometric parameter	[-]
$\dot{\gamma}$	shear rate	[s^{-1}]
γ_{Al}	stoichiometric ratio c_{A10}/c_{B0}	[-]
δ	optical pathlength	[m]
ε	molar extinction coefficient	[$m^2 \cdot mol^{-1}$]
ε_{turb}	rate of turbulent energy dissipation	[$W \cdot kg^{-1}$]
Θ	dimensionless time	[-]
λ	wavelength	[nm]
μ	viscosity	[Pa·s]
ξ	stoichiometric ratio c_{A20}/c_{A10}	[-]
ρ	fluid density	[$kg \cdot m^{-3}$]
σ	shear stress	[Pa]
τ	mean residence time	[s]
ϕ	angle	[º]
ψ	segregation parameter of NETmix® static mixer	[-]

Subscripts/superscripts

0	initial
1*o*	reaction $A_1 \rightarrow o-R$
2*o*	reaction $p-R \rightarrow S$
2*p*	reaction $A_1 \rightarrow p-R$
2*p*	reaction $o-R \rightarrow S$
3	reaction $A_2 \rightarrow Q$
*A*1	1-naphthol
*A*2	2-naphthol
app	apparent
B	Diazotized sulfanilic acid
calc	calculated
CSTR	for the CSTR
exp	experimental
inj	at the injectors
min	minimum value for the variable
new	new value for the variable
oc	optical cell
old	old value for the variable
op	observation point
$o-R$	2-[(4'-sulfophenyl)azo]-1-naphthol
PFR	for the PFR
$p-R$	4-[(4'-sulfophenyl)azo]-1-naphthol
Q	1-[(4'-sulfophenyl)azo]-2-naphthol
R	sum of $o-R$ and $p-R$
S	2,4-bis[(4'-sulfophenyl)azo]-1-naphthol
t	time
x	denotes the component in the x direction
y	denotes the component in the y direction
∞	infinitive

Abbreviations

AA	Ascorbic Acid
ADC	Analog to Digital Converter
CCD	Charge-Couple device
CFD	Computational Fluid Dynamics
CHNS	Carbon, Hydrogen, Nitrogen and Sulphur
CPU	Central Processing Unit
CSTR	Continuous Stirred Tank Teactor
DCIP	2,6-Dichlorophenolindophenol
FCUL	Faculdade de Ciências da Universidade de Lisboa
FEUP	Faculdade de Engenharia da Universidade do Porto
GRG	Generalized Reduced Gradient
HEC	Hydroxyethyl Cellulose
HNMR	Hydrogen Nuclear Magnetic Resonance
ICAT	Instituto de Ciência Aplicada e Tecnologia
LDA	Laser Doppler Anemometry
LIF	Laser-Induced Fluorescence
LSRE	Laboratory of Separation and Reaction Engineering
MB	Mass Balance
PFR	Plug-Flow Reactor
PIV	Particle Image Velocimetry
PLIF	Planar Laser-Induced Fluorescence
RGB	Red, Green and Blue
RIM	Reaction Injection Molding
RTD	Residence Time Distribution
TLC	Thin Layer Chromatography
UV	Ultra Violet
vis	Visible

1. Introduction

1.1 Motivation and Relevance

The success and efficiency of many industrial processes depend on the mixing conditions of the materials. From an engineering point of view mixing is a phenomenon that appears in many technologies and affects products quality.

Comparatively to the chemically passive flows, when mixing is accompanied by chemical reaction many new problems arise, whose are absent in the first case. If there are several competing reactions occurring simultaneously whose reaction lifetimes are approximately the same as the time scale of the mixing process, the relative progress of the reactions will be governed by the mixing process and products distribution, consequently, the yield will be surely affected. Thus, the knowledge of the influence of mixing on the behavior of a chemical process is of decisive importance in the control and optimization of the distribution of the products formed, allowing and/or helping to improve their yields, making better use of raw materials and reducing the formation of by-products, simplifying the purification of the products. Such topics are likely to be of most relevance in chemical engineering and industrial chemistry, but also to be of interest in mechanical engineering and fluid mechanics as well as environmental science and engineering (Baldyga and Bourne, 1999).

Examples of industries where mixing plays a key role include fine chemicals and pharmaceuticals, petrochemicals, biotechnology, polymer processing, paints and automotive

finishes, cosmetics and consumer products, food, drinking water and wastewater treatment (Paul et al., 2004). Chemical reactions such as combustion, biological growth, neutralization, precipitation and continuous polymerization are frequently present in the production line of those industries and have their product quality conditioned by the mixing processes.

In order to solve some of those problems related with mixing quality, some research teams have been developed their investigation in this field. For instance, several kind of mixing devices, including static mixers, are being tested in the precipitation processes, where the degree of mixing strongly influences the shape and size distribution of precipitate particles (Muhr et al., 1997; Lopes et al., 2005a; McCarthy et al., 2007; Wu et al., 2007; Silva et al., 2008). Another example arrived from the polymer industry, where the demands of a vast range of new products are imposed by the progress of the today's society. Thus, new technologies have been developed and improved their performance, such as the Reaction Injection Molding (RIM) for polyurethane production. This technology is used for processes where the products have a complex structures and rheology making the control of the yield and product distribution experimentally challenging (Kolodziej et al., 1982; Kusch et al., 1989; Coates and Johnson, 1997; Lopes et al., 2005b; Erkoç et al., 2007).

For these reasons, the prediction of mixing effects is very important for process design and its improvement, which can be made through relatively simple mathematical models that provide a better understanding of what actually occurs in a reactor. However, in order to validate these models other tools are required namely, experimental techniques able to characterize the mixing quality at their different scales: macromixing, mesomixing and micromixing (defined in Chapter 2).

Nowadays, the assessment of mixing at molecular scale – micromixing – constitutes a challenge for many researchers related to the design and conception of mixer devices. The existing techniques for mixing characterization can be subdivided in two main categories: physical and chemical methods, as it will be shown in Chapter 2. The development, the improvement and the knowledge about these techniques are of a great importance in the sight of the recurrent needs of mixing assessment studies.

This thesis has a purpose to give a contribution in this field, by the knowledge for the improvement than can be done for a chemical method and its subsequent application on the characterization of micromixing in emergent reactors used in actual industry.

1.2 Thesis Objectives and Layout

The field of mixing in chemical engineering is very wide and diverse. Therefore, this work will be restricted to those phenomena where mixing and chemical reaction are closely linked in liquid single-phase media. This research field, involving chemical reaction and fluid flow, requires information from several fields such as physical organic chemistry and fluid mechanics. The purely physical aspects of mixing will not be considered, although this important operation also poses unsolved problems to industry.

Thus, one of the objectives of this work is to investigate one chemical method, also called *test reaction system*, suitable for the mixing characterization investigations, extending its range of application to reactors where the flow fluids have high viscosities. This test system should be able to be implemented in any reactor and not be specific for a single one, i.e. have a large applicability among the reactors involving reagents and/or products with high viscosities.

There exists in the literature several test systems generally developed for micromixing studies in aqueous non-viscous medium. From these, a set of test reactions that have been widely used in mixing studies during the last two decades (Bourne et al., 1990; Bourne et al., 1992a) were selected to be studied in this work. The set of test reactions chosen were classified in two distinct test systems here denoted as: *simplified test system* and *extended test system*.

The kinetics of these set of reactions in aqueous non-viscous medium have been widely reported in the literature, but there is no common accepted values for their rate constants (Bourne et al., 1985; Bourne et al., 1990; Wenger et al., 1992). Thus a kinetic study in aqueous solution was performed with the aim to clarify possible remaining doubts around these reactions.

The main kinetic study was then carried out in an aqueous viscous medium, once this data for high viscosity values are not available in the literature. Another objective of this part of the work was the selection of a water-soluble additive to raise the solution viscosity. This additive follows certain key properties such as being an inert, being added in low percentage and maintaining the Newtonian behavior of the fluid; these properties are often expected industrially in a given additive.

The stopped-flow technique is generally used in the study of the kinetics of fast reactions. Problems with concentration gradients within the observation cell were detected

(Nunes, 1996), which becomes more relevant as the rate of reaction increases. A new methodology was developed for the mathematical treatment of kinetic data, which corrects those gradients.

The feasibility of the studied test reactions for the micromixing characterization in non-viscous and in viscous media was evaluated and validated respectively in: NETmix® static mixer and in the mixing chamber of a RIM machine, which constituted the final goal of the present work (see Chapter 5).

Besides this first introductory chapter, the layout of this dissertation consists of the following chapters.

Chapter 2 provides a review of the most relevant studies published in the last years in the area of micromixing characterization. Major studies in both experimental and simulation areas were selected from abundant available information. Special attention was focused on publications dealing with test reactions, since they are the most relevant for this work.

Chapter 3 offers a detailed description of the stopped-flow technique, for which a new data processing methodology was developed and constitutes an innovation of this work. Data processing and error estimations based on statistical principles are also described. More, the application limits of the equipment to perform kinetic studies were also here established.

Detailed information about the synthesis, purification and identification steps of the chemicals involved in both test system is given in Chapter 4. In this chapter the main experimental kinetics results both in aqueous non-viscous and viscous media are presented as well as the rheological studies performed during the selection of an additive to raise de viscosity of aqueous solutions.

The plausibility of the studied reactions as test systems is shown in Chapter 5, which provides the results of micromixing characterization in two reactors/mixing devices:

- NETmix® static mixer – where the simplified test system was used in aqueous non-viscous medium in order to quantify the mixing intensity in the Reynolds number ranging $Re = 5$ to $Re = 700$. The reaction pattern visualization study is also presented and assisted the interpretation of the mixing experimental results. Macromixing simulation study was also performed in order to evaluate the influence

of the reagents feed scheme and network geometry in the product distribution at static mixer outlet.

- Mixing chamber of RIM machine – once the usual flowing fluids of this reactor are viscous, the solutions here used had a viscosities of $20\,\mathrm{mPa \cdot s}$. Tracer flow visualization experiments are shown for Reynolds numbers ranging from $\mathrm{Re} = 100$ to $\mathrm{Re} = 500$. They allow to verify the calibration of the pumps systems and simultaneously to observe the evolution of the flow pattern among the Reynolds numbers studied. The effect of this parameter in the mixing intensity was investigated by using of the extended test system. The main results are here presented in the range $75 \leq \mathrm{Re} \leq 600$.

Finally, the main conclusions, remarks, achievements and problems encountered during this study can be found in the Chapter 6. Suggestions and challenges for future experimental and simulation work are also outlined.

2. Micromixing: State-of-the-Art

2.1 Introduction

Today's consumer society requires more, better quality and innovative products from a wide variety of industries, such as the production of plastics and synthetic resins, man-made fibres, polymers, paints and varnishes, drugs and pharmaceuticals, agricultural chemicals, food and drinks. All of these industries have one point in common: the raw materials are converted into final products by means of chemical reactions in an environment that involves fluid flow. *Reactive mixing* is a terminology commonly used to denominate this kind of process, where mixing and chemical reactions can occur simultaneously.

Mixing is a generic term that implies homogenization or reduction on the variability of concentration, temperature, pressure, etc. Considering this homogenization, it is necessary to regard the scale at which this variability exists and at which the various mixing mechanisms reduce variability (Danckwerts, 1953b). In the process of mixing in continuous or semi-continuous reactor, one can distinguish three different scales of mixing: macromixing, mesomixing and micromixing.

Macromixing is the process of mixing at the macroscopic scale, i.e., on the scale of the whole vessel and corresponds to the large-scale flow processes that cause the occurrence of large-scale distributions such as the residence time distribution (RTD) or the distribution of mean

concentration. Therefore, macromixing determines the ambient concentrations for the other two scales: mesomixing and micromixing.

The *mesomixing* process refers to the dispersion of fresh feed stream shortly after it enters a reactor, i.e., mixing at a scale roughly comparable with the size of the reagent feed pipe, i.e., it corresponds to mixing phenomena which occur on a scale smaller than macromixing but larger than micromixing (Baldyga and Bourne, 1992).

Finally, *micromixing*, the last mixing stage, refers to the set phenomena that promote contact of the elements at the microscopic or molecular scales and is characterized by the fine texture of the fluid and by the dynamic environment renovation around each molecule. This forms the central objective in this thesis.

Although the inhomogeneity related to the meso and macromixing processes has only an indirect effect on the chemical reaction, this effect can be very strong. More, in so-called reactive mixing, the micromixing should always be considered since reaction is a molecular-scale process. For example, when reagents are initially in separated streams, they need to be brought into contact by mixing on a molecular scale, in order to promote reaction. In practice, three cases can happen: (i) total segregation of reagents or absence of mixing, and therefore no reaction occurs; (ii) complete mixing or absence of segregation; (iii) incomplete mixing or partial segregation, where the product distributions are unexpected.

Usually a mixing device (impeller, static mixer, etc.) is used with the purpose to promote a complete mixing. However, not always this objective is completely attained. The search for the optimal operation conditions, the development of new mixers designs and the enhancement of techniques to characterize the mixing quality are frequent research fields of some important industries and subject of study of a large number of academic teams.

This chapter is organized this way. Section 2.2 gives an historical perspective of mixing. In Section 2.3 some topics about the importance of mixing are outlined. Section 2.4 is reserved to state the techniques to monitoring the mixing quality and some published examples are reported. In Section 2.5 it is referenced the importance of the experimental technique – test systems – for the micromixing modeling; some micromixing models are briefly mentioned. The final conclusions of this chapter are presented in Section 2.6.

2.2 Historical Perspective

Perhaps due to the complexity of the phenomena involved, the development of know-how in the micromixing research field has been slow. Several researchers have given important contributes for the comprehension of mixing phenomena and their influence on chemical reaction performance, but only a few have dedicated most of their investigation to this subject. Here a brief historical retrospective of the main contributions is presented.

As referred by van Krevelen (1958), Damköhler (1937) was one of the first researchers to show the great influence of flow factors and boundary layer phenomena on the gross result of chemical reactions. Since then ever more attention has been made to the effects of fluid flow, mixing, mass and heat transfer, and to the influence of the physical fine structure of reacting substances. Nevertheless, the literature of the 1940s and early 1950s on this subject is scarce and most of research work consisted of applying the methods of engineering fluid mechanics to stirred tanks (Bourne and Rohani, 1983).

The years 1952 and 1953 marked a turning point, when Danckwerts published important papers addressing residence time distribution (Danckwerts, 1953a) and quality of mixing and its quantitative definition and determination (Danckwerts, 1953b). Later, this author distinguished macromixing and micromixing processes (Danckwerts, 1958), and showed how the residence time distribution function, RTD, can be used to describe macromixing. While the residence time distribution is susceptible of direct experimental measurement, only in the case of isothermal first-order reactions it completely determines the performance of a reactor. Fundamental and classical concepts, such as: scale and intensity of segregation (Danckwerts, 1958) as well as the extremes of maximum mixedness and complete segregation as limiting cases of micromixing (Zwietering, 1959) were introduced. These publications constituted important advances in the mixing field research and are today still an essential part of any consideration of “mixing on the molecular scale”.

During the 1960s, several models were developed to represent the mixing processes, but little experimental research was performed and this limited their advance. Micromixing began to deviate from reality, because although most models required a physical basis (e.g. fluid mechanics), the model parameters were rarely known independently but were rather fitted (Bourne, 1984). Weinstein and Adler (1967) and Nishimura and Matsubara (1970) have proposed specific models for micromixing processes and calculated the effect of various

degrees of segregation on the steady-state conversion obtained in a reactor operating with a single feed stream of premixed reagents (Spencer et al., 1980).

From the 1970s to the 1980s some points started to be clarified, namely (Angst et al., 1982): (i) the inhomogeneity at the molecular scale develops if the half-life time which would be required by chemical reaction in a homogeneous solution is of the same order as or less than the half-life for micromixing in the absence of reaction; (ii) micromixing proceeds by molecular diffusion in small fluid elements which are being gradually strained. Although, many theoretical models had already been proposed (e.g. Mao and Toor 1970; Nishimura and Matsubara, 1970; Chen, 1971; Treleaven and Tobgy, 1971; Nauman, 1975; Ottino et al., 1979) unfortunately their number greatly exceeded that of the available experimental results so that the progress in understanding micromixing was slow. The application of this research to industrial processes was still incipient, although considered important in some cases. Bourne (1984) refers that micromixing influence is important in certain special cases such as in polymerization processes where micromixing plays an important role on the molecular weight distribution of polymers and in the cases of reactions involving inline mixing of reagents (for instance flames).

Villermaux (1983) in a general review entitled “Mixing in chemical reactors” wrote: “The end of this survey leaves us with the feeling that research on mixing in chemical reactors is a very lively area, where problems have been attacked from several directions (turbulence theory, residence time distribution and mixing earliness, segregation and micromixing…). If the major concepts have been identified, there is still a need for a unified theory allowing *a-priori* predictions from the sole knowledge of physicochemical properties and operating parameters, even if encouraging progress has been made in this direction”. A large amount of phenomenological models exist in the literature for representing intermediate micromixing processes in flow reactors, although most of them are more or less equivalent. Villermaux (1983) suggested that more experimental data on real reactors is needed, where the reactive tracer method seemed to be especially promising to correlate the micromixing parameters to the physicochemical properties of the mixture and the operating conditions of the reactor.

The late 1980s and the 1990s were marked by a clarification and consolidation of concepts and by significant progress in the micromixing area. The required experimental data appeared, due mostly to the important publications of J. Bourne and co-workers (Bourne et al., 1981; Bourne et al., 1985; Bourne et al., 1990; Bourne et al., 1992a), which developed a chemical method to characterize micromixing. This chemical system has been widely used and it is still

used nowadays. More recently, J. Villermaux and his research team (Fournier et al., 1996a; Fournier et al., 1996b; Guichardon et al., 2000) developed another chemical system to characterize mixing at molecular scale.

The 90s decade was also fruitful on the micromixing modeling field. Micromixing models had been actively studied for more than 30 years, especially in three scientific areas: chemical engineering, fluid mechanics and combustion (e.g. Ottino, 1980; Heeb and Brodkey, 1990; Barresi et al., 1992; Wenger et al., 1993; Kaminsky et al., 1996; Sheikh and Vigil, 1998; Tsai and Fox, 1998). Initially studies in these areas seem to ignore each others, but with increasing exchange of information and with the important experimental information supplied by the chemical methods outlined above these models became more convergent, reliable and realistic (Villermaux and Falk, 1996).

Previously, the majority of the academics studies had been concerned in conventional design of reactors (batch, semi-batch and continuous stirred tank reactors), with mixing of miscible fluids (gases or Newtonian liquids) and very simple reaction schemes involving one or two reactions. However, industrial needs were now more demanding and addressed more complex situations: very viscous and non-Newtonian liquids, multiphase systems (gas-liquid, liquid-solid, gas-liquid solid suspensions), and complex transformations involving simultaneously a large number of species and reactions.

With the recent progress in the micromixing field, conditions were created for the advancement of more complex situations in order to provide the industry needs. New studies included mixers with different geometries such as static mixers (Lopes et al., 2005a; Laranjeira, 2006) and impinging jets (Schaer et al., 1999). The viscosity of the fluids involved in the processes studied increased (Guichardon and Falk, 2000) and reactors of liquid-solid suspensions were also the subject of research (Aoun et al., 1996; Mahajan and Kirwan, 1996; Zauner and Jones, 2000a; Zauner and Jones, 2000b; McCarthy et al., 2007; Wu et al., 2007).

Software tools, in constant development, help those studies of more complexity. In particular, Computational Fluid Dynamics (CFD) has an important role on the coupling of local micromixing models with macroscopic description of the flow (Bourne, 1993; Trambouze, 1996; Fox, 1998; Hjertager et al., 2002; Marchisio and Barresi, 2003; Ekambara et al., 2006). Nevertheless, the available commercially CFD software does not include a complete integrated system, which includes a flowsheet modeling, reactor hydrodynamics modeling, and fully integrated complex reaction models.

In the present state of knowledge a rigorous deductive theory of the coupling between mixing and reaction is unattainable (Baldyga and Bourne, 1999). Although much work has been done to model the process of micromixing (see, for example, Patterson, 1981; David and Villermaux, 1987; Baldyga and Bourne, 1989; Cassiani et al., 2007; Soleymani et al., 2008), there still exists no way to predict its effects for an arbitrary reactor design and reaction kinetics. As in the past, and probably due to the nature and the complexity of the involved phenomena, the progress in this field is slow and needs to be continued today and in the future.

2.3 The Importance of Mixing

Mixing phenomena in chemical reactors may be considered either from the point of view of fluid mechanics in the framework of the turbulence theory or from the perspective of chemical engineering approach of the macro/micromixing theory. In fact, both are complementary. The mixing phenomena at macro and meso-scales are better known and understood than micro-scale phenomena. As a starting point, it is useful to analyze the main mechanisms, which are responsible for mixing at those scales. Thus, in turbulent mixing, the kinetic energy input into the system is dissipated by viscous deformation during the following cascade of mixing mechanisms (see Figure 2.1): (1) the distribution of fluid throughout the vessel by *bulk convection*; (2) the formation of daughter vortices, which grow (by *turbulent diffusion* or *inertial-convective* mixing) and engulf new surround fluid; (3) further deformation of daughter vortices ultimately resulting in a lamellar structure - *momentum diffusion* - where *molecular diffusion* can eliminate regions of segregation in a local flow that is laminar (Johnson and Prud'homme, 2003).

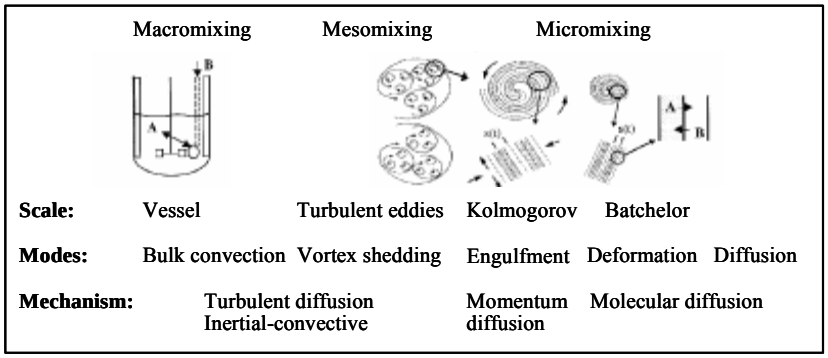

Figure 2.1 Turbulent mixing mechanisms through the several scales (adapted from Johnson and Prud'homme (2003)).

The Kolmogorov scale provides a limit where turbulent forces are balanced by viscous forces. Below this scale, appears the Batchelor scale, which provides a limiting scale where the rate of molecular diffusion is equal to the rate of dissipation of turbulent kinetic energy (Kresta and Brodkey, 2004).

When chemical reaction is slow relative to the time scale for mixing of the reagents, the only information about the flow needed to describe the course of reaction is the bulk or macroscopic flow pattern, i.e., micromixing effects can generally be neglected in comparison with macromixing effects. The outcome of the reaction is then determined by the reaction kinetics and the stoichiometric ratio of the reagents. There is, however, experimental evidence, taken from various fields of chemistry, that product distributions cannot always be predicted from chemical kinetics alone. This is not due to an inadequate description of reactions, but can be interpreted in a consistent manner as the result of a limited rate of mixing of the reagents; consequently chemical conversion can be entirely controlled by mixing, inducing significant variations in the distribution of products. This situation arises when reaction is fast relative to the attainable mixing rate, so that physical factors (e.g. rate of stirring and solvent viscosity) also contribute to determining yield and selectivity. Practical examples such as: combustion and reaction in liquid suspensions, biological growth, continuous polymerization, and reactions in viscous media are especially illustrative in this respect (Villermaux, 1983; Baldyga and Bourne, 1999). Therefore, in these cases macromixing knowledge is not enough, and it is also necessary a micromixing assessment.

2.4 Monitoring Mixing Quality

The characterization techniques of the state of mixing can be subdivided in two main categories: physical and chemical methods.

2.4.1 Physical Methods

The residence time distribution (RTD) measurement is the classic method generally used on the assessment of macromixing, that is the spatial distribution of materials on the macroscopic scale (i.e., large compared to molecular dimensions) – (Danckwerts, 1953a; Nadeau et al., 1996). This technique consists of a *non-reactive tracer* stimulus-response, with the injection of a step or pulse tracer (electrolyte, dye, miscible liquid having a different refractive index, etc.) into the reactor at a particular position and the measurement of tracer concentration

directly through a physical property (electrical conductivity, pH, optical density, refractive index, light absorption, fluorescence, radioactivity, etc.) at the reactor outlet, as a function of time. However, this method has important limitations, namely: (i) a given RTD does not correspond to a single flow pattern and, for instance, the sequence in which the fluid passes through various regions is not singly defined; (ii) the RTD is insufficient to describe the mixing and reaction of two (or more) feed streams one with each other, in particular since the moment at which mixing occurs cannot be uniquely determined; and (iii) it is not possible to decide from those measurements whether still smaller samples (and in particular those at the molecular level) are chemically homogeneous or not, i.e., it gives no information about the extent of micromixing (Bourne, 1984).

In some cases, tracer concentrations are measured simultaneously at several locations, for the monitorization of large-scale fluid motion, on samples whose size falls in the range of 1 mm (1 μL or roughly = 10^{20} molecules) to few centimeters, depending upon the analytical method (Ranade, 1992; Nienow et al., 1997; Chang et al., 1999; Buchmann and Mewes, 2000). Such measurements reveal nothing about homogeneity on finer scales due to their spatial (sample size) and time resolution (probe time response) limitations. Moreover, the probes implementation can exert flow perturbations and their size can not be reduced bellow certain dimensions for mechanic reasons.

Visualization techniques (optical methods) were also developed for the characterization of mixing, such as the study of trajectories within a flowing fluid and by measuring its velocity. These trajectories are materialized by the use of a marker, i.e., small dimension particles with the same density of the fluid, and can be visualized and recorded by laser beams and video cameras. Laser Doppler Anemometry (non-intrusive), Particle Image Velocimetry, Laser-Induced Fluorescence and Planar Laser-Induced Fluorescence (allows quantitative concentration measurements) are examples of visualization techniques.

However, most of optical methods are intrinsically limited to eddies bigger than 100 μm (much larger than Batchelor microscale), which is still beyond the range of small structures which control chemical reaction. Thus, the equipment spatial and time resolutions limit these visualization techniques to macromixing studies (Villermaux and Falk, 1996).

Chen and co-workers (1993) developed a High Speed Stroboscopic Microscopic Photography visualization technique characterized by high spatial (6.7 μm) and time (8 μs) resolutions to

study the performance of the fluid elements in the meso- and micromixing processes. The spatial resolution attainable with the better visualization techniques is comparable to the Kolmogorov scale (several hundreds of micrometers), but the finest scale such as the Batchelor scale (few micrometers) seems to be almost inaccessible.

More recently, Buchmann and Mewes (1998, 2000) developed a technique involving both physical and chemical methods. The technique consists on the simultaneous injection of an inert and a reacting dye into the reactor. The inert dye serves as a tracer for macromixing scale, whereas the vanishing of the reacting dye shows the micromixing scale. The concentration fields of the dyes are measured simultaneously by transluminating the reactor from three directions with superimposed laser beams of different wavelength. This tomographical dual wavelength technology enables the measurement of the local intensity of segregation at a multitude of points inside the reactor. The light absorption by the dyes is measured with RGB-CCD cameras (rate of deliver pictures=25 Hz) and these projections are used for the tomographic reconstruction of the concentration fields.

In short, physical methods are well suited to macromixing studies but cannot compete with chemical methods (see Section 2.4.2) for the study of mixing at the molecular scale. Macromixing studies generally give information on the large scale concentration distribution, which in turn influences reactions rates. Although necessary, these studies are not sufficient to describe the whole mixing process in the reactor, and for the study of the effects of mixing on chemical reactions.

2.4.2 Chemical Methods

The direct local determination of the scale and intensity of segregation is difficult, because this would require measurements on the molecular scale. During the last 25 years several chemical methods were developed to characterize the molecular scale of mixing sensitive.

These methods use test systems, called *reactive tracers* or more frequently *test reactions*, which are dependent on the reagent mixing. This dependency is shown by their product distribution, since they are considered as *molecular probes* (Bourne et al., 1992a; Villermaux et al., 1992). The technique consists in the injection of the reagents into the mixing reactor, and after spontaneous reactions, the products distribution is determined by sampling the fluid at outlet of reactor if the system is continuous, or from the mixture in the reactor otherwise.

The micromixing state is inferred from measurements of reaction rate and thus the mechanisms and kinetics of the test reactions need to be comprehensively known for their implementation.

Mixing sensitive reactions have kinetics of order different from (often greater than) unity. Thus, the homogeneous first-order or pseudo-first order reaction belongs to the group of reactions that are not sensible to the mixing degree, and for which the RTD knowledge is sufficient to determine the output of the reactor, since the chance of a molecule reacting depends solely on the duration of its stay in the reactor. On the other hand, reactions with non-linear kinetics (such as those normally encountered), where the probability for molecule to react depends on which other molecules it encounters during its stay in the reactor, are influenced by micromixing. Thus, test reactions belong to this last group of reactions and a great deal more information is required to predict the output of the reactor (Bourne, 1984).

The following characteristics should be fulfilled by a set of test reactions (Bourne et al., 1977a; David and Villermaux, 1987; Bourne et al., 1992a).

- Two or more reagents are involved so that contacting between these is controlled by micromixing.
- Rapid, irreversible, second-order kinetics with few (preferably two) products and no side reactions are desirable.
- It should be possible to write a full reaction mechanism, including the kinetics of every step. The effects of temperature, solvent, ionic strength, pH and concentration of a homogeneous catalyst should be known.
- A trace of the history of mixing must be kept in the system in the form of one or several stable products.
- At least one of the reactions must be faster than the micromixing processes. In practice this implies that in liquids reaction times for the fastest step are less than 0.1 second. Rate constants differing by approximately 2 orders of magnitude are suitable.
- A routine, inexpensive, and accurate instrumental analytical method is sought.
- Low concentrations of highly reactive reagents, which should be directly available on the market and sufficiently pure that they require no further purification, are sought.

- Water is the preferred solvent, and the solubility of reagents and products should be known and not exceed in micromixing measurements. Adequate solubility allows variations in concentrations and volume ratios, which are important experimental variables. If a viscosity increase is required, low concentrations of the additive are desirable to avoid interference on the reaction kinetics.
- Suitability of the reaction system for use on a technical scale, e.g. in scale-up studies; this requires consideration of factors like hazards (fire, explosion, toxicity, corrosion, volatility, effluent disposal, etc.), light sensitivity and cost of reagents must be pondered. A potential test reaction can be reduced to an acceptable level by simple and cheap measures.

However, the use of test reactions on study of mixing in reactors also presents some disadvantages (David and Villermaux, 1987):

- The instantaneous conversion has to be deduced from the concentration of reagents or products and this requires specific sensors with short response times.
- The maximum sensitivity to micromixing effects is achieved when the reaction time is of the same order of magnitude as the space-time and/or the micromixing time. Consequently, the number of reactions, which are available for these experiments, is limited and this may lead to unusual short space times in liquid phase.

Strictly speaking, the statement that a particular reaction is mixing-sensitive is incomplete and potentially misleading. What one means is that such sensitivity is manifested under a particular set of experimental conditions, namely: when the characteristic reaction time is of same order of the mixing characteristic time (the time required for the reagents to diffuse to one another and being into intimately contact). This subject is discussed in more detail in Section 5.2.

In the literature (e.g. Fournier, 1994; Baldyga and Bourne, 1999; Patterson et al., 2004), several candidates to test reactions can be found. However, it is uncertain whether these reactions satisfy all the above criteria for test reactions. It is probably correct to state that no set of reactions completely satisfies these criteria. The several test systems found in the literature can be grouped in three main stoichiometric types:

1. Single reactions: $A + B \rightarrow R$;
2. Competitive-consecutive reactions: $A + B \rightarrow R$, $R + B \rightarrow S$;
3. Competitive-parallel reactions: $A + B \rightarrow R$, $C + B \rightarrow S$.

In Sections 2.4.3 and 2.4.4, several practical examples of them are shown as well as some of their advantages and limitations.

2.4.2.1 Single Fast Reactions

Single fast reactions usually involve the neutralization of a strong mineral acid with a base represented by the following scheme: $A + B \xrightarrow{k_1} R$.

These are instantaneous or very fast reactions with a characteristic reaction time shorter than the mixing characteristic time. They are suitable for turbulent tubular reactors where reagent conversions as function of distance and time can be followed (Baldyga and Bourne, 1999). Single reactions can not be used alone but they can be implemented coupled with other techniques (e.g. optical methods). Table 2.1 summarizes the cases of single test reactions reported in the literature.

Table 2.1 Test reactions of type $A + B \rightarrow R$ (Fournier et al., 1996b).

Reference	**Reagent** A	**Reagent** B	**Rate constant** (25°C) $[\mathrm{m^3 \cdot mol^{-1} \cdot s^{-1}}]$
Worrel and Eagleton, 1964 Keairns and Manning, 1969	Sodium thiosulphate	Hydrogen peroxide	$k_1 = 2.83 \times 10^{-4}$
Keeler *et al*., 1965 Torrest and Ranz, 1970 Miyairi *et al*., 1971	Ammonium hydroxide	Acetic acid	
Mao and Toor, 1971	Hydrochloric acid	Sodium hydroxide	$k_1 = 1.4 \times 10^{8}$
	Maleic acid	Sodium hydroxide	$k_1 = 3 \times 10^{5}$
	Nitrilotriacetic acid	Sodium hydroxide	$k_1 = 1.4 \times 10^{4}$
	Carbon dioxide	Sodium hydroxide	$k_1 = 8.32$
Méthot and Roy, 1973	Sodium thiosulphate	Sodium bromoacetate	$k_1 = 10^{-5}$ at 20°C
Larosa and Manning, 1964 Zoulalian and Villermaux, 1970 Goto *et al.*, 1975 Lintz *et al*., 1975 Makataka and Kobayashi, 1976	Ethyl acetate	Sodium hydroxide	$k_1 = 1.34 \times 10^{-4}$ at 20°C
Aubry, 1972 Klein *et al*., 1980	Nitromethane	Sodium hydroxide	$k_1 = 2 \times 10^{-2}$ at 20°C

2.4.2.2 Multi-Step Fast Reactions

Fast reactions whose product distribution is dependent of the mixing quality require competitive steps. These may occur in a competitive-consecutive scheme

$$\begin{aligned} A + B &\xrightarrow{k_1 \to \infty} R \\ R + B &\xrightarrow{k_2} S \end{aligned} \tag{2.1}$$

or in a competitive-parallel scheme

$$\begin{aligned} A + B &\xrightarrow{k\infty} R \\ C + B &\xrightarrow{k_3} Q \end{aligned} \tag{2.2}$$

where the first step is quasi-instantaneous and the rate of the second step is comparable to that of the micromixing process.

This kind of reaction schemes have the advantage of keeping the memory of mixing efficiency through the distribution of products, i.e., the product distribution is limited by the consumption of the limiting reagent, which makes them well suitable for micromixing studies. Thus, a limited amount (lower than that given by stoichiometry) of B must be added to A ($N_{A0} > N_{B0}$ or $F_{A0} > F_{B0}$) in the case of a competitive-consecutive reaction scheme or to the mixture of A and C ($N_{A0} + N_{C0} > N_{B0}$ or $F_{A0} + F_{C0} > F_{B0}$) in the case of a competitive-parallel reaction scheme, so that both reactions stop by total consumption of B.

Table 2.2 and Table 2.3 show some examples of consecutive and parallel reaction schemes.

Among these reactions, some are not fast enough to characterize micromixing, some make use of organic reagents, which may be hazardous and pernicious for the environment and only a few of them are commonly used. Below, it will be exposed some details about the four test systems mainly used and reported in the literature.

As stated in Section 2.2, the most frequently used competitive-consecutive reaction system was developed by Bourne and co-workers in the early 1980s (Bourne et al., 1981). The test reaction is the azo coupling between 1-naphthol, A_1, and diazotized sulfanilic acid, B, having two products (R=monoazo and S= bisazo), which are dyes. In fact, the reaction produces

two isomers of monoazo dye, the *para* and the *ortho* form. However, at the beginning (Bourne et al., 1981) the reactions involving the ortho product were not taken into account. Afterwards, the percentage of $o-R$ and $p-R$ formed (under certain physicochemical conditions) were determined and the new reaction scheme comprises now four reactions (in Chapter 4 and 5 more details are given about this system).

Table 2.2 Test reactions of type $A+B \rightarrow R$, $R+B \rightarrow S$ (adapted from Fournier et al. (1996b)).

Reference	**Reagent** A	**Reagent** B	**Rate constant** (25°C) $[\mathrm{m^3 \cdot mol^{-1} \cdot s^{-1}}]$
Paul and Treybal, 1971 Bourne and Rohani, 1983	1-Tyrosine	Iodine	$k_1 = 3.5 \times 10^{-2}$ $k_1/k_2 = 9.2$
Zoulalian and Villermaux, 1974	*p*-Cresol	Iodine	$k_1 = 3.25$ $k_2 = 1.28$ (pH=11)
Zoulalian, 1973 Troung and Méthot, 1976	Glycol diacetate	Sodium hydroxide	$k_1 = 5.14 \times 10^{-4}$ $k_2 = 2.27 \times 10^{-4}$
Bourne et al., 1977b	Resorcinol	Bromine	$k_2 = 10^2$
Nabholz and Rys, 1977	Prehnitene Isodurene Durene	Nitronium salt	$k_2 = 3 \times 10^{-1}$ $k_2 = 4 \times 10^{-2}$ $k_2 = 10^{-1}$ $k_1/k_2 > 100$
Bourne and Kozicki, 1977	1,3,5-Trimetoxybenzene	Bromine	$k_1/k_2 \cong 27$
Bourne et al., 1990	1-Naphthol	Diazotized sulfanilic acid	$k_1 = 1.3 \times 10^4$ $k_2 = 2.7$

This test system has been widely used on micromixing studies in several types of mixers and reactors (e.g. Kusch et al., 1989; Bourne and Maire, 1991). However, it has been also criticized by several authors, who pointed out some disadvantages such as the temperature sensitivity of the reagents, their not straightforward preparation and the difficulty to obtain the spectrum of product S (Wenger et al., 1992; Fournier, 1994).

The analytical errors and the risk of side reactions (involving the product S) restrict the application of this test system to mixers whose rates of turbulent energy dissipation is less than $200-400$ W.kg^{-1} (Bourne et al., 1992a).

Table 2.3 Test reactions of type $A + B \rightarrow R$, $C + B \rightarrow S$ (adapted from Fournier et al. (1996b)).

Reference	**Reagent A**	**Reagent B**	**Reagent C**	**Rate constant** (25°C) $[\mathrm{m^3 \cdot mol^{-1} \cdot s^{-1}}]$
Treleaven and Tobgy, 1973	1- Naphthol-6-sulphonic acid	4-sulphophenyl diazonium chloride	4-Toluene diazonium chloride	$k_1 = 18.3$ $k_2 = 2.46 \times 10^{-1}$
Miyawaki *et al.*, 1975	Ammonia	Carbon dioxide	Sodium hydroxide	$k_1 = 4 \times 10^{-1}$ $k_2 = 9.3$
Phelan and Stedman, 1981	Hydrazine	Nitrous acid	Hydrogen azide	$k_1 = 6.67$
Paul et al., 1992	Hydrochloric acid	Sodium hydroxide	Organic solvent	
Bourne and Yu, 1994	Hydrochloric acid	Sodium hydroxide	Ethyl chloroacetate	$k_1 = 1.3 \times 10^{8}$ $k_2 = 3.10 \times 10^{-2}$
Bourne and Yu, 1994	Hydrochloric acid	Sodium hydroxide	Methyl chloroacetate	$k_1 = 1.3 \times 10^{8}$ $k_2 = 5.13 \times 10^{-2}$
Fournier et al., 1996b; Guichardon et al., 2000	Borate ion	Sulphuric acid	Iodide and iodate	$k_1 = 10^{8}$ $k_2 = f(I)$
Baldyga et al., 1998	Hydrochloric acid	Sodium hydroxide	2,2-dimethoxypropane	$k_1 = 0.6$

Note: All rate constants shown in Table 2.1, Table 2.2 and Table 2.3 are referent to a non-viscous medium.

In order to enlarge the range of applicability of the previous test system, the same research team improved it by introducing a fifth reaction corresponding to the azo coupling between 2-naphthol, A_2, and the diazotized sulfanilic acid with a unique monoazo dye product, Q. Thus, the kinetics scheme becomes more complex with consecutive-competitive and parallel-competitive steps simultaneously (see Chapter 4 and 5), but the analytical method and the data treatment are not significantly affected.

The improved system allows to extend the mixing investigations to higher energy dissipation rate devices, because the fifth reaction is faster than the second couplings of diazotized sulfanilic and the monoazo isomers of R. The problems associated with the limited stability of the bisazo dye, S, stated before, persist but are now less significant. Other disadvantages

relative to the chemicals are also present in this test reaction system. The main advantage of simultaneously coupling 1-and 2-naphthols is that the coupling of 2-naphthol is much faster than the secondary couplings of 1-naphthol, which makes it possible to resolve higher energy dissipation rates (up to $10^5\,\mathrm{W\cdot kg^{-1}}$) (Bourne et al., 1992a).

The competitive neutralization of hydrochloric acid and alkaline hydrolysis of monochloroacetate (methyl or ethyl) esters with sodium hydroxide investigated by Bourne and Yu (1994) is competitive (parallel) test system easy to implement. However, they are limited to weaker flow fields (e.g. stirred tanks) where the energy dissipation rates should not exceed $1\,\mathrm{W\cdot kg^{-1}}$ and $10\,\mathrm{W\cdot kg^{-1}}$ for ethyl ester and methyl ester system, respectively (Baldyga and Bourne, 1999).

The iodide-iodate test reaction was proposed by Villermaux and co-workers (Fournier et al., 1996b; Guichardon et al., 2000) as an alternative system to assess micromixing. The method involves an acid-base neutralization and an oxidation reaction, called the Dushman reaction according to the following steps

$$H_2BO_3^- + H^+ \rightleftarrows H_3BO_3 \tag{2.3}$$

$$5I^- + IO_3^- + 6H^+ \leftrightarrow 3I_2 + 3H_2O \tag{2.4}$$

In the presence of a local excess of acid, iodine is produced and instantaneously complexed by I^- in the form of I_3^-, which can be measured by spectrophotometric absorption. This additional equilibrium makes the test reaction scheme slightly more complex than the simple scheme above.

$$I_2 + I^- \leftrightarrow I_3^- \tag{2.5}$$

The first reaction is a neutralization and may be considered instantaneous. The rate of the second one is comparable to the rate of the micromixing process, and it has been studied since 1888. However, in spite of its extensive use in analytical chemistry, its kinetics is still uncertain (Fournier et al., 1996b).

This test reaction system has a few drawbacks: the reagents are expensive; the products of the reaction have to be rapidly analyzed, preferably within a minute after the end of the reaction, in order to avoid disproportionation and iodine losses; the medium is oxidizing, thus cannot

be used without care in any kind of equipment; the complex kinetics for the second reaction, Equation 2.4, and the difficulty to determine a correct kinetics rate expression could compromise a quantitative interpretation of data by micromixing models for the determination of micromixing times (Fournier, 1994; Guichardon, 1996).

Recently, this last test reaction system has been the most used system in the micromixing studies by different investigators (e.g. Ferrouillat et al., 2006; Chua et al., 2007; Assirellia et al., 2008). However, in this work the more recent test reaction system investigated by Bourne´s team (Bourne et al., 1992a) was used. This decision was made based on the several drawbacks stated above to the iodide-iodate test system as well as the selected test system was being widely used by several research teams in the micromixing assessment studies at the beginning of this work.

From the mixing studies by using a test system it is generally calculated a parameter, based in its product distribution, commonly denoted as *segregation index* or *product yield*. The values of that parameter give a quantitative description of the degree of micromixing. However, it is more valuable for reactor design and operation to have a physically meaningful parameter related to the segregation index. This is achieved by use of models which simulate the mixing processes. However, many assumptions are made during the derivation of those models and they need to be validated.

2.5 Test Systems and Micromixing Modeling

The literature reports several kinds of methods that can be used to evaluate the predictions of models claiming to describe the coupling between mixing and chemical reaction. As stated in Section 2.4.1, methods based on physical phenomena such as optical methods do not have enough resolution to characterize mixing at molecular scale. Conversely, chemical methods (test systems) have been widely used and offer the best way to attain that objective.

Once a model has been validated, its time constants can be applied industrially to suggest the directions in which to change various operating variables in order to effect the desired change of product distribution. According to Bourne (1984), this will be possible at a qualitative level (the model can only predict quantitatively if sufficient information is available), but is also important.

During the last fifty years, the micromixing models developed and reported in the literature are diverse. Depending on the role played by fluid mechanics, they can be roughly classified into two categories: phenomenological models and mechanistic models.

Models of phenomenological nature try to infer formal laws for interaction and segregation decay without explicitly referring to the underlying processes, which may account for these mechanisms. Such models try to involve only parameters that can be independently fitted to theories of turbulence or determined from laboratory measurements. They involve segregated zones, exchange fluxes, recycle streams, etc., similarly to the classical RTD models but on a more local and microscopic basis (Villermaux and Falk, 1996; Baldyga and Bourne, 1999).

These models have been successful to some extent, but their practical application usually involves previous experimental identification of the system. Moreover, the models are often abstract, contain functions or constants having no direct physical meaning, they are not able to yield *a priori* predictions or scale-up rules, and are difficult to apply in practice. However, they have a larger degree of generality and may be applied to a wider range of systems than mechanistic models designed for specific purposes. *The Coalescence and Dispersion Model*, *Interaction by Exchange with the Mean (IEM Model*) and *Multi-environment Models* are examples of this category.

Mechanistic or physical models constitute the second approach of models for micromixing simulation. They are based on elementary idealized mechanisms identified by fluid mechanics, mainly diffusive, convective and turbulent phenomena that enable to simulate the mixing process.

Fundamentally, it is clear that the best agreement between theoretical predictions and experimental data in a wide range of operating conditions is obtained with this kind of models, containing the basic mechanisms of the real mixing process (David and Villermaux, 1987). They allow *a priori* predictions as long as the flow characteristics are known. Some examples of models are: *Lamellar Model*, *Engulfment, Deformation, Diffusion (EDD) Model* and *E-Model*.

For more details about both categories of models see for example Baldyga and Bourne (1999).

The current and promising Computational Fluid Dynamics (CFD) codes have been more and more used to simulate the mixing by numeric resolution of the equations that govern the flow

and mass transfer mechanisms. In the context of a CFD calculation, micromixing is on a scale that is smaller than a typical computational cell and the models that it uses are not sufficient to provide all the details of local and complex micromixing phenomena. A key issue is to include mechanistic micromixing models into CFD codes. However, the different formulations of micromixing models (Lagrangian) and CFD model (Eurelian) could makes difficult the task (Fox, 1998).

2.6 Conclusion

To successfully implement on an industrial scale a chemical reaction developed in the laboratory, many hurdles are usually encountered. Often, these are related to difficulties in maintaining the same temperature, pressures and level of homogeneity of the reagents on a large scale. To scale-up issues, there is a strong interaction between reaction and the thermodynamic, hydrodynamic and mass-transfer processes in the reactor. The micromixing models suitably validated can be a very helpful tool to aid the engineer to understand all these phenomena and to design a productive and efficient operation. In addition, the models should be as reliable as possible, to make it possible to predict the yield and selectivity of micromixing controlled reactions and/or to obtain operating conditions ensuring the same product quality upon scale-up from laboratory to industrial conditions.

At present, the test systems are important tools on the design of new mixing devices, as stated in Section 2.1. Besides, they are the best experimental method capable to validate the micromixing models, because they allow quantifying the mixing quality at molecular scale. However, before its implementation in micromixing assessment studies, their reactions must be fully chemically characterized (reaction kinetics, analytical methods, hazards, etc.). Seeing that, all of those reactions are fast or instantaneous, its own characterization requires suitable equipment/technique, i.e., the reaction kinetic studies must be performed in high-tech equipments with short times response and resolution.

Chapter 3 is dedicated to one of those equipments – the stopped-flow reaction analyzer once, the present research work intent to the enlargement of applicability to a high aqueous viscous medium of the Bourne's improved test system (simultaneous coupling between 1- and 2-naphthol and diazotized sulfanilic acid). Consequently, the kinetic reactions should be re-determined for the new conditions and a suitable instrument is required.

3. The Stopped-Flow Technique

3.1 Introduction

Recent developments and improvements on the simulation of transport processes in chemical reactors increasingly demand more accurate and unambiguous experimental data on chemical reaction kinetics. The kinetic of fast reactions in liquid solutions have been obtained for many years by flow techniques. Three main categories of flow instruments are classified by their flow velocity and time of observation (Chance, 1974):

- *Constant* or *continuous-flow* − the flow stream is maintained at constant velocity and the extent of reaction is measured at different distances from the reagents mixing point, usually in a sequence of discharges.
- *Accelerated-flow* − the distance at which the extent of reaction is measured is constant and the flow rate is varied during a single discharge.
- *Stopped-flow* − the mixture of the reagents flows up to the observation point, stops there and the extent of reaction is measured as a function of time. This technique was developed for "slower" reactions, where ideally the time resolution of this method is sufficient to allow: (i) the optical cell to be filled with mixed but unreacted constituents and (ii) the total course of the reaction to be observed. In practice, however, significant progress of the reaction may have occurred during the course between the mixing and observation points, as it will be shown along this chapter.

The stopped-flow method is the most widely used of all the fast reaction techniques. Its vast application embrace kinetics studies of organic and inorganic reactions and of enzyme processes in biochemistry (Robinson, 1986). It was selected in this work for the kinetic study of a group of fast reactions – test reactions – as it will be shown in Chapter 4. Thus, special attention is given to this technique in the current chapter, where some details and limitations are discussed. Basically in this technique, the reagents are injected through piston driven syringes into individual tubes that converge in a T-mixer and *mixing chamber*, where the reagents streams are mixed (see Figure 3.1). The reacting mixture continues its flow at a constant rate within the single tube of the *mixing chamber* and is driven into a transparent *optical cell*, where concentrations can be measured by a spectrophotometric method. After some time the flow is halted, and the concentrations of the stopped mixture are dynamically monitored.

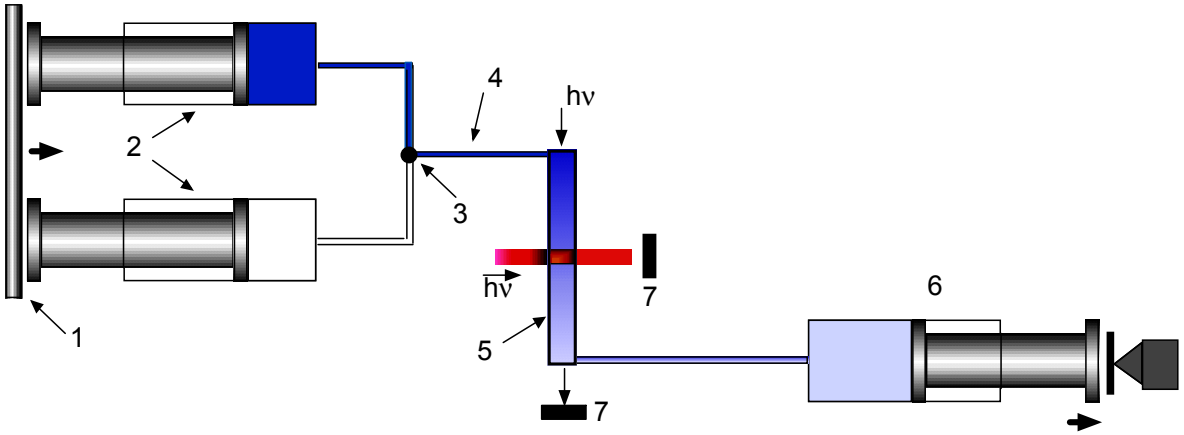

Figure 3.1 Schematic diagram of the flow system from stopped-flow technique.

The data interpretation of this technique can be strongly influenced by the quality of mixing and by the concentration gradients in the optical cell, mainly when the characteristic reaction time is of the order of the characteristic flowing time (Nunes, 1996). This characteristic flowing time, the *dead time*, results from the physical separation between the first point of mixing and the detector, and was defined, by Dickson and Margerum (1986), as the time during which the physical and the chemical processes, initiated by mixing, proceed without detection. This parameter is important to set an upper limit on the reaction rate for which an instrument is effective, since the ultimate limitation on time resolution in these flow systems arises from the finite time required for mixing (Bradley, 1975). This upper limit depends on

the geometry and hydrodynamics of the instrument and the concentration monitoring technique used, as it will be shown in Section 3.2.2.

The aim of this chapter is to establish the limits of applicability of the stopped-flow equipment used in the kinetics studies that will be described in Chapter 4 and to present a methodology for the data treatment analysis. Thus, the equipment setup is introduced in Section 3.2.1 and some of its inherent limitations are discussed in more detail in Section 3.2.2. Section 3.2.3 is reserved to the development of a comprehensive mathematical model that allows the determination of the rate constant by a multiple parameters fit that simultaneously takes into account the concentration gradient along the length of the cell for a pseudo-first order reaction. The experimental part carried out to determine the dead time of the equipment and the respective results is presented in Section 3.2.5. The main conclusions are summarized in Section 3.3.

3.2 Stopped-Flow Equipment

The commercial SX.18MV Reaction Analyzer Stopped-Flow apparatus from Applied Photophysics was used in this work. This equipment consists in three main parts: (i) a spectrophotometer, (ii) a flow system and (iii) a 32-bit RISC workstation. The equipment setup and details about its operation mode are described in the next section.

3.2.1 Setup and Operation

The SX.18MV stopped-flow reaction analyzer is a fully modular purpose designed system whose performance can be extended with several options. In this work, SK.1 Spectrakinetic was the option used, which is the basic single wavelength, single mixing, absorbance, fluorescence detection capability. It provides steady-state scanning and automated kinetic acquisitions over a selected wavelength range, with a temporal resolution of 10 μs per spectrum. The wavelength signal/noise optimization is totally automated and reference scan ("blank") subtraction in each spectrum is made internally using software installed in the workstation, which also controls the system, data acquisition and analysis.

An overview of the SX.18MV stopped-flow apparatus can be observed in Figure 3.2 and its three main parts are described in the next three sections.

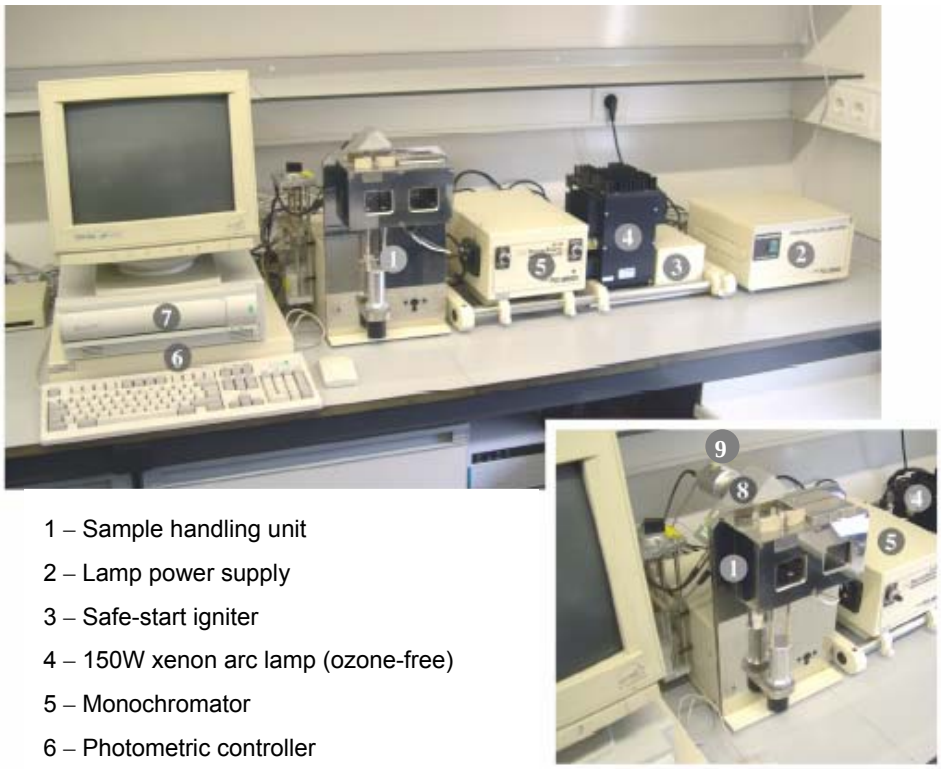

Figure 3.2 Photos of stopped-flow reaction analyzer, model SX.18MV from Applied Photophysics (adapted from Laranjeira (2006))

3.2.1.1 Spectrophotometer

The equipment used in this work for the production of a beam light and its detection after the reagents pass through the optical cell is summarized in this section. A lamp power supply unit provides a stable lamp output, which together with a *safe-start* igniter system, does not affect sensitive electronic equipment support to the ozone free xenon lamp (cuts off at 250 nm), a general purpose lamp for operation mainly in the visible. After the lamp housing, the monochromator is mounted, fitted with a 250 nm holographic grating, and programmable from the workstation. The output monochromator is connected to the sample handling unit's optical cell (see Section 3.2.1.2) through a light guide, referred as the *optical coupler*. The optical coupler has two optional positions in the orthogonal viewing ports of the cell block (see Section 3.2.1.2) as well as the absorbance photomultiplier, giving a choice of 2 mm and 10 mm pathlengths. The absorbance photomultiplier is always in the opposite viewing port of the optical coupler. Conversely, the fluorescence photomultiplier, which is not used in this work, is located in a normal position to the optical coupler.

3.2.1.2 Sample Handling Unit

Figure 3.1 shows a schematic diagram of the flow system composed of the handling unit, the optical detection cell and the stop unit. The handling unit consists of two drive syringes (filled by two reservoir syringes) whose plungers are moved by a pneumatic ram operated at the recommended pressure of $8\,\text{bar}$ (using compressed air). This unit (drive syringes, flow lines and optical cell) is immersed in a thermostat bath, which temperature is controlled by an external circulating bath (Neslab RTE-111M). Downstream of the driving syringes, the reagents are set in contact in the mixing chamber, $V_{\text{mc}} = 10\times10^{-9}\,\text{m}^3$, and flow down through the optical cell, $V_{\text{oc}} = 20\times10^{-9}\,\text{m}^3$, a silica square tube of length $\ell_{\text{oc}} = 10\,\text{mm}$, with two orthogonal viewing ports, giving a choice of $\delta = 2$ mm or $\delta = 10$ mm optical pathlengths, as it was already stated in the previous section. The reacting mixture is flushed out from the cell into the auto-stop unit, and when the flow fills completely the stop syringe, the movement of its plunger closes a micro-switch, initiating the recording of time and concentration signal changes in the detector. In this way, information relating to concentration changes of reagents, intermediate species and end products can be accurately measured for kinetic analysis and reaction modeling.

The flow circuit is chemically inert, free of stainless steel and the flow line is made of Teflon (PTFE) material. However, the more recent equipment upgrades, the flow line material is of PEEK (PolyEtherEtherKetone) which promotes a better flow integrity with much lower possibility of leakage and a slight improvement in dead time due to higher tube rigidity. For the actual material and optical cell dimension, the equipment supplier points out $1\,\text{ms}$ for the dead time value, and recommends the application limit for measurements of rates up to $1500\,\text{s}^{-1}$.

3.2.1.3 Workstation

The signal coming from the photomultiplier reaches the photometric unit, which is connected to the 32 bit RISC-processor based workstation with the ARM/Digital SA-110 CPU running at 200 MHz. The workstation is also composed by an Acorn computer fitted with IIC communication card and 12 bit ADC card.

3.2.1.4 Operation Conditions

In this work, when the flowing fluids are aqueous non-viscous, the injection flow rate value used was high enough to insure turbulent flow with Reynolds number values greater than 10^4 in the mixing chamber and in the optical cell. The injection volume could be adjustable and the value used was of approximately $V_{inj} = 240 \times 10^{-9}\ \mathrm{m}^3$, in order to allow the flush-out of the old chemicals from the optical cell and to achieve steady-state continuous flow during the reagents injection. Under these conditions the average flow rate is approximately $16 \times 10^{-6}\ \mathrm{m}^3 \cdot \mathrm{s}^{-1}$. In order to further minimize the effect of mixing, every kinetic experiment reported here is the average of eight runs.

The external-trigger mode was used to set the initial time for data collection. This means that the ADC card and workstation wait until the leaf trigger on the stop unit is closed before monitoring the detectors for changes in the concentration values. Therefore, the reported initial time instant, $t = 0$, corresponds to the instant when the solution flow ends.

3.2.2 Limitations of the Stopped-Flow Technique

In the first stage of the stopped-flow technique a steady-state flow must be established and the time to reach it depends on the reagents flow rate and on the geometry of the mixing chamber and optical cell. The geometry determines the necessary solution volume to be pushed through the optical cell, and the flow rates are determined by the necessary gas pressure to move the drive syringes, which is dependent on the viscosity of the solution being pushed and on the flow geometry. While the solution flows at a steady rate, the average age of the fluid at the observation point in the optical cell is constant and equal to the dead time, t_d, taken as the residence time between the first point of mixing and the centre of the optical cell. Modern stopped-flow equipment has a characteristic dead time of the order of $1\,\mathrm{ms}$. If mixing is perfect, the reagent concentrations will be maintained constant locally. In reality small concentration fluctuations are observed, resulting from incomplete mixing. This is particularly relevant for stopped-flow equipment with very small values for the characteristic dead time.

When the fluid fills the stop unit (see Figure 3.1), time starts to be recorded as well as the concentration data. In the second stage of the stopped-flow technique, the flow is brought to a halt by rapidly stopping the drive syringe and the reaction proceeds with time, hypothetically following, at every point of the optical cell, the dynamics of a closed batch reactor. The

concentration dynamics at this stage can be measured as a function of time, t, starting from the instant when the flow is halted.

Since the solution does not stop instantaneously, there is a short transition period, measured by the stoppage time, t_0, between continuous flow and batch conditions where the velocity of the fluid sharply decreases to zero and competition between chemical reaction and other physical mixing processes is present. When the fluid finally stops, the age of the solution in the optical cell is greater than the dead time and equals the sum of dead time and stoppage time. The final result is that the zero-time recorded in the observed time, t, is different from the zero-time of reaction of the solution retained in the cell for kinetic studies.

From the concentration history after the stoppage of the flow within cell, kinetic data is obtained assuming the batch reactor model. The time for flow stoppage cannot be resolved unambiguously. The usual determination of the so called dead time by Dickson and Margerum (1986), based on first order kinetics, is obtained disregarding the concentration gradients along the optical cell resulting from the initial flow condition, and the existence of mixing effects in the initial stages.

Later, Dunn and co-workers (1996) applied experimentally the mathematical treatment developed by Meagher and Rorabacher (1994), where concentration gradients are taken into account for a second-order reversible kinetics, but totally neglecting the non-linear effects of the mixing problem inside the optical cell. In this case, as well in other fast reactions with non-linear kinetics, it is required to use the kinetic time (reaction time) in the analysis instead of the observed time (stopped-flow internal recorded time). With the available stopped-flow measuring technology, this is not very critical for reaction kinetics with characteristic times greater than 10 ms and for low viscosity liquids, but for more viscous fluids and very fast reactions these two aspects can be critical for kinetics studies. In these cases, models of mixing and reaction will need to consider local conditions such as composition, reaction rate, etc. (Baldyga and Bourne, 1999).

Under this panorama, the determination of the dead time as well as the stoppage time is a crucial task, which must precede the use of the stopped-flow equipment in a kinetic study of fast reactions. Due to the inherent limitations of the technique exposed above, the next section is reserved to the presentation of a comprehensive mathematical model that takes into account the concentration gradient along the length of the cell and the different observed and kinetic

times scales. Later, times constants t_d and t_0 are determined by fitting the model to the data resultant from experiments performed in the stopped-flow by using a test reaction (see Section 3.2.4) in a pseudo-first order condition. Thus, the model was developed for pseudo-first order kinetics and is presented in the next section.

3.2.3 Stopped-Flow Dynamics Modeling for Pseudo-First Order Kinetics

In terms of the flow dynamics, the flowing circuit between the T-mixer, where the reagents have the first contact, and the optical cell, the stopped-flow technique has two distinct stages: continuous flow and stopped flow.

3.2.3.1 Continuous Flow

As already discussed during the continuous-flow stage the kinetic rate measurements are usually made under the assumption of plug-flow, i.e., that all fluid elements move with the same velocity (Bradley, 1975). When the fluids are aqueous non-viscous, the imposed Reynolds number characteristic for the flow of the reagent solution is high enough ($Re>10^4$) to promote turbulence. Rapid radial turbulent exchange or mixing and extensive homogenization occur over any cross-section of the tube or cell, i.e., fluid elements on the centre-line exchange rapidly with those on the periphery and the radial velocity and concentration distributions becomes flattened. However, there is an axial concentration gradient through the flow system, since reaction is occurring during the flow, and concentrations at different positions along the tube correspond to different reaction times. For a reaction $A+B\xrightarrow{k}\text{Products}$, when using a large excess of one of the reagents, $c_{B0} >> c_{A0}$, the reaction can be considered as a pseudo-first order. The apparent rate constant, k_{app}, is dependent on c_{B0}, $k_{\text{app}} = k\,c_{B0}$, and the reaction scheme becomes $A\xrightarrow{k_{\text{app}}}\text{Products}$.

For this pseudo-first order kinetics the local mass balance for the concentration of reagent A, c_A, is given by

$$\frac{dc_A}{dV} = \frac{r_A}{q} = -\frac{k_{\text{app}}}{q} c_A \tag{3.1}$$

where V is the volume and q is the solution volumetric flow rate.

Integration of Equation 3.1 between the first reagent contact point at the T-mixer, and any *observation point* results in:

$$c_A\left(V_{\text{op}}\right) = c_{A0}\exp\left(-k_{\text{app}}\frac{V_{\text{op}}}{q}\right) = c_{A0}\exp\left(-k_{\text{app}}t_d\right) \qquad (3.2)$$

where $c_A\left(V_{\text{op}}\right)$ is the concentration at the observation point, c_{A0} is the concentration at the T-mixer, and V_{op} is the volume of solution contained between T-mixer and the point of observation. This point will be always considered at midway of the observation cell and therefore V_{op}/q corresponds to the equipment *dead time*, t_d.

The concentration profile between the T-mixer and the optical cell is strongly influenced by the kinetic constant, k_{app}, as shows Figure 3.3.

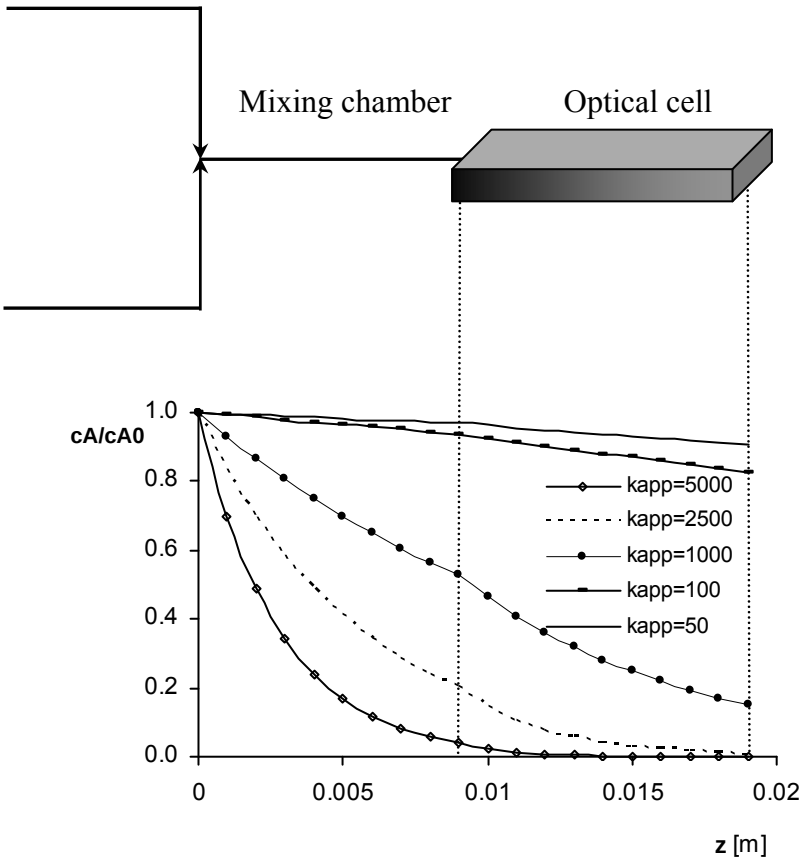

Figure 3.3 *Effect of k_{app} in the concentration profile along the flowing circuit of the stopped-flow equipment. $\vartheta_{\text{mc}} = 14.04\ \text{m}\cdot\text{s}^{-1}$ and $\vartheta_{\text{oc}} = 7.94\ \text{m}\cdot\text{s}^{-1}$. [$k_{app}$]=[$s^{-1}$].*

The concentration profile along the optical cell can be expressed in terms of a local axial co-ordinate, z_{oc}, varying between zero at the inlet of the optical cell up to the optical cell length, ℓ_{oc}, as:

$$c_A(z_{oc}) = c_{A0}\exp\left(-k_{app}\frac{V_{mc}}{q}\right)\exp\left(-\frac{k_{app}}{\vartheta_{oc}}z_{oc}\right) = c_{A0}\exp\left(-k_{app}t_{mc}\right)\exp\left(-\frac{k_{app}}{\vartheta_{oc}}z_{oc}\right) \quad (3.3)$$

where V_{mc} is the volume of the mixing chamber, t_{mc} is the mixing chamber residence time, and, ϑ_{oc} is the solution velocity in the optical cell.

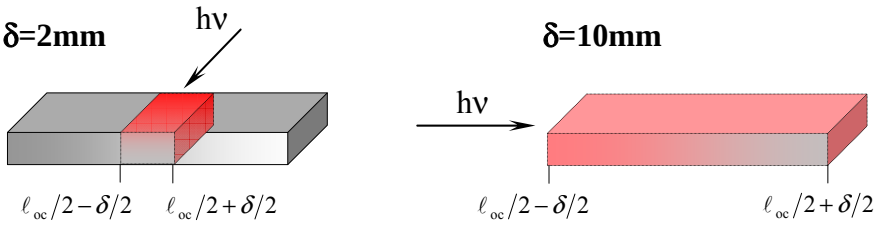

Figure 3.4 Volume of optical cell scanned during the absorbance measurements for the two optional optical pathlengths.

If concentrations are measured at the observation point in the optical cell using a spectrophotometric technique, then concentrations are not measured at one fixed point, but actually measured along an optical path of thickness δ (see Figure 3.4). The detector will register the average concentration between $\ell_{oc}/2-\delta/2$ and $\ell_{oc}/2+\delta/2$ and in effect, measuring a space average concentration at the observation point, $\langle c_A\rangle_{op}$, that can be calculated as:

$$\begin{aligned}\langle c_A\rangle_{op} &= \frac{1}{\delta}\int_{\ell_{oc}/2-\delta/2}^{\ell_{oc}/2+\delta/2} c_A(z_{oc})\,dz_{oc} = \frac{c_{A0}}{\delta}\exp\left(-k_{app}t_{mc}\right)\int_{\ell_{oc}/2-\delta/2}^{\ell_{oc}/2+\delta/2}\exp\left(-\frac{k_{app}}{\vartheta_{oc}}z_{oc}\right)dz_{oc} = \\ &= \frac{2\vartheta_{oc}c_{A0}}{\delta k_{app}}\exp\left(-k_{app}t_{mc}\right)\exp\left(-k_{app}t_{op}\right)\sinh\left(\frac{k_{app}\delta}{2\vartheta_{oc}}\right)\end{aligned} \quad (3.4)$$

where $t_{op} = \ell_{oc}/2\vartheta_{oc}$ is the residence time in the optical cell up to the observation point. Taking into consideration that $t_d = t_{mc} + t_{op}$ and introducing two geometry parameters for the cell and detector, respectively $\alpha = 2V_{mc}/V_{oc}$ and $\beta = \delta/\ell_{oc}$, Equation 3.4 can be rearranged and normalized as:

$$\frac{\langle c_A \rangle_{op}}{c_{A0}} = \frac{\alpha+1}{\beta k_{app} t_d} \sinh\left(\frac{\beta k_{app} t_d}{\alpha+1}\right) \exp\left(-k_{app} t_d\right) = f\left(\beta/(\alpha+1), k_{app} t_d\right) \exp\left(-k_{app} t_d\right) \quad (3.5)$$

where the existence of a correction factor function, $f\left(\beta/(\alpha+1), k_{app} t_d\right)$, becomes clear that is always greater than 1. This correction factor is represented in terms of $(f-1)\times 100\%$, the percentual relative deviation value, in the form of a contour line map in Figure 3.5. It is clear that for values of $k_{app} t_d$ larger than 1, the correction factor can be larger than 10%, becoming determinant for kinetic data analysis.

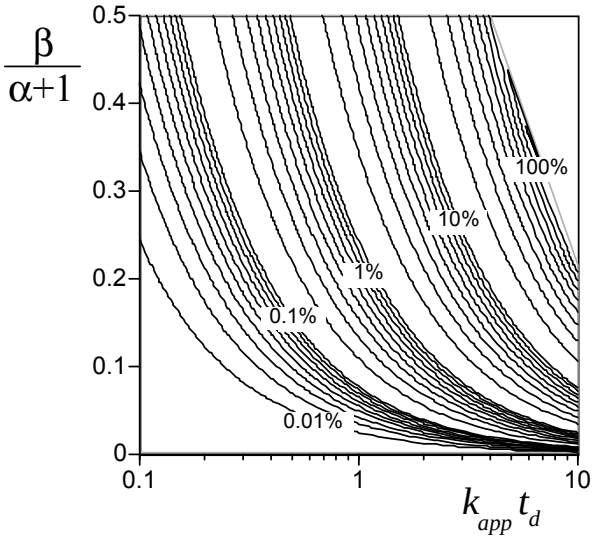

Figure 3.5 Contour line map of percentual relative deviation value, $(f-1)\times 100\%$.

3.2.3.2 Stopped Flow

The second stage of the stopped-flow technique starts when the flow is stopped at time $t = 0$. At this instant, if the solution has completely stopped, then any point is the optical cell will follow a closed batch reactor dynamics, and therefore the concentration history will evolve with time according to:

$$\frac{\langle c_A(t) \rangle_{op}}{c_{A0}} = f\left(\beta/(\alpha+1), k_{app} t_d\right) \exp\left(-k_{app} t_d\right) \exp\left(-k_{app} t\right) \quad (3.6)$$

where concentration space averaging is taken into consideration.

Actually, even if the flow is stopped instantaneously the fluid is still kept in motion locally. This is due to several possible reasons, such as cell and tube elasticity, and most probably to the inertia of liquid vortices characteristic of turbulent flows. Some evidence of these facts

will be shown later, but the immediate impact is that there is a finite time interval, the stoppage time, t_0, necessary to stop all the motion of the reacting solution. During this period, mixing between parts of fluid from different axial and radial positions is still taking place. The mixing process dies off very rapidly due to viscous dissipation, but as will be shown later, this *stoppage time* is of same order of magnitude as the dead time for stopped-flow equipment used to study very fast chemical reactions. Therefore, only after this stoppage time, should the local concentration dynamics be governed by a closed batch reactor law and in consequence Equation 3.6 should be modified to account for this delay, as follows:

$$\frac{\langle c_A(t)\rangle_{\text{op}}}{c_{A0}} = f\left(\beta/(\alpha+1), k_{\text{app}}\, t_d\right)\exp\left(-k_{\text{app}} t_d\right)\exp\left(-k_{\text{app}}\left(t-t_0\right)\right) \qquad (3.7)$$

Equations 3.5 and 3.7 form the basis for kinetic data interpretation for the stopped-flow experiments. These are two equations with three parameters, k_{app}, t_d and t_0, which will be calculated from the experimental stopped-flow curves. The pseudo-first order constant, k_{app}, obtained for a particular concentration of excess reagent, c_{B0}, is not the main objective of the research. The aim is to obtain the rate constant, k, for the second order reaction. Therefore, stopped-flow curves must be generated for a range of values of c_{B0}, and the validity of the proposed form of rate equation for the studied concentration range must be tested.

To obtain the values of the three parameters from the experimental curves, the following four step iterative procedure was implemented:

1. Give reasonable initial estimates for values of k, t_d and t_0.

2. For all these values, the stopped-flow curves of the different c_{B0} values, and only for the instant $t = 0$, are calculated as it follows:

   - compute: $\langle c_A\rangle_{\text{op}} / c_{A0}$ from Equation 3.5;

   - compute the total deviation parameter, D_0^2, from experiments:

$$D_0^2 = \sum_{\text{for all } c_{B0}} \left(\frac{\langle c_A\rangle_{\text{op}}}{c_{A0}} - \frac{Abs(t=0)}{Abs_0} \right)^2 \qquad (3.8)$$

- find by an optimization scheme to determine the value of the dead time, t_d, that minimizes D_0^2.

3. With the new value of t_d, for all the stopped-flow curves of the different c_{B0} values select only the time values where the first order assumption is valid, with the last used value for k:

   - compute: $\langle c_A(t)\rangle_{\text{op}} / c_{A0}$ from Equation 3.7;

   - compute the total deviation parameter, D_t^2, from experiments:

$$D_t^2 = \sum_{\text{for all } c_{B0}} \left(\frac{\langle c_A(t)\rangle_{\text{op}}}{c_{A0}} - \frac{Abs(t)}{Abs_0} \right)^2 \tag{3.9}$$

   - find by an optimization scheme for the determination of the rate constant k values, and of the stoppage time, t_0, that minimizes D_t^2.

4. For the newly found set of values $(k, t_d, t_0)_{\text{new}}$, compare with the previous set $(k, t_d, t_0)_{\text{old}}$, and, if different, iterate again by proceeding back to step 2. Otherwise the set $(k, t_d, t_0)_{\text{new}}$ is the best estimate for the three parameters.

In this work, it was found that this proposed four step iterative scheme, with two optimization processes involved, converged rapidly to a good and suitable solution as it will be presented in the next section.

3.2.4 Dead Time and Stoppage Time Determination

3.2.4.1 Experimental Procedure

The test reaction used in this work is the reducing reaction of 2,6-dichlorophenolindophenol by L-ascorbic acid, referred to as DCIP and AA, respectively (Tonomura et al., 1978), whose reaction is:

$$\text{DCIP} + \text{AA} \xrightarrow{k} \text{Products} \tag{3.10}$$

It is represented schematically by $A + B \xrightarrow{k} \text{Products}$. Under large excess of ascorbic acid, that is, if its initial concentration, c_{B0}, is at least one order of magnitude greater than the concentration of DCIP, c_{A0}, the reaction can be considered as a pseudo-first order. The apparent rate constant, k_{app}, is dependent on c_{B0}, $k_{\text{app}} = k\, c_{B0}$, and the reaction scheme becomes $A \xrightarrow{k_{\text{app}}} \text{Products}$ (Tonomura et al., 1978; Matsumura et al., 1990).

A solution $0.5\,\text{mM}$ of DCIP (Riedel-de Haën 33125) in water containing 10% (v/v) 2-propanol and $0.2\,\text{M}$ of NaCl was prepared. In order to achieve different apparent rate constants, various AA (Riedel-de Haën 33034) solutions at different concentrations, 2 to $120\,\text{mM}$, were prepared using HCl/NaCl ($0.2/0.2\,\text{M}$) as an ionic strength buffer. Fresh solutions were prepared daily. The experiments were carried out at 25°C with injection of equal volumes of each reagent resulting in a mixture solution with $\text{pH} = 2.0$.

The solution absorbance was measured against time at 524 nm (Tonomura et al., 1978) using both the 2 and $10\,\text{mm}$ optical pathlengths. At this wavelength, the DCIP absorbance is near its maximum value, and none of the other reagent and products exhibit significant absorbance. The initial absorbance at the mixing point, Abs_0, of the colored reagent was determined independently using a blank run (no AA) under the same pH and ionic strength conditions as those for the kinetic study.

The concentration of DCIP should be less than 1 mM in order to avoid precipitation problems of that dye and the AA concentration must be much greater than that DCIP to ensure a pseudo-order kinetics.

3.2.4.2 Results and Selection of Kinetic Data

The experimental results for the reaction between AA and DCIP are shown in Figure 3.6 for the (a) $2\,\text{mm}$ and (b) $10\,\text{mm}$ optical pathlengths, where the time resolution of each series is $25\,\mu\text{s}$. The physical and chemical conditions of the experiments were described above. The Lambert-Beer law was tested in both cases for the various concentrations used. To provide an improved quality data record for analysis, particularly at higher AA concentrations, the referred 8 runs average ensured a more reliable value for the absorbance signal.

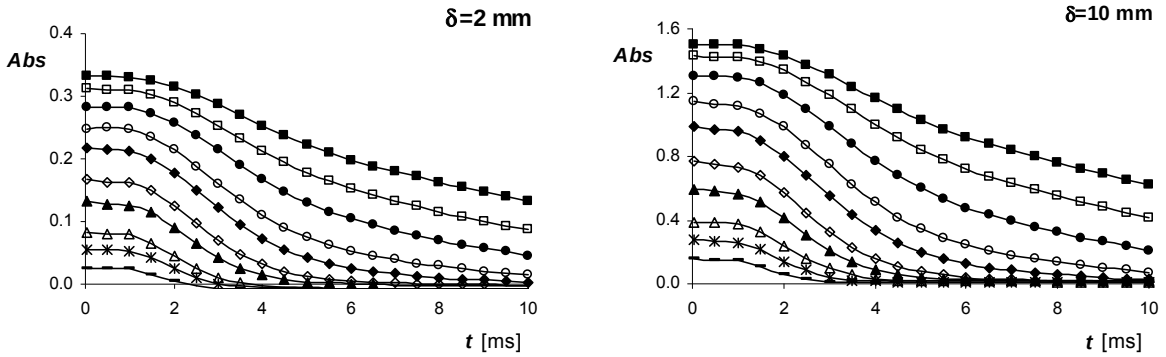

(a) (b)

Figure 3.6 *Experimental values of absorbance for the optical pathlengths: (a)* 2 mm*; (b)* 10 mm. *(*$c_{B0} = 0.25$ mM *and* c_{A0}*:* ■ 2.5 mM, □ 3.5 mM, ● 5 mM*;* ○ 7.5 mM, ♦ 10 mM, ◊ 15 mM, ▲ 20 mM, Δ 30 mM, ∗ 40 mM, - 60 mM).

To implement the model developed in Section 3.2.3, it must be ensured that only the data for which the 1st order process hypothesis is valid, was used. Data below the sensitivity limits of the equipment was neglected. Graphic visualization on the normalized logarithmic absorbance scale for different values of the initial c_{B0} reagent, as it is shown in Figure 3.7, allow an appropriate selection of the curves that present a first order behavior and the respective time range where it occurs.

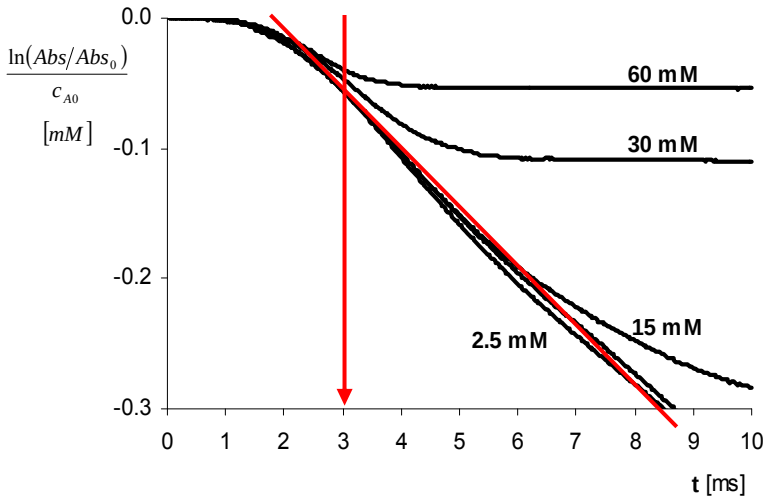

Figure 3.7 *Diagram of experimental data selection to use on fitting model.*

The region near time $t = 0$ in Figure 3.7 is characterized by a plateau, i.e., the absorbance is constant in time and represents the continuous flow stage or steady state flow. The chemicals

in the cell are constantly being replenished; hence the signal amplitude remains constant. The solution average age in the cell is constant and is equal to the dead time. After the flow is stopped, the solution velocity decreases until it stops ($t_0 \cong 3$ ms); up to this time, as it is expected, the curve does not present a first order behavior: instead of an exponential law shape, it has a sigmoidal behavior. Measurements taken during the time interval of this deceleration effect must be neglected since they could affect the subsequent concentration gradient following the cessation of the flow (Dunn et al., 1996). Finally, for larger time values the reaction proceeds with an exponential decay of the signal back to the final base line amplitude. This behavior is characteristic of pseudo-first order kinetics, and provides the results that are used by the optimization model for the determination of k, t_d and t_0.

Also, only the data recorded in the range $c_{B0} \leq 10$ mM, where linearity holds for the deduced relationship of the test reaction, can be safely considered reliable. Although for higher values of c_{B_0} pseudo-first order conditions must exist, the half-life reaction times become near or smaller than the cell dead time with consequent high yield reactions. In such cases, the detected signal decrease (in the stop flow stage) was small and often very close to the signal noise. As shown in Table 3.1, for $c_{B0} > 10$ mM in the steady state stage the reaction yield (calculated by Equation 3.11) is always greater than 50%. Moreover, in the course of the transition stage where the results are discarded due to segregation problems, the remaining reagents are practically all consumed and the signal change in the final region is very poor. These problems become more relevant for the $\delta = 2$ mm data, where most of changes occur within the first 2 ms after the stoppage of the flow. Thus, there is almost no signal change to monitor.

$$X = \frac{Abs_{0_{theor}} - Abs_{ss}}{Abs_{0_{theor}}} \times 100 \qquad (3.11)$$

Table 3.1 *List of the reagents ascorbic acid and DCIP solutions (after mixing) for the experiments to determine de dead time. Calculated initial half-life values based on (Tonomura et al., 1978) rate constant $k = 50\,\mathrm{m^3 \cdot mol^{-1} \cdot s^{-1}}$ (1); observed absorbance during the steady state stage(2); reaction yield (3).*

			$\delta = 10\,\mathrm{mm}$ $Abs_{0_{theor}} = 1.703$		$\delta = 2\,\mathrm{mm}$ $Abs_{0_{theor}} = 0.3787$	
c_{AA}[mM]	c_{DCIP}[mM]	$^{(1)}t_{1/2}$[ms]	$^{(2)}Abs_{ss}$	$^{(3)}X$(%)	$^{(2)}Abs_{ss}$	$^{(3)}X$(%)
1.0	0.25	13.86	1.640	4	0.364	4
2.5	0.25	5.55	1.504	12	0.331	13
3.5	0.25	3.96	1.426	16	0.311	18
5.0	0.25	277	1.300	24	0.282	25
6.5	0.25	213	1.203	29	0.265	30
7.5	0.25	1.85	1.126	34	0.249	34
8.0	0.25	1.73	1.105	35	0.240	37
10.0	0.25	1.39	0.968	43	0.215	43
12.5	0.25	1.11	0.824	52	0.186	51
15.0	0.25	0.9	0.753	56	0.163	57
20.0	0.25	0.7	0.583	66	0.128	66
30.0	0.25	0.46	0.384	77	0.080	79
40.0	0.25	0.35	0.263	85	0.054	86
50.0	0.25	0.28	0.192	89	0.038	90
60.0	0.25	0.23	0.149	91	0.025	93

3.2.4.3 Conventional Treatment

According to the usual data treatment to determine the dead time parameter for stopped-flow instruments and first order kinetic constants (Tonomura et al., 1978; Dickson and Margerum, 1986), k_{app} values were also determined for each individual curve by fitting the exponential relationship $Abs = Abs_0 \exp(-k_{app} t)$. The value of k was calculated from the slope of the straight line $k_{app} = k c_{A0}$, as shown in Figure 3.8. It was also corrected by the mixing rate with the relationship suggested by Dickson and Margerum, $1/k_{obs} = 1/k_{real} + 1/k_{mix}$, for the pseudo-first order rate constant. The respective results are presented in the Figure 3.9.

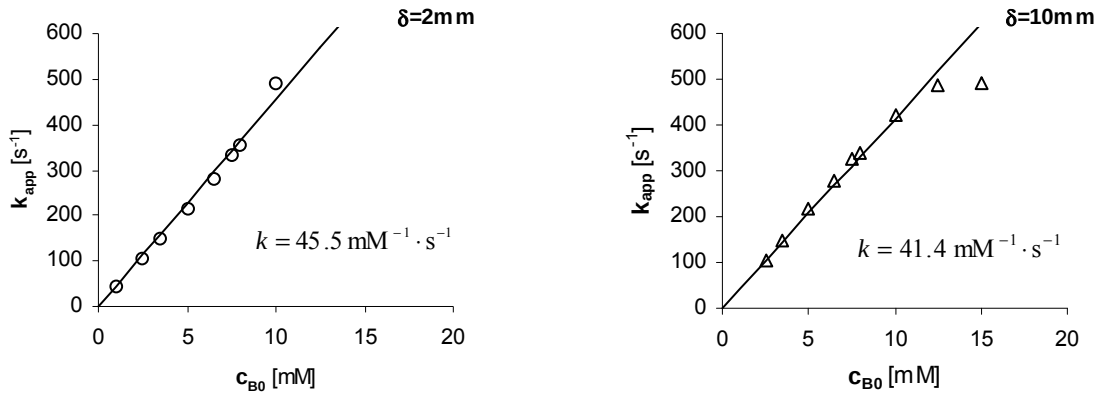

(a) (b)

Figure 3.8 The dependence of apparent rate constant (determined by usual methodology) on ascorbic acid concentration for optical pathlengths: (a) 2 mm*; (b)* 10 mm.

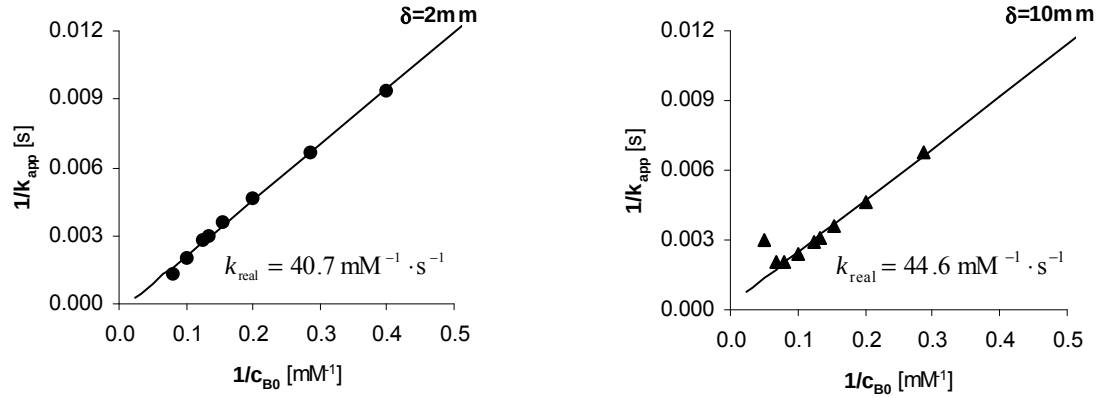

(a) (b)

Figure 3.9 Rate constant correction suggested by Dickson and Margerum (1986). (a) 2 mm *optical pathlength; (b)* 10 mm *optical pathlength.*

The measured rate constants were plotted against ascorbate concentrations (see Figure 3.8) in order to establish the extent of non-linearity at higher ascorbic concentrations. Non-linearity occurs for $c_{B0} > 10$ mM, with a different k_{app} behavior for both optical pathlengths. For higher c_{B_0} values, only the last part of the curve of the chemical reaction can be analyzed, as the early part data is lost within the dead time of instrument and during the stoppage stage. Consequently, the sigmoid part of the decay curve has an increasing effect on the k_{app} deviation, as seen by an increasing underestimation of the rate constant (see Figure 3.9b). Furthermore, for $\delta = 2$ mm an opposite effect is observed, i.e. the rate constants were overestimated.

$$c_A(t) = c_{A0} \exp\left(-k_{app}\left(t + t_d\right)\right) \tag{3.12}$$

The comparisons between the stopped-flow curves with the predictions of the conventional treatment (by Equation 3.12) are presented in Figure 3.10. Discrepancies are observed between model and experimental curves for the 10 mm optical pathlength. Similar behavior was observed for 2 mm.

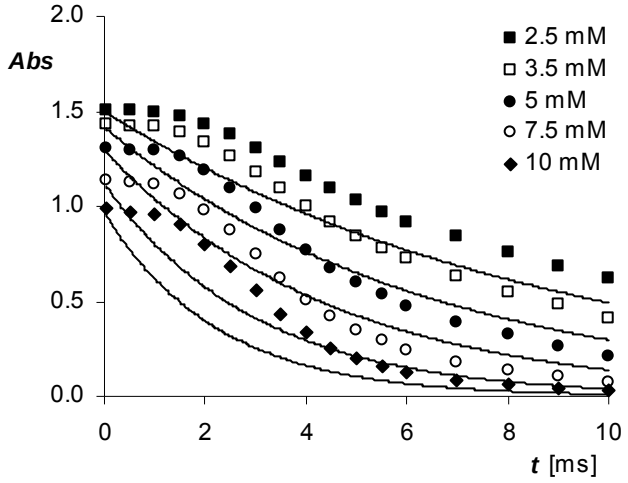

Figure 3.10 Comparisons between the experimental (symbols) and the predictions of the conventional treatment (curves) values of absorbance for $\delta = 10$ mm.

In order to obtain a better fitting between the experimental results and the predicted by the theoretical model, an alternative data treatment based on the model deduced in Section 3.2.3, is proposed in the next section.

3.2.4.4 Proposed Data Treatment

The experimental series used for the data treatment proposed in this work were the same selected in the previous section. The methodology was already described in Section 3.2.3. It consists in the determination of the constants t_d, t_0 and k by fitting of the model Equations 3.5 and 3.7 to the experimental results, which is performed using the proposed iterative scheme (see Section 3.2.3.2), and using the Excel® Solver tool for the optimization steps. This tool uses a generalized reduced gradient (GRG2) non-linear algorithm (Partin, 1995). The obtained values of k, t_d and t_0 are shown in Table 3.2 with the graphic comparison between experimental and fitted values shown in Figure 3.11. In Table 3.2 it is also summarized the rate constants and dead times values obtained by the conventional treatment of Section 3.2.4.3.

Table 3.2 Summary of the constants k, t_d and t_0 obtained by the proposed and conventional data treatment.

	Proposed treatment		**Conventional treatment**	
	$\delta = 2$ mm	$\delta = 10$ mm	$\delta = 2$ mm	$\delta = 10$ mm
k [mM^{-1}s^{-1}]	45.2	44.0	41.7	44.6
t_0[ms]	1.6	1.6	---	---
t_d[ms]	1.3	1.3	1.1	1.3

Using the proposed fitting model for concentration gradient corrections, the determined values for the three variables for both optical pathlengths are within acceptable agreement. The rate constants are the same within an acceptable 3% error. Similar t_0 values as well as the dead time, t_d, values were obtained for both pathlengths. Relatively to the conventional treatment, the results obtained are not so concordant for both optical pathlengths with errors greater than 5%. The rate constants obtained by both methods are smaller than the value published by Tonomura and co-workers (1978), that is $k = 50\ \mathrm{mM^{-1} \cdot s^{-1}}$.

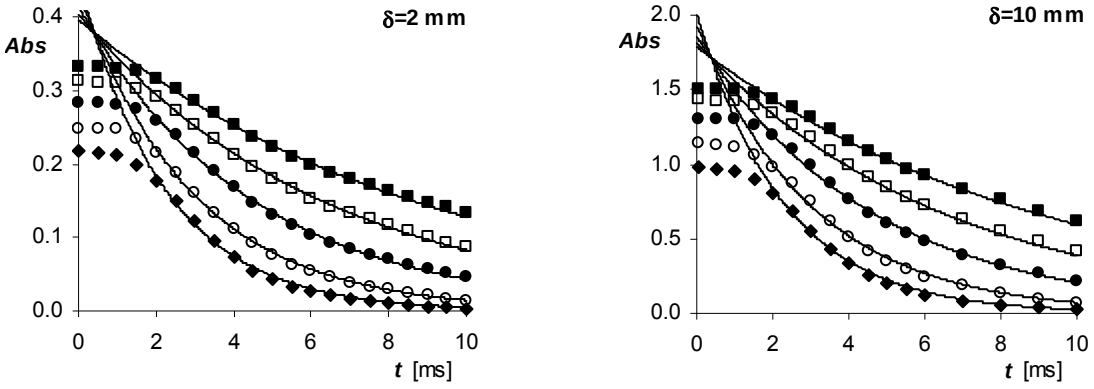

(a) (b)

Figure 3.11 Comparison between experimental (symbols) and best fitting (curves) values of absorbance for: (a) 2 mm *optical pathlength; (b)* 10 mm *optical pathlength.* (c_{A0} *:* ■ 2.5 mM , □ 3.5 mM , ● 5 mM ;○ 7.5 mM , ♦ 10 mM).

The graphic representation of the curves predict by the model here proposed allows to infer about the flow dynamics, mixing process and reaction. Thus, the examination of the experimental data of Figure 3.11 shows that during the period of flow stoppage ($0 < t < 2\,\text{ms}$) the absorbance is decreasing not as rapidly as the expected by the fitting model. When separate feed streams are used, such as in the stopped-flow technique, more segregation means less contact between the initially separated reactants and lower reactions rates (Baldyga and Bourne, 1999). So, these results reveal the presence of segregation in this time interval that can be attributed to the deceleration process and local eddy movements, since the stoppage process cannot be carried out instantaneously.

For longer times, $t > 2\,\text{ms}$, where the stop flow is ensured, good agreement between the experimental data and the fitting model is observed. This result is also shown in Figure 3.9, where the absorbance deviations between the experimental data and the model predictions are presented, and where a good and consistent fit for all excess reagent concentrations for large values of time and both optical pathlengths is observed. These results confirm that local mixing dominates for the initial $3-4\,\text{ms}$ of the data acquisition.

3.3 Conclusions

Prior to using a stopped-flow instrument in kinetics studies, its performance must be evaluated to establish its detection limits in terms of signal intensity and time resolution. For the SX.18MV stopped-flow spectrometer, with a $20\,\mu\text{L}$ optical cell, the lower limit here observed for absorbance measurements is 0.01. The supplier, Applied Photophysics, gives a time resolution of $10\,\mu s$ per spectrum and recommends the application of the equipment for kinetic rates smaller than $1500\,\text{s}^{-1}$, which was also found in this work (see Figure 3.7). Thus, the reactions to be studied by using this equipment should have a characteristic time greater than $1\,\text{ms}$.

The presence of concentration gradients in the observation cell cannot be ignored in any kinetic study, although it is of no consequence for the determination of a first order rate constant. However, in this last case, the concentration gradient becomes important when the objective is the determination of the time scale correction parameter. As shown in this chapter, the t_d values obtained with gradient correction were in good agreement using both

optical pathlengths in contrast with those determined by the conventional methodology, i.e., without gradient correction.

The suggested data treatment methodology allows the accurate and simultaneous determination of flow rate (from the dead time value), rate constant and t_0 parameter with data collected using any optical pathlength. It also allows the same determination of parameters in another record time mode; since there are other options of time acquisition (e.g. start the recording just before the drive syringe motion). In this case the t_0 will be different.

The observed time scale offset is only equal to the dead time when the stoppage of the flow was instantaneous. In the used instrument this is not the case and the offset is equal to the $t_0 - t_d$ parameter.

To avoid significant deviations during the rate constant determination, a reaction half-life time of the order or less than the cell dead time must be avoided, since most absorbance changes then occur during the stoppage flow stage and after that the signal change becomes so small that it is no longer distinguishable from the background noise.

For the presented experimental conditions the kinetic analysis was restricted to data points greater than $3\ \text{ms}$ from the time of the instrument triggering. However, this value as well the value $1.3\ \text{ms}$ for t_d, will change if the injection volume, pressure or solution viscosity changes. In this case the values must be recalculated for the new conditions.

In Chapter 4 this stopped-flow apparatus is used for the kinetic studies of fast reactions under non-viscous medium and viscous medium ($20\ \text{mPa}\cdot\text{s}$), and the experiments presented in Section 3.2.4 are repeated for the new conditions. Rheolate 255 was used the additive (as it will be seen on next chapter, Section 4.4.1) to increase the reagents solutions viscosity up to $20\ \text{mPa}\cdot\text{s}$. The data treatment was similar to the presented in Section 3.2.4.3 and the values obtained for t_d and t_0 were $2.2\ \text{ms}$ and $1.8\ \text{ms}$, respectively. The increase of viscosity with a shift in Reynolds number in the direction of laminar flow causes an increase of both quantities.

The knowledge about the stopped-flow technique, acquired along the experiments presented above as well as the modeling results, constitute an important support for the kinetic measurements performed by using this equipment, as it will be shown in Chapter 4.

4. Test Reaction Systems: Kinetic Study

4.1 Introduction

Recently, there has been significant recognition of the importance of viscous mixing in the chemical processes industry. For example, it is well known that chemical processes which involve fast competitive reactions are strongly influenced by mixing at the molecular scale. Micromixing effects increase with viscosity, and these can be relevant to the quality of some industry products, as in the food, pharmaceutical, synthetic-fiber and plastics-processing industries. In order to improve the quality of these products, better knowledge on micromixing processes in viscous media has to be obtained.

One of the most used experimental tools for the characterization of mixing is the use of the test reactions, as it was described in Chapter 2. In this work, the chosen test reaction is the simultaneous coupling of 1-naphthol, A_1, and 2-naphthol, A_2, with diazotized sulfanilic acid, B:

$$A_1 + B \xrightarrow{k_{1o}} o - R \qquad \text{(instantaneous)} \qquad (4.1)$$

$$A_1 + B \xrightarrow{k_{1p}} p - R \qquad \text{(instantaneous)} \qquad (4.2)$$

$$o - R + B \xrightarrow{k_{2p}} S \qquad \text{(fast)} \qquad (4.3)$$

$$p - R + B \xrightarrow{k_{2o}} S \qquad \text{(fast)} \qquad (4.4)$$

$$A_2 + B \xrightarrow{k_3} Q \qquad \text{(fast)} \qquad (4.5)$$

These reactions were investigated by Bourne and co-workers in aqueous solution. Initially, only the first four reactions, referring to 1-naphthol and its derivates, were studied (Bourne et al., 1985; Bourne et al., 1990). However, 1-naphthol/diazotized sulfanilic acid coupling revealed to be too slow to characterize the micromixing in high-intensity devices, having a limit to determining energy dissipation rates up to $200 - 400\ \mathrm{W \cdot kg^{-1}}$ (Bourne et al., 1992a). To expand this application limit, Bourne's team (Bourne et al., 1992a) proposed a fifth reaction (Equation 4.5), allowing micromixing characterization in systems/mixers with energy dissipation rates on the order of $10^5\ \mathrm{W \cdot kg^{-1}}$, in aqueous solutions.

Thus, the kinetics of these reactions in aqueous solution is well known. Some studies have been performed assuming the same kinetics obtained in aqueous solution applied to the studies of micromixing in viscous media (Bourne et al., 1989; Gholap et al., 1994; Bourne et al., 1995). In these works the effect of viscosity and composition of media was neglected.

In this work it was considered important to study of the influence of the viscosity on kinetics of the test reaction system, the principal goal of this chapter. Nevertheless, initially the kinetic study was also performed in aqueous (non-viscous) medium. The results obtained were compared with the published data, with the aim to validate the technique and the experimental procedure.

Previously to the kinetic study of test reaction system, the $o-R$, $p-R$, S and Q colored products were synthesized following published procedures (Bourne et al., 1990; Bourne et al., 1992a). These compounds (except S) were isolated, purified and identified using the following techniques:

- ^{1}H NMR , hydrogen (*proton*) nuclear magnetic resonance spectroscopy;
- CHNS elementary analysis;
- Measurement of humidity and ashes contents;
- Atomic absorption spectrometry;
- UV/vis spectrophotometry.

4.2 Chemicals

The test reaction system studied in this work is represented in a simple way by Equations 4.1 to 4.5 and they can be seen in more detail in Figure 4.1. There are three azo coupling reactions where the diazotized sulfanilic acid, B, is always one of the reagents. In the primary coupling, the 1-naphthol, A_1, is the other reagent producing two monoazo isomer dyes (*o*-R and *p*-R). The secondary couplings are between B and the monoazo isomers forming the bisazo dye, S. Finally the 2-naphthol, A_2, reacts with B in the third coupling where Q is produced.

Before the kinetic study it is essential to obtain some physical and chemical properties of the reagents and products involved. To this extent pure reagents and products were obtained, some of which were available on the market and others had to be synthesized, isolated and purified. Particularly:

- A_1 and A_2 are available on the market;
- B is obtained from the diazotization of sulfanilic acid which is available on the market;
- $o-R$ is not available and was synthesized and purified;
- $p-R$ and Q are available on the market as Orange I and Orange II, respectively, but due to their low purity to this application, they were synthesized;
- S is not available on the market, and its synthesis is described in detail in Section 4.2.5.

Spectrophotometry UV/vis was the analytical technique employed for the kinetic measurements since the reaction products are colored. Therefore, to accurately determine the concentration of each dye in the reaction mixture, the molar extinction coefficients, ε, of the pure dyes must be known. These coefficients constitute the calibration spectra of the species and were determined based in the Lambert-Beer law.

$$Abs(\lambda) = \varepsilon(\lambda)\,\delta\,c \tag{4.6}$$

where $Abs(\lambda)$ is the absorbance at a given wavelength, λ, $\varepsilon(\lambda)$ represents the extinction coefficient, δ is the optical pathlength and c is the solution concentration of the pure chemical.

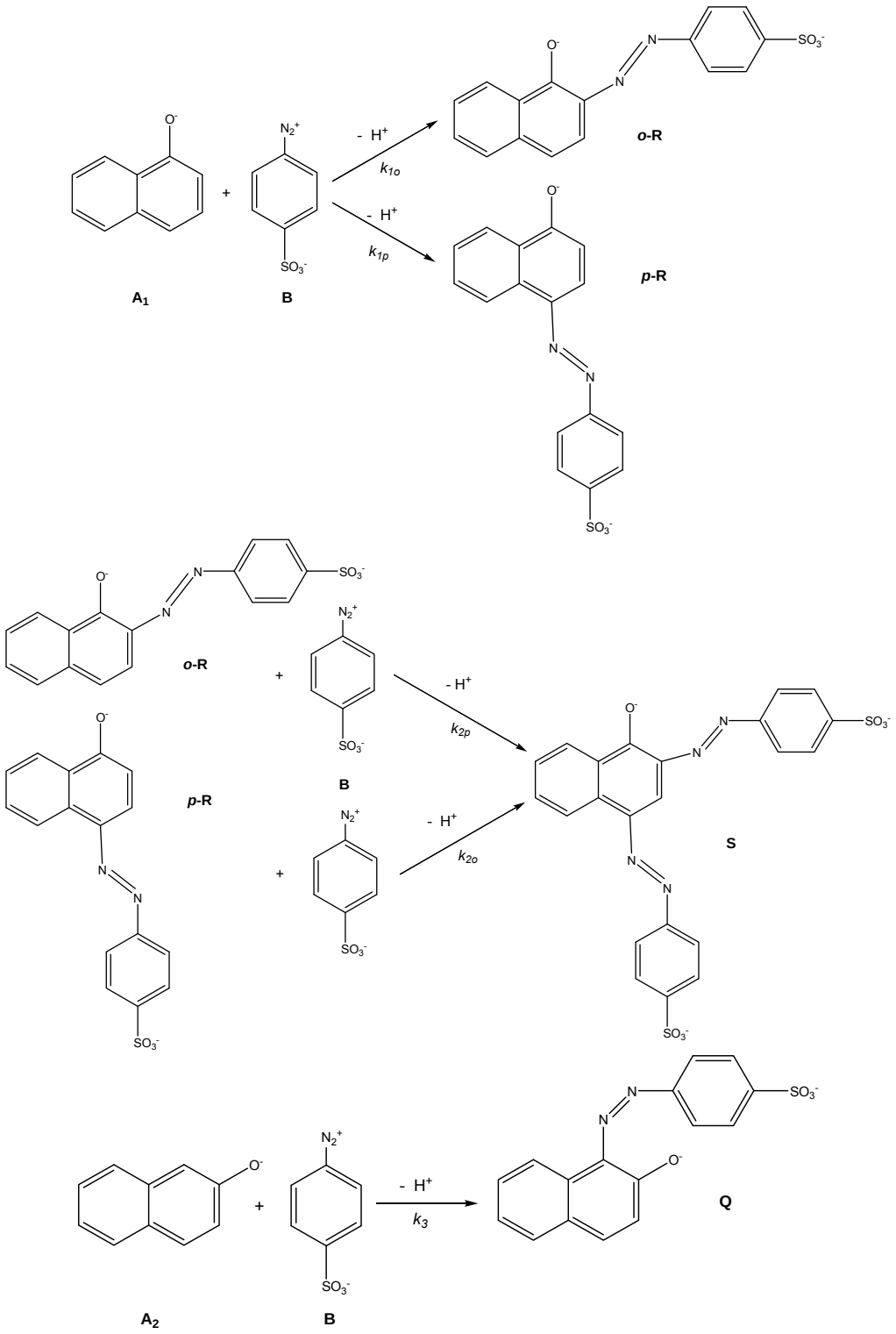

Figure 4.1 Diazo coupling reactions between 1 and 2-naphthol and diazotized sulfanilic acid (Bourne et al., 1992a).

4.2.1 1- and 2-Naphthols (A_1 and A_2)

The 1- and 2-naphthol have the molecular formula $C_{10}H_8O$, with different chemical structures as shown in Figure 4.2, and a molecular weight of $144.17\ g \cdot mol^{-1}$. In this work they were used with a purity of $99+\%$ (ACROS 12819 and 1808, respectively).

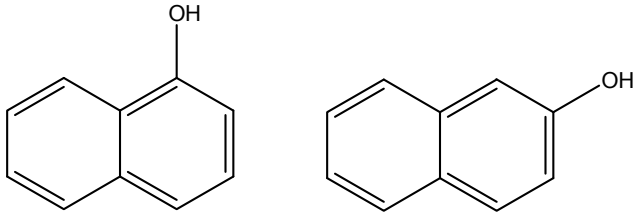

1-Naphthol **2-Naphthol**

Figure 4.2 Structural representation of 1 and 2-naphthol.

4.2.1.1 Preparation

The solubility in water of 2-naphthol is $6.9\ mol \cdot m^{-3}$ at $20^{\circ}C$ (ACROS). The 1-naphthol is slightly soluble in water but very soluble in ethanol. The aqueous solution of this reagent can be prepared by dissolving it in a very small quantity of ethanol and adding this to water. The 1-naphthol initially forms a fine precipitate which then rapidly redissolves. Following this procedure, Bourne and Tovstiga (1985) measured the solubility of 1-naphthol in water in the range $285 - 305\ K$; the results are reported in the Table 4.1.

Table 4.1 Solubilities of 1-naphthol in water at various temperatures (Bourne and Tovstiga, 1985).

T [K]	284.7	293.1	298.0	304.6
Solubility [$mol \cdot m^{-3}$]	4.78	6.26	9.09	11.49

The water used in the preparation of 1- or 2-naphthol was previously deionized and stripped of dissolved oxygen by a nitrogen stream. Both solutions were stored in glass vessels under exclusion of light and at below room temperature. Fresh solutions were prepared everyday.

These reagents were alkaline-buffered with $Na_2CO_3/NaHCO_3$ to a pH of 10 just before coupling, as it will be described below (Sections 4.3.1.1 and 4.3.4.1).

4.2.1.2 Identification

The solutions concentrations of 1- and 2-naphthol were checked by spectrophotometry, comparing with previous published spectra data.

4.2.1.3 UV/vis spectra

Aqueous non-viscous solutions of 1- and 2-naphthol were prepared using reagent concentrations in the range $0.1-0.2\ \text{mol}\cdot\text{m}^{-3}$ (buffered to $\text{pH}=10$, $I=444.4\,\text{mol}\cdot\text{m}^{-3}$). The spectra were scanned at 25°C and the molar extinction coefficients, ε, were determined. Their average values were calculated and stored to give the calibration spectra useful for the kinetic study, as shown in Figure 4.3 and Figure 4.4.

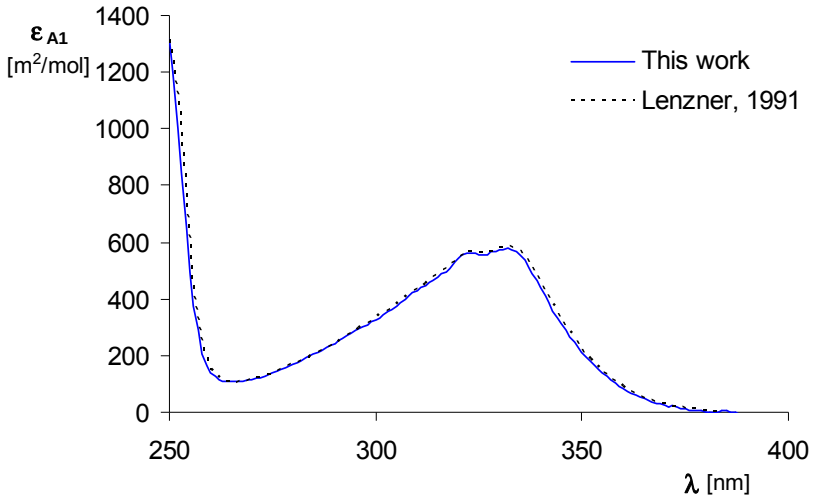

Figure 4.3 Molar extinction coefficients of 1-naphthol ($I=444.4\ \text{mol}\cdot\text{m}^{-3}$, $\text{pH}=9.9$, $\mu=1\ \text{mPa}\cdot\text{s}$ and $T=25^{\circ}\text{C}$). — Experimental and --- published (Lenzner, 1991).

A good agreement between experimental and previously published spectra for both naphthols was obtained. These curves depend on the experimental conditions, and therefore, they should be re-determined if those conditions change. These spectra were determined under the same experimental conditions of the kinetic study in aqueous non-viscous media. For the kinetic study in aqueous viscous medium these spectra were also determined and will be reported later.

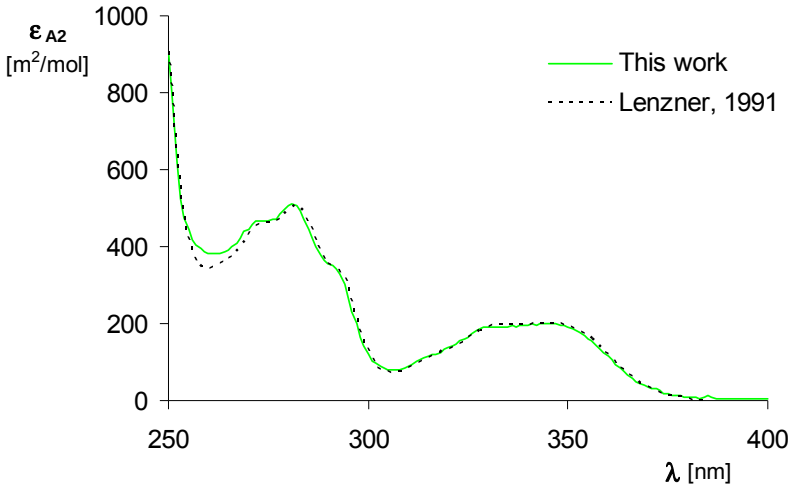

Figure 4.4 Molar extinction coefficients of 2-naphthol ($I = 444.4\ \text{mol}\cdot\text{m}^{-3}$, $\text{pH} = 9.9$, $\mu = 1\ \text{mPa}\cdot\text{s}$ and $T = 25^{\circ}\text{C}$). — Experimental and --- published (Lenzner, 1991).

4.2.1.4 Stability and Toxicity

1 and 2-naphthol are stable in solution for a few hours. It is recommended their preparation everyday.

Their specific toxicity (mutagenesis, carcinogenesis) has not been reported. However, in Appendix A some emergency overviews and potential health effects are presented.

4.2.2 Diazotized Sulfanilic Acid (*B*)

4.2.2.1 Preparation

The diazotized sulfanilic acid can be prepared by the diazotization of sulfanilic acid (Fluka 86090), which is an primary arylamine. In acid solution, this reagent is a zwitterion (ion with double opposite charge), and it is relatively insoluble. On the other hand, its base (see Figure 4.5) is soluble up to $10\ \text{g}\cdot\text{L}^{-1}$.

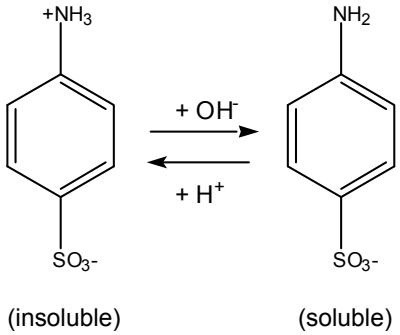

Figure 4.5 Sulfanilic acid: acid/base equilibrium.

Sulfanilic acid is commercialized as a free acid and can be dissolved by adding the required amount of sodium carbonate as shown in Figure 4.6.

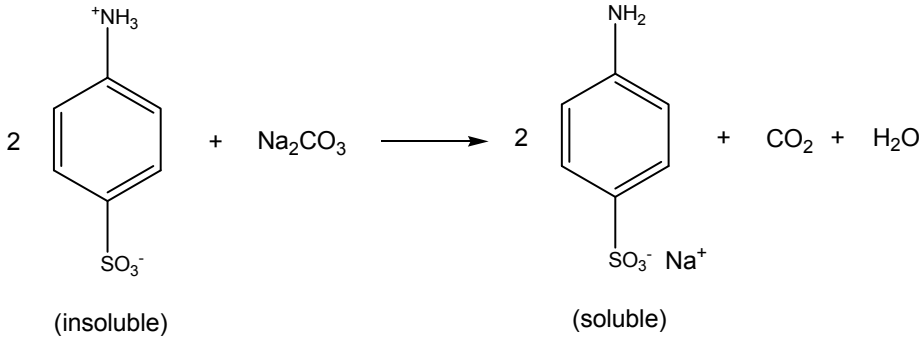

Figure 4.6 Solubilization of sulfanilic acid (free acid).

Once dissolved, sulfanilic acid can be diazotized. The diazotization reaction, discovered by Peter Griess in 1858 (Kirk-Othmer, 1982), involves three components: an arylamine (sulfanilic acid: $^{-}O_3SC_6H_4NH_2$), a mineral acid (hydrochloric acid: HCl) and a source of nitrous acid (sodium nitrite: $NaNO_2$) (Saunders and Allen, 1985). The overall equation for this reaction is given by:

$$^{-}O_3SC_6H_4NH_2 + 2\,HCl + NaNO_2 \rightarrow {}^{-}O_3SC_6H_4N_2Cl + NaCl + 2\,H_2O \qquad (4.7)$$

Diazotization is conducted at 275-277 K using both HCl and $NaNO_2$ in 4% excess, and the excess nitrite is destroyed after diazotization by adding urea. The solution is stored in a glass vessel under exclusion of light and below room temperature.

The low temperature at which this reaction takes place is advantageous because the solubility of free nitrous acid is greater, which means that there is less danger of the nitrous gases escaping from the acid medium. At the same time, the low temperature enhances the stability of the diazotized sulfanilic acid (Zollinger, 1961). In Figure 4.7 shows an example of the degradation reaction of diazotized sulfanilic acid that can occur at higher temperatures.

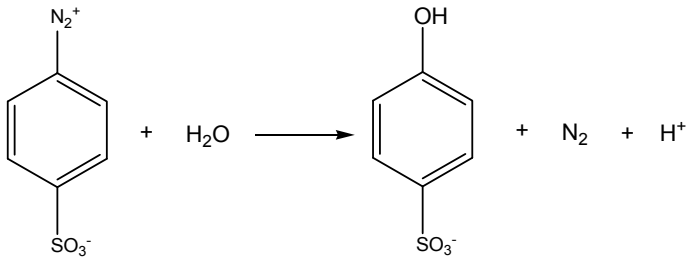

Figure 4.7 Degradation of diazotized sulfanilic acid at high temperatures.

Although the theoretical requirement of hydrochloric acid is two equivalents, in agreement with Equation 4.7, the use of HCl in excess is recommended to prevent the formation of triazen (Saunders and Allen, 1985). In this work, an excess of 4% was used (Bourne et al., 1985).

During the diazotization reaction, the pH value should be kept below 2 to avoid the reaction between the diazotized sulfanilic acid and the sulfanilic acid, producing a diazomino compound, as shown in Figure 4.8.

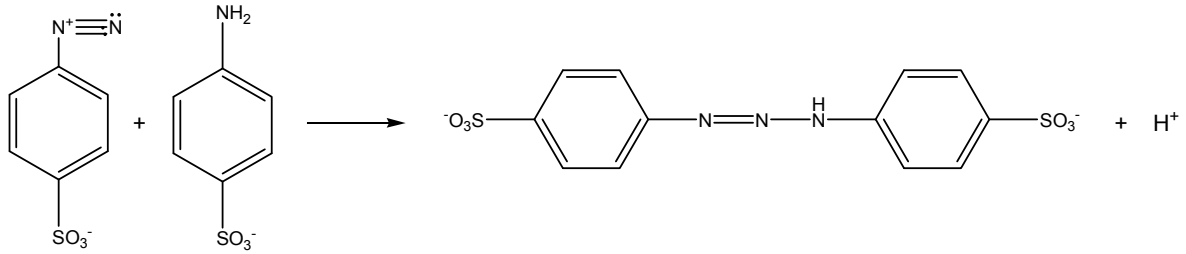

Figure 4.8 Degradation of diazotized sulfanilic acid at high pH during the diazotization.

The diazotizing agent is produced from nitrous acid, for which the source is the sodium nitrite. Its formation mechanism is depicted in Figure 4.9.

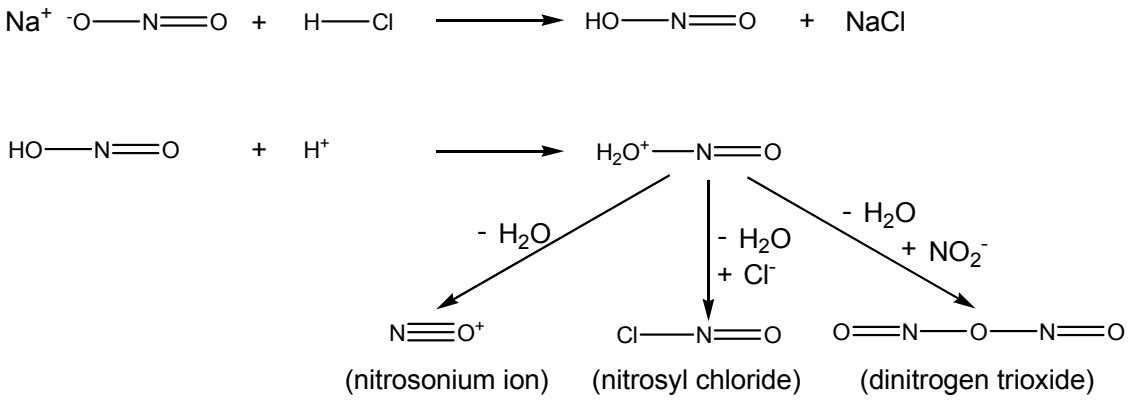

Figure 4.9 Mechanism of diazotizing agent formation.

Depending on the pH, diazotization proceeds via a different derivative of nitrous acid because, on the one hand, the rate of formation of these derivatives varies in different ways with pH and, on the other, the derivatives exhibit different rates of diazotization of the amine. It has been suggested that at low pH, the diazotizing agent is the nitrosonium ion (Zollinger, 1961).

In contrast to the acid, sodium nitrite should not be added in excess, because an excess of nitrous acid exerts a very unfavourable influence on the stability of diazo solutions (Zollinger, 1961). However, if an excess is used (as suggested by Bourne and co-workers (1985)) nitrous acid can be destroyed after diazotization is completed, by the addition of urea (NH_2CONH_2) or sulphamic acid ($OHSO_2NH_2$). These compounds are able to convert nitrous acid into nitrogen, as shown in Equations 4.8 and 4.9.

$$NH_2CONH_2 + 2\,HNO_2 \rightarrow CO_2 + 2\,N_2 + 3\,H_2O \qquad (4.8)$$

$$OHSO_2NH_2 + HNO_2 \rightarrow H_2SO_4 + N_2 + H_2O \qquad (4.9)$$

In spite of the decomposition being faster using sulphamic acid, in this work urea in the 4% of nitrite excess was used, because when using sulphamic acid in a strongly acid solution, the following side reaction with the diazo compound is possible (Zollinger, 1961):

$$^{-}O_3SC_6H_4N_2^{+} + OHSO_2NH_2 + H_2O \rightarrow {}^{-}O_3SC_6H_4NH_3^{+} + H_2SO_4 + N_2 \qquad (4.10)$$

The excess of nitrous acid should be verified by making a test with an external indicator - moist potassium iodide starch paper - which exhibits an immediate blue colouration in the presence of nitrite ions. However, it is crucial to wait a few minutes between the end of the diazotization reagents mixing and this test, because towards the end of the diazotization the reaction with nitrous acid is slow (Vogel, 1964).

Once the quantity of nitrite used in excess on the diazotization it is known, the amount of urea to be added for its removal is calculated by the respective destruction reaction stoichiometry.

Owing to the solubility problems in acid media, the diazotization of the sulfanilic acid is processed by the so-called “indirect method” (Zollinger, 1961), where nitrite is added to the approximately neutral sulfanilic acid solution, which is then run into ice-cooled and stirred hydrochloric acid solution. The formation of the diazonium salt takes places quickly - forming a white precipitate – and prevents precipitation of the free acid.

An example of experimental procedure to prepare 0.01 mol of diazotized sulfanilic acid is:

1. Dissolve 0.5300 g of Na_2CO_3 (0.005 mol) in approximately 100 mL of water;
2. Add 1.7319 g (0.01 mol) of sulfanilic acid (free acid form) to the previous solution;
3. In parallel, prepare an aqueous solution of HCl, by adding 1.9 mL of 37 % concentrated HCl ($d = 1.09$) at ± 50 mL of water;
4. Cool, both solutions, in a ice bath up to 2-4ºC;
5. Dissolve 0.7176 g of $NaNO_2$ in the sulfanilic solution of step 2;
6. Drop, while stirring, the sulfanilic acid and nitrite solution into the HCl solution. The diazotized sulfanilic acid formed precipitates and the diazotization reaction is complete almost as soon as all solution has been added;
7. Add 0.012 g of urea, soon after;
8. Dissolve the precipitate in water. The total solution volume should be 1 L and the concentration of the diazotized sulfanilic acid about 10 $mol \cdot m^{-3}$.

The diazotized sulfanilic acid is considered to be obtainable in 100% yield by this method.

4.2.2.2 Stability and Toxicity

This compound is colourless, absorbs in the UV region but it is sensitive to light. For these reasons, its concentration can be checked by the coupling solutions of 0.0525 $mol \cdot m^{-3}$ 1-naphthol and of 0.05 $mol \cdot m^{-3}$ diazotized sulfanilic acid with intensive stirring or in the stopped-flow apparatus. This reaction produces monoazo dyes and by spectrophotometric analysis the mass balance can be made. In the present work, the mass balance always closed within $\pm 2\%$, indicating that the diazotization was completed.

The diazotized sulfanilic acid is stable for several hours when kept in slurry form in an ice bath. The precipitate should not be isolated because it is an explosive material when dried. The solutions of this reagent should be preparared every half-day and stored in dark bottles to avoid the light exposure.

The diazotized sulfanilic acid is unstable for alkaline pH, where it passes by a complex transition into covalent union with the hydroxyl anion to form the weak diazotate anion $Ar\,N_2O^-$ (Saunders and Allen, 1985).

At room temperature the solubility of this salt is up to $60\,mol\cdot m^{-3}$ (Baldyga and Bourne, 1999).

In the literature, no hazards information related with diazotized sulfanilic acid was found. Information about potential health effects and emergency overviews of sulfanilic acid are pointed in Appendix A.

4.2.3 4-[(4-Sulfophenyl)azo]-1-naphthol (*p-R*)

In the test reaction in study, the dye $p-R$ is simultaneously a product (see Equation 4.2) and a reagent (see Equation 4.4).

In order to make the kinetic study of the reaction where $p-R$ is a reagent, it is necessary to obtain this isomer isolated and in pure solid form. This compound is available on the market under the name of Orange I (Sigma&Aldrich 75360). However, its 90% of purity was not satisfactory for this work and the observed UV/vis spectrum was different from the published (Bourne et al., 1990; Wenger et al., 1992). Consequently, it was necessary to proceed to the synthesis and purification of this compound, following some of the procedures referred in the literature (Belevi et al., 1981; Bourne et al., 1990; Wenger et al., 1992).

In the next sections, details of the experimental procedure as well as the identification results of the final product by different techniques are presented.

4.2.3.1 Synthesis and Purification

Following the procedure described in Section 4.2.2, sulfanilic acid was diazotized and $0.01\,mol$ was added dropwise at room temperature to $0.01\,mol$ $(1.442\,g)$ of 1-naphthol dissolved in $75\,mL$ of buffered ethanol. It was observed the formation of a dark-brown solution, which was heated up to $60^{\circ}C$ left for 2 hours and finally cooled over several hours to room temperature (Bourne et al., 1990). The resulting dark-green precipitate was filtered, rinsed 3 to 4 times with 50% aqueous ethanol and finally it was dried.

Thin layer chromatography (TLC) was used for the qualitative assessment of the precipitate purity. Even after the various rinses, TLC still indicated impurities by showing two spots, one pink and one orange ($p-R$).

With the aim to achieve a better result, the solid was divided into five fractions to be submitted to different processes of isolation/purification.

1. Column chromatography (solid support - silica gel; eluent - chloroform:methanol);
2. Preparative thin layer chromatography, TLC (stationary phase - silica gel; liquid phase – ethyl acetate: methanol);
3. Recrystallization from aqueous ethanol;
4. Rinse with 50% aqueous ethanol;
5. Rinse with organic solvent (ethanol and ethyl ether 1:4 v/v).

For the first fraction column chromatography using silica gel as the solid support chloroform:methanol as solvent was tried but the separation was not satisfactory.

Thin layer chromatography, TLC (stationary phase - silica gel; liquid phase – ethyl acetate:methanol) was used on the second fraction, and a good separation was observed. However, only a small amount of $p-R$ was recovered from the plate in each sample, and thus for the present work this technique became unsuitable.

Triple recrystallization from aqueous ethanol tried on another fraction was unsuccessful.

The fourth fraction was rinsed 20 times with 50% aqueous ethanol. The fifth fraction was rinsed with an organic solvent mixture (ethanol:ethyl ether 1:4 v/v). In both cases, the experimental procedure comprised also the evaluation by TLC, of the impurities still remaining in the dry solid and in the waste solution: first, by direct TLC plate observation where the coloured spots were easily detected; second, using an ultraviolet (UV_{254}) camera; and finally, using an iodine vapours camera.

On the evaluation by TLC of both fractions (fouth and fifth) the starting point was firstly to dissolved the dried solid in water and different TLC eluent mixtures were tested in order to attain a good spots separation, namely ethanol:chloroform (1:1 v/v), methanol:chloroform (1:1 v/v) and ethyl acetate:methanol (1.8:1 v/v). This last solvent mixture was the best one on the spots separation in any of the two solid fractions.

Besides the two common variables that affect the TLC results, namely: the composition of the eluent (mixtures more or less polar) and the visualization/development techniques employed for spots identification, in this work it was seen that the solvent where the solid is dissolved in also affected the separation of the spots.

In this work, when the TLC tests performed after each rinsing step showed just the orange spot, the water solvent was changed for ethanol. It was observed that the pink spot reappeared which means that the solid was still impure. New rinsings succeeded up to pink spot vanishing. Then, one changes the solvent again to methanol and, even tenuous, the pink spot reappeared.

As the precipitated was submitted to numerous rinsings, a significant mass loss of $p-R$ was observed, and thus the product was accepted as pure as soon as the pink spot was very tenuous after rinsing. The fraction that was rinsed with ether:ethanol was the only one that followed for the next step – the identification, because it exhibited a more tenous pink spot.

4.2.3.2 Identification of $p-R$

Identification and characterization of $p-R$ was done using different techniques, such as: humidity and ashes content, atomic absorption spectroscopy, elemental analysis, nuclear magnetic resonance (^{1}HNMR) and UV/vis spectrophotometry.

Humidity and ashes content

The humidity content was low ($0.9\,\%$), which is indicative that there are no water molecules crystallized on the $p-R$ chemical structure. The ashes content, determined at $650^{\circ}\mathrm{C}$ over 2 hours, was of $0.8\,\%$ which is a low value and indicative of the inexistence of minerals in this compound. Both analyses were performed in ICAT laboratory from FCUL-Faculdade de Ciências da Universidade de Lisboa, Portugal.

Atomic absorption spectroscopy

Sodium ion was not detected by atomic absorption spectroscopy. This result is in good agreement with the low value of ashes, which means that the purified $p-R$ precipitate obtained in this work is in the form of free acid. The same conclusion was obtained by other authors (Bourne et al., 1990; Wenger et al., 1992).

In short, from these analysis it is predicted the chemical formula $HOC_{10}H_6N{=}NC_6H_4SO_3H$ for $p-R$ with theoretical molecular weight of $328.34\ \mathrm{g\cdot mol^{-1}}$.

Elemental analysis

Three samples of $p-R$ solid were submitted to CHNS (carbon, hydrogen, nitrogen and sulphur) elemental analysis done at ICAT-FCUL. The standard used in this analysis was the sulphanilamide ($C_6H_8N_2SO_2$). The results presented in the Table 4.2 are the average of all samples and respective standard deviations. In the same table it is also reported the results published by Wenger and co-workers (1992) and the theoretical values predicted when using the chemical formula specified above.

Table 4.2 Elemental analysis of p-R (free acid).

Reference	**% C**	**% H**	**% N**	**% S**
This work	58.31 ± 0.59	3.48 ± 0.14	8.38 ± 0.13	6.96 ± 0.29
Wenger et al. (1992)	58.55	3.71	8.49	---
Theoretical	58.52	3.68	8.53	9.76

The difference between experimental and theoretical values should not be greater than 0.4% to validate the purity of the compound. Wenger and co-workers (1992) obtained good results, but they did not present the sulphur content. The results obtained in this work fulfil the criteria for all atoms except for sulphur, where the difference is 2.8%. In spite of this, one can say that $p-R$ is in a high level of purity, because the experimental values of CHNS elemental analysis are very close to the initially predicted. Moreover, the next characterization technique will corroborate this assertion.

Nuclear magnetic resonance

Proton nuclear magnetic resonance – ^{1}HNMR – is another analytical technique that can be used to assess compound purity. For the ^{1}HNMR spectrum determination, a little quantity of dried solid was weighed and dissolved in deuterium water. The analysis was made by a laboratory of the Chemical Department of Universidade de Aveiro and the result is shown in Figure 4.10.

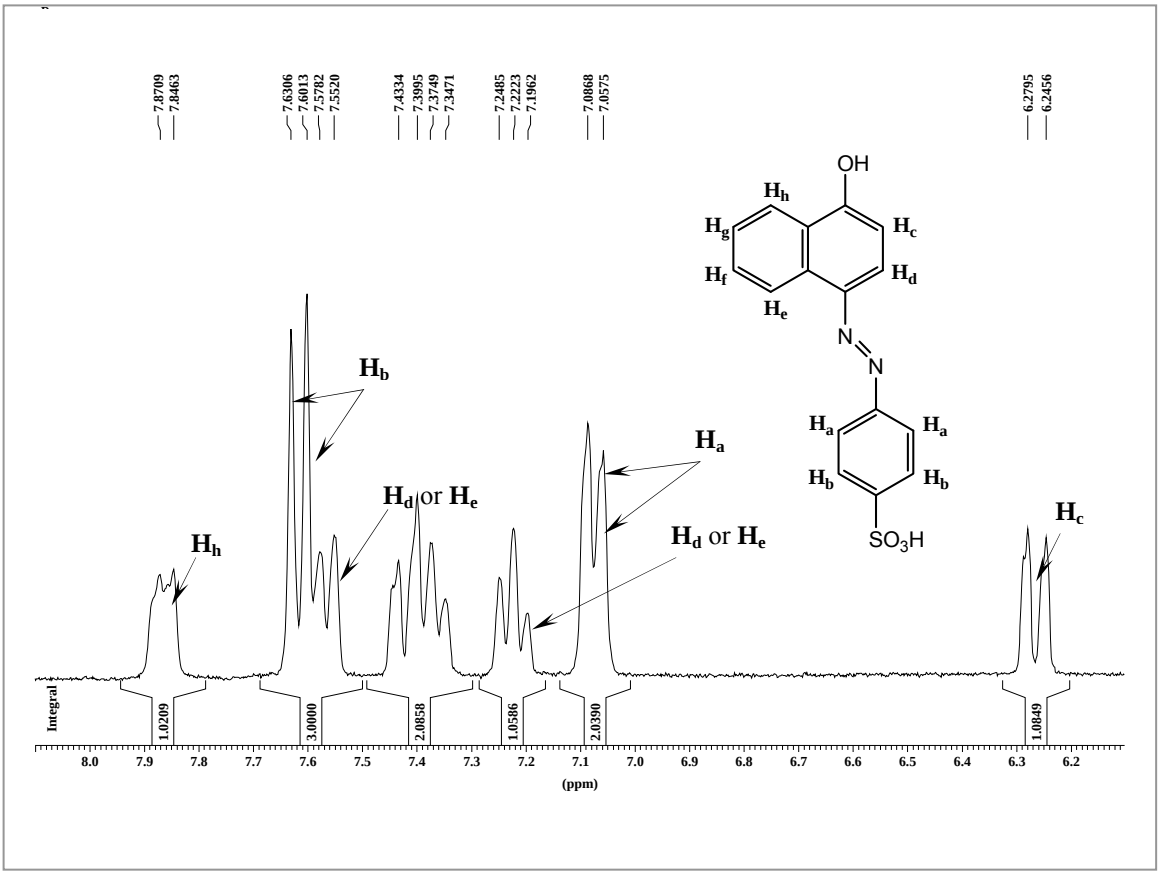

Figure 4.10 ^{1}*HNMR spectrum of* $p-R$.

On the $p-R$ molecule there are ten hydrogen atoms bonded to the three rings. Accordingly to their protection level, they were identified as H_a, H_b, and so on as shown in Figure 4.10. The order of appearance of these hydrogen atoms in the ^{1}HNMR spectrum depends on their protection level. In this way, the most unprotect hydrogen, H_h, is the first to appear at $7.85\ \text{ppm}$, followed by both H_b atoms up to the most protected, H_c, which appears at $6.26\ \text{ppm}$. The third group of peaks (around 7.4 ppm) corresponds to duplet and triplet overlapping. Hence, most of the $p-R$ molecule hydrogen atoms can be identified in the above spectrum, which means that this compound has a significant purity level.

Spectrophotometry

The last technique used to characterize the purity of this monoazo isomer was UV/vis spectrophotometry. It is opportune to point out that $p-R$ isomer is a pH indicator (7.6-8.9) showing an orange colour in acid medium, with maximum absorbance wavelength, $\lambda_{max} = 470\ \text{nm}$, changing to red colour in basic medium with $\lambda_{max} = 510\ \text{nm}$. Thus, its UV/vis spectrum depends on the solution pH.

To follow the kinetic reactions where this isomer is involved, its spectrum must be known on the same experimental conditions of the kinetic studies, namely: pH, ionic strength, *I*, viscosity, solvent, temperature, etc.

The spectrum was determined in aqueous non-viscous medium, at $25^{\circ}\mathrm{C}$, $I = 444.4\ \mathrm{mol \cdot m^{-3}}$ and $\mathrm{pH} = 9.9$, by using $Na_2CO_3/NaHCO_3$ as a buffer, which are the same conditions of the published spectra as well as the experimental conditions of the first part of the kinetic study performed in this work (see Section 4.3). Aqueous solutions with different concentrations of this dye were prepared by weighing masses based on theoretical molecular weight present before. The molar extinction coefficients, $\varepsilon_{p-\mathrm{R}}$, were calculated accordingly to Equation 4.6 and they are the average values of all determined spectra, as shown in Figure 4.11.

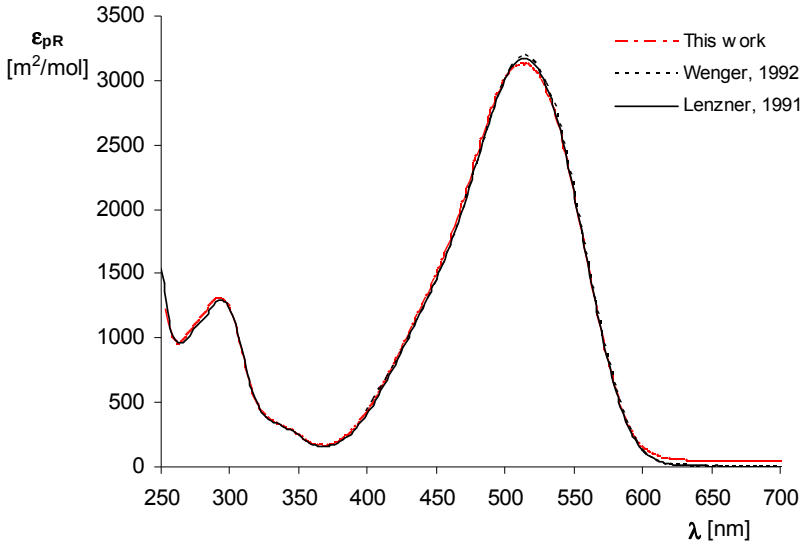

Figure 4.11 *Comparison of spectra obtained in this work and on earlier publications (Lenzner, 1991; Wenger et al., 1992).* $I = 444.4\ \mathrm{mol \cdot m^{-3}}$, $\mathrm{pH} = 9.9$, $\mu = 1\ \mathrm{mPa \cdot s}$ *and* $T = 25^{\circ}\mathrm{C}$.

From Figure 4.11 one can see a good agreement between published spectra and the one obtained in this work. The maximum extinction coefficient of the present work, near of 515 nm (see Table 4.3), is about 1.2 % and 1.8 % lower than the ones obtained by Lenzner and Wenger, respectively. These differences are not considered relevant.

Table 4.3 Comparison between maximum $\varepsilon_{p-\mathrm{R}}$, and respective $\lambda\,[\mathrm{nm}]$, obtained in this work and on earlier publications.

Reference	ε_{p-R} max $[\mathrm{m}^2 \cdot \mathrm{mol}^{-1}]$	$\lambda\,[\mathrm{nm}]$
This work	3133	515
Lenzner (1991)	3171	514
Wenger et al. (1992)	3190	515

In summary, the results obtained by these characterization techniques allow to infer that the purity of the synthesized $p-R$ solid is high. This conclusion is crucial to carry out kinetics studies by using this isomer as a pure reagent (see Equation 4.4).

4.2.3.3 Stability and Toxicity

Bourne and co-workers (1990) detected a partial decomposition of neutral solution of $p-R$ after 2-3 months, but they also observed that it kept unchanged for many months in a drying oven (45°C, 100 mbar) and in brown glass bottles.

In this work, it was verified that the $p-R$ powder stored in a brown glass bottle at room temperature and on the exsicator maintain its UV/vis spectrum after two years. In a buffered solution ($0.2\ \mathrm{mol} \cdot \mathrm{m}^{-3}$) stored with light exclusion and at $4°\mathrm{C}$, it showed after three days a small decrease of absorbance at $\lambda_{\max}$ (around 7%) indicating a slight degree of decomposition. Thus, for the kinetics studies the solutions of this compound were prepared daily.

Although this compound is commercialized, there is no information about its hazards for the human health.

4.2.4 2-[(4-Sulfophenyl)azo]-1-naphthol (*o-R*)

Similarly to the *para* isomer, the *ortho* isomer ($o-R$) was synthesized, purified and its purity assessed by several analytical techniques such as atomic absorption spectroscopy, elemental analysis, ^{1}HNMR and UV-vis spectrophotometry.

4.2.4.1 Synthesis and Purification

$o-R$ was prepared from β-naphthoquinone using the method of Bourne and co-workers (1990), where 0.025 mol (3.954 g) of this reagent (ACROS 17123) was dissolved in 50 mL of glacial acetic acid (Sigma-Aldrich A9967) which acts as catalyst, at room temperature and then poured into a suspension of 0.025 mol (4.801 g) of phenylhydrazine-*p*-sulfonic acid (ACROS 41178) in 50 mL of water. The *ortho* isomer is formed accordingly to the reaction scheme shown in Figure 4.12.

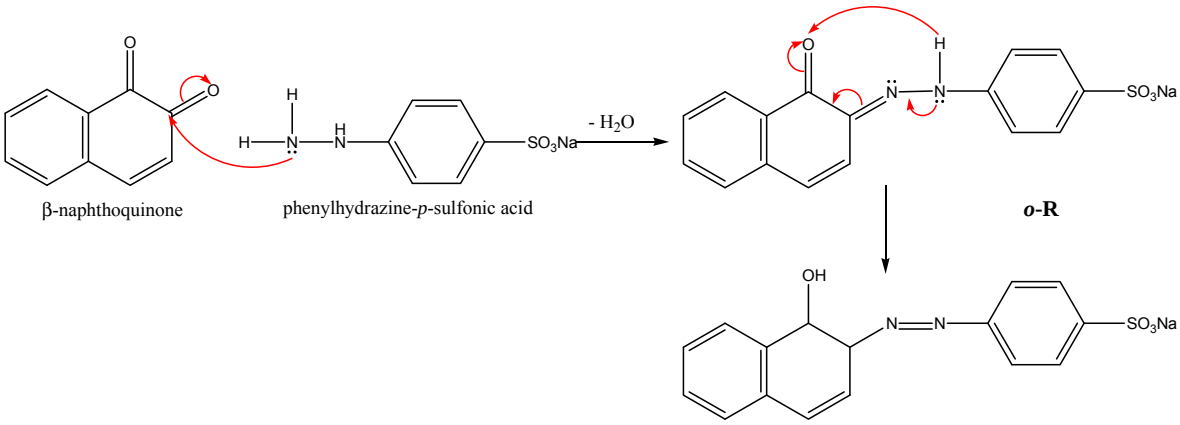

Figure 4.12 Reaction synthesis of $o-R$.

After stirring for 24 hours, the partially precipitated dye was dissolved in a small quantity of water and separated from the unconverted reagents by filtration. The dye was precipitated by adding $(2-3\,\text{g})$ of sodium chloride and filtered, in order to remove the water soluble impurities. The precipitate was then submitted to a purification process by recrystallization and hot filtration to remove the insoluble impurities.

In few words, these purification steps are resumed to:

1. The impure $o-R$ crystals were dissolved in the minimum amount of the selected hot solvent;
2. Then, this saturated solution was filtered to remove the insoluble impurities, retained on the filter;
3. The filtered solution was slowly cooled first to room temperature and then in an ice bath. As the solution is cooled the solubility of compounds in solution decreases and the desired $o-R$ is recrystalized from solution without the soluble impurities;
4. The "pure" $o-R$ is finally recovered by filtration and dried.

The first three steps were repeated five times with water as solvent and finally once with water:ethanol solution (1:1 v/v). Between each purification cycle, the presence of impurities was checked by TLC, using eluent ethanol:chloroform 1:1 v/v as eluent. At the last cycle, the TLC still showed two oranges spots, one corresponds to the desired $o-R$ and the other, very tenuous, relating to an impurity. Moreover, after making the double of purification cycles performed by Bourne and co-workers (1990) and once the spot of impurity was tenuous it was considered that the product was almost pure, it was submitted for identification.

4.2.4.2 Identification of $o-R$

Humidity and ashes contents

The percentage of humidity founded in the $o-R$ sample was 0.6%, which means that the crystals of this isomer are dehydrated. The high content of ashes determined (19.0%) could be justified by the presence of sodium in the $o-R$ chemical structure. One hypothesis for this content of ashes is that the *ortho*-isomer is in the form of monosodium salt with the chemical formula: $HOC_{10}H_6N{=}NC_6H_4SO_3Na$ and the sodium remains in the ashes as Na_2SO_4. In this way, the theoretical content of ashes is 20.3% and the difference to the experimental value is only 1.3%.

Atomic absorption spectroscopy

By atomic absorption spectroscopy a sodium content of 5.71% it was detected, when 6.57% is the predicted theoretical value by using the formula presented above. This result consolidates the hypothesis raised previously. Thus, and similarly to the results obtained by other authors (Bourne et al., 1990; Wenger et al., 1992), the $o-R$ crystals synthesized in this work are in the form of monosodium salt, having a theoretical molecular weight of $350.33\ g\cdot mol^{-1}$.

Elemental analysis

The CHNS elemental analysis to the $o-R$ crystals was made by the same laboratory and procedure described before for the other monoazo isomer. The average results and respective standard deviations are presented in the Table 4.4, where it can also be seen the values published by Wenger and co-workers (1992) and the theoretical values predicted by using the monosodium chemical formula referred above.

Table 4.4 Elemental analysis of $o-R$ (sodium salt).

Reference	% C	% H	% N	% S
This work	54.46 ± 0.25	2.93 ± 0.12	7.83 ± 0.08	7.76 ± 0.06
Wenger et al. (1992)	54.84	3.14	8.00	---
Theoretical	54.86	3.16	8.00	9.15

Such as in the $p-R$ elemental analysis, the contents of carbon, hydrogen and nitrogen do not differ more that 0.4% from the theoretical. However, for sulphur the difference is slightly larger, namely 1.39%.

Nuclear magnetic resonance

Figure 4.13 represents the ^{1}HNMR spectrum of $o-R$, which was determined by the same way of the ^{1}HNMR spectrum of $p-R$.

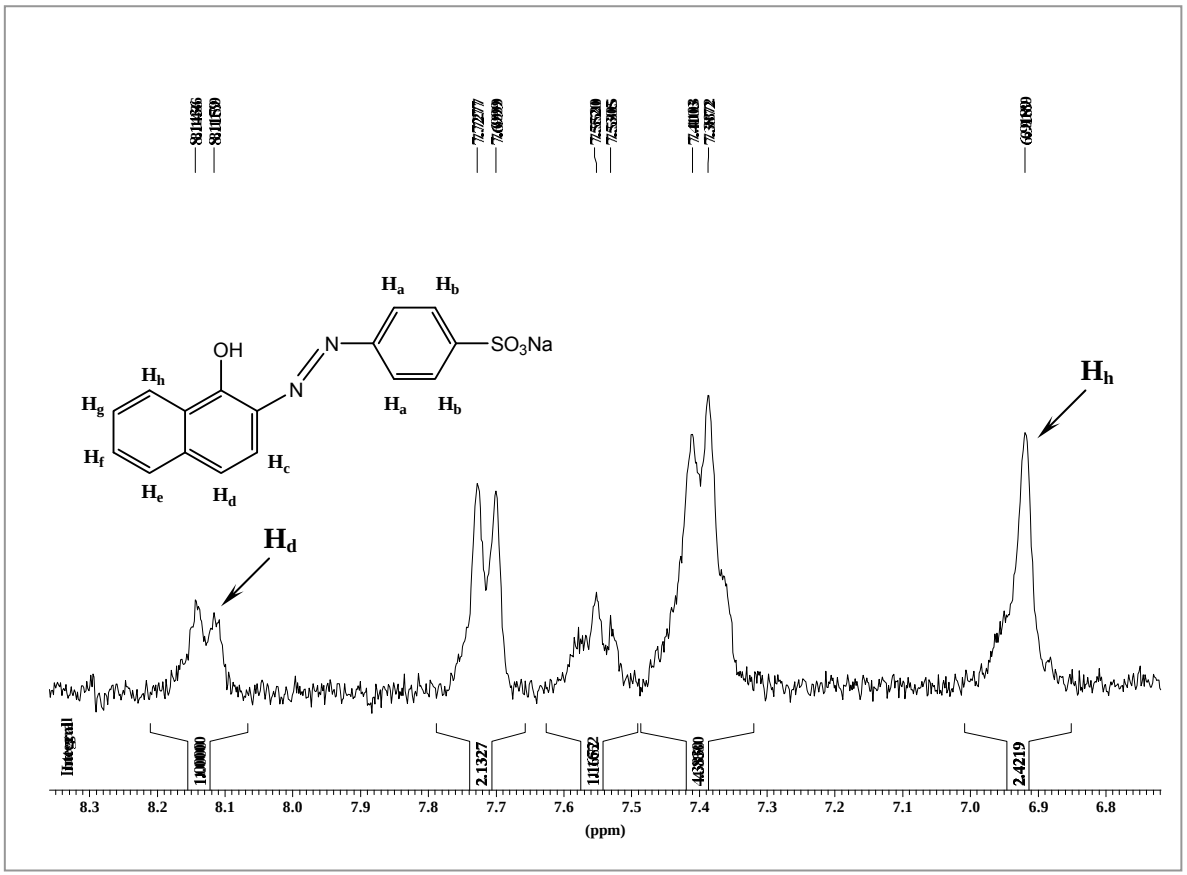

Figure 4.13 ^{1}HNMR spectrum of $o-R$.

The various hydrogen atoms of the $o-R$ molecule were identified by their protection level as shown in Figure 4.13, but in the ^{1}HNMR spectrum it is not possible to identify all hydrogen atoms, except the more protected, H_d, and unprotected, H_h, which appear at $8.1\,\text{ppm}$ and $6.9\,\text{ppm}$, respectively.

This NMR spectrum could compromise the conclusions about the purity level of compound in analysis but, taking into account the results presented before, this result could be atrributed to an external interference on this spectrum, such as the presence of non-deuterium water, e.g. the crystals used for this analysis could be hydrated.

Spectrophotometry

The molar extinction coefficients of $o-R$, ε_{o-R}, were determined for the same physico-chemical conditions of the spectrum of $p-R$ shown above, i.e. at $I = 444.4\,\text{mol}\cdot\text{m}^{-3}$, $\text{pH} = 9.9$, $\mu = 1\,\text{mPa}\cdot\text{s}$ and $T = 25^\circ\text{C}$. The results depicted on Figure 4.14 are the average of spectra solutions with different concentrations ($0.05 - 0.1\ \text{mol}\cdot\text{m}^{-3}$).

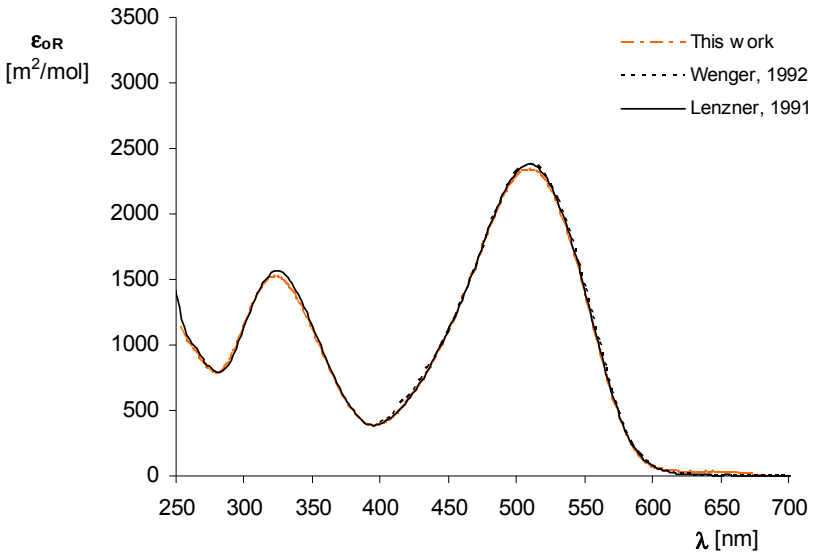

Figure 4.14 *Comparison between ε_{o-R} obtained in this work with that obtained on earlier publications (Lenzner, 1991; Wenger et al., 1992). $I = 444.4\,\text{mol}\cdot\text{m}^{-3}$, $\text{pH} = 9.9$, $\mu = 1\,\text{mPa}\cdot\text{s}$ and $T = 25^\circ\text{C}$.*

The spectrum obtained in this work is similar to those previously published (Lenzner, 1991; Wenger et al., 1992), which is an indication that the synthesized compound is pure. The maximum absorbance is registered at 510 nm where the value of ε_{o-R} is $2338\,\mathrm{m}^2 \cdot \mathrm{mol}^{-1}$ in this work, $2382\,\mathrm{m}^2 \cdot \mathrm{mol}^{-1}$ in the spectrum obtained by Lenzer (1991) and $2380\,\mathrm{m}^2 \cdot \mathrm{mol}^{-1}$ by Wenger et al. (1992). The deviation between Lenzner result and that obtained in this work is about 1.8%.

In conclusion, all used techniques to identify the $o-R$, except the NMR, allow the conclusion that this isomer is isolated in monosodium salt form, with a good level of purity. Thus, the kinetic studies were performed with the solid obtained as described above.

4.2.4.3 Stability and Toxicity

Like other isomer, the crystals of $o-R$ were stored in a brown glass bottle, at room temperature and on the exsicator. After two years the UV/vis spectrum of this compound did not change. Moreover, in neutral solution and after several days, this dye presented the same spectrum. Bourne and co-workers (1990) obtained similar results. Nevertheless, all necessary solutions for the kinetic studies were freshly prepared.

No references to this chemical about human health hazard were found in the bibliography.

4.2.5 2,4-Bis[(4-sulfophenyl)azo]-1-naphthol (*S*)

The dye S, also called bisazo dye, is a product of both reactions 4.3 and 4.4. The knowledge of its UV/vis spectrum is necessary for accurate quantification of its concentration in micromixing or kinetic studies where it is involved.

Published reference spectra for this dye have shown substantial variations among researchers, both in shape and magnitude, as it is illustrated in Figure 4.15. These differences are usually related with problems in its isolation, purification and quantification.

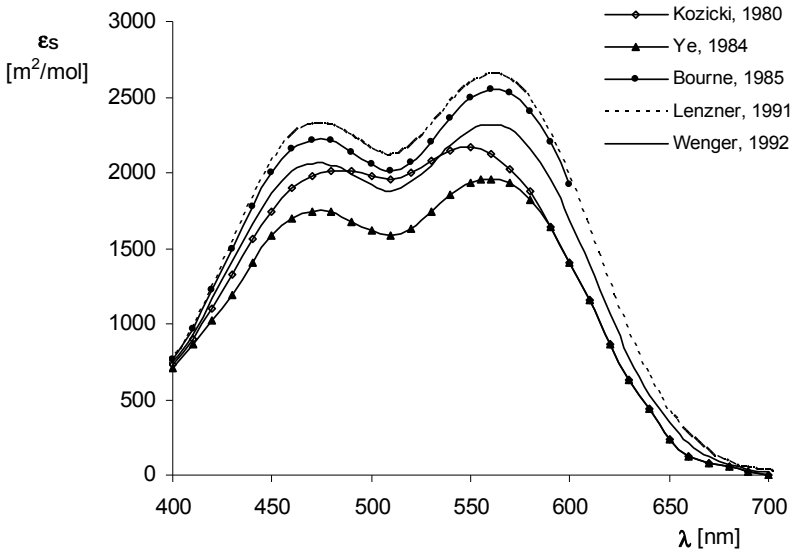

Figure 4.15 Previously reported visible spectra for bisazo dye S (Wenger et al., 1992).

These spectra were obtained with different methods as described by Wenger et al. (1992):

- Kozicki (1981) – The dye was synthesized by coupling equimolar quantities of diazotized sulfanilic acid, *B*, and *p-R*. A solid product was precipitated, dried and weighed without any purification step.
- Ye (1984) – The bisazo dye was prepared following the same procedure of Kozicki, but purification steps were introduced, by washing the dried solid with 1:1 v/v ethanol/water solution 12 times until paper chromatography showed only one spot.
- Bourne *et al.* (1985) – The dye was prepared in the same way referred above, and the crude product was separated by thin-layer chromatography. A small quantity of S was recovered from the plate and quantified by titration with titanium (III) chloride.
- Bourne *et al*. (1990) or Lenzner (1991) – This sample was obtained by coupling one mole of $o-R$ with less than one mole of diazotized sulfanilic acid. The spectrum of S was determined directly from the aqueous solution, by assuming 100 % yield and subtracting out the spectrum of the residual $o-R$.
- Wenger *et al*. (1992) – The same procedure as Kozicki was used. It was unsuccefully tried the purification step by washing the solid with 95% ethanol 12 times, after which the paper chromatography still indicated impurities. Nevertheless, they considered that the solid was reasonably pure and used it for the spectrum determination.

Most of the published spectra of S have basically the same saddle shape, but differ in magnitude. The inexistence of similar spectra in the literature led to the independent determination of the spectrum for the bisazo dye in this work. For this purpose, S was synthesized by using both coupling reactions, $p-R+B$ and $o-R+B$ as described below.

4.2.5.1 Synthesis of S from Reaction $p-R+B$

Excluding Bourne et al. (1990), all published spectra were determined by coupling *p-R* and diazotized sulfanilic acid, B. Problems inherent to this method were reported (Bourne et al., 1985; Bourne et al., 1990; Wenger et al., 1992), such as the instability of *S* in presence of diazonium ions, which leads to a loss of this dye to form unstable products (diazo ether, radicals, etc.) and the persistence of an impurity after many solid purification (wash/recrystalization) steps.

The strategy used in the present work was:

- Purified $p-R$ ($0.4\ \mathrm{mol\cdot m^{-3}}$) and B were injected in the stopped-flow apparatus under standard conditions ($I = 444.4\ \mathrm{mol\cdot m^{-3}}$, $\mathrm{pH} = 9.9$ by using a $Na_2CO_3/NaHCO_3$ buffer). Several sets of experiments were carried out by varying the stoichiometric ratio of $p-R$ to B ($1 < c_{p-R0}/c_{B0} \leq 1.75$), always using $p-R$ in excess;

- After some seconds, the absorbance of the final solution was measured over visible range wavelengths;

- A conversion of 100% was assumed and the excess of $p-R$ was subtracted from the absorbance spectrum;

- The exctintion coefficients of S were calculated.

The purpose of using an excess of $p-R$ was to minimize the occurrence of side reactions between B and S. If both $p-R$ and S compete for B and the monoazo isomer is in excess, that competition will be favourable to $p-R$, avoiding by this way the degradation of S.

The results are presented in Figure 4.16 and can be compared with earlier published spectra.

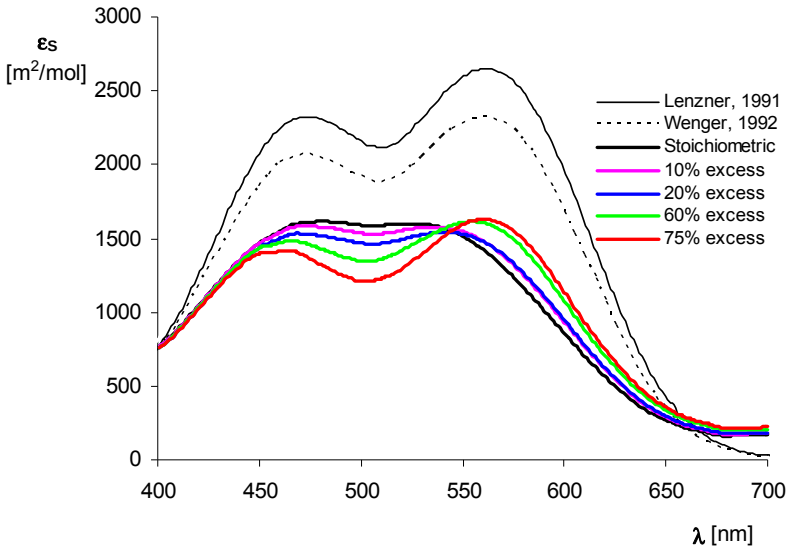

Figure 4.16 *Comparison between bisazo dye spectra obtained in this work, by coupling reaction* $p-R+B \rightarrow S$*, using different stoichiometric ratio of* $p-R$ *to* B *(shown as percentage of* $p-R$ *in excess of that of* B*), and of earlier publications. Experimental conditions:* $I = 444.4\ \text{mol}\cdot\text{m}^{-3}$, $\text{pH} = 9.9$, $\mu = 1\ \text{mPa}\cdot\text{s}$ and $T = 25^{\circ}\text{C}$.

Figure 4.16 shows that for the stoichiometric ratio and for lower excess of $p-R$, the spectra did not exhibit a saddle shape. This is due to the presence of impurities deriving from side reactions and/or an yield lower than 100%, and thus the quantity of $p-R$ subtracted from the spectrum was lower than the existing in solution. Since $p-R$ has an absorbance maximum near $510\,\text{nm}$, where S has an absorbance minimum, the curve tends to flatten the saddle shape if $p-R$ is also present in solution.

As the excess of $p-R$ increases, the curves become bimodal, which means that the loss of S by side reactions decreases. However, the degradation of S never disappeared as shown by the difference between the published and all experimental curves of the current work. After this unsuccessful attempt for the determination of the S spectrum directly from aqueous solution, the compound was isolated using thin-layer chromatography. First, S was synthesized by coupling equimolar quantities of buffered $p-R$ and B. Then, the solution was submitted to an evaporation process to concentrate the desired compound. Finally, S was isolated by using a silica chromatographic plate with an eluent consisting of ethyl acetate and methanol in proportions 2:1 (v/v). A good separation between the purple (S) and the orange (impurity) spots was observed. Problems arise on the extraction of bisazo dye from the silica. Several solvents were used without success, such as ethyl acetate, ethyl ether,

dichloromethane, chloroform and acetone. The extraction capability of ethanol was weak and good results were obtained both with water or methanol, although these latest solvents should not be used because they also dissolve the silica present in the TLC plate. However, this experiment proceeded only for a qualitative determination of the S spectrum, with the aim to evaluate the shape of this curve. Thus, recovered solid was dried and weight 0.0236 g to dissolve in a $5\,\text{mL}$ of buffered aqueous solution ($I = 444.4\,\text{mol}\cdot\text{m}^{-3}$). The absorbance spectrum of this solution was determined and it is shown in Figure 4.17. Despite the saddle shape, the curve has a second peak lower than the first, contradicting the expectations. There is no apparent reason for this fact except some interference occurred by the presence of the silica.

Since the curve shape was different from the one expected, the quantification step of S was not carried out.

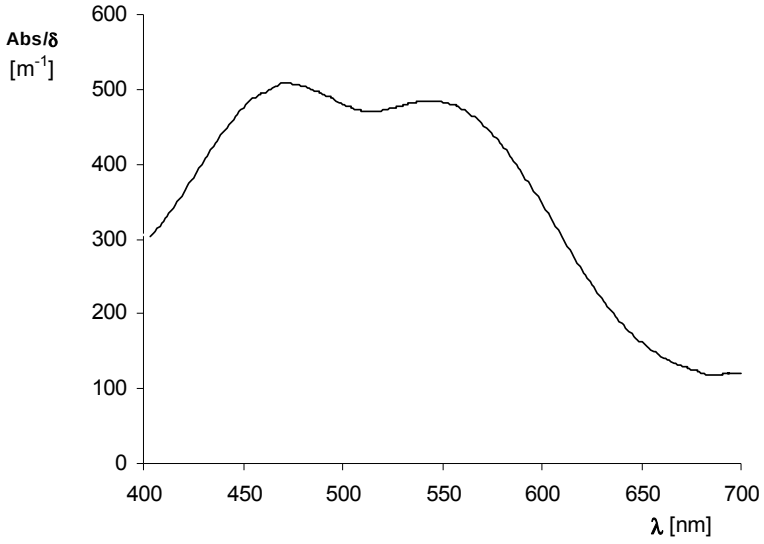

Figure 4.17 Absorbance spectrum of S isolated by thin-layer chromatography.
$I = 444.4\,\text{mol}\cdot\text{m}^{-3}$, $\text{pH} = 9.9$, $\mu = 1\,\text{mPa}\cdot\text{s}$ and $T = 25^{\circ}\text{C}$.

No more attempts were made to isolate *S* in a crystalline form by TLC because the quantities obtained by this method are very small.

4.2.5.2 Synthesis of S from Reaction $o-R+B$

The spectrum of S was directly obtained using the solution resulting from the coupling reaction of $o-R$ and B, without isolation or purification steps. The experimental procedure was similar of the described in the preceding section, i.e., on the stopped-flow several sets of experiments with different stoichiometric ratios ($1 \le c_{o-R0}/c_{B0} \le 1.5$; $c_{o-R0} = 0.2\ \text{mol}\cdot\text{m}^{-3}$) were carried out. It was also assumed a yield of 100%, and the excess of $o-R$ was subtracted from the recorded absorbance spectrum. Figure 4.18 shows some of the obtained results, where it can be seen a good agreement with those published by (Lenzner, 1991). The calculated extinction coefficients attributed to S differed only by a few parts per thousand.

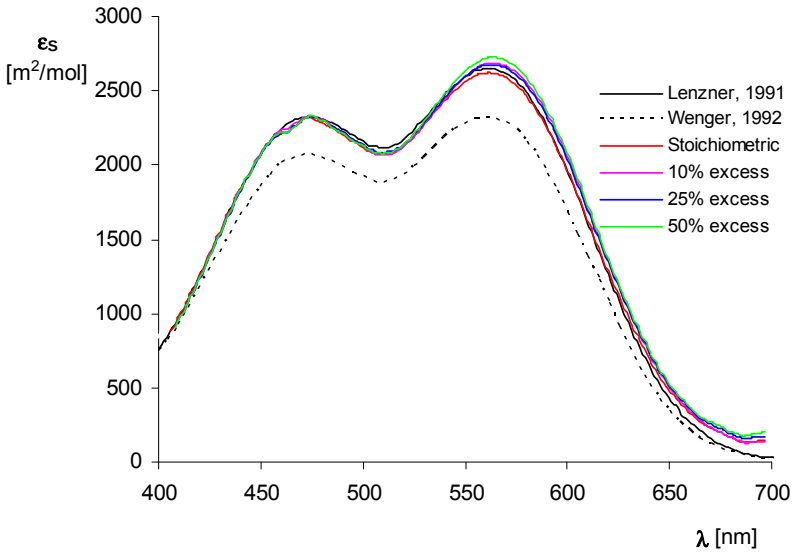

Figure 4.18 Comparison between bisazo dye spectra obtained in this work, by coupling reaction $o-R+B \rightarrow S$, using different stoichiometric ratio of $o-R$ to B (shown as percentage of $o-R$ in excess of that of B), and of earlier publications. $I = 444.4\ \text{mol}\cdot\text{m}^{-3}$, $\text{pH} = 9.9$, $\mu = 1\ \text{mPa}\cdot\text{s}$ and $T = 25^{\circ}\text{C}$.

Other experiments were carried out by varying the initial reagent concentrations ($0.01-0.1\ \text{mol}\cdot\text{m}^{-3}$) in equimolar proportion. The obtained spectra were coincident in the majority of the cases founded in literature. The average experimental spectrum is presented in Figure 4.19 and will be used during this work.

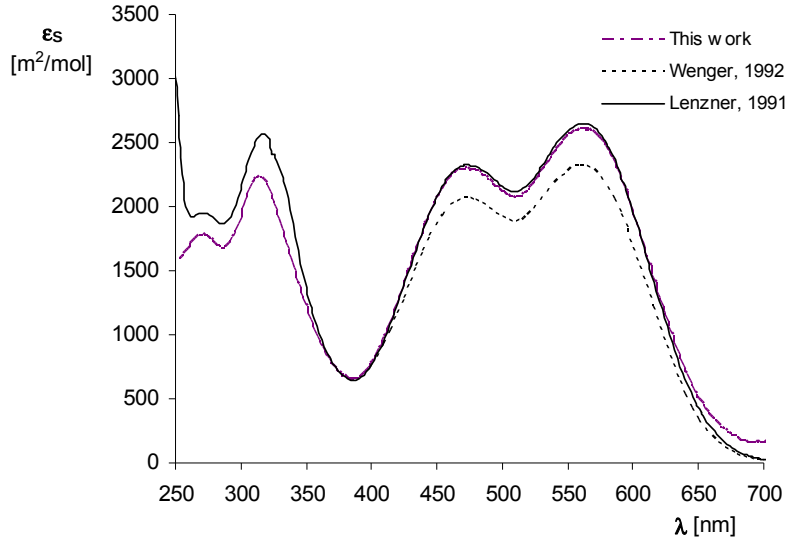

Figure 4.19 Comparison between bisazo dye S UV/vis spectrum obtained in this work and in earlier publications. $I = 444.4\ \text{mol}\cdot\text{m}^{-3}$, $\text{pH} = 9.9$, $\mu = 1\ \text{mPa}\cdot\text{s}$ and $T = 25^{\circ}\text{C}$.

In the visible light region, there are two peaks and one minimum on the *S* spectrum. The wavelengths at which they are observed are listed in Table 4.5. The differences among this work and the other authors are not significant.

Table 4.5 Maxima and minimum wavelength of S spectra

Reference	$\lambda_{1^{st}\,\text{peak}}$	λ_{min}	$\lambda_{2^{nd}\,\text{peak}}$
This work	473	511	559
Wenger *et al.*, 1992	474	508	562
Lenzner, 1991	475	510	560

Wenger and co-workers (1992) suggested one way to compare the shape of the spectra, by defining an index of purity

$$I_p = \frac{\varepsilon_{S\,\text{max}}}{\varepsilon_{S\,\text{min}}} \tag{4.11}$$

where $\varepsilon_{S\,\text{max}}$ and $\varepsilon_{S\,\text{min}}$ are respectively the maximum and minimum extinction coefficients of S.

Table 4.6 shows the values of the index of purity of S using the spectra wavelengths listed in Table 4.5.

Table 4.6 Index of purity of S.

Reference	$\varepsilon_{S\,1^{st}\,peak}/\varepsilon_{S\,min}$	$\varepsilon_{S\,2^{nd}\,peak}/\varepsilon_{S\,min}$	$\varepsilon_{S\,470nm}/\varepsilon_{S\,510nm}$	$\varepsilon_{S\,560nm}/\varepsilon_{S\,510nm}$
This work	1.11	1.26	1.10	1.23
Wenger et al. (1992)	1.10	1.23	1.10	1.23
Lenzner, 1991	1.10	1.25	1.10	1.25

In spite of the difference in magnitude of the Wenger et al. (1992) curve (see Figure 4.19), the indexes of purity are similar to the other curves.

From Figure 4.19 it was already observed the similarity in magnitude between the curve obtained in this work and that published by Lenzer (1991). The indexes of purity are a quantitative confirmation of this fact.

4.2.5.3 Stability and Toxicity

Comparatively to the monoazo dyes, the bisazo dye solutions have much lower stability, and so all measurements should be done as soon as possible. In this work a quantitative study of its instability was not done. However, Bourne and co-workers (1990) referred that solutions having concentrations near $3\ \mathrm{mol\cdot m^{-3}}$ were stable for 1-2 hours, whereas in more diluted solutions for the spectrophotometric analysis (near $0.035\ \mathrm{mol\cdot m^{-3}}$) their stability can reach 4-5 hours.

As in Bourne and co-workers (1985), in this work it was registered the degradation of bisazo dye S by excess of diazotized sulfanilic acid, B (diazonium ions), which is observable by the change of colour solution from violet to yellow. In order to check this instability a further set of experiments in the stopped-flow were done by coupling $o-R$ and diazotized sulfanilic acid. The initial concentrations of $o-R$ were constant ($0.05\ \mathrm{molm^{-3}}$) and the concentration of diazotized sulfanilic acid was increased from 0.1 to $1.0\ \mathrm{molm^{-3}}$, so that a 2 to 20-fold excess of B was created.

Figure 4.20 shows the results of these experiments. It is possible to see that in neither experiment the yield of $o-R$ to S exceeds 85%. Initially the concentration of the bisazo dye increases due to the slow decomposition caused by the side reaction with excess diazonium ion occurs. This decomposition becomes faster and more significant for greater stoichiometric ratio $r = c_{B0}/c_{o-R0}$.

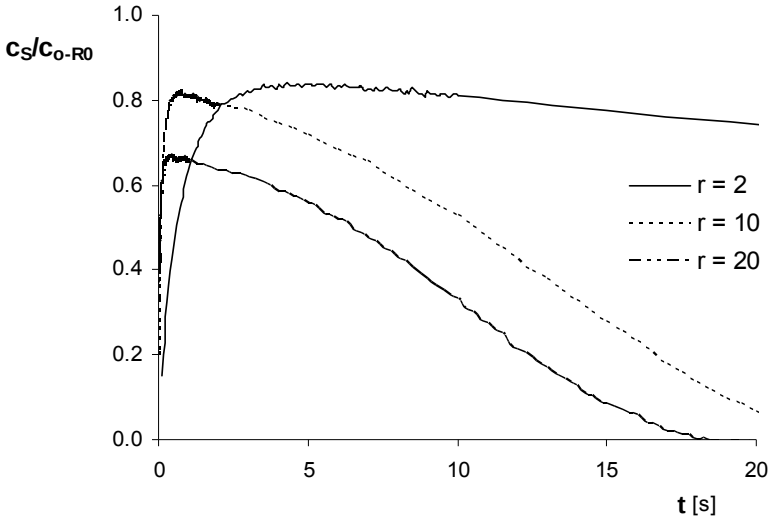

Figure 4.20 Degradation of S in presence of excess of diazotized sulfanilic acid. $I = 444.4\ \text{mol}\cdot\text{m}^{-3}$, $\text{pH} = 9.9$, $\mu = 1\ \text{mPa}\cdot\text{s}$ and $T = 25^{\circ}\text{C}$.

No references about human health hazard were found to this chemical in consulted bibliography.

4.2.6 1-[(4-Sulfophenyl)azo]-2-naphthol (*Q*)

4.2.6.1 Synthesis and Purification of Q

Q is a chemical compound known as Orange II (CI-colour index- Acid Orange 7; CI 15510), but due to the low purity of the commercial samples, in this work it was synthesized as the product resulting from the azo coupling reaction between 2-naphthol, A_2, and diazotized sulfanilic acid, B (see Equation 4.5). Since Q is not simultaneously a reagent and a product (as is the case of monoazo dyes), its synthesis was done just for the determination of its UV/vis spectrum. The experimental procedure was used (Vogel, 1964; Bourne et al., 1992a):

1. 1.4420 g (0.01 mol) of 2-naphthol were dissolved in 15 mL of ethanol and cooled to about 3°C;

2. A suspension of diazotized sulfanilic acid (1.7300 g, 0.01 mol) was added dropwise to the previous solution and stirred. The temperature should not be allowed to rise above 5°C (Kirk-Othmer, 1982). The precipitation of the orange dye was observed;

3. The final solution was slowly stirred at the room temperature for about 3 hours;

4. The remaining solution was warmed to $50-60^{\circ}C$ during 1 hour and the precipitate was redissolved;

5. Approximately 3 g of sodium chloride (which decreases the solubility of the dye) were added to the solution to induce the precipitation;

6. The solution was allowed to cool spontaneously at room temperature for 1 hour and then cooled in ice until crystallization is complete;

7. The precipitate was filtered and washed once with a small amount of 50% acetone solution and then three times with 50% aqueous ethanol solution.

After the precipitate was dried, the first purity test was done by TLC with ethyl acetate:chloroform:methanol (1:1:1 v/v) as eluent, and only one spot was observed.

The identification of the crystals of *Q* was carried out by elemental analysis and spectrophotometry. Humidity and ashes contents were also determined.

4.2.6.2 Identification of Q

Humidity and ashes contents

The percentage of humidity of *Q* crystals obtained was 4.4%, which reveals that this compound is hydrated. Considering that each molecule of *Q* is hydrated with one molecule of water, its chemical formula is $HOC_{10}H_6N{=}NC_6H_4SO_3Na.H_2O$ corresponding to a molecular weight of $368.34\ g\cdot mol^{-1}$. In this molecule, the theoretical humidity content is 4.9%, differing just by 0.48% from the experimental value obtained.

A content of ashes of 17.3% was obtained, in a good agreement with the results obtained by Bourne et al. (1992).This value is an indicative of the presence of sodium, and assuming that *Q* is in the form of a monosodium salt monohydrated and that sodium is present in the form of Na_2SO_4, the predicted theoretical value for the ashes content is 19.3% which is in resonable agreement with the experimental value.

Elemental analysis

Similarly to the monoazo dyes, three samples of Q dye were submitted to CHNS elementary analysis and the average values and standard deviation are shown in Table 4.7, as well as the respective theoretical predictions considering two alternatives for the hydratation state of the Q molecule.

Table 4.7 Elemental analysis of Q (sodium salt). (1) dehydrated; (2) monohydrated.

	% C	% H	% N	% S
This work	51.82 ± 0.16	2.93 ± 0.09	7.39 ± 0.02	5.11 ± 0.04
Theoretical(1)	54.86	3.16	8.00	9.15
Theoretical(2)	52.17	3.56	7.61	8.70

If the Q molecule is considered to be dehydrated, the difference between the experimental and the theoretical values exceeds 0.4% (maximum recommend difference) for all C, N and S atoms. Considering Q to be a monohydrated molecule, these differences decrease to 0.4% for the C and N atoms, but for the H and S atoms these difference are 0.63% and 3.60%, respectively.

The discrepancy between the theoretical and experimental values for the sulphur atom was previously observed in the monoazo dyes analysis, and despite the relative large difference observed for the hydrogen atom, it can be assumed that these synthesized crystals of Q are monohydrated and with an acceptable degree of purity.

Spectrophotometry

In the determination of the UV/vis spectrum of Q two procedures were adopted. One was to prepare different aqueous solutions with known concentrations ($0.1-0.5\ \mathrm{mol\cdot m^{-3}}$) by dissolving weighed quantities of the solid. These solutions were buffered with $Na_2CO_3/NaHCO_3$ to pH=9.9 and $I = 444.4\ \mathrm{mol\cdot m^{-3}}$. The absorbance values were measured in the spectrophotometer of the stopped-flow apparatus and the extinction coefficients were calculated using Equation 4.6. The pink curve shown in Figure 4.21 represents the average of all experimental curves.

The other procedure consisted on the azo coupling reaction between 2-naphthol, A_2, and diazotized sulfanilic acid, B. In the stopped-flow apparatus, solutions of A_2 (buffered) and of B with different concentrations ($0.025 - 0.1\,\text{mol}\cdot\text{m}^{-3}$) were injected, always in the stoichiometric ratio of $1:1$. After a few seconds, it was assumed a yield of 100% and the absorbance values were measured over the UV/vis wavelength range. The cyan curve in Figure 4.21 represents the average extinction coefficients obtained from the experimental absorbance curves.

In order to test the validity of the assumption of 100% of yield, another set of experiments were performed by using different stoichiometric ratios c_{A20}/c_{B0}, namely from 1.5 to 15. The excess of A_2 should prevent any eventual side reaction between Q and B. To obtain the Q extinction coefficients curves from the experimental absorbance curves of these solutions, it was necessary to subtract the contribution of the excess of A_2, specifically on the UV region (see Figure 4.4). The obtained results were very similar to the cyan curve of the Figure 4.21, which means that the assumption is correct.

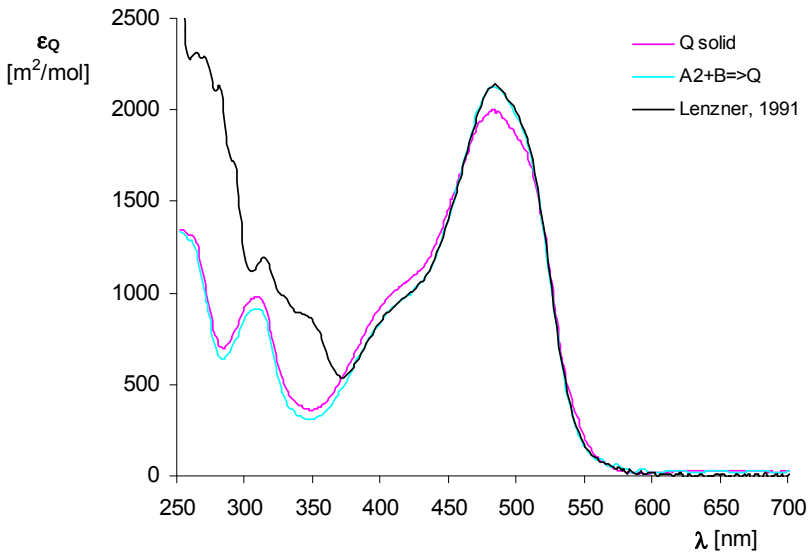

Figure 4.21 Comparison between the UV/vis spectrum of Q, obtained in this work and by Lenzner (1991). $I = 444.4\,\text{mol}\cdot\text{m}^{-3}$, $\text{pH} = 9.9$, $\mu = 1\,\text{mPa}\cdot\text{s}$ and $T = 25^{\circ}\text{C}$.

The two experimental curves obtained in this work have similar shapes but in the maximum region they differ by about 6%, which can be attributed to the purity level of the synthesized solid mentioned in the elemental analysis.

Figure 4.21 also shows the spectrum of Q obtained by Lenzner (1991), where Q was synthesized and purified using a similar procedure. In the visible region, the curve obtained directly from the reaction $A_2 + B$ is coincident with the Lenzner curve, having a maximum at $480\ \text{nm}$. However, they diverge both in shape and in magnitude within the UV region. For all kinetic and micromixing studies in this work, the Q spectrum was assumed to be represented by the cyan curve.

4.2.6.3 Stability and Toxicity

In crystal form, Q can be stored in a hermetic dark flask under the exclusion of light for up at least six years without loosing its properties.

The stability of buffered solutions of Q (prepared by the two ways described before), stored at 4ºC under the exclusion of the light, was evaluated for over two months and no change was registered.

Q is stable in the presence of an excess of diazotized sulfanilic acid. This is an important point for micromixing studies, so there are restrictions on the range of concentrations to be used and on the time for quantification of this dye in a mixture.

The dye Q is classified as nongenotoxic, and a carcinogenic effect has not been indicated. More information is listed in Appendix A.

4.3 Kinetic Study in Aqueous non-Viscous Medium

For test reaction system, knowledge of the reaction kinetics is crucial for its implementation in the micromixing studies. Naturally kinetic data should be obtained in the same physico-chemical conditions (pH, ionic strength, temperature, solvent, viscosity) as its future applications.

The test reaction system that constitutes the reactions between 1- and 2-naphthol and diazotized sulfanilic acid has been studied by Bourne and co-workers and largely used by this and other research teams. Although this reaction system has been used on micromixing characterization for both viscous (Bourne et al., 1989) and non-viscous media (Bourne et al., 1992b), the reported kinetics data (Bourne et al., 1985; Bourne et al., 1990; Bourne et al., 1992a) was only obtained for aqueous non-viscous medium.

One of the objectives of this work is the micromixing characterization on a mixing device (for example, in a RIM machine as described Chapter 5), where the viscosity of the fluids is higher than that for water. Thus, the main objective of this chapter is the determination of the kinetics of the test reaction under different conditions, instead of assuming that they are unchangeable (Bourne et al., 1989; Gholap et al., 1994). Nevertheless, the kinetic study was first conducted in aqueous non-viscous medium in order to compare with published data and to validate the experimental and data treatment procedures here adopted. Afterwards, the kinetics was studied in aqueous viscous medium, after choosing of a suitable additive to increase the viscosity.

Usually, the main parameters determined in a kinetic study are: the reaction's order (global and partial), the kinetics rate constant, k, and the activation energy, E_a. In the present work, the experimental plan and data treatment were carried out based on the assumption that all reactions (from 4.1 to 4.5) were of global second order – first order for each reagent – according to literature information (Bourne et al., 1990; Bourne et al., 1992a). However, it is known that the reactions mechanisms and kinetics are generally more complex. Thus, for each reaction, the rate constant and the activation energy were calculated.

All kinetics experiments were carried out in a stopped-flow apparatus from Applied Photophysics, as described in the Chapter 3. In any experiment, the reagents proportion was equal or greater than the stoichiometric ratio, where the diazotized sulfanilic acid, B, was always the limiting reagent, due to the following reasons:

- In the case of reaction 4.1 or 4.2, using the diazotized sulfanilic acid as the limiting reagent reduces the occurrence of reactions 4.3 or 4.4, which simplifies the treatment of the resulting data;

- In the case of reactions 4.3 and 4.4 it is essential in order to avoid/minimize the occurrence of side reactions (see Section 4.2.5.3.);

- For reaction 4.5 there is no restriction to use an excess of B, since none of the previous problems occur.

The concentration of the reagents should be judiciously chosen so as to acquire the most possible and relevant information for the kinetic study, i.e., the major part of the curve with higher reaction rates should be caught. The upper limit for second-order rate constants that

can be observed by a given method is approximately the reciprocal of the smallest half-time that can be measured on the sensitivity of the spectrophotometer. Thus, for reactions with a very high rate constant under ordinary conditions, one way to follow the kinetics is to work at lower concentrations, keeping in mind that the highest second-order rate constant accessible by a given method depends as much on the sensitivity of the technique to low concentrations of reagent as on the least time-interval that it can resolve (Caldin, 1964).

In other words, when the reactions are fast, some problems may arise to follow their kinetics. The technique used in this work takes actions in order to make the reaction slower: (i) to decrease the reagents concentration, together with two alternative optical pathlengths (2 and 10mm) and (ii) to decrease the temperature.

Absorbances of the reaction products at the respective λ_{max} were recorded as function of time. The time range for data acquisition varied from $10\ ms$, for the fastest reactions (reactions 4.1 and 4.2), up to $50\ s$ for the slowest reactions (reactions 4.3 and 4.4). The number of points per series was always 400, thus the resolution time varied from $0.025\ ms$ to $125\ ms$.

Two different cases of experiments and respective data treatment were developed in order to account for the different types of reagents and/or products in each reaction. Case 1 pertains to reactions 4.1, 4.2 and 4.5 that have colourless reagents and dye products, while Case 2 refers to reactions 4.3 and 4.4 where one of the reagents and the product are coloured.

For Case 1, a series of experiments was run with reagent concentration ratio between 1 and 20. Since the reaction products are dyes, the kinetic was followed by absorbance measurements at their maximum wavelength. An example of data series is shown in Figure 4.22a. In the stopped-flow equipment for each experiment, the data acquisition was done during different time intervals with the purpose to get the most detailed information.

From the series acquired at lower time intervals, more detailed information is obtained on the reaction kinetics where the reaction rates are higher. On the other hand, using higher time intervals during the acquisition, the most important is the value acquired for Abs_{∞}, when the reaction is finished, or almost finished. This value is useful, for example, to test the mass balance of the reaction system.

Before the data treatment, some values of each data series or even a complete data series are discarded according to given criteria, namely:

- All absorbance values acquired during the first $3\ \text{ms}$ are neglected, because they refer to a transient period of the continuous stopped-flow stage (for more details see Chapter 3);
- When the registered maximum absorbance value is lower than 0.1 that series is rejected due to sensitivity problems of the spectrophotometer;
- The mass balance should always be checked by comparing the initial concentration of limiting reagent, B, with the final concentrations of the products. Whenever this balance does not close within a minimum error of 3%, the series is discarded;
- Finally, the application of the SX.18MV stopped-flow spectrometer, having an optical cell with $20\ \mu\text{L}$, is for rates inferior than $1500\ \text{s}^{-1}$ and there were chosen series with characteristic reaction time, $t_{reaction} = 1/k\,c_{B0}$, greater than $1\ \text{ms}$.

The next step is the determination of the kinetics rate constant, by fitting the assumed kinetic model to the experimental data. Moreover, by assuming a second-order reaction, the kinetic models were derived for both scenarios: ignoring and not ignoring the concentration profile in the optical cell. The final equations are summarized below.

- Optical cell concentration profile is neglected:

$c_{A0} = c_{B0}\ (r = 1)$

$$\frac{c_R(t)}{c_{B0}} = 1 - \frac{1}{1 + k c_{B0}(t_d + t - t_0)} \tag{4.12}$$

$c_{A0} > c_{B0}\ (r > 1)$

$$\frac{c_R(t)}{c_{B0}} = \frac{1 - \exp\left[-Da\left(1 - \frac{c_{B0}}{c_{A0}}\right) - k\,(c_{A0} - c_{B0})(t - t_0)\right]}{1 - \frac{c_{B0}}{c_{A0}}\exp\left[-Da\left(1 - \frac{c_{B0}}{c_{A0}}\right) - k\,(c_{A0} - c_{B0})(t - t_0)\right]} \tag{4.13}$$

- Optical cell concentration profile is taken into account:

$c_{A0} = c_{B0}\ (r = 1)$

$$\frac{\langle c_R(t)\rangle}{c_{B0}} = 1 - \frac{\alpha+1}{2\beta\, Da}\ln\left[\frac{1+Da(1+\beta/(\alpha+1))+k\,c_{A0}(t-t_0)}{1+Da(1-\beta/(\alpha+1))+k\,c_{A0}(t-t_0)}\right] \tag{4.14}$$

$c_{A0} > c_{B0}\ (r > 1)$

$$\frac{\langle c_R(t)\rangle}{c_{B0}} = 1 + \frac{c_{A0}}{c_{B0}}\frac{\alpha+1}{2\,\beta\, Da}\ln\left[\frac{\left[1-\frac{c_{B0}}{c_{A0}}\exp\left[-Da\left(1-\frac{c_{B0}}{c_{A0}}\right)\left(1+\frac{\beta}{\alpha+1}\right)\right]-k(c_{A0}-c_{B0})(t-t_0)\right]}{\left[1-\frac{c_{B0}}{c_{A0}}\exp\left[-Da\left(1-\frac{c_{B0}}{c_{A0}}\right)\left(1-\frac{\beta}{\alpha+1}\right)\right]\right]-k(c_{A0}-c_{B0})(t-t_0)}\right] \tag{4.15}$$

Here c_{A0} is the initial concentration of 1 or 2-naphthol ($A = A_1 = A_2$), after mixing with diazotized sulfanilic acid with a initial concentration of B, c_{B0}; $c_R(t)$ is the concentration of the reaction product ($o-R$, $p-R$ or Q respectively for reactions 4.1, 4.2 and 4.5) at time t, α and β are geometric parameters defined in Chapter 3, $Da = k\,c_{A0}\,t_d$ is the Damkhöler number, k is the kinetics rate constant and t_d and t_0 are the dead time and the time constant of the stopped-flow apparatus, respectively, as defined in Chapter 3.

The fitting of the models to the experimental values was done using the Excel® Solver tool (see Figure 4.22b), to minimize the deviation function of Equation 4.16 using reasonable initial estimates for values of t_0 and k.

$$D^2 = \sum_r\left[\sum_{t=3\text{ms}}^{t}\left(\frac{Abs_t}{Abs_\infty}-\frac{c_R(t)}{c_{B_0}}\right)^2\right]_r \tag{4.16}$$

Note that t_0 is a parameter that should depend only on the flow-rate, which was the same in all experiments, and thus t_0 should be a constant. However it was verified that the fitting worked better if t_0 was allowed to be an adjustable parameter.

Finally, the experimental curves are compared with those predicted by the kinetic model, using the fitted variables (see Figure 4.22c).

Figure 4.22 shows a summary of the procedure used in Case 1 type reactions with colourless reagents and dye product(s).

Case 1: colourless reagents and dye product(s)

Experimental data series

- Different reagent ratios $r = c_{A0}/c_{B0}$

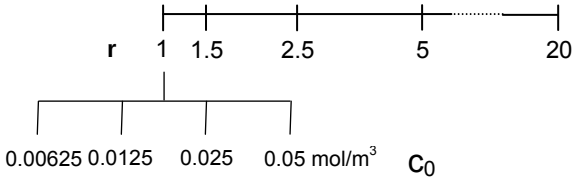

- Absorbance acquisition data at λ_{max} of the reaction product for several acquisition times

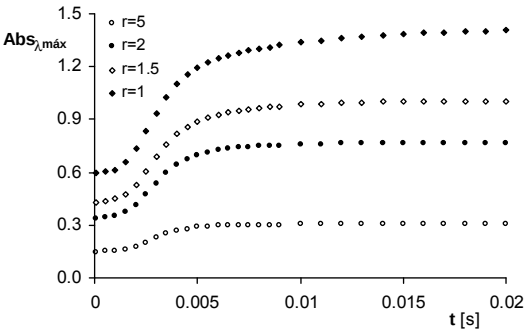

(a)

Discard data criteria:

- Time range $t < 3$ ms
- $Abs_{\infty} < 0.1$
- Mass balance, MB:

$$\left|\frac{c_{B0}\delta\varepsilon_R - Abs_{\infty}}{c_{B0}\delta\varepsilon_R}\right| \times 100 > 3\%$$

- Characteristic reaction time:

$$t_{reaction} = \frac{1}{k\,c_{B0}} < 1\text{ms}$$

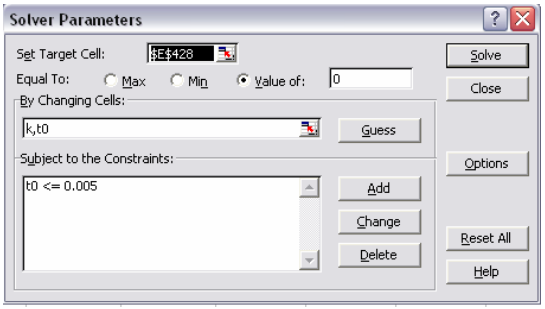

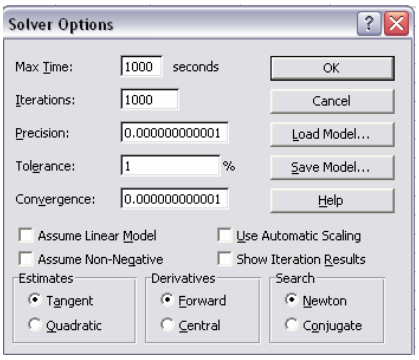

(b)

Data treatment:

- Excel® Solver tool
- Minimize $D^2 = \sum_r \left[\sum_{t=3\text{ms}}^{t} \left(\frac{Abs_t}{Abs_{\infty}} - \frac{c_R(t)}{c_{B_0}} \right)^2 \right]_r$
- Fit variables: t_0 and k

Experimental vs predicted results:

- Graphic comparison between experimental and the predicted curves by assuming the theoretical kinetic model, and using the fit variables determined before.

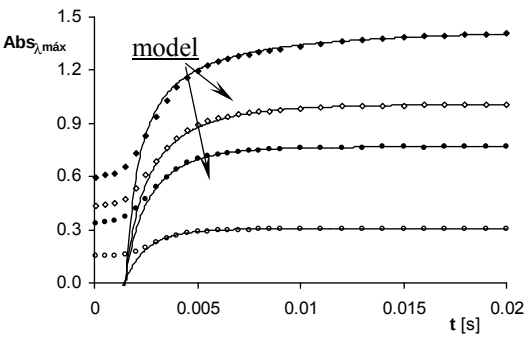

(c)

Figure 4.22 Procedure for the determination of the kinetic model, in reactions with colourless reagents and dye product(s).

Case 2 refers to reactions that have simultaneously one of the reagents and the product coloured. Whereas the kinetics is followed by spectrophotometry, some difficulties could arise if the spectra of both dyes overlap. Reactions 4.3 and 4.4 are the slowest reactions of this micromixing test system and belong to this type of data treatment. The lowest reaction rates bring advantages to this acquisition data technique; some of the limitations verified for fast reactions here are neglected, namely: (i) the loss of some important data due to the dead time of the equipment; (ii) and the concentration profile into the optical cell.

Although the concentration profile into the optical cell could be neglected, the equations were worked out and are presented below. They can be obtained from the general reaction $A+B \rightarrow R$ by replacing of A to R and R to S, respectively:

- Optical cell concentration profile is neglected:

$c_{R0} = c_{B0} \ (r = 1)$

$$\frac{c_S(t)}{c_{B0}} = 1 - \frac{1}{1 + k c_{B0}\left(t_d + t - t_0\right)} \tag{4.17}$$

$c_{R0} > c_{B0} \ (r > 1)$

$$\frac{c_S(t)}{c_{B0}} = \frac{1 - \exp\left[-Da\left(1 - \frac{c_{B0}}{c_{R0}}\right) - k\left(c_{R0} - c_{B0}\right)\left(t - t_0\right)\right]}{1 - \frac{c_{B0}}{c_{R0}}\exp\left[-Da\left(1 - \frac{c_{B0}}{c_{R0}}\right) - k\left(c_{R0} - c_{B0}\right)\left(t - t_0\right)\right]} \tag{4.18}$$

- Optical cell concentration profile is considered:

$c_{R0} = c_{B0} \ (r = 1)$

$$\frac{\langle c_S(t)\rangle}{c_{B0}} = 1 - \frac{\alpha + 1}{2\beta\, Da}\ln\left[\frac{1 + Da\left(1 + \beta/(\alpha+1)\right) + k\, c_{R0}\left(t - t_0\right)}{1 + Da\left(1 - \beta/(\alpha+1)\right) + k\, c_{R0}\left(t - t_0\right)}\right] \tag{4.19}$$

$c_{R0} > c_{B0}\ (r > 1)$

$$\frac{\langle c_S(t)\rangle}{c_{B0}} = 1 + \frac{c_{R0}}{c_{B0}} \frac{\alpha+1}{2\,\beta\,Da} \ln\left[\frac{\left[1 - \frac{c_{B0}}{c_{R0}} \exp\left[-Da\left(1-\frac{c_{B0}}{c_{R0}}\right)\left(1+\frac{\beta}{\alpha+1}\right)\right] - k(c_{R0}-c_{B0})(t-t_0)\right]}{\left[1 - \frac{c_{B0}}{c_{R0}} \exp\left[-Da\left(1-\frac{c_{B0}}{c_{R0}}\right)\left(1-\frac{\beta}{\alpha+1}\right)\right]\right] - k(c_{R0}-c_{B0})(t-t_0)}\right] \quad (4.20)$$

Here c_{R0} is initial the concentration of reagent R (*ortho* or *para* monoazo isomer) after mixing with diazotized sulfanilic acid, B, with concentration c_{B0}; $c_S(t)$ is the bisazo product concentration at time t; the Damkholer number here is defined as $Da = k\,c_{R0}\,t_d$.

In Case 2 the data series were obtained for reagent concentration ratios (*ortho* or *para* isomer/diazotized sulfanilic acid) between 1 and 20. Since the stopped-flow equipment used did not have a photodiode-array detector, an alternative way to attain absorbance measurements against time for different wavelengths was to carry out one run for each wavelength, and assuming that the unique condition (parameter) that changes between each run is the wavelength. Figure 4.23 shows an example of a typical kinetics experiment for reaction $R + B \rightarrow S$, where it is observable the absorbance evolution along time. For the standard physico-chemical conditions, R had a maximum absorbance around 510 nm and it is visible its transformation into the product S, through the appearance of a bimodal curve.

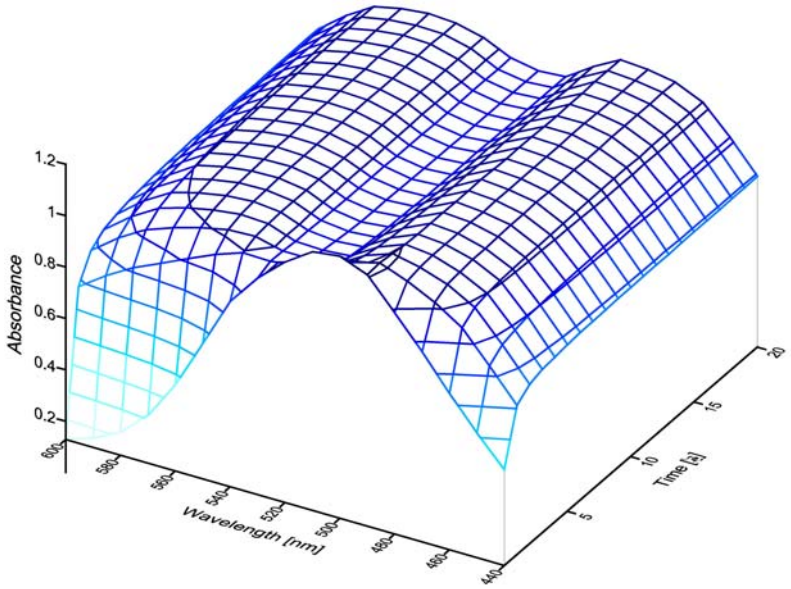

Figure 4.23 *Example of absorbance evolution over wavelength and time during a kinetics experiment of monoazo dye and diazotized sulfanilic acid.* $I = 444.4\ \mathrm{mol \cdot m^{-3}}$, $\mathrm{pH} = 9.9$, $\mu = 1\ \mathrm{mPa \cdot s}$ and $T = 25^{\circ}\mathrm{C}$.

From Figure 4.24a it is clear that most of the UV/vis spectra of $o-R$ or $p-R$ overlap with the S spectrum. However, in the range $550-650$ nm the ratio $\varepsilon_S/\varepsilon_R$ is high, so this wavelength range was chosen for the data acquisition.

The selection of the experimental data acquisition was based on the following assumptions:

- For the reasons presented in the Case 1, all absorbance values acquired during the first 3 ms were neglected. However, for reactions 3 and 4 no experiments had any point acquired in that time interval;

- The curves with absorbance values systematically lower than 0.1 presented noise due to sensitivity limit of the spectrophotometer, and for this reason they were discarded;

- The mass balance verification was always done by comparing the initial concentration of the limiting reagent, B, and the final concentration of the product. Whenever it did not close within a minimum error of 3% the series was discarded.

In all these experiments, $c_{R0} \geq c_{B0}$, and, from the mass balance, it is considered that $c_R = c_{R0} - c_S$. Assuming that R and S absorb independently in the chosen range of wavelengths and that the Lambert-Beer law is valid at the concentration levels used, the absorbance at any instant t, for a given wavelength, can be calculated by:

$$Abs_t = c_{R0}\,\varepsilon_R\,\delta + c_S(t)(\varepsilon_S - \varepsilon_R)\delta \tag{4.21}$$

The reaction stops when $c_{B0} = 0$ and from that moment $c_R = c_{R0} - c_{B0}$ and $c_S = c_{B0}$. This absorbance, Abs_∞, can be calculated from Equation 4.21 to give:

$$Abs_\infty = c_{R0}\,\varepsilon_R\,\delta + c_{B0}(\varepsilon_S - \varepsilon_R)\delta \tag{4.22}$$

The mass balance verification is done by comparing the absorbance value calculated from the above equation with the experimental value obtained from the flattened part of the absorbance curve, against time.

Using the Excel® Solver tool the rate constant was determined by the minimization the deviation function given by

$$D^2 = \sum_{\lambda=550\,\mathrm{nm}}^{650\,\mathrm{nm}} \left[\sum_{t=3\,\mathrm{ms}}^{\mathrm{t}} \left(\left(\frac{Abs_t}{Abs_\infty} \right)_{\exp} - \frac{1 + c_S(t)/c_{R0}\left(\varepsilon_S/\varepsilon_R - 1\right)}{1 + c_{B0}/c_{R0}\left(\varepsilon_S/\varepsilon_R - 1\right)} \right) \right]_\lambda \qquad (4.23)$$

where $\left(Abs_t/Abs_\infty\right)_{\exp}$ refers to experimental values; $c_S(t)$ is given by one of the Equations 4.17 to 4.20; ε_R and ε_S come from the respective spectra, previously determined.

In short, it was obtained the kinetics rate constant – the fit variable - common to all data series in the wavelength range $550 - 650$ nm. Comparison between the curves predicted by the model with the experimental curves is illustrated in Figure 4.24c.

This procedure was repeated for each experiment and new rate constants were obtained. The average of all values is the rate constant of the reaction in study. Figure 4.24 shows a summary of the procedure used in Case 2 type for reactions with dye reagent and product.

Case 2: dye reagent and dye product

Experimental data series

- Different reagent ratios $r = c_{R0}/c_{B0}$

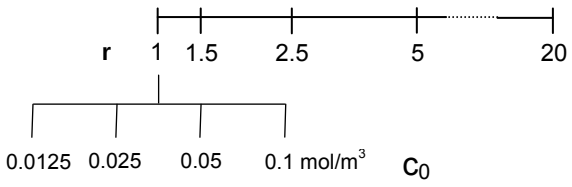

- Absorbance acquisition data at $550-650\,\text{nm}$ for several acquisition times

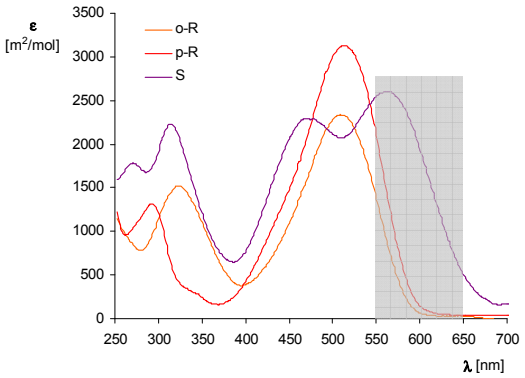

(a)

Discard data criteria:

- Time range $t < 3$ ms
- $Abs < 0.1$
- Mass balance, MB:

$$\left|\frac{c_{R0}\,\varepsilon_R\,\delta + c_{B0}(\varepsilon_S - \varepsilon_R)\delta - Abs_\infty}{c_{R0}\,\varepsilon_R\,\delta + c_{B0}(\varepsilon_S - \varepsilon_R)\delta}\right| \times 100 > 3\%$$

Data treatment:

- Excel® Solver tool
- Minimized function

$$D^2 = \sum_{\lambda=550\,\text{nm}}^{650\,\text{nm}} \left[\sum_{t=3\,\text{ms}}^{t} \left(\frac{Abs_t}{Abs_\infty} - \frac{1 + c_S(t)/c_{R0}\,(\varepsilon_S/\varepsilon_R - 1)}{1 + c_{B0}/c_{R0}\,(\varepsilon_S/\varepsilon_R - 1)} \right) \right]_\lambda$$

- Fit variable: k

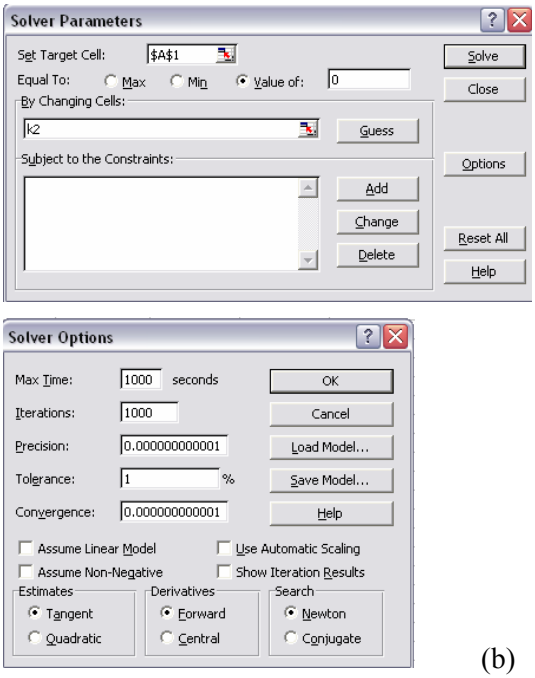

(b)

Experimental vs predicted results:

- Graphic comparison between the experimental and the predicted curves by the assumed kinetic model, using a fitted k.

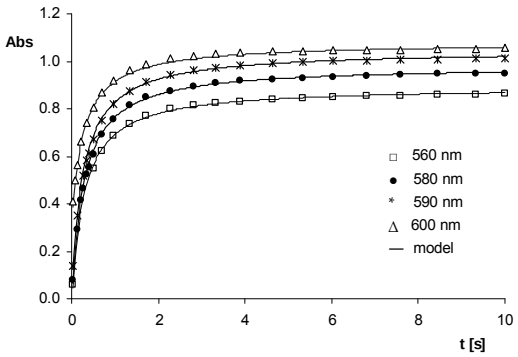

(c)

Figure 4.24 *Procedure for the determination of the kinetic model, in reactions with a dye reagent and a dye product.*

The results obtained in the kinetic study for each reaction are presented in the next sections.

4.3.1 Reactions 1 and 2: $A_1 + B \rightarrow o-R + p-R$

The azo coupling reaction between 1-naphthol (A_1) and diazotized sulfanilic acid (B) is an electrophilic aromatic substitution. The nucleophilic and electrophilic species are the 1-naphthol and diazotized sulfanilic acid, respectively. This coupling occurs preferentially in the *para* position of the 1-naphthol, but *ortho* isomer is also formed although at a lower percentage. The *ortho*:*para* isomer ratio depends on several factors, such as: the nature of the solvent, the pH of the medium, the temperature of coupling and the presence of catalysts (Zollinger, 1961; Saunders and Allen, 1985).

Thus the first coupling includes reactions 1 and 2 and forms simultaneously the two monoazo dyes ($o-R$ and $p-R$). The rate constants of those reactions could not be determined individually and the scheme of reactions 1 and 2 can be simplified by:

$$\begin{aligned} A_1 + B &\xrightarrow{k_{1o}} o-R \\ A_1 + B &\xrightarrow{k_{1p}} p-R \\ \hline A_1 + B &\xrightarrow{k_1} R \end{aligned} \qquad (4.24)$$

Where $k_1 = k_{1o} + k_{1p}$ is calculated from kinetic runs and represents the total rate constant. Product R represents the sum of monoazo dyes, i.e., $c_R = c_{o-R} + c_{p-R}$. According to $o-R/p-R$ ratio, which must be determined (see 4.3.1.3), k_1 can be divided into the desired individual rate constants:

$$k_{1o} = \frac{c_{o-R}}{c_R} k_1 \qquad (4.25)$$

$$k_{1p} = \frac{c_{p-R}}{c_R} k_1 \qquad (4.26)$$

The acid-base equilibrium is fundamental to the kinetics of the azo coupling, since it influences the predominance of the reactive species: 1-naphtholate (A_1O^-) and diazonium ions (ArN_2^+). Thus, the coupling reactions should be carried out in a medium such that acid-base equilibriums favour as much as possible the presence of those species.

4.3.1.1 Determination of the Optimum pH

The corresponding equilibrium of reactive species 1-naphtholate and diazonium ions are (Bourne et al., 1981):

$$A_1OH \xleftrightarrow{K_{A1}} A_1O^- + H^+ \tag{4.27}$$

$$ArN_2^+ + H_2O \xleftrightarrow{K_1} ArN_2OH + H^+ \xleftrightarrow{K_2} ArN_2O^- + 2H^+ \tag{4.28}$$

From Equation 4.27 it results,

$$\begin{cases} K_{A_1} = \dfrac{c_{A_1O^-}\, c_{H^+}}{c_{A_1OH}} \\ c_{A_1 0} = c_{A_1OH} + c_{A_1O^-} \end{cases} \Rightarrow c_{A_1O^-} = \frac{K_{A_1}}{K_{A_1} + c_{H^+}} c_{A_1 0} = \frac{c_{A_1 0}}{1 + 10^{(pK_{A_1} - pH)}} \tag{4.29}$$

where $K_{A1} = 9.36$ at $25\,^{\circ}C$ (Baldyga and Bourne, 1999).

In Equation 4.28 very little diazohydroxide (ArN_2OH) is produced, and the equilibrium is basically between the diazotate (ArN_2O^-) and the diazonium ions (ArN_2^+) (Saunders and Allen, 1985):

$$\begin{array}{l} ArN_2^+ + H_2O \xleftrightarrow{K_1} ArN_2OH + H^+ \\ ArN_2OH \quad \xleftrightarrow{K_2} ArN_2O^- + H^+ \\ \hline ArN_2^+ + H_2O \xleftrightarrow{K_1K_2} ArN_2O^- + 2H^+ \end{array} \tag{4.30}$$

and

$$\begin{cases} K_1K_2 = \dfrac{c_{ArN_2O^-}\, c_{H^+}^2}{c_{ArN_2^+}} \\ c_{B0} = c_{ArN_2^+} + c_{ArN_2O^-} \end{cases} \Rightarrow c_{ArN_2^+} = \frac{c_{B0}}{1 + K_1K_2 / c_{H^+}^2} = \frac{c_{B0}}{1 + 10^{(2pH - pK_1 - pK_2)}} \tag{4.31}$$

where $pK_1 + pK_2 = 20.96$ at $25\,^{\circ}C$ (Baldyga and Bourne, 1999).

Equations 4.29 and 4.31 show the pH-dependence of the reactive ions, of the first coupling reaction, related to the total concentrations of 1-naphthol, $c_{A_1 0}$, and diazotized sulfanilic acid, c_{B0}. Figure 4.25 shows the pH dependence, where it is evident that an increase in pH

increases the concentration of reactive naphtholate ions, but reduces the concentrations of diazonium ions. Therefore, the optimum pH corresponds to the point at which the product of the reactive species concentrations is maximized. This point corresponds to the intersection of the two curves, $c_{A10^-}/c_{A10} = f(\mathrm{pH})$ and $c_{ArN_2^+}/c_{B0} = f(\mathrm{pH})$, and occurs for $\mathrm{pH} = 1/3\left(\mathrm{p}K_{A_1} + \mathrm{p}K_1 + \mathrm{p}K_2\right)$.

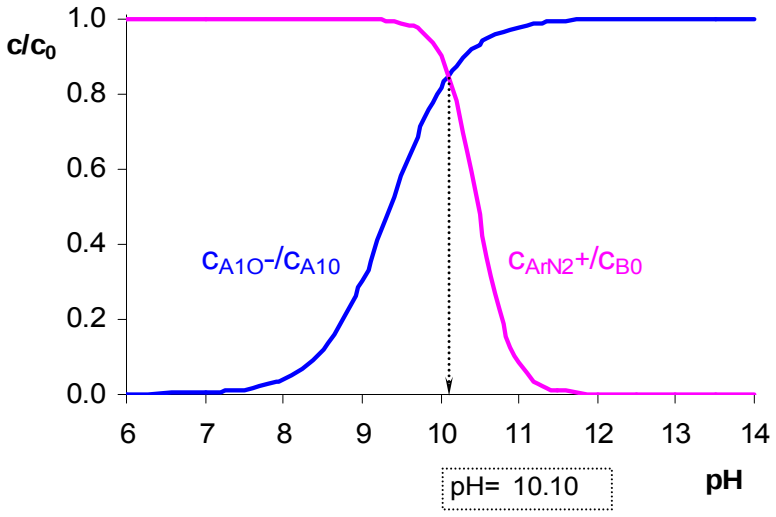

Figure 4.25 pH dependence of the reactive species for the first coupling reaction.

In short, at 25 °C the optimum pH for the first coupling reaction is near 10. As it will be shown later, the same pH value is also recommended for the other reactions studied in the present work. Hence, in the micromixing experiments and in the kinetic studies this pH value should be ensured and fixed.

Due to instability problems of diazonium ion in neutral/alkaline aqueous solutions it is appropriate to buffer the 1-naphthol reagent solution and never the diazotized sulfanilic acid solution.

4.3.1.2 Ionic Strength

The active form of diazotized sulfanilic acid is a zwitterion $\left({}^{-}\mathrm{O_3S(C_6H_4)N_2^+}\right)$, carrying no net charge ($Z_D = 0$). Its activity should therefore be independent of the ionic strength of the solution. It means that this parameter should exert no influence on the rate constants where this diazonium ion participates, i.e., it has no primary salt effect as expressed by Bronsted's equation (see for example Zollinger (1961)).

$$\log k = \log k_{I=0} + \frac{2 Z_D Z_C \alpha \sqrt{I}}{1 + \beta a \sqrt{I}} \tag{4.32}$$

where Z_D and Z_C are the charges on the reactive forms diazonium ion and 1-naphtholate, respectively, I the ionic strength, and $k_{I=0}$ and k_I the rate constants at ionic strengths zero and I, respectively, α and β are constants and a is the average minimum distance between the ions.

Bourne and co-workers studied the importance of the ionic strength in this test reaction system, establishing the value of $444.4\ \text{mol}\cdot\text{m}^{-3}$, by using $111.1\ \text{mol}\cdot\text{m}^{-3}$ for both sodium carbonate and sodium bicarbonate. Owing to the protons released during these coupling reactions, a buffer solution is needed to avoid local pH gradients (at molecular scale) development which would influence the product distribution (Bourne et al., 1988; Bourne and Gablinger, 1989).

The most recent published kinetic studies about this test reactions system done by the Bourne team (Bourne et al., 1992a) were performed at the standard conditions 25°C, $I = 444.4\ \text{mol}\cdot\text{m}^{-3}$ and pH=9.9. In view of the objectives established for this part of this chapter, these conditions will be kept. Moreover, for these standard experimental conditions and previously to the kinetic study it is opportune to know the monoazo dyes isomer ratio formed.

4.3.1.3 $o-R/p-R$ ratio

According to the information reported above, the knowledge of the $o-R/p-R$ ratio is important to calculate the rate constants of the reactions 1 and 2. Since this ratio depends on nature of the solvent, pH and temperature, it should be determined if any of those parameters is changed. In the current work, this ratio was determined for two different standard conditions respecting to viscous and non-viscous aqueous medium. Nevertheless, in each one of the cases it was assumed that the isomer ratio is independent on the temperature.

The experimental procedure used to obtained the $o-R/p-R$ ratio was done by adding $50\ \text{mL}$ of diazotized sulfanilic acid solution to $50\ \text{mL}$ of 1-naphthol (alkaline-buffered with $222.2\ \text{mol}\cdot\text{m}^{-3}$ each of $\text{Na}_2\text{CO}_3/\text{NaHCO}_3$), forming a equimolar solution, with intensive

stirring at room temperature. When the coupling is completed, all monoazo isomers capable to be formed are in solution with pH 9.9 and $I = 444.4\ \text{mol}\cdot\text{m}^{-3}$. Their quantification is made by two-component spectrophotometric analysis. However, under the actual conditions this analysis gives inadequate resolution between these isomers due to their overlapping spectra (see Figure 4.26 a).

Better resolution of isomers is achieved if the pH was acid, because the spectra overlapping disappear, as shown Figure 4.26b. Therefore, 100 mL of alkaline solution with dyes should be neutralized by adding 33.3 mL of 1N HCl and making up to 200 mL with KCl/HCl buffer (pH=0.95, $I = 200\ \text{mol}\cdot\text{m}^{-3}$) (Lenzner, 1991). The final measured pH is 1.2 and the ionic strength $I = 233\ \text{mol}\cdot\text{m}^{-3}$.

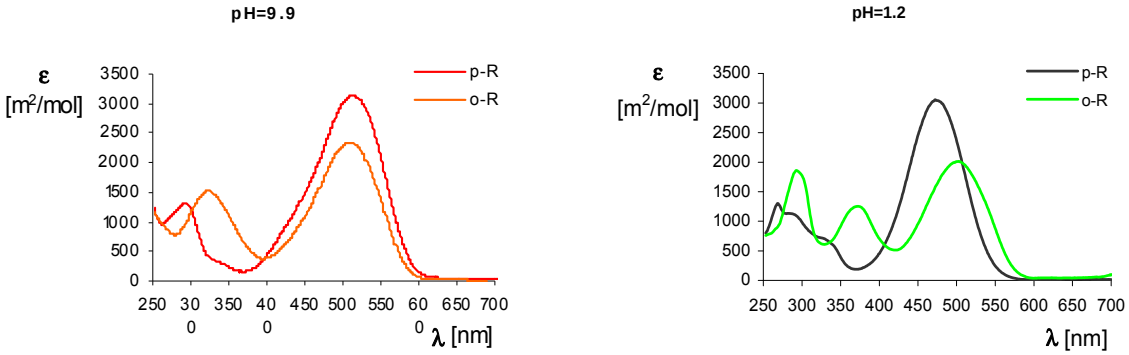

Figure 4.26 *$o-R$ and $p-R$ spectra comparison in aqueous non-viscous medium at: (a) $I = 444.4\ \text{mol}\cdot\text{m}^{-3}$, pH=9.9; (b) $I = 233\ \text{mol}\cdot\text{m}^{-3}$, pH=1.2.*

The next step was to determine the UV/vis spectrum of this acid solution, containing the isomer dyes to be quantified, over a range $250-700$ nm with a wavelength interval of 1 nm.

Assuming that the Lambert-Beer law is valid and that the dyes absorb light independently, the absorbance at a given wavelength over a optical pathlength, δ, can be estimated by:

$$Abs_{\text{calc}} = \varepsilon_{o-R}\, c_{o-R}\, \delta + \varepsilon_{p-R}\, c_{p-R}\, \delta \qquad (4.33)$$

where ε_{o-R} and ε_{P-R} are respectively the molar extinction coefficients of $o-R$ and $p-R$ at the same experimental conditions.

From Equation 4.33, an absorbance curve, Abs_{calc}, can be calculated, based on reasonable estimations of both isomers concentrations c_{o-R} and c_{p-R}. Then, by using the Excel®solver tool, that curve can be fitted to the experimental curve Abs_{exp}, where the fitting variables are naturally c_{o-R} and c_{p-R}. This is done through the minimization of the deviation function

$$D^2 = \sum_{300\,\text{nm}}^{550\,\text{nm}} \left(Abs_{\text{exp}_\lambda} - Abs_{\text{calc}\,\lambda} \right)^2 \tag{4.34}$$

over the wavelengths range of $300 - 550$ nm.

Using reagents concentrations in the range $0.0125 - 0.05\ \text{mol} \cdot \text{m}^{-3}$ (after mixing), several experiments were done. From these experiments, where the mass balances closed around $\pm 1\%$, the average percentage of the isomers was 6% for *ortho* and 94% for *para* isomer, which is in reasonable agreement with the results obtained by Bourne and co-workers (1990) of 7% and 93%, respectively.

Once it is known the $o-R/p-R$ ratio, suitable conditions of pH and I to perform the reactions and the isomers spectra in those conditions, all requirements to proceed with the kinetic study are fulfilled.

4.3.1.4 Determination of the Rate Constant and Activation Energy

Equation 4.24 represents the reaction between 1-naphthol and diazotized sulfanilic acid, with a simplified scheme. However, the reaction mechanism is more complex, involving intermediate products which were studied in more detail for example in Bourne and co-workers (1981, 1985).

The partial orders of the reagents A_1 and B were not determined here, since the reaction mechanism equation has been verified many times (Bourne et al., 1985) and the partial orders of 1 were obtained. The reaction rate is given by

$$r_R = k_1\, c_{A1}\, c_B \tag{4.35}$$

The product R represents the sum of monoazo isomers. Its UV/vis spectrum is given by:

$$\varepsilon_R = 0.06\, \varepsilon_{o-R} + 0.94\, \varepsilon_{p-R} \tag{4.36}$$

The maximum extinction coefficient of R is $3071\,\mathrm{m}^2\cdot\mathrm{mol}$ at $510\,\mathrm{nm}$, thus the kinetic was followed by recording absorbances over time at this wavelength. In agreement with the experimental data procedure described for Case 1, the value of ε_R is only required for the mass balance verification.

A wide set of experiments was conducted in order to determine the rate constant k_1 at $25^\circ\mathrm{C}$, $I = 444.4\ \mathrm{molm}^{-3}$, pH=9.9 and $\mu = 1\,\mathrm{mPa}\cdot\mathrm{s}$. The concentration of the reagent 1-naphthol was $6.25\times10^{-3} - 0.1\ \mathrm{mol}\cdot\mathrm{m}^{-3}$ and the concentration of diazotized sulfanilic acid was used with a ratio ($r = \gamma_{A1} = c_{A10}/c_{B0}$) in the range $1 \le r \le 20$. For different reasons not all experiments were succeeded well, namely: the upper or lower limits of the spectrophotometer were exceeded; the reaction time was lower than the stopped-flow dead time and the loss of kinetic data was significant; the mass balance did not close, etc. This last problem was recurrent for almost all experiments where $r > 5$, thus they were discarded from the data treatment. Table 4.8 summarizes the values of k_1 obtained in the experiments, using the correction of concentration profile in the optical cell (Equations 4.13 and 4.15).

In the experiments where $c_{A10} = c_{B0}$, Bourne and co-workers (1985) observed an initial concentration-dependency for $1 \le r \le 5$. In order to evaluate that "strange" effect, the experimental results obtained for stoichiometric reagents ratio were treated separately. The resulting kinetics rate constants are summarized in the Table 4.8 on the column for $r = 1$. The legends of the columns $1 < r \le 5$ and $1 \le r \le 5$ refers to series included on the deviation function (Equation 4.16), where the serie $r = 1$ was excluded and included, respectively. It was observed that all curves of the model had a good fitting to the experimental results. Thus, even for stoichiometric ratio, it can be considered that the second-order kinetic law represents conveniently the behavior of the first azo coupling reaction.

Table 4.8 *Rate constant* $k_1\,[\mathrm{m^3\cdot mol^{-1}\cdot s^{-1}}]$ *at* $I = 444.4\ \mathrm{mol\cdot m^{-3}}$, $\mathrm{pH} = 9.9$, $\mu = 1\ \mathrm{mPa\cdot s}$ and $T = 25^{\circ}\mathrm{C}$.

$\delta\,[\mathrm{mm}]$	$c_{A0}\,[\mathrm{mol\cdot m^{-3}}]$	Experiment	$r = 1$	$1 < r \le 5$	$1 \le r \le 5$	MB[(1)]
2	0.05	# 1	20378	18597	19510	3.23%
		# 2	22010	19977	20706	0.31%
10	0.025	# 1	19163	18980	19047	1.97%
		# 2	17699	18390	18200	1.48%
		# 3	18219	18619	18619	1.17%
	0.05	# 1	18704	19685	19432	0.90%
		# 2	22952	18142	22051	2.15%

[(1)]MB=mass balance

From the results presented in the Table 4.8, it is not evident any concentration-dependency of k_1, as it was registered by Bourne and co-workers (1985). This author suggested two causes for the occurrence: characteristic reaction times lower than mixing time of the stopped-flow equipment used and local pH gradients problems. With the available information it can be said that perhaps the performance of their stopped-flow is the main justification for the different observations, once the equipment used in this work is different and provided with more recent technology.

Only the shaded values in the Table 4.8 were used to calculate a mean value of the kinetics rate constant k_1 presented in the Table 4.9; the other values were excluded because they increased the standard deviation or because the mass balance verification was not satisfactory.

It should be mentioned two points:

- When the profile concentration into the optical cell is ignored, the maximum difference observed for the rate constant was nearly 1%, thus the simple model might be used is this case;
- The values of t_0 found were in the range $2.4 - 2.8$ ms.

Table 4.9 *Rate constants for reaction 1 and reaction 2 at* $I = 444.4\ \text{mol}\cdot\text{m}^{-3}$, $\text{pH} = 9.9$, $\mu = 1\ \text{mPa}\cdot\text{s}$ *and* $T = 25^{\circ}\text{C}$.

Rate constant $[\text{m}^3\cdot\text{mol}^{-1}\cdot\text{s}^{-1}]$	**This work**	**Bourne (1990)**
k_1	18824 ± 533	13159 ± 480
k_{1o}	1129 ± 32	921 ± 34
k_{1p}	17695 ± 501	12238 ± 446

The values of k_{1o} and k_{1p} and the respective standard deviations presented in Table 4.9 were calculated from Equations 4.18 and 4.19, respectively. These values differ significantly from those obtained by Lenzner (Bourne et al., 1990; Lenzner, 1991).

The conclusion of the kinetic study of this reaction was done by the determination of the influence of temperature on the rate constant, using the Arrhenius equation:

$$k = k_0 e^{-\frac{E_a}{RT}} \tag{4.37}$$

where k_0 is the Arrhenius parameter or frequency factor, E_a is the activation energy, T is the temperature and $R = 8.314\ \text{J}\cdot\text{mol}^{-1}\cdot\text{K}^{-1}$.

Several experiments were conducted at different temperatures in the range $288 - 308\ \text{K}$ to determinate E_a and k_0. The final average results are shown in Figure 4.27.

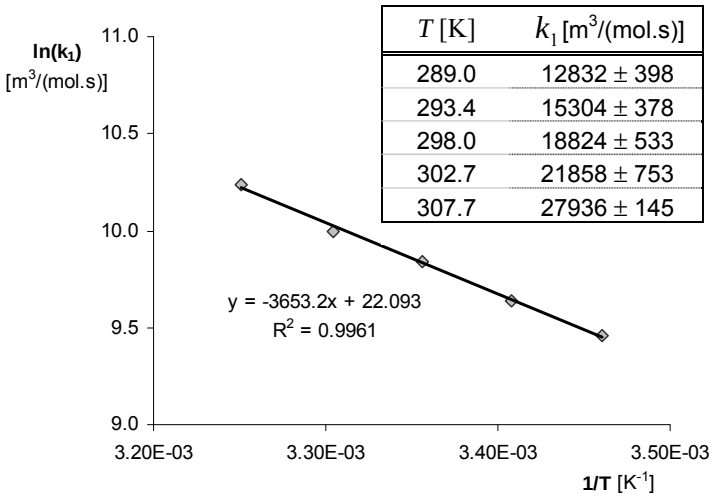

Figure 4.27 *Linearization of Arrhenius equation for the determination of the activation energy for reaction* $A_1 + B \rightarrow R$ *(*$I = 444.4\ \text{mol}\cdot\text{m}^{-3}$, $\text{pH} = 9.9$ and $\mu = 1\ \text{mPa}\cdot\text{s}$*).*

The experimental results have a good correlation with the linearization of the Arrhenius equation. The values of E_a and k_0 from the trend line equation are summarized in Table 4.10.

Table 4.10 Activation energy and Arrhenius parameter for the first azo coupling reactions at $I = 444.4\ \text{mol}\cdot\text{m}^{-3}$, $\text{pH} = 9.9$ *and* $\mu = 1\ \text{mPa}\cdot\text{s}$.

	This work	**Bourne (1985)**
E_a [J·mol^{-1}]	3.037×10^4	3.05×10^4
k_0 [m^3·mol^{-1}·s^{-1}]	3.934×10^9	---

The activation energy value obtained in this work is very similar to previously published values (Bourne et al., 1985; Bourne et al., 1990). No published value of k_0 for comparison was found.

It must be noted that the values presented in Table 4.10 refer to the global reaction $A_1 + B \rightarrow R$. Nevertheless, similarly to Bourne et al. (1990) assumption, it seems reasonable to use this activation energy for k_{1o} and k_{1p} in the temperature range studied.

4.3.2 Reaction 3: $o-R + B \rightarrow S$

The kinetics of the coupling between the $o-R$ and B is presented in this section. First, it is convenient to evaluate if the predefined standard is suitable to the occurrence of this reaction, specifically which concerns the pH value.

4.3.2.1 Determination of the Optimum pH

In the present reaction, the reactive species are the naphtholate form of $o-R$, $o-RO^-$ and the diazonium ion, ArN_2^+. The equilibrium of ArN_2^+ is described in Section 4.3.1.1 and the equilibrium of $o-R$ is given by:

$$o\text{-}ROH \xleftrightarrow{K_{oR}} o\text{-}RO^- + H^+ \qquad (4.38)$$

The dependence of the reactive specie on pH is given by the relationship:

$$\begin{cases} K_{oR} = \dfrac{c_{o\text{-}RO^-}\, c_{H^+}}{c_{o\text{-}ROH}} \\ c_{o-R0} = c_{o\text{-}ROH} + c_{o\text{-}RO^-} \end{cases} \Rightarrow c_{o\text{-}RO^-} = \frac{K_{oR}}{K_{oR} + c_{H^+}}\, c_{o-R0} = \frac{c_{o-R0}}{1+10^{(pK_{oR}-pH)}} \qquad (4.39)$$

where $pK_{oR} = 9.17$ at 25 °C (Baldyga and Bourne, 1999). c_{o-R0} is the total concentration of $o-R$.

The dependence on pH is similar to that in Figure 4.25. A pH increase has a negative effect over the diazonium ion but favours the specie $o-RO^-$. Thus, there exists an optimum pH value given by $pH = 1/3\left(pK_{oR} + pK_1 + pK_2\right)$, for this second coupling reaction. At 25 °C, this pH value is 10.03, which means that the $pH = 9.9$ established on the standard conditions is also suitable for this reaction.

4.3.2.2 Determination of the Rate Constant and Activation Energy

In the experiments performed to determine the kinetics rate constant, the concentration of purified $o-R$ used was in the range $0.0125 - 0.1\ \text{mol}\cdot\text{m}^{-3}$. The ratio c_{o-R}/c_{B0} varied from 1 to 20. The solutions of $o-R$ were buffered with $222.2\ \text{mol}\cdot\text{m}^{-3}$ for both $Na_2CO_3/NaHCO_3$ given a $I = 888.8\ \text{mol}\cdot\text{m}^{-3}$. In this way, when mixing the $o-R$ and B solutions in the stopped-flow, the final solution has an half value of ionic strength and $pH = 9.9$.

The measurements of absorbance as a function of time were done at ten values of wavelength in the range $550 - 650$ nm (in steps of 10 nm). The choice of the wavelength range follow the criteria of the least overlapping of the $o-R$ and S spectra and for which the ratio $\varepsilon_S/\varepsilon_{o-R}$ attained the highest values. The experiments were conducted at four values of temperatures, all in the range $288.5 - 303.0$ K. The data acquisition times were in the range $5 - 50$ s, and since the number of points per series is 400 it means a time resolution between $0.0125 - 0.12$ s.

The data treatment followed the procedure described before for Case 2. The kinetics rate constants and respective standard deviations are shown in Figure 4.28. The mass balances of

the series closed within 2%. It was observed a good fitting between experimental data and the curves predicted by the kinetic model assumed, i.e., the experimental data are well represented by a global second order reaction model.

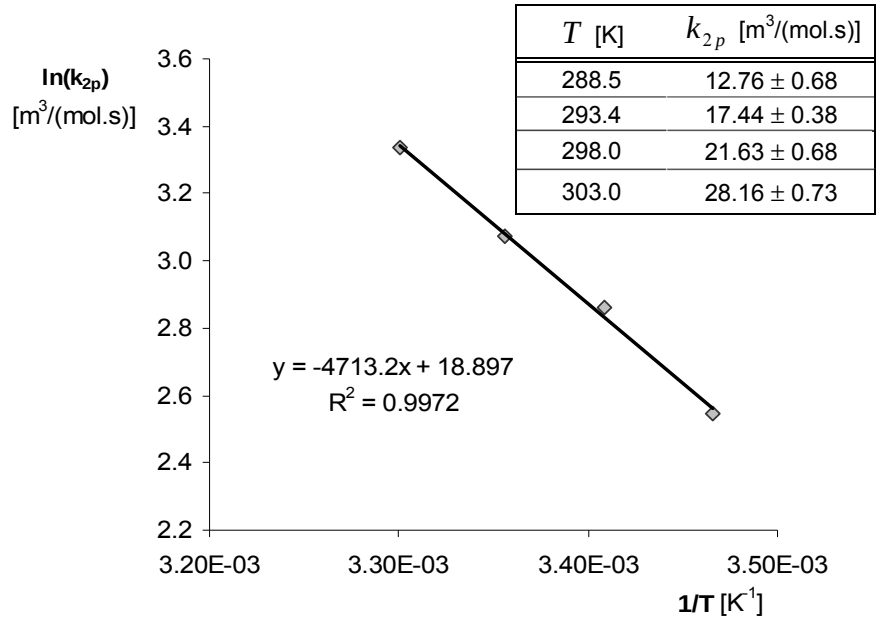

T [K]	k_{2p} [m³/(mol.s)]
288.5	12.76 ± 0.68
293.4	17.44 ± 0.38
298.0	21.63 ± 0.68
303.0	28.16 ± 0.73

Figure 4.28 Linearization of Arrhenius equation for the determination of the activation energy for reaction $o - R + B \rightarrow S$ *(*$I = 444.4\ \text{mol}\cdot\text{m}^{-3}$, $\text{pH} = 9.9$ and $\mu = 1\ \text{mPa}\cdot\text{s}$*)*

For the temperature range studied, the experimental results of k_{2p} show a good correlation coefficient on the linearization of the Arrhenius equation (Equation 4.37), as shown in Figure 4.28. The activation energy and the frequency factor is calculated from the straight line equation and are presented in the Table 4.11, together with the values published by (Bourne et al., 1985; Bourne et al., 1990). The value of E_a obtained in this work is in good agreement with Bourne's result.

Table 4.11 *Rate constant for reaction $o-R+B \rightarrow S$ (at $I = 444.4\ \text{mol}\cdot\text{m}^{-3}$, $\text{pH} = 9.9$, $\mu = 1\ \text{mPa}\cdot\text{s}$ and $T = 25^{\circ}\text{C}$), activation energy and frequency factor.*

	This work	**Bourne (1990)**
k_{2p} [$\text{m}^3\cdot\text{mol}^{-1}\cdot\text{s}^{-1}$] at 25°C	21.63 ± 0.68	22.25 ± 0.25
E_a [$\text{J}\cdot\text{mol}^{-1}$]	3.919×10^4	3.874×10^4
k_0 [$\text{m}^3\cdot\text{mol}^{-1}\cdot\text{s}^{-1}$]	1.611×10^8	---

It is also reported in the Table 4.11 the average value of k_{2p} at 25°C for comparison with Bourne et al. (1990). The result obtained in this work differs by 2.8% from the value obtained by Bourne. This difference can be considered rather significant and could be attributed to the purity level of synthesized solid $o-R$ or to experimental errors.

4.3.3 Reaction 4: $p-R+B \rightarrow S$

The fourth reaction in the test reaction system in study corresponds to the coupling between the *para* monoazo isomer ($p-R$) and the diazotized sulfanilic acid (B). Similarly to the reactions presented before, the pH value has a relevant influence in the predominance of the reactive species in this reaction.

4.3.3.1 Determination of the Optimum pH

The reactive species for diazotized sulfanilic acid, B, is the diazonium ion $Ar\text{N}_2^+$ and for $p-R$ is the naphtholate form $p-R\text{O}^-$. The equilibrium for B was reported in Section 4.3.1.1 and for $p-R$ is given by

$$p\text{-}R\text{OH} \xleftrightarrow{K_{p_R}} p\text{-}R\text{O}^- + \text{H}^+ \tag{4.40}$$

From the above equation it can be shown that

$$\begin{cases} K_{pR} = \dfrac{c_{p\text{-}R\text{O}^-}\, c_{\text{H}^+}}{c_{p\text{-}R\text{OH}}} \\ c_{p-R0} = c_{p\text{-}R\text{OH}} + c_{p\text{-}R\text{O}^-} \end{cases} \Rightarrow c_{p\text{-}R\text{O}^-} = \frac{K_{pR}}{K_{pR} + c_{\text{H}^+}}\, c_{p-R0} = \frac{c_{p-R0}}{1+10^{(\text{p}K_{p\text{R}} - \text{pH})}} \tag{4.41}$$

where c_{p-R0} is the total concentration of $p-R$ and $pK_{pR} = 8.26$ at $25^{\circ}\mathrm{C}$ (Baldyga and Bourne, 1999).

In the reaction in study, the pH has an opposite effect on the reactive species, i.e., an increase of pH has a positive effect in the predominance of $p-R\mathrm{O}^{-}$ but a negative effect for the existence of $Ar\mathrm{N}_2^{+}$. So, there is an optimum pH value, corresponding to the intersection of the concentration curves of both reactive species against pH. This value can be calculated by $\mathrm{pH} = 1/3\left(\mathrm{p}K_{pR} + \mathrm{p}K_1 + \mathrm{p}K_2\right)$. The obtained value in this case is 9.73 at $25\ ^{\circ}\mathrm{C}$, which means that the $\mathrm{pH} = 9.9$ established previously for the standard condition is also appropriate for this reaction.

4.3.3.2 Determination of the Rate Constant and Activation Energy

The reaction in study is the slowest reaction of the group of five belonging to the test reaction system. This fact has consequences in the time intervals for data acquisition, which varied from 20 to 100 s. This time scale is greater when compared with the dead time of the stopped-flow and problems with loss of important information on the kinetics determination are here absent.

The absorbance of the mixtures was recorded in the stopped-flow spectrophotometer at several wavelengths $550-650$ nm (in steps of 10 nm). The experiments covered a reagent ratio of $1 \le c_{p-R}/c_{B0} \le 20$ and the concentrations of $p-R$ were in the range $6.25\times10^{-3} - 0.05\ \mathrm{mol\cdot m^{-3}}$. Since the solutions of B are unstable in alkaline pH, the solutions of the reagent $p-R$ should be buffered in order to ensure a $I = 444.4\ \mathrm{mol\cdot m^{-3}}$ after mixing with B in the stopped-flow. The way to prepare the buffered reagent is the same described for $o-R$ in Section 4.3.2.2.

When the $\delta = 2$ mm optical pathlength was used, the series corresponding to $c_{p-R}/c_{B0} > 7.5$ were discarded in most cases, because the experimental curves presented significant noise levels.

In order to determine the constants of the Arrhenius equation (Equation 4.37) a set of experiments were done at four distinct temperatures in the range $288.5-303$ K. A compilation of the average values obtained for the kinetics rate constants is shown in Figure 4.29, as well as the respective standard deviations.

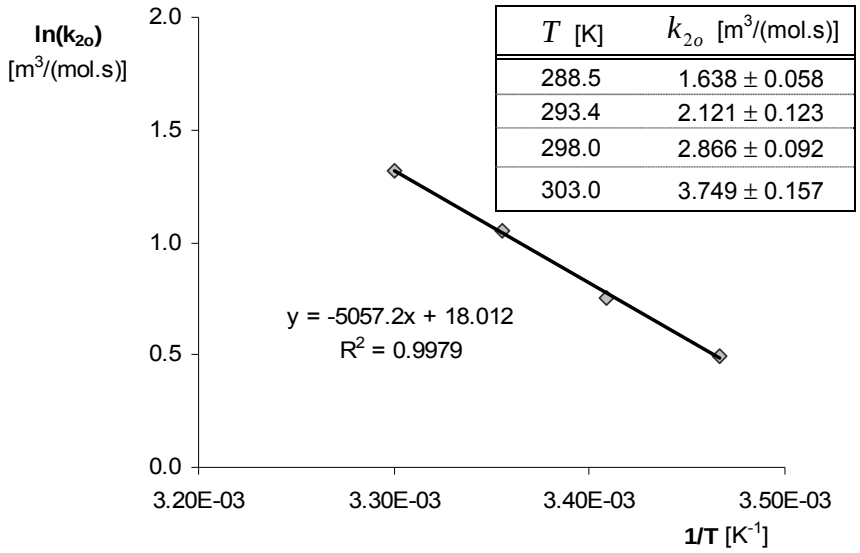

Figure 4.29 Linearization of Arrhenius equation for the activation energy determination of the reaction $p - R + B \rightarrow S$ *(*$I = 444.4\ \text{mol} \cdot \text{m}^{-3}$, $\text{pH} = 9.9$ and $\mu = 1\ \text{mPa} \cdot \text{s}$*).*

The values for the activation energy and for the frequency factor, calculated from the trend line equation of Figure 4.29 are shown in Table 4.12. Both E_a and k_0 values obtained in this work are in good agreement with the results published by (Bourne et al., 1990). This author assumed that both reactions with monoazo isomers and diazotized sulfanilic acid had the same E_a and k_0 values. In fact, the results obtained in this work allow concluding that the activation energy could be considered to be equal for both reactions, but the frequency factors are different.

For easier comparison, Table 4.12 also shows the kinetics rate constant value obtained in this work and the value published by (Bourne et al., 1990), at 25°C. The k_{2o} obtained in the present work differs 56% from the Bourne result. This expressive difference could be due to the purity level of the solids used.

Table 4.12 Rate constant for reaction $p-R+B \rightarrow S$ (at $I = 444.4\ \text{mol}\cdot\text{m}^{-3}$, $\text{pH} = 9.9$, $\mu = 1\ \text{mPa}\cdot\text{s}$ and $T = 25^{\circ}\text{C}$), activation energy and frequency factor.

	This work	**Bourne (1990)**
k_{2o} [$\text{m}^3\cdot\text{mol}^{-1}\cdot\text{s}^{-1}$] at 25°C	2.866 ± 0.092	1.835 ± 0.018
E_a [$\text{J}\cdot\text{mol}^{-1}$]	4.205×10^4	3.874×10^4
k_0 [$\text{m}^3\cdot\text{mol}^{-1}\cdot\text{s}^{-1}$]	6.643×10^7	1.063×10^7

4.3.4 Reaction 5: $A_2 + B \rightarrow Q$

The coupling of 2-naphthol, A_2, with diazotized sulfanilic acid, B, is the last reaction to be studied.

This reaction is only required for micromixing characterization in systems with energy dissipation rates greater than $200 - 400\ \text{W.kg}^{-1}$ (Bourne et al., 1992a), that is the upper limit of sensitivity of the "simplified" test reaction system, composed of only the four reactions (see Chapter 2).

The reagent 2-naphthol has three possible positions on the ring to be coupled by the diazonium ions, but the coupling occurs only at the 1 position. Citing (Saunders and Allen, 1985): "No satisfactory explanation as to why the azo group cannot enter in the 3 position emerged until Wheland pointed out that of the three mesomeric forms of 2-naphthol (a) and (b) contain Kekulé benzene rings and have less energy than (c); the form (c) is therefore not favoured and consequently little or no coupling occurs at 3." (see Figure 4.30)

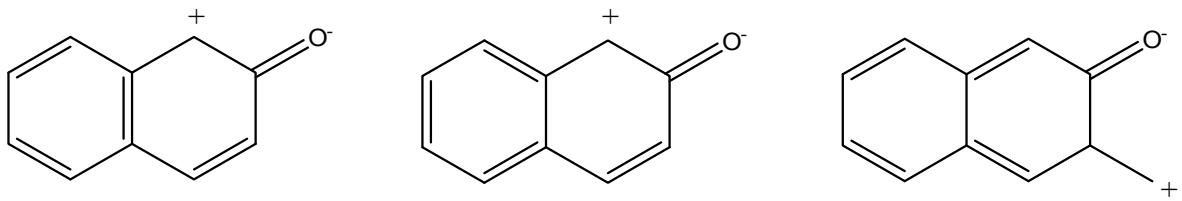

(a) **(b)** **(c)**

Figure 4.30 Mesomeric forms of 2-naphthol (Saunders and Allen, 1985).

In this azo coupling reaction, the reactive species are the 2-naphtholate, A_2O^-, and the diazonium ions. The pH value has an opposite effect in the predominance of these species, existing an optimum value for reaction occurrence. The optimum pH value will be determined in the next section.

4.3.4.1 Determination of the Optimum pH

The equilibrium involving diazonium ion and its pH dependence equation was presented before by Equations (4.28, 4.30 and 4.31). The equilibrium of 2- naphtholate is represented by:

$$A_2\mathrm{OH} \xleftrightarrow{K_{A_2}} A_2\mathrm{O}^- + \mathrm{H}^+ \tag{4.42}$$

The relationship between $A_2\mathrm{O}^-$ and pH is given by

$$\begin{cases} K_{A_2} = \dfrac{c_{A_2\mathrm{O}^-}\, c_{\mathrm{H}^+}}{c_{A_2\mathrm{OH}}} \\ c_{A_2 0} = c_{A_2\mathrm{OH}} + c_{A_2\mathrm{O}^-} \end{cases} \Rightarrow c_{A_2\mathrm{O}^-} = \frac{K_{A_2}}{K_{A_2} + c_{\mathrm{H}^+}}\, c_{A_2 0} = \frac{c_{A_2 0}}{1 + 10^{\left(\mathrm{p}K_{A_2} - \mathrm{pH}\right)}} \tag{4.43}$$

where $c_{A_2 0}$ is the total concentration of 2-naphthol and $pK_{A_2} = 9.54$ at $25\ ^\circ\mathrm{C}$ (Bourne et al., 1992a).

An increase of pH promotes the predominance of the reactive species 2- naphtholate and has and opposite effect in the diazonium ion. The ideal pH for the occurrence of this reaction corresponds to the value that maximizes both reactive species. This value can be calculated by $\mathrm{pH} = 1/3\left(\mathrm{p}K_{A_2} + \mathrm{p}K_1 + \mathrm{p}K_2\right)$. It was obtained a value of pH equal to 10.17 at $25\ ^\circ\mathrm{C}$.

Similarly to the other four reactions, the $\mathrm{pH} = 9.9$ of the standard conditions is also suitable for the reaction between 2-naphthol and diazotized sulfanilic acid, for which the kinetic study is presented next.

4.3.4.2 Determination of the Rate Constant and Activation Energy

The kinetic study of the reaction between A_2 and B was performed in the stopped-flow apparatus, with concentrations of buffered A_2 in the range $0.025 - 0.05\ \mathrm{mol \cdot m^{-3}}$ and with reagents ratio in the range $1 \le c_{A_2 0}/c_{B0} \le 20$. The kinetics was followed by absorbance measurements as a function of time, at $480\ \mathrm{nm}$, the wavelength corresponding to the maximum of the UV/vis spectrum of the product of the reaction, Q (see Figure 4.21).

For the determination of the activation energy and the frequency factor, a set of experiments was done in the temperature range $288.8 - 302.9\ \mathrm{K}$.

The problems related with the loss of data sometimes existing on the kinetic study of fast reactions (using the present analytical technique) did not occur here. For the concentrations used, the characteristic reaction times were always higher than the dead time of the equipment.

The data treatment followed the procedure explained before for Case 1, and the partial orders of the reaction were set to be one. With this kinetic model, it was observed a good fitting between the curves of the model and the experimental results.

The average values of the kinetics rate constant, k_3, and respective standard deviations are shown in Figure 4.31.

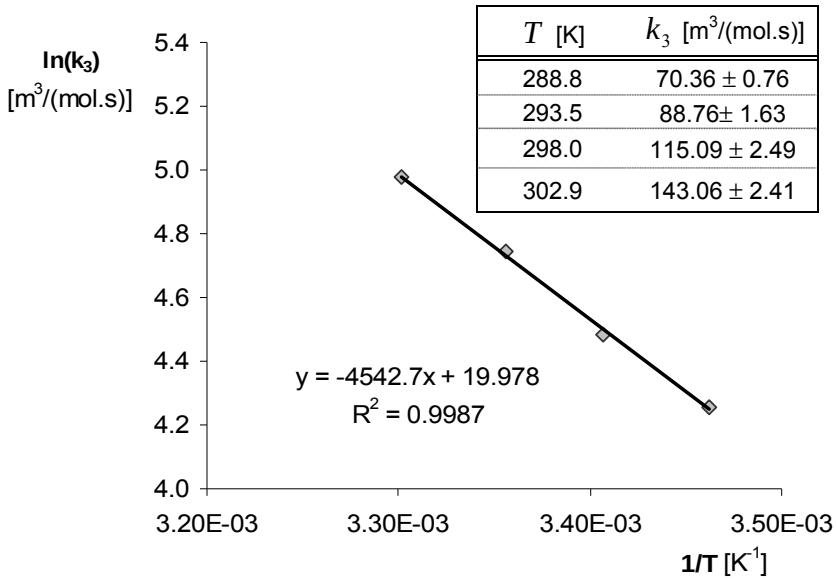

Figure 4.31 Linearization of Arrhenius equation for the determination of the activation energy for reaction $A_2 + B \rightarrow Q$ *(*$I = 444.4\ \text{mol} \cdot \text{m}^{-3}$, $\text{pH} = 9.9$ and $\mu = 1\ \text{mPa} \cdot \text{s}$*).*

Table 4.13 summarizes the constants of the Arrhenius equation obtained in the present work. No published values for comparison were founded. At the standard conditions, the value of k_3 differs from Bourne's value by about 7.6%.

Table 4.13 Rate constant for reaction $A_2 + B \rightarrow Q$ *(at* $I = 444.4\ \text{mol}\cdot\text{m}^{-3}$, $\text{pH} = 9.9$, $\mu = 1\ \text{mPa}\cdot\text{s}$ *and* $T = 25^\circ\text{C}$*), activation energy and frequency factor.*

	This work	**Bourne (1992)**
k_3 $[\text{m}^3\cdot\text{mol}^{-1}\cdot\text{s}^{-1}$ at 25°C	115.09 ± 2.49	124.52 ± 1.02
E_a $[\text{J}\cdot\text{mol}^{-1}]$	3.710×10^4	---
k_0 $[\text{m}^3\cdot\text{mol}^{-1}\cdot\text{s}^{-1}]$	3.605×10^8	---

The previously presented kinetic study allowed the validation of the experimental procedure and data treatment for comparison with the published results. As it was shown, at the standard conditions both results (published and obtained in this work) for the rate constants are not very different. In short, it can be said that the main objectives of this section were attained.

4.4 Kinetic Study in Aqueous Viscous Medium

Before the kinetic study in aqueous viscous medium, it was necessary to select an additive to add to the aqueous solutions in order to increase the viscosity. In this section, it will be presented the selection of a suitable additive, followed by its rheological and reactivity/stability study. Then, for the chosen additive, it will be evaluated its effect on the UV/vis spectra of the reagents and products. Finally, the kinetic study will be presented.

4.4.1 Additive Selection to Increase the Viscosity

The concept of viscosity, μ, is given by Newton's postulate, in which the shear stress σ is related to the velocity gradient, or shear rate $\dot{\gamma}$, through the equation (see for example Barnes et al., 1997):

$$\sigma = \mu\,\dot{\gamma} \tag{4.44}$$

In a simplistic way, saying that a fluid exhibits a Newtonian behavior means that μ is independent of $\dot{\gamma}$, under constant temperature and pressure.

A convenient way to raise the viscosity of aqueous solutions is by use of an additive – thickener - that should preferably exhibit the following properties (Bourne et al., 1989; Guichardon, 1996):

- Newtonian flow behavior;
- A significant increase in viscosity at low concentrations of the additive;
- Viscosity independent of pH;
- Inert in presence of the chemicals in use;
- No influence on the analytical method;
- Soluble in water;
- Non-toxic and biodegradable.

An additive that fulfills all the properties referred above and those results in solutions with a viscosity near $100\ \mathrm{mPa \cdot s}$ was searched. This value was previously practiced by Teixeira (2000) and Santos (2003) in experiments performed in the mixing chamber of a RIM head machines, whose micromixing characterization is one of the aims of this research work (as it will be seen in Chapter 5).

As a starting point, the literature searched for similar works where some additive was used to increase the viscosity of aqueous solutions. The selected additives were first characterized by two simple tests:

- Reactivity in presence of the reagents 1-naphthol, A_1, and diazotized sulfanilic acid, B. Aqueous solutions of 1-naphthol (buffered with $\mathrm{Na_2CO_3/NaHCO_3}$) and diazotized sulfanilic acid were prepared, separately. Both solutions contained a certain percentage of the chosen additive and were stored in the freezer during 60 minutes approximately. Fresh solutions were also prepared and added to the respective older stored solutions, i.e., $A_1(\mathrm{old}) + B(\mathrm{fresh})$, $A_1(\mathrm{fresh}) + B(\mathrm{old})$, and so on. The spectra of the resulting solutions were determined and compared with the spectra of the solution obtained by the addition of both fresh reagents.

- Newtonian or non-Newtonian behavior. For this test, it was used the rheometer (Paar Physica, UDS 200 model) presented in Figure 4.32, where a fluid sample is placed in the measuring thermostatized unit, controlled by an electronic interface connected to a computer for data acquisition.

  This measuring unit can work as a simple viscometer and has two operating options: concentric-cylinder mode and cone-and-plate mode. The last configuration was used in this study, with a MK 24 cone reference.

  The viscosity measurements were carried out at $20^{\circ}\mathrm{C}$, using a shear rate range $0.1 \le \dot{\gamma} \le 5000\ \mathrm{s}^{-1}$, to cover those experienced by fine-scale vortices where micromixing occurs (Bourne et al., 1995).

Figure 4.32 Paar Physica rheometer.

From the literature search, it was found that carboxymethyl cellulose (CMC) was used by Bourne an co-workers (1989) as a thickener, on the reaction system composed by the first four reactions of the test system (Equations 4.1 to 4.4), but due to its rheological non-Newtonian behavior, it was considered to be non-ideal. Gholap and co-workers (1994) investigated several additives in order to increase the viscosity of aqueous reagent solutions. They found additives that exhibited a pH-dependent viscosity such as: the polyacrylic acid PAA, xanthan gum and poly-alkyl alcohols (Polyox). They observed that large quantities of sortibitol were required and that the CMC did not fulfil most of the properties described above. HEC, hydroxyethyl cellulose (Natrosol-GR) was recognized, by those researchers, to be a good additive, having a solution viscosity almost independent of pH and a Newtonian flow behavior at low concentrations (< 1 wt.%). For example, a solution of HEC with a concentration of 0.7 wt.% gives a viscosity of 11.5 $\mathrm{mPa \cdot s}$.

Guichardon (1996) used glycerol in the iodine/iodate test reaction, obtaining solutions with viscosity of up to 170 mPa·s with Newtonian behavior. At first, this non-polymeric additive seemed to be an interesting option. However, in order to increase the viscosity significantly the glycerol needs to be used at high concentrations meaning that the solvent for a chemical reaction is changed with a possible simultaneous change in the reaction kinetics (Baldyga and Bourne, 1999).

Aqueous solutions of glycerol at several ratios were prepared. Their rheological behavior was evaluated and confirmed as Newtonian fluids (Nunes et al., 2001). To prepare a 20 mPa·s viscosity solution, a high glycerol concentration - about 72% - is necessary. This concentration can be undesirable from the kinetics point of view. The glycerol reactivity was analysed in presence of reagents A_1 and B with 72% of glycerol. After one hour, B was degraded to a high extent in the presence of glycerol. This fact shows that this additive cannot be used.

The second additive studied was hydroxyethyl cellulose (synonymous HEC, 250 HHBR, Natrosol®, *Aqualon*), a polymer used in the food and paint industries. This additive family (250 GR, "Natrosol") was also used by Bourne and co-workers (Baldyga et al., 1995; Bourne et al., 1995) to prepare solutions of up to 8 mPa·s. Under the conditions used in their experiments (low additive concentrations, low temperature, limited contact time, etc.) HEC did not react with the other ions in solution. In this work Newtonian behavior for low concentration solutions of the additive (0.1%, $\mu = 5\,\text{mPa}\cdot\text{s}$) is observed (Nunes et al., 2001), however for concentrations of 0.25% or higher, the polymeric solutions exhibit a shear-dependent viscosity, typical of non-Newtonian fluids. The viscosity decreases with increase in shear rate, giving rise to what is called *shear-thinning* behavior or pseudoplasticity (Barnes et al., 1997).

Even though HEC solutions do not react with the test reaction reagents, their non-Newtonian behavior make them unsuitable for this work, since the viscosity of 8 mPa·s is lower than the desired value of 100 mPa·s.

The diversity of the additives employed in similar works (with the intended properties) revealed to be scarse. The search was extended to the other commercial additives used in the paints industry, namely: the family of Rheolates (from *Elementis Specialities*), which are polymeric organic products. Three species of the Rheolate, 350, 212 and 255, were investigated. According to the supplier information, Rheolate 350 is a polyether polyol and

Rheolate 212 is a polyether polyurethane resin solution in water, and both form, in aqueous solutions, fluids with Newtonian properties.

The rheograms of solution with various concentrations of Rheolate 350 (10, 15 and 20 wt.%) and Rheolate 212 (1, 10 and 20 wt.%) were determined and it was confirmed their Newtonian behavior (Nunes et al., 2001). For example, to prepare 20 mPa·s solutions about 15% of Rheolate 350 and 20% of Rheolate 212 was necessary. The reactivity test of these two additives was positive in the presence of diazotized sulfanilc acid, disallowing their application in the present work.

Rheolate 255 is a polyurethane polymer solution (25%) in a mixture of water/diethylene glycol ether (60%/15%). The rheogram of this additive in pure form showed its non-Newtonian behavior, as it was previously referred by its supplier. However, when used in diluted aqueous solutions (2-3 wt.%) it exhibits Newtonian behavior over shear rates in the range $0.1 - 5000\ s^{-1}$ as shown in Figure 4.33a. Solutions with a viscosity of 20 mPa·s can be obtained using 3.8 wt.% of the additive (see Figure 4.33b). In this case, the Newtonian behavior is ensured up to shear rates of $3000\ s^{-1}$ (see Figure 4.34). For higher additive concentrations this limit decreases.

Roughly, the upper limit of application for this additive providing a Newtonian behavior is in solutions having a Rheolate 255 mass percentage of 3.8 wt.%, resulting in aqueous solutions with viscosity of 20 mPa·s.

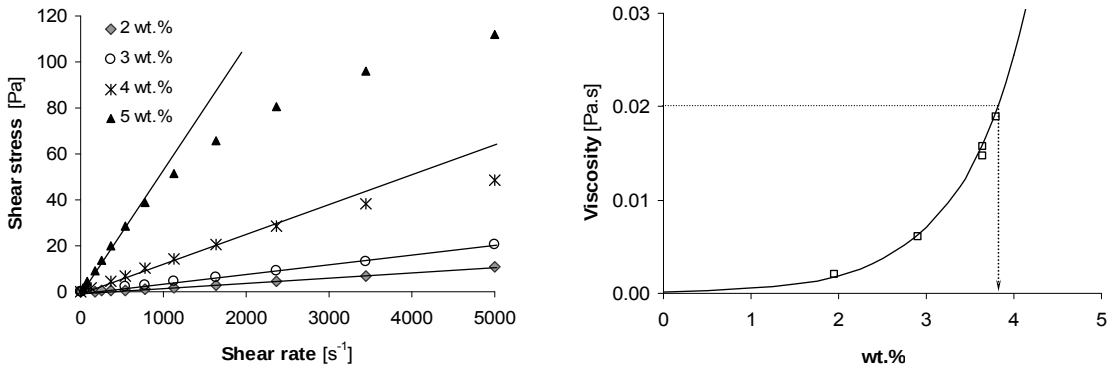

(a) (b)

Figure 4.33 (a) Shear stress vs. shear rate of Rheolate 255 aqueous solutions ($T = 20^{\circ}C$); (b) Viscosity vs Rheolate 255 solutions mass percentage ($T = 20^{\circ}C$).

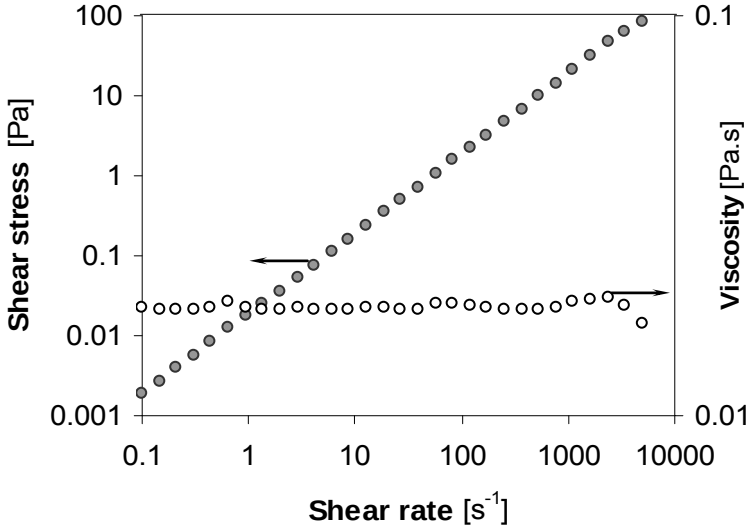

Figure 4.34 Shear stress vs. shear rate and viscosity vs. shear rate of Rheolate 255 aqueous solutions (3.8 wt.%, $T = 20^{\circ}\mathrm{C}$).

In reactivity tests with Rheolate 255 aqueous solutions (3.8 wt.%), solubility problems arose in the preparation of the buffer solutions with $Na_2CO_3/NaHCO_3$, $222.2\,mol\cdot m^{-3}$ of each in order to obtain a $I = 444.4\ mol\cdot m^{-3}$ after mixing with diazotized sulfanilic acid (as it was done before). The problem was solved by reducing those concentrations by one half ($111.1\ mol\cdot m^{-3}$ each one).

The first tests were performed with a "small" free sample provided by *Elementis Specialities*. Rheolate 255 solutions with $\mu = 20\ mPa\cdot s$ did not react with any reagent or product involved in the test reaction system, except again for the diazotized sulfanilic acid, which presented degradation lower than 5% during about 120 minutes of contact.

Considering the difficulties to find an ideal additive that matches all proposed properties, Rheolate 255 seemed to be the best from the rheological and chemical points of views. Thus, it was chosen to proceed with the kinetic studies and, later, with micromixing characterization in a specific mixing device.

The second Rheolate 255 package showed some differences when compared with the first sample. The mass percentages to prepare aqueous solutions with the previously determined viscosities, were readjusted, e.g. to obtain a solution with $\mu = 20\ mPa\cdot s$ the percentage passed from 4.3 wt.% to 3.8 wt.% . Figure 4.33b was constructed with the polymer of this new package. Another alteration observed was related with its reactivity in the presence of

diazotized sulfanilic acid, where the degradation levels of this reagent increased significantly (about 50% in 2.5 hours); the initial colourless solutions of B becomes yellowish. The discovery of the origin of the problem was not direct. However, the pH of the polymer was measured at a value of approximately 9. Due to the instability of the diazotized sulfanilic acid in alkaline medium, a pre-neutralization of the polymer with HCl before using it with the test reaction chemicals was adopted.

The aqueous viscous solutions of diazotized sulfanilic acid after the pre-neutralization step with HCl, had a pH of 3-4. The reactivity tests were repeated and it was obtained 2-3% of diazotized sulfanilic acid degradation at the end of 2 hours, which was considered acceptable.

The reactivity tests were extended to the other compounds, such as A_1, A_2, $o-R$, $p-R$ and Q. Buffered solutions were prepared and absorbance measurements made over the UV/vis wavelength range. The absorbance recordings were repeated after a few hours and the solutions were stored at $4\,^{\circ}\mathrm{C}$ with the exclusion of light (on the refrigerator). In the presence of Rheolate 255 (3.8 wt.%), it was not perceptible any degradation of A_1 and A_2 after 2 hours or 26 hours for the dyes, $o-R$, $p-R$ and Q.

Rheological studies were performed with the 3.8 wt.% solutions. These solutions showed a pH-independent viscosity ($4 \le \mathrm{pH} \le 10$) and non-thixotropic (viscosity independent of the flow history). Their viscosity variation with temperature was determined, for $\dot{\gamma} = 10^3\ \mathrm{s}^{-1}$, and in the range $288-303\ \mathrm{K}$ may be represented by the relationship: $\mu = 2.446 \times 10^{-12} e^{6.675\times10^3/T}$; where T is the temperature $[\mathrm{K}]$ and μ the viscosity $[\mathrm{Pa}\cdot\mathrm{s}]$.

Summing up, from the five additives evaluated in this work (see Table 4.14), Rheolate 255 fulfils most of the properties established for an ideal thickener: Newtonian flow behavior (up to $\dot{\gamma} = 3000\ \mathrm{s}^{-1}$); low concentrations of the additive used to attain significant increase in viscosity (3.8 wt.% to obtain $\mu = 20\ \mathrm{mPa}\cdot\mathrm{s}$); pH-independent viscosity; inert (up to 120 min); water soluble; non-toxic (except the diethylene glycol ether which makes part of the Rheolate 255). The influence on the analytical method and on reactions kinetics will be investigated in the next sections.

Note: the supply form of all additives studied is in solution, except the Natrosol which is in powder form. Its humidity was determined and considered in the respective study.

Table 4.14 Summary of the additives studied and their reactivity and rheological behavior.

Additive	**Reactivity**	**Rheology**
Glycerol	Reactive	Newtonian
Hydroxyethyl cellulose - Natrosol®[(1)] 250	Inert	Non-Newtonian
Rheolate 350[(2)]	Reactive	Newtonian
Rheolate 212[(2)]	Reactive	Newtonian
Rheolate 255[(2)]	Inert	Newtonian[(3)]

[(1)]Aqualon; [(2)]Elementis Specialities; [(3)]Under conditions specified in the text.

The standard conditions for the kinetic studies in aqueous viscous medium are: $I = 222.2\ \text{mol}\cdot\text{m}^{-3}$, $\text{pH} = 10$, $\mu = 20\ \text{mPa}\cdot\text{s}$ and $T = 20^{\circ}\text{C}$.

Compared with the standard conditions of the non-viscous medium, the ionic strength decreased due to the difficulties founded in the buffer solubility, however, the pH value is kept constant. The temperature of 20°C is the average room temperature of the laboratory, where the micromixing studies were performed (as it will be seen in Chapter 5).

4.4.2 Make up Aqueous Viscous Solutions

The preparation of the viscous aqueous chemical (reagents and products) solutions was done by two methods depending on the reagent: (i) a first method for the diazotized sulfanilic acid, B, that requires a pre-neutralizing additive step; (ii) a second method for the remaining chemicals (A_1, A_2, $o-R$, $p-R$ and Q).

4.4.2.1 Diazotized Sulfanilic Acid

On the preparation of the viscous solutions of the diazotized sulfanilic acid three distinct solutions were necessary:

1. "Concentrated" diazotized sulfanilic acid aqueous solution, prepared accordingly to the procedure described in Section 4.2.2;

2. Neutralizing solvent - 10^{-3} N HCl. This solution was prepared by diluting 5 mL of 0.1N HCl in water with a final volume of 500 mL. The 0.1N HCl solution was prepared by adding 2.07 mL of 37% concentrated HCl (d=1.09) to water completing a total volume of 250 mL;

3. Rheolate 255 with density of 1.03 $g \cdot cm^{-3}$ at 20°C.

Depending on the reagent concentration and viscosity of the desired solution, the proportion of the three solutions varies. In the last section, the viscosity was pre-defined to be always 20 $mPa \cdot s$, which is attained with 3.8 wt.% of Rheolate 255. Thus, to prepare 25 mL of $c_B = 0.1\ mol \cdot m^{-3}$ with that viscosity, the procedure is:

1. 0.95 g of Rheloate 255 is weighed;

2. 22.8 mL of neutralizing solvent is added and the solution is stirred until an homogeneous solution is observed;

3. 1.25 mL of diazotized sulfanilic acid "concentrated" is added, with a concentration of 2.0 $mol \cdot m^{-3}$.

All diazotized sulfanilic acid solutions prepared following this procedure had a pH between 3 and 4.

4.4.2.2 Remaining Chemicals

The solutions of the remaining chemicals, 1 and 2-naphthols (A_1 and A_2), monoazo isomers ($o-R$, $p-R$) and Q, which are available in powder form, were prepared following the procedure desbribed below:

1. First, a known "concentrated" solution of the respective chemical in water was prepared;
2. In parallel, the suitable mass of Rheolate 255 was mixed in a certain volume of water in order to have a 3.8 wt.% of the additive in the final solution (after adding a certain volume of the previous solution);
3. A mass of buffer $Na_2CO_3/NaHCO_3$ is added, in order to have the desired ionic strength in the final solution;
4. The volume of the concentrated chemical solution to the previous viscous buffered solution is added. For stability reasons, when the chemical is A_1 or A_2, this step should be made fresh, i.e., a few minutes before the use of the solution.

A practical example is the preparation of 25 mL aqueous viscous solution of 1-naphthol with $c_{A1} = 0.1\ \text{mol}\cdot\text{m}^{-3}$ and $I = 444.4\ \text{mol}\cdot\text{m}^{-3}$ for the subsequent use in a kinetic study (where it is mixed with diazotized sulfanilic acid given a final ionic strength of $I = 222.2\ \text{mol}\cdot\text{m}^{-3}$):

1. The "concentrated" aqueous solution of A_1 is prepared, for example $c_{A1} = 2.0\ \text{mol}\cdot\text{m}^{-3}$, following the procedure described in Section 4.2.1, but suppressing the buffering step;
2. 0.95 g of Rheolate 255 (with density of $1.03\ \text{g}\cdot\text{cm}^{-3}$ at 20°C) is weighed and 22.8 mL of water is added. It is necessary to stir until it is observed an homogeneous solution;
3. 0.2944 g of Na_2CO_3 and 0.2333 g of $NaHCO_3$ to the previous viscous solution is added;
4. Finally, and just before using the solution in preparation, 1.25 mL of the "concentrated" aqueous solution with a concentration of $2.0\ \text{mol}\cdot\text{m}^{-3}$ is added.

The product S was prepared by coupling $o-R$ (buffered) with diazotized sulfanilic acid, with both solutions prepared following the procedure described above.

In any experiment of this work, even in the viscous medium, the reagent and product solutions were dilute, so that their contribution for the ionic strength could be neglected.

In the next section it is evaluated the influence of the selected additive on the analytical method. This is made by the comparison of the UV/vis spectra of the reagents and products in aqueous viscous medium with the same spectra in aqueous non-viscous medium, determined in Section 4.3.

4.4.3 Reagents and Products UV/vis Spectra

The UV/vis spectra of all reagents - except that of the diazotized sulfanilic acid - and products of the test reaction system were determined in the standard conditions previously established for the viscous medium: $I = 222.2\ \text{mol}\cdot\text{m}^{-3}$, $\text{pH} = 9.9$, $\mu = 20\ \text{mPa}\cdot\text{s}$ and $T = 20^{\circ}\text{C}$.

As it was explained before, due to the instability in the presence of light, the quantification of the diazotized sulfanilic acid is always made indirectly, thus its UV/vis spectrum was not determined.

Several solutions with different concentrations ($0.025 - 0.1\ \text{mol}\cdot\text{m}^{-3}$) of A_1, A_2 and the purified $p-R$ and $o-R$, following the procedure described in Section 4.4.2.2 were prepared. The absorbances of these solutions were measured in the UV/vis wavelength range and the extinction coefficients were calculated by using the Lamber-Beer law (Equation 4.6). The average of all spectra obtained for each chemical is shown in Figure 4.35, where they can be compared with those obtained in aqueous non-viscous medium, presented in Section 4.3.

The Rheolate 255 and water curves represent the aqueous viscous and aqueous non-viscous solutions, respectively. It is important to call attention to the fact that the viscosity value is not the only parameter that has changed between the two curves; the temperature and the ionic strength are also different. However, it was confirmed that this change (only for the used values) did not alter the curves, i.e., in aqueous non-viscous medium, the obtained curves for $I = 222.2\ \text{mol}\cdot\text{m}^{-3}$ and $T = 20^{\circ}\text{C}$ did not differ from from the curve referenced as water. So, any observed difference in the curves is a consequence of the presence of the new solvent.

In Figure 4.35a and Figure 4.35b, a slight displacement between the spectrum in viscous and non-viscous (water) medium can be observed. The shape of the curves was also modified slightly.

The spectrum of $p-R$ (Figure 4.35c) undergoes alterations by a displacement of 8 nm in its wavelength of maximum absorbance. For $o-R$ (Figure 4.35d) no alteration is observed in the visible region of the spectrum.

For the reasons presented in Section 4.2.5, the product S was not obtained in a solid form. Thus, making the reaction between $o-R$ and B in aqueous viscous medium, assuming a 100% yield, the absorbance of the resulting solution was measured and the spectrum was determined (see Figure 4.35e). The spectrum of S is again bimodal, even in the presence of the Rheolate 255 additive, but some changes are registered both in magnitude and in position relatively to the wavelength axis. They are summarized in Table 4.15 as well as the indices of purity of S, calculated by using Equation 4.11.

Table 4.15 Summary of the differences found between the S spectra in viscous ("Rheolate 255") and non-viscous ("Water") medium.

		Rheolate 255	**Water**
1st maximum	$\varepsilon_{máx}$ [m²/mol] =	2106	2297
	λ [nm] =	480	473
minimum	ε_{min} [m²/mol] =	1802	2070
	λ [nm] =	516	511
2nd maximum	$\varepsilon_{máx}$ [m²/mol] =	2184	2604
	λ [nm] =	571	559
	IP_1=	1.17	1.11
	IP_2=	1.21	1.26

Finally, the spectrum of Q shown in Figure 4.35f was obtained directly from the resulting solution of the coupling of 2-naphthol and diazotized sulfanilic acid, assuming a yield of 100%. In the presence of Rheolate 255 the curve maintained the shape of the curve in aqueous non-viscous solution, but decreased its intensity in the region of its maximum absorbance.

A curious fact around the spectrum of Q was observed. The spectrum here named by "Rheolate 255" is coincident with that obtained in aqueous non-viscous medium when the purified solid of Q is used (see pink curve of the Figure 4.21). Moreover, the spectrum determined by preparing a solution with Q solid following the procedure described in Section 4.4.2.2, is also coincident with these spectra. In summary, the single spectrum of Q which is not coincident with the others is the one that was prepared by the reaction $A_2 + B$ in aqueous non-viscous solution. However, several experiments were made to confirm this result. No reason is found for this fact.

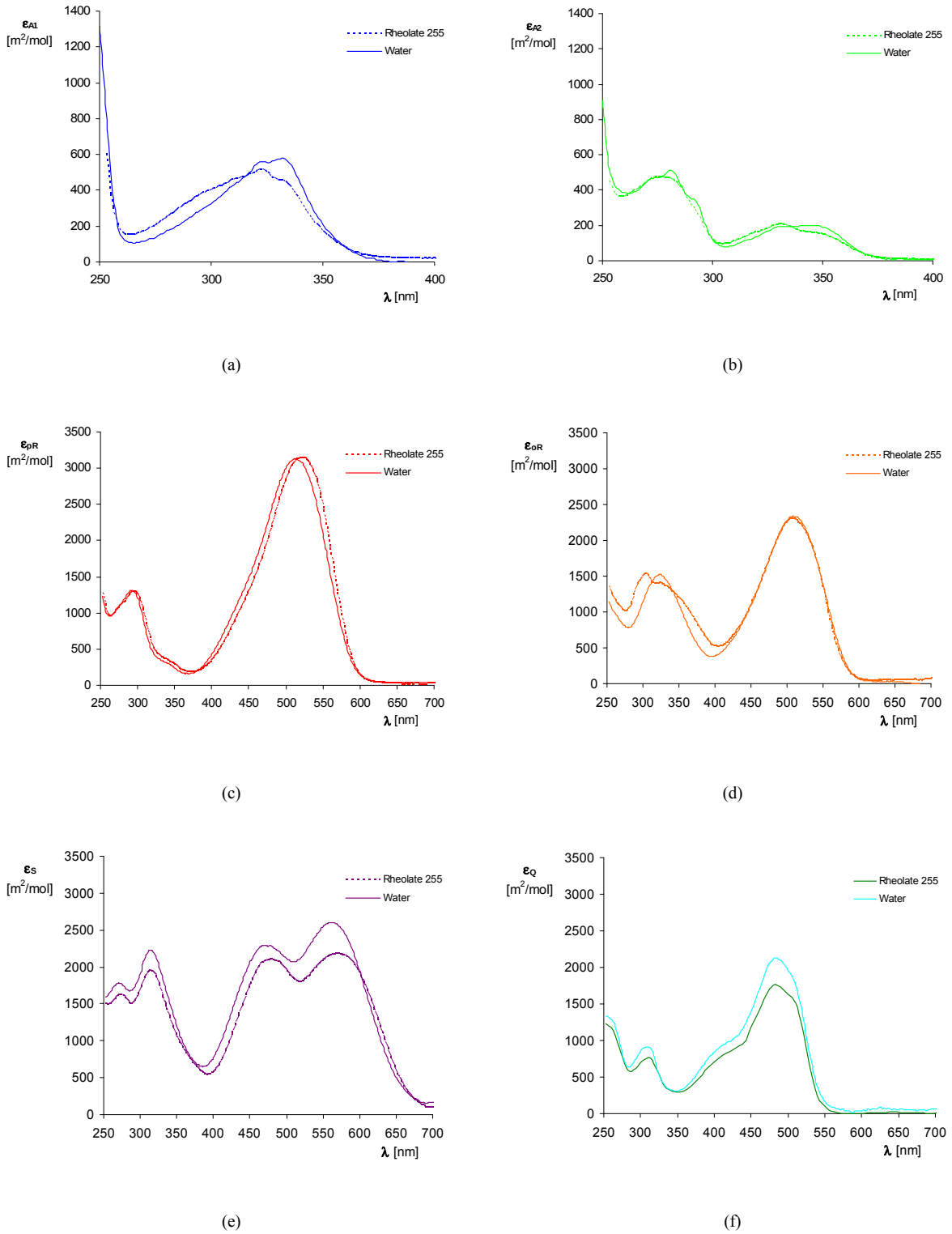

Figure 4.35 *Comparison between the UV/vis spectrum in aqueous non-viscous solution* ($I = 444.4\ \mathrm{mol \cdot m^{-3}}$, $\mathrm{pH} = 9.9$, $\mu = 1\ \mathrm{mPa \cdot s}$ and $T = 25^{\circ}\mathrm{C}$) *and the UV/vis spectrum in aqueous viscous solution* ($I = 222.2\ \mathrm{mol \cdot m^{-3}}$, $\mathrm{pH} = 9.9$, $\mu = 20\ \mathrm{mPa \cdot s}$ and $T = 20^{\circ}\mathrm{C}$). *(a) 1-naphthol; (b) 2-naphthol; (c)* $p-R$*; (d)* $o-R$*; (e)* S *and (f)* Q.

A summary of all spectra is presented in Figure 4.36.

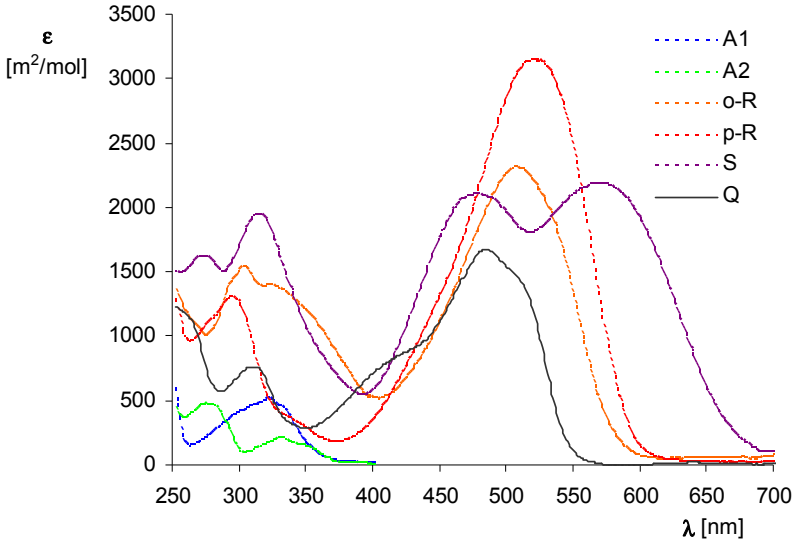

Figure 4.36 *UV/vis spectra in aqueous viscous solution of all chemicals involved in the test reaction system* ($I = 222.2\ \text{mol}\cdot\text{m}^{-3}$, $\text{pH} = 9.9$, $\mu = 20\ \text{mPa}\cdot\text{s}$ *and* $T = 20^{\circ}\text{C}$).

The observed differences in the spectra, due to the presence of the additive Rheolate 255 in 3.8 wt.%, should not be classified as significant; however, these spectra in the new standard conditions are essential in order to proceed with the kinetic study of the reactions where the chemicals participate.

4.4.4 Influence of the Additive on the Rate Constants

In the selection of a thickener to be used in solutions where the reactions will take place, it is desirable that it does not change the respective kinetics. That is one of the reasons why it is better to use a low percentage of the additive to achieve the desired viscosity. However it is always advisable to re-determine the kinetics when the solvent changes.

When using the simplified test reactions system (the first four reactions) in viscous medium with 1 wt.% of HEC (Gholap et al., 1994) no influence was observed on the reaction rate constants of the second azo couplings. Moreover, the influence of the HEC on the kinetics of the primary couplings was not investigated, because these authors considered that those reactions are instantaneous, i.e., "A_1 and B do not co-exist in solution: therefore the rate constants of these primary couplings need not to be known with high accuracy". A similar study was made by Bourne and co-workers (1989), when using the CMC as additive. It was

observed that the k_{2o} fell by 2.7% when using 0.4 wt.% CMC and by 4.5% when using 0.6 wt.% CMC solutions.

In this work, it was decided to evaluate the influence of the Rheolate 255 in 3.8 wt.% on the kinetics of all five reactions. The kinetic studies, in aqueous viscous medium, were done in the same stopped-flow apparatus used for the study of the test reaction in aqueous non-viscous medium.

The experimental plan and data treatment were very similar to that described in Section 4.3, named as Case 1 and Case 2, so that in the next sections it will be presented the results of the reaction rate constants obtained and detailed information on the procedures already described in the previous section were surpressed.

The activation energy and the frequency factor from the Arrhenius law were also determined. It is understood that the viscosity changes with the temperature, and in these experiments the percentage of Rheolate 255 was always 3.8 wt.%. The interest of that determination was only to compare with the values previously obtained with solutions where the additive was absent (aqueous non-viscous medium).

4.4.4.1 Reaction 1 and Reaction 2: $A_1 + B \rightarrow o-R$ *and* $A_1 + B \rightarrow p-R$

As it was already observed, it is not possible to study the kinetics of reactions 1 and 2 separately. The global reaction $A_1 + B \rightarrow R$ (where $R = o-R + p-R$) is studied and knowing the ratio of *ortho* and *para* monoazo isomers, it is possible to calculate the rate constant of each reaction individually.

The ratio $o-R/p-R$ was re-determined for the new solvent. The experimental procedure followed was the same described in Section 4.3.1.3, but the concentrations of some chemical species differed. In this case, 50 mL of diazotized sulfanilic acid solution was added to a 50 mL of 1-naphthol (alkaline-buffered with 111.1 $\text{mol}\cdot\text{m}^{-3}$ of both $Na_2CO_3/NaHCO_3$) equimolar solution, with intensive stirring at room temperature. When the coupling is completed, the quantities of monoazo isomers should be quantified by two-component spectrophotometric analysis. However, at the actual conditions: $I = 222.2\ \text{mol}\cdot\text{m}^{-3}$ and pH=9.9 the spectra of $o-R$ and $p-R$ overlap (see Figure 4.37a). Better resolution of isomers is achieved whether the pH solution was acid, because their spectra overlapping

disappear, as shown Figure 4.37b. Therefore, the 100 mL of alkaline solution with dyes should be neutralized by adding 33.3 mL of 0.5N HCl and making up to 200 mL with NaCl/HCl buffer (pH=0.95, $I = 200\ \text{mol}\cdot\text{m}^{-3}$). The final measured pH is 1.2 and the ionic strength $I = 150\ \text{mol}\cdot\text{m}^{-3}$.

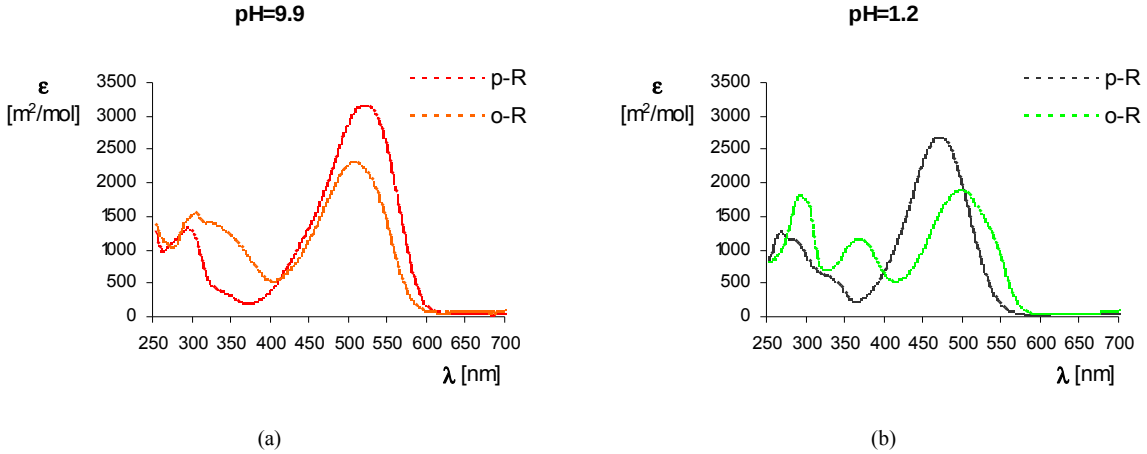

Figure 4.37 *$o-R$ and $p-R$ spectra comparison in aqueous viscous medium at:* (a) $I = 222.2\ \text{mol}\cdot\text{m}^{-3}$, $\text{pH} = 9.9$; (b) $I = 150\ \text{mol}\cdot\text{m}^{-3}$, $\text{pH} = 1.2$.

The percentages of $o-R$ and $p-R$ obtained were 10% and 90%, respectively, while for the aqueous non-viscous medium 6% for $o-R$ and 94% for $p-R$ had been previously obtained. Thus, it can be concluded that the presence of the Rheolate 255 in 3.8 wt.% had a small influence on the *ortho/para* ratio. In fact, it was already known that this ratio could be considerably influenced by the solvent where the reaction occurs. This can arise from alteration on the relative stabilization, by the solvent molecules, of the transition states for the attack on the *ortho* and *para* positions. However it can also be considered the possibility of the electrophilic species being different in the two different solvents (Sykes, 1977).

The kinetics of the coupling between 1-naphthol and diazotized sulfanilic acid was followed at three wavelengths, 500, 510 and 520 nm, in order to determine the maximum absorbance of $o-R$ (510 nm) and of $p-R$ (520 nm). The experimental plan and the data treatment followed the procedure describe above as Case 1.

The constants E_a and k_0 of the Arrhenius equation were determined based on experiments performed at four temperatures in the range $288.4-303\ \text{K}$. The obtained values for those constants and average values for rate constant k_1 are listed in Table 4.16.

The values of k_{1o} and k_{1p} were calculated by using Equations 4.25 and 4.26, i.e., $k_{1o} = 0.10\, k_1$ and $k_{1p} = 0.90\, k_1$.

Table 4.16 Rate constants for reaction $A_1 + B \rightarrow R$ (at $I = 222.2\ \text{mol}\cdot\text{m}^{-3}$, $\text{pH} = 9.9$ and $\mu = 20\ \text{mPa}\cdot\text{s}$), activation energy and frequency factor.

T [K]	k_1 [$\text{m}^3\cdot\text{mol}^{-1}\cdot\text{s}^{-1}$]	E_a [$\text{J}\cdot\text{mol}^{-1}$]	k_0 [$\text{m}^3\cdot\text{mol}^{-1}\cdot\text{s}^{-1}$]
288.4	11873 ± 780	2.694×10^4	8.815×10^8
293.1	13554 ± 547		
298.2	16677 ± 685		
303.0	20283 ± 817		

The k_1 values obtained in aqueous viscous medium are around 11% (see Figure 4.27) lower than the values found for the aqueous non-viscous medium. Indeed, the viscosity was not the unique parameter that changed between these media; the ionic strength was reduced to one half. However, some experiments were performed in aqueous non-viscous medium with $I = 222.2\ \text{mol}\cdot\text{m}^{-3}$ and the obtained values did not differ from those obtained with $I = 444.4\ \text{mol}\cdot\text{m}^{-3}$. This allows to conclude that the differences verified between both media can be attributed to the new solvent, i.e., to the additive/thickener.

The observed decrease of the rate constant is reflected in the value of k_0, which also decreased with the change of the medium. The decrease in the activation energy can be considered rather significant.

4.4.4.2 Reaction 3: $o - R + B \rightarrow S$

The experimental plan and data treatment followed in the kinetic of second coupling reaction between $o - R$ and B was described above as Case 2. The kinetics was followed by absorbance measurements in the range $550 - 650$ nm, seeing that it corresponds to the region of both $o - R$ and S spectra where $\varepsilon_S / \varepsilon_{o-R}$ attains the maximum values. The experiments were conducted at several temperatures in the range $293.4 - 307.9$ K. The obtained results of the rate constants for the different temperatures are presented in Table 4.17, as well as the values of E_a and k_0. The result at 34.9 °C was excluded due to its high standard deviation.

Table 4.17 Rate constants for reaction $o - R + B \rightarrow S$ (at $I = 222.2\ \text{mol}\cdot\text{m}^{-3}$, pH = 9.9 and $\mu = 20\ \text{mPa}\cdot\text{s}$), activation energy and frequency factor.

T [K]	k_{2p} [$\text{m}^3\cdot\text{mol}^{-1}\cdot\text{s}^{-1}$]	E_a [$\text{J}\cdot\text{mol}^{-1}$]	k_0 [$\text{m}^3\cdot\text{mol}^{-1}\cdot\text{s}^{-1}$]
293.4	14.06 ± 0.07	5.210×10^4	2.622×10^{10}
298.2	19.07 ± 0.24		
302.9	27.49 ± 1.00		
307.9	29.94 ± 7.47		

The value of k_{2p} is lower when the Rheolate 255 is present in the solvent; at $20.4\ ^\circ\text{C}$ the difference is about 19% (see Figure 4.28).

The activation energy is of the same order of magnitude in both media: viscous and non-viscous, but the frequency factor, k_0, increased two orders of magnitude. There is no apparent reason and explanation for this occurrence.

4.4.4.3 Reaction 4: $p - R + B \rightarrow S$

The kinetics of reaction between $p - R$ and B followed a very similar way to the preceding reaction. The average values of k_{2o} for several temperatures are presented in Table 4.18. The E_a and k_0 values are also shown on the same table and were calculated excluding the k_{2o} value referent to 34.9°C, in order to increase the correlation coefficient of the trend line.

Once again, it is observed a fall of the kinetics rate constant in the presence of Rheolate 255. At 20.4°C the registered difference for k_{2o} is greater than for k_{2p} (see Figure 4.29) by about 40%.

The activation energy is of the same order of magnitude and similarly to the previous reaction, the frequency factor increases two orders of magnitude.

Table 4.18 Rate constants for reaction $p-R+B \rightarrow S$ (at $I = 222.2\ \text{mol}\cdot\text{m}^{-3}$, $\text{pH} = 9.9$ and $\mu = 20\ \text{mPa}\cdot\text{s}$), activation energy and frequency factor.

T [K]	k_{2o} [$\text{m}^3\cdot\text{mol}^{-1}\cdot\text{s}^{-1}$]	E_a [$\text{J}\cdot\text{mol}^{-1}$]	k_0 [$\text{m}^3\cdot\text{mol}^{-1}\cdot\text{s}^{-1}$]
293.3	1.278 ± 0.021	6.033×10^4	7.294×10^{10}
298.0	2.045 ± 0.039		
302.9	2.799 ± 0.106		
307.9	3.175 ± 0.078		

4.4.4.4 Reaction 5: $A_2 + B \rightarrow Q$

The kinetics of reaction between 2-naphthol and diazotized sulfanilic acid was studied following the procedure described in Section 4.3 as Case 1. The experiments were performed at four values of temperature in the range $293.4 - 307.5$ K and the absorbance measurements over time were conducted at 480 nm.

The average values of the rate constant, k_3, and respective standard deviations are shown in Table 4.19. The values for the activation energy and for the frequency factor do not differ (in order of magnitude) from the obtained in the aqueous non-viscous medium (see Table 4.13).

Table 4.19 Rate constants for reaction $A_2 + B \rightarrow Q$ (at $I = 222.2\ \text{mol}\cdot\text{m}^{-3}$, $\text{pH} = 9.9$ and $\mu = 20\ \text{mPa}\cdot\text{s}$), activation energy and frequency factor.

T [K]	k_3 [$\text{m}^3\cdot\text{mol}^{-1}\cdot\text{s}^{-1}$]	E_a [$\text{J}\cdot\text{mol}^{-1}$]	k_0 [$\text{m}^3\cdot\text{mol}^{-1}\cdot\text{s}^{-1}$]
293.4	95.0 ± 1.3	3.622×10^4	2.690×10^8
298.2	121.4 ± 1.9		
303.1	155.8 ± 2.3		
307.8	190.0 ± 5.3		

Contrarily to the influence observed in the rate constants of the other four reactions, in the current study the additive Rheolate 255 increased slightly the value of k_3. The registered difference between both media is around 7% at $20\,^{\circ}\text{C}$.

4.5 Conclusions

Some relevant conclusions and remarks can be withdrawn from the work developed and presented in this chapter.

The kinetics of the reactions belonging to the test system should be previously known for the working up of the experimental plan for micromixing characterization and also for the validation of the simulation programs of micromixing processes.

The test system studied refers to the azo coupling between 1 and 2-naphthols and diazotized sulfanilic acid. The analytical technique used to follow the kinetics of the reactions was the UV/vis spectrophotometry. Thus, the spectra of reagents and products involved needed to be determined. For that, $p-R$, $o-R$ and Q were synthesized, isolated/purified in a solid form and identified. The purity of the synthesized chemicals was demonstrated by most of the identification techniques employed. This result had a particular interest in the case of both monazo isomers; seeing that they are also reagents (Equations 4.3 and 4.4), and their existence in a solid and pure form was required for the kinetic studies.

The spectra of bisazo dye, S, were determined directly from the resulting solution after reaction of $o-R$ and B, by assuming a 100% yield. The observed low success attained in its synthesis from the reaction between $p-R$ and B (see Section 4.2.5.1) was attributed to the fact that this reaction is slower, which gives more opportunity to the occurrence of side reactions (between B and S, as shown Figure 4.20).

To compare with the published data, the spectra of the reagents and products were first determined in the same physico-chemical conditions (here called "standard conditions of the non-viscous medium"). The UV/vis spectra of A_1, A_2, $p-R$ and $o-R$ obtained in the present work were very similar to the published data. The spectrum of Q obtained by using the synthesized solid differed in magnitude from the published values, however, it is coincident with the published spectrum when Q is produced in solution without purification and isolation steps. In the literature it was found a controversy around the spectrum of S. The spectrum obtained in this work is similar to the published by Bourne et al. (1990), however the experimental procedure followed was similar to that recommended by these authors.

The diazotized sulfanilic acid is the common reagent in all reactions here studied. Due to its high sensitivity to light, its spectrum was not possible to be determined. When it was

necessary to verify its concentration, this was made by an indirect method, performing the reaction $A_1 + B$.

Having obtained all spectra of the reagents and products, this work continued with the kinetic study. This part comprised two distinct kinetic studies, with different standard conditions: (i) aqueous non-viscous medium ($I = 444.4\ \text{mol}\cdot\text{m}^{-3}$, $\text{pH} = 9.9$, $T = 25°\text{C}$ and $\mu = 1\ \text{mPa}\cdot\text{s}$) and (ii) aqueous viscous medium ($I = 222.2\ \text{mol}\cdot\text{m}^{-3}$, $\text{pH} = 9.9$, $T = 20°\text{C}$ and $\mu = 20\ \text{mPa}\cdot\text{s}$). The reason for the study in non-viscous medium was to compare with the literatures values and by this way to validate the methodology adopted. The second part of the kinetic study, in viscous medium, was to extend the application limits of the test reaction to systems with higher viscosity.

It is important to mention that the diazotized sulfanilic acid is unstable in neutral or alkaline solution, so that the reactions were conducted in a dilute aqueous solution at pH 9.9. This was achieved by buffering the other reagent solutions which will react with diazotized sulfanilic acid (A_1, A_2, $p-R$ or $o-R$), with Na_2CO_3/$NaHCO_3$ in excess of the quantities needed to neutralize the protons formed in the coupling and initially present in the acidic B-solution ($\text{pH} \cong 2$) (Bourne et al., 1985). In this way, the pH of the solution did not change during the reactions.

The rate constants, the activation energy and the frequency values for the five reactions in aqueous non-viscous medium are presented in Table 4.20.

Table 4.20 Summary of the rate constants ($I = 444.4\ \text{mol}\cdot\text{m}^{-3}$, $\text{pH} = 9.9$, $\mu = 1\ \text{mPa}\cdot\text{s}$ and $T = 25°\text{C}$), E_a and k_0 obtained in this work.

	k_i [$\text{m}^3\cdot\text{mol}^{-1}\cdot\text{s}^{-1}$]	E_a [$\text{J}\cdot\text{mol}^{-1}$]	k_0 [$\text{m}^3\cdot\text{mol}^{-1}\cdot\text{s}^{-1}$]
$A_1 + B \xrightarrow{k_{1o}} o-R$	1129 ± 32	3.037×10^4	3.934×10^9
$A_1 + B \xrightarrow{k_{1p}} p-R$	17695 ± 501	3.037×10^4	3.934×10^9
$o-R + B \xrightarrow{k_{2p}} S$	21.63 ± 0.68	3.919×10^4	1.611×10^8
$p-R + B \xrightarrow{k_{2o}} S$	2.866 ± 0.092	4.205×10^4	6.643×10^7
$A_2 + B \xrightarrow{k_3} Q$	115.09 ± 2.49	3.710×10^4	3.605×10^8

The majority of the values are in good agreement with those published by Bourne's team (team that dedicated their investigation to the test reaction system in study), with exception of k_1 ($k_1 = k_{1o} + k_{1p}$) and k_{2o}, where the differences were considered significant.

All five reactions are fast, so that to follow their kinetics suitable equipment (in the present case, the stopped-flow apparatus), with short time response and with an efficient reagents mixing device, is required. Any limitation or problem in these demanded characteristics has high repercussions on the first azo couplings because they are "instantaneous" reactions. One reason for the registered differences in k_1 values could be that the equipment used for the kinetic study was different from that used by other research groups.

The difference encountered in the k_{2o} value can be attributed to the purity level of the solids used.

The values of E_a and k_0 obtained in the presented work are of the same order of magnitude as the published.

The correction of the profile concentration in the optical cell was irrelevant in this study, since the differences between the values of k_1 (most unfavourable scenario) were about 2 or 3% when the profile was neglected. However the developed tool could be useful in other kinetics studies, involving reactions even more rapid and equipment with other geometric parameters (α and β).

These five second-order rate constants refer to stoichiometric reagent concentrations (e.g., 1-naphthol), not to the reactive species (e.g. 1-naphtholate ion). Conversion to this basis may be made using the pK values, given in the previous sections, when required. All concentrations referred in this work are relative to the total concentration c_{i0} and not to the reactive specie. The kinetics is refered to this concentration, too.

The second part of the kinetic study, in aqueous viscous medium, was conducted in different standard conditions. Besides the viscosity, the temperature and the ionic strength were changed. The temperature selected had as reference the average value of the ambient laboratory temperature. The ionic strength needed to be modified due to a solubility problem of the buffer in the new solvent.

It was necessary to choose an additive to increase the aqueous solution's viscosity. The choice of the additive, for the simultaneous reaction of 1- and 2-naphthol and diazotized sulfanilic acid, was not an easy assignment. The diazotized sulfanilic acid is an unstable compound, being light sensitive and unstable in aqueous solutions ($\mathrm{pH} > 7$) requiring storage at low

temperature ($<5^{\circ}\mathrm{C}$) to minimize its decomposition. The diazonium ions can suffer several kinds of reactions such as nucleophilic substitution SN1 and SN2, reduction reactions, and other problems (Morrison and Boyd, 1983). The presence of an additive in solution, mainly in high concentrations, can promote those unwanted reactions. The degradation of this reagent by the various additives studied can be explained by the medium composition, namely nucleophilic groups as hydroxyl in the glycerol case. Although HEC also contains hydroxyl groups in the side chains as well as in the cellulose backbone, it did not attack diazotized sulfanilic acid, due to its low concentration.

From the other polymers investigated (from the Rheolate family) the one that presented less instability for diazotized sulfanilic acid was Rheolate 255. However, it was needed to make a polymer pre-neutralization because its solution was alkaline ($\mathrm{pH} = 9$).

The fact of Rheolate 255 being inert in the presence of the present chemical compounds, together with its Newtonian flow behavior up to concentrations $3.8\,\mathrm{wt.\%}$ and to shear stress of $3000\,\mathrm{s}^{-1}$, make it the best additive. To ensure the Newtonian behavior in a wide shear rate range, it was necessary to limit the value of viscosity to $20\,\mathrm{mPa\cdot s}$. Despite this value of viscosity being inferior to that initially desired ($100\,\mathrm{mPa\cdot s}$), it is the highest value used with the present test reaction system.

Because of the small quantities of additive necessary to obtain highly viscous solutions, it is expected that the polymer does not influence the kinetics. The results obtained from the kinetic study are summarized in Table 4.21.

The kinetic results for higher viscosity media were not directly correlated with the previous work on non-viscous media. Two possible reasons can explain this fact: (i) chemical interference of the additive with reactions or (ii) mixing limitations due to the lower Reynolds number in the mixing chamber of stopped-flow apparatus. The Reynolds number in the flow system of stopped-flow apparatus is greater than 10^4, in mixing solutions with viscosity of the order of $1\,\mathrm{mPa\cdot s}$, ensuring turbulent flow in the mixing chamber, however when the viscosity rises twenty times the flow regime changes to laminar and mixing problems can arise.

Except for k_3, all kinetic constants decreased in the presence of the additive. The percentages of that decrease were not the same among the reactions, being greater for the second coupling with the *para* isomer.

Table 4.21 Summary of the rate constants ($I = 222.2\ \text{mol}\cdot\text{m}^{-3}$, $\text{pH} = 9.9$, $\mu = 20\ \text{mPa}\cdot\text{s}$ and $T = 20 \pm 0.5^{\circ}\text{C}$), E_a and k_0 obtained in this work.

	$k_i\ [\text{m}^3\cdot\text{mol}^{-1}\cdot\text{s}^{-1}]$	$E_a\ [\text{J}\cdot\text{mol}^{-1}]$	$k_0\ [\text{m}^3\cdot\text{mol}^{-1}\cdot\text{s}^{-1}]$
$A_1 + B \xrightarrow{k_{1o}} o-R$	1355 ± 55	2.694×10^4	8.815×10^8
$A_1 + B \xrightarrow{k_{1p}} p-R$	12199 ± 492	2.694×10^4	8.815×10^8
$o-R + B \xrightarrow{k_{2p}} S$	14.06 ± 0.07	5.210×10^4	2.622×10^{10}
$p-R + B \xrightarrow{k_{2o}} S$	1.278 ± 0.021	6.033×10^4	7.294×10^{10}
$A_2 + B \xrightarrow{k_3} Q$	95.0 ± 1.3	3.622×10^4	2.690×10^8

It is important to call attention to the fact that the kinetics rate constants of Table 4.20 and Table 4.21 can not be compared directly due to the different standard conditions, i.e., the viscosity is not the only different parameter, but mainly the temperature. The ionic strength is also different but a separate study proved that this parameter did not influence those values in the evaluated range ($222.2 \le I \le 444\ \text{mol}\cdot\text{m}^{-3}$), which was expected due to the fact that the diazotized sulfanilic acid is a zwitterion.

Some final remarks:

- In any experimental series for both media (viscous and non-viscous) for the data treatment, the fit between the experimental curves and the curve of the theoretical model adopted was very good, which means that the kinetics of those reactions are well represented by a global second order model (first order in each reagent);
- Dyes can associate when the concentration is sufficiently high. The observed linearity between absorbance and concentration indicates that association did not occur here, i.e., the linearity of the Lambert-Beer law for the concentration range used was verified;
- Bourne et al. (1990) described as significant the effect of ionic strength on extinction coefficient but it was not quantified. In this work this was not verified in the range $222.2 - 888.8\ \text{mol}\cdot\text{m}^{-3}$;
- The practical information given by Bourne and co-workers (1985) and here confirmed about the spectrophotometric analysis of product mixtures, the occurrence of a side reaction (degradation of the bisazo dye by excess diazonium ions) and its influence on the analysis, and the kinetics of the coupling reactions.

5. Micromixing in NETmix® and RIM Reactors

5.1 Introduction

In many sectors of the chemical industry it is very well known problems resulting from an inefficient mixing process and the subsequent important economic and environmental effects (e.g. in controlling the formation and emission of by-products). Solid waste incineration, dyestuffs and polymer production are examples of processes where those problems can arise.

Chemical reaction is unaffected by mixing if the reagents are completely mixed down to the molecular scale (micromixing) before significant reaction occurs. However, when the time constants of the reactions are on the order of or smaller than those of the relevant heat and mass transfer processes, the product distribution and quality of the fast, multiple reactions can be affected (Bourne, 1993).

At pilot scale the mixing of low-viscosity liquids is generally attained after about $1\,\mathrm{ms}$ for liquid volumes of the order of microliters or for small volumetric flow rates ($\mu\mathrm{L}\cdot\mathrm{s}^{-1}$). An example is the stopped-flow apparatus employed on the kinetic study stated in Chapter 3 and Chapter 4. Conversely, such rapid mixing is not easily obtained on the industrial scale, except for prohibitively excessive inputs of power. Turbulence is generally used to promote this rapid mixing and the short time contact of the liquids ($\leq 1\,\mathrm{s}$) (Demyanovich and Bourne, 1989; Forney and Gray, 1990).

Nowadays, the development of efficient mixing devices with industrial applications constitutes the main goal of many research teams. The present work arose in a research team at LSRE/FEUP, where two different technologies for static mixing were developed: (i) the NETmix® static mixer and reactor (Lopes et al., 2005a; Laranjeira, 2006) and (ii) a T-mixer (also called mixing chamber) used in reaction injection molding, RIM, technology (Teixeira, 2000; Santos, 2003; Lopes et al., 2005b). These two mixing devices were studied by both computational fluid dynamics (CFD) simulation and experimental characterization using various techniques such as: (i) visualization of flow fields by laser doppler anemometry (LDA) and particle image velocimetry (PIV) techniques, (ii) macro and micromixing assessment.

The test reaction system discussed in Chapter 4 was used on the micromixing characterization studies of the two mixers. In fact, the five reactions studied can constitute two distinct test systems for mixing characterization: reaction between 1-naphthol and diazotized sulfanilic acid and the simultaneous reaction between 1 and 2-naphthol and diazotized sulfanilic acid, here denoted by *simplified test system* and *extended test system*, respectively.

In this work, the simplified test system was used in aqueous non-viscous medium to characterize the mixing quality on the NETmix® static mixer device (see Section 5.3) whereas the extended test system was applied in aqueous viscous medium on a mixing chamber of RIM machine (see Section 5.4).

Owing to analytical and kinetics factors, both test systems have limitations and range of applicability on the micromixing characterization studies, which are discussed in more detail in Section 5.2.

5.2 Range of Application and Limitations of the Test Systems

When a chemical reaction is used to test the micromixing quality of a particular device, the relative rates of mixing and reaction must be considered. These rates can be expressed by their respective characteristics times: the characteristic reaction time, $t_{\text{reaction}} = 1/k\,c_0^{n-1}$ (where c_0 is the initial concentration of limiting reagent and n is the global reaction order), and the characteristic mixing time, t_{mixing}, i.e., the time required for the reagents to diffuse to one another. Thus, the relative values of t_{reaction} and t_{mixing} express competition between reaction and mixing, which lead to different product distributions and can be classified as (Baldyga and Bourne, 1999; Paul et al., 2004):

- $t_{mixing} << t_{reaction}$ - *chemical* or *slow regime*. Homogenization is fast and precedes reaction. The product distribution is chemically controlled and it depends on the initial stoichiometric reagents ratio and the ratio of the rate constants.
- $t_{mixing} >> t_{reaction}$ - *fully-mixing* or *instantaneous regime*. Reaction is extremely fast, but the actual rate is limited by the rate of mixing by diffusion. The product distribution is controlled by mixing degree.
- $t_{mixing} \approx t_{reaction}$ - *mixing-controlled* or *fast regime*. Reaction rate is lower than predicted from kinetics, but higher than predicted from diffusion without reaction, i.e., the rate is influenced by physical and chemical factors. In this regime, both the mixing and kinetics determine the product distribution.

The effect of mixing should be observed in the last two cases, i.e., a chemical reaction becomes mixing-controlled if $t_{reaction}$ is of the order of or smaller than that of the mixing process. However, the maximum sensitivity to micromixing effects is achieved when the reaction time is of the same order of magnitude as the micromixing time, i.e., in the mixing-controlled regime. It should be also noted that the reaction can be classified as slow when compared with micromixing, but fast or instantaneous when compared with mesomixing or macromixing (Baldyga and Bourne, 1999).

It could be misleading the statement that a particular reaction is mixing sensitive, because this sensitivity is manifested under a particular set of experimental conditions. For instance if the goal is to have the reaction less sensitive or even independent of the mixing degree, in some cases, it could be achieved by diluting the reagents, lowering the temperature or increasing intensity of mixing in order to change from a condition where $t_{mixing} \leq t_{reaction}$ to another where $t_{mixing} > t_{reaction}$ (Bourne, 1984).

In the case of using a test reaction system to perform the micromixing assessment studies, the objective is exactly the opposite, i.e., the test system should be mixing-sensitive. Consequently, the experiments must be operated in only (micro)mixing-controlled regime and the effects of macro- and mesomixing have to be excluded. Thus, the experimental conditions should be wisely selected in order to attain this regime, taking into consideration that each test system has intrinsic limitations and range of applicability, which are presented in Sections 5.2.1 and 5.2.2 for the simplified and for the extended test systems, respectively.

5.2.1 Simplified Test System

The so-called simplified test system is composed by the competitive and consecutive (series) reactions between 1-naphthol, A_1, and diazotized sulfanilic acid, B, and can be translated by the simplified scheme:

$$\begin{aligned} A + B &\xrightarrow{k_1} R \\ R + B &\xrightarrow{k_2} S \end{aligned} \tag{2.1}$$

where $R = o-R + p-R$; $k_1 = k_{1o} + k_{1p}$ and $k_2 = \%o-R\, k_{2p} + \%p-R\, k_{2o}$.

This simplified way to translate the reaction scheme is useful for two reasons: (i) the mass balance equations are more easily deductible and workable and (ii) the limitation of the analytical method demands it, because the three-component ($o-R$, $p-R$, S) spectrophotometric analysis at pH 9.9 has been found to give inadequate resolution between the monoazo isomers due to their overlapping spectra (see Figures 4.11 and 4.14).

In the micromixing characterization studies, the above reactions should run with less than the stoichiometric quantity of B, i.e., $N_{A10}/N_{B0} > 0.5$, usually $N_{A10}/N_{B0} > 1$. In this way, any quantity of S formed indicates poor mixing at the molecular level.

The product distribution of this test system is usually characterized by the fraction of the limiting reagent B which is converted to secondary product S, defined as (Bourne et al., 1990):

$$X_S = \frac{2c_S}{c_{o-R} + c_{p-R} + 2c_S} = \frac{2c_S}{c_R + 2c_S} \tag{5.1}$$

This parameter, X_S, is called the segregation index or selectivity in S and decreases as the mixing quality increases. It also signals the extent to which the reagents are segregated on the molecular scale. The value of X_S ranges between zero and unity depending on whether the regime is slow or instantaneous, respectively. The left side scheme of Figure 5.1 shows a simple and elucidative example of both regimes and their effect in the X_S values.

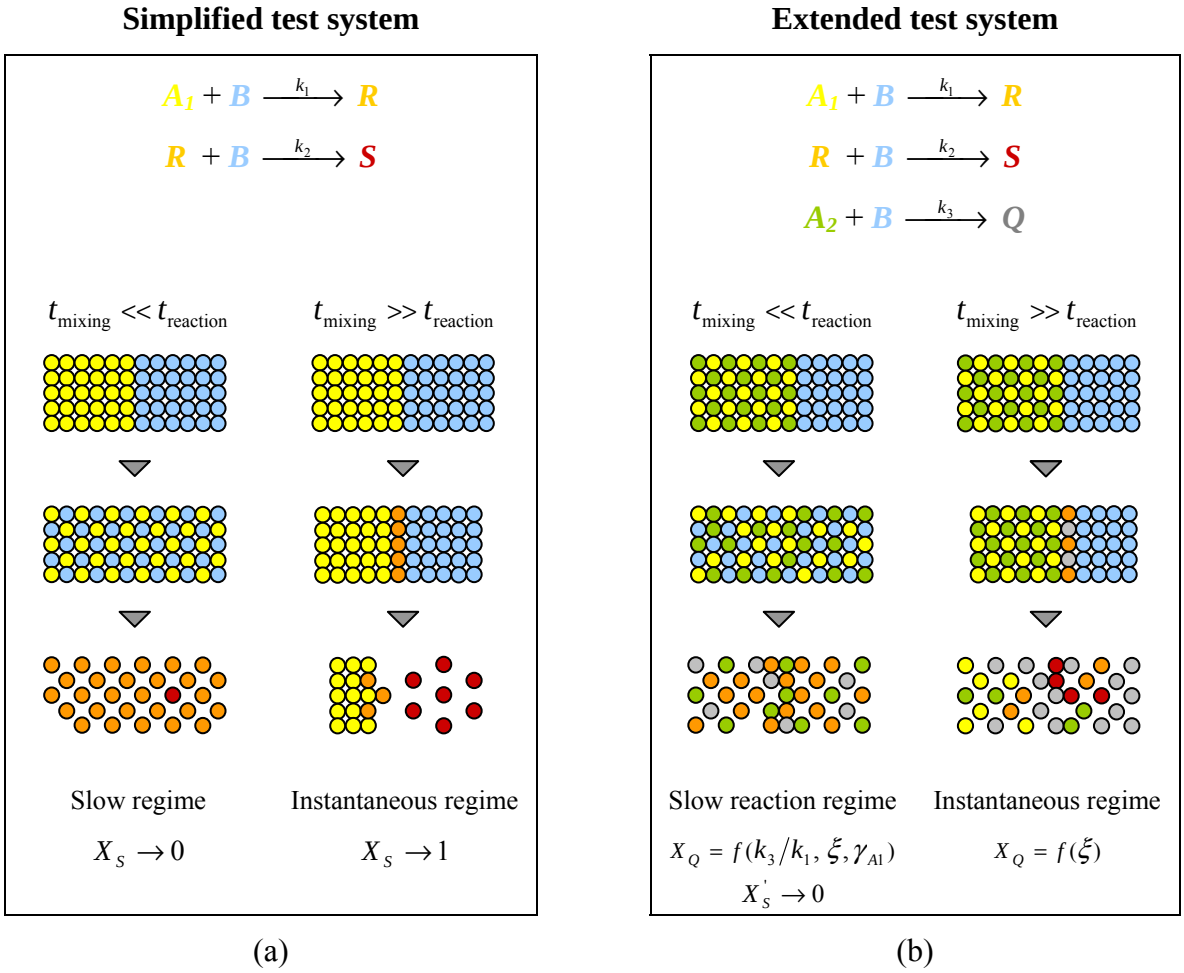

Figure 5.1 *Effect of the mixing and reaction times relative values in the product distribution for: (a) consecutive-competitive reactions; (b) competitive-consecutive-parallel reactions.*

It was considered that a cloud of each reagent A_1 (yellow balls) and B (blue balls) brought in contact, where B is the limiting reagent. The product distribution as well as X_S differ considerably between the slow and the instantaneous regime.

5.2.1.1 Slow Regime

In the slow regime, mixing occurs rapidly and finishes before significant chemical reaction takes place. Seeing that $k_1 >> k_2$, the B molecules have scarce opportunity to be in contact with R molecules (orange balls) to produce S (red balls). Thus, the reaction stops when the molecules B are extinct. In the final reaction mixture there is present mainly the product R and the quantity of S produced is virtually zero. In addition, in this regime the yield of R and X_S are governed by the ratios k_1/k_2 and c_{A10}/c_{B0} .

For example, assuming the following conditions, $I = 444.4\ \text{mol}\cdot\text{m}^{-3}$, $\text{pH} = 9.9$, $\mu = 1\ \text{mPa}\cdot\text{s}$ and $T = 20\ ^\circ\text{C}$ the ratio k_1/k_2 is 5.311×10^3 (see Sections 4.3.1 to 4.3.3), the influence of c_{A10}/c_{B0} on X_S value was determined for the cases where the reaction occurs in: (i) a plug-flow (batch or semi-batch) reactor, PFR; and (ii) in a continuous stirred tank reactor, CSTR. The steady-state values for both reactors are shown in Figure 5.2.

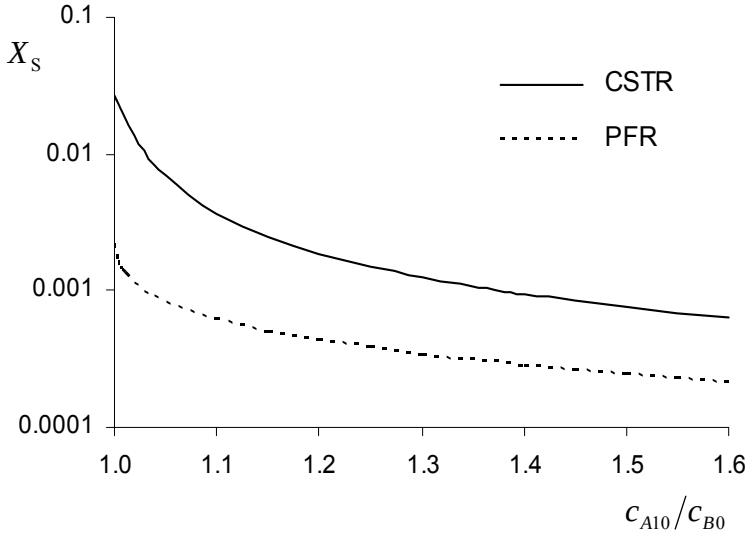

Figure 5.2 Influence of c_{A10}/c_{B0} on the value of X_S for PFR and CSTR in slow regime, $k_1/k_2 = 5.311\times10^3$.

The values of the Figure 5.2 were obtained by solving the non-linear algebraic equation of the following mass balance

$$2\frac{c_{A1}}{c_{A10}} + \frac{c_R}{c_{A10}} + \frac{c_{B0}}{c_{A10}} - 2 = 0 \tag{5.2}$$

where c_R/c_{A10} depends on the reactor design: for a PFR, batch or semi-batch reactor

$$\frac{c_R}{c_{A10}} = \frac{1}{1-k_2/k_1}\left[(1-X_{A1})^{k_2/k_1} - 1 + X_{A1}\right] \tag{5.3}$$

and for a CSTR

$$\frac{c_R}{c_{A10}} = \frac{X_{A1}(1-X_{A1})}{1-(1-k_2/k_1)X_{A1}} \tag{5.4}$$

and $X_{A1} = (c_{A10} - c_{A1})/c_{A10}$.

From Figure 5.2, it can be seen that the formation of S in the slow regime can be increased by decreasing the initial stoichiometric ratio between A_1 and B. However, any value of X_S is below the limit of the sensibility of the analytical technique used – spectrophotometry, established by Bourne and co-workers (1990) as $X_S = 0.04\,(\pm 0.003 - 0.004)$.

5.2.1.2 Instantaneous Regime

In the instantaneous regime, the time constant for reaction is much shorter than that for mixing. The rate of consumption of the reagents is infinitely high and the zone of reaction is restricted to the boundary surface between A-rich and B-rich regions. In this case, any R formed no longer survives due to overexposure to B, reacting to form S. The final product mixture is composed practically only by S and unreacted A, so that $X_S \to 1$. In this way, X_S is not chemical-controlled and independent on the kind of reactor.

This regime represents the situation of the extreme segregation and the maximum value of X_S in achieved. However, the higher values of X_S can not be experimentally practiced with the present test system due to the occurrence of side reactions evolving the product S. Bourne and co-workers (1990) referred the value of 0.4 as the upper limit of X_S.

5.2.1.3 Applicability of the Simplified Test System

The simplified test system has a range of applicability in studying micromixing, where X_S should fall in the range 0.04-0.4. The limited stability of S is the responsible for the upper limit of X_S. Besides, it also demands a reaction mixture analysis within a few hours of taking a sample always followed by a mass balance check.

A micromixing experiment planning should be made in order to work on the fast regime, where the sensitivity to mixing is higher. For example, when the study refers to a high intensive mixing device, where the characteristic mixing time is short, sometimes it is necessary to increase the temperature in order to also decrease the reaction time ($t_{\text{reaction}} = 1/k_1 c_{B0}$). This can be also be attained by increasing the reagents concentration, however this option is limited by the solubility of 1-naphthol and diazotized sulfanilic acid, which is $9.1\ \text{mol}\cdot\text{m}^{-3}$ and $60\ \text{mol}\cdot\text{m}^{-3}$, respectively.

The lower limit of X_S restricts the application of the simplified test system to mixers whose rates of turbulent energy dissipation is less than $200-400\mathrm{W}\cdot\mathrm{kg}^{-1}$ (Bourne et al., 1992a). The study of more intense mixing devices, e.g. rotor stator mixers and static mixers ($100-5000\ \mathrm{W}\cdot\mathrm{kg}^{-1}$) could be reached by using a faster reaction (Bourne and Maire, 1991), and thus the introduction of the extended test system.

5.2.2 Extended Test System

The extended test system results from the addition of a third reaction (or fifth reaction, if it is considered the reactions of the isomers of R), between 2-naphthol, A_2, and diazotized sulfanilic acid, B, to the simplified test system. The general reaction scheme is traduced by:

$$A_1 + B \xrightarrow{k_1} R \tag{4.24}$$

$$R + B \xrightarrow{k_2} S \tag{5.5}$$

$$A_2 + B \xrightarrow{k_3} Q \tag{4.5}$$

The new test system appeared in order to answer the need to perform micromixing studies in high intensity mixing devices, where the range of applicability of the simplified test system is exceeded. The addition of the third reaction, faster than the secondary azo coupling reactions, allows a decrease of the characteristic reaction time

$$t_{\text{reaction}} \approx \frac{1}{k_3 c_{B0}} \tag{5.6}$$

In the extended test system, the product distribution can be defined by two variables: the fraction of the limiting reagent B which is converted to S and to Q, denoted by $X_S^{'}$ and X_Q, respectively (see Equations 5.7 and 5.8).

$$X_S^{'} = \frac{2\,c_S}{c_{o-R} + c_{p-R} + c_Q + 2\,c_S} = \frac{2\,c_S}{c_R + c_Q + 2\,c_S} \tag{5.7}$$

$$X_Q = \frac{c_Q}{c_{o-R} + c_{p-R} + c_Q + 2\,c_S} = \frac{c_Q}{c_R + c_Q + 2\,c_S} \tag{5.8}$$

Usually a single solution containing both naphthols is prepared for the micromixing studies. When this solution is brought into contact with the diazotized sulfanilic acid solution, different product distributions are possible, depending of the kind of regime: slow, fast or instantaneous.

The experimental conditions (e.g. initial reagents concentration ratios) should be suitable chosen in order to perform the mixing characterization under the fast regime, where $t_{\text{mixing}} \approx t_{\text{reaction}}$. The product distribution for this regime is not possible to predict without models that relate mixing and chemical reaction. Conversely and similarly to the description for the simplified test system, the product distribution in the slow and instantaneous regimes are easily predictable.

Figure 5.1b shows a schematic example of a possible product distribution obtained in both slow and instantaneous regimes. It was considered that an equimolar solution of 1-naphthol (yellow balls) and 2-naphthol (green balls) was brought in contact with the limiting reagent solution, the diazotized sulfanilic acid (blue balls).

5.2.2.1 Slow Regime

In slow regime, mixing is faster than reaction so that the three reagents (A_1, A_2 and B) would be intimately mixed before any extension of reactions occurs. Thus, after the limiting reagent has been fully consumed, the product distribution is determined by the initial stoichiometric ratios and the kinetics. Since the primary couplings reactions (Equation 4.24 and 4.5) are much faster than the secondary reaction (Equation 5.5), very little S is formed so that it can be discarded in this regime. Only R and Q are formed, thus $X_S^{'}$ is approximately zero and $X_Q = f(k_3/k_1, \xi = c_{A10}/c_{A20}, \gamma_{A1} = c_{A20}/c_{B0})$.

Note that the reaction given by the Equation 5.5 can be discarded in this regime.

The influence of the initial stoichiometric ratios on X_Q is evaluated, when the limiting reagent is fully consumed, for the cases of PFR (batch or semi-batch reactors) and CSTR, as follows.

For a PFR, batch or semi-batch reactor, the mass balance to both naphthols in the reactor results in

$$\frac{dc_{A_1}}{dc_{A_2}} = \frac{k_1}{k_3}\frac{c_{A_1}}{c_{A_2}} \Rightarrow \frac{c_{A_1}}{c_{A_{10}}} = \left(\frac{c_{A_2}}{c_{A_{20}}}\right)^{k_1/k_3} \tag{5.9}$$

The reactions stop when $c_B = 0$ and the mass balance of this limiting reagent results in

$$\frac{c_{A1}}{c_{A10}} = 1 + \xi - \xi w - \frac{1}{\gamma_{A1}} \tag{5.10}$$

where $w = c_{A2}/c_{A20}$, which is the fraction of unreacted 2-naphthol, $\xi = c_{A20}/c_{A10}$ and $\gamma_{A1} = c_{A10}/c_{B0}$ represent the initial stoichiometric ratios.

Substituting Equation 5.9 on Equation 5.10, it results in:

$$w^{k_1/k_3} + \xi w - 1 - \xi + \frac{1}{\gamma_{A_1}} = 0 \tag{5.11}$$

This non-linear equation relates the yield of A_2, c_{A2}/c_{A20}, with both initial stoichiometric reagents ratios and the ratio of kinetic constants, k_1/k_3. Its resolution enables calculating subsequently the segregation index X_Q:

$$X_Q = (1 - w)\,\gamma_{A_1}\xi \tag{5.12}$$

Figure 5.3 shows the effect of some initial stoichiometric ratios on the segregation index, X_Q, for the experimental solutions referred above. $\xi = 0$ corresponds to the simplified test system case. For a given ξ, an increase of the ratio between 1-naphthol and diazotized sulfanilic acid results in the decrease of X_Q. On the other hand, keeping γ_{A_1} constant, an decrease of ξ decreases X_Q, which can attain values below the limit of analytical error.

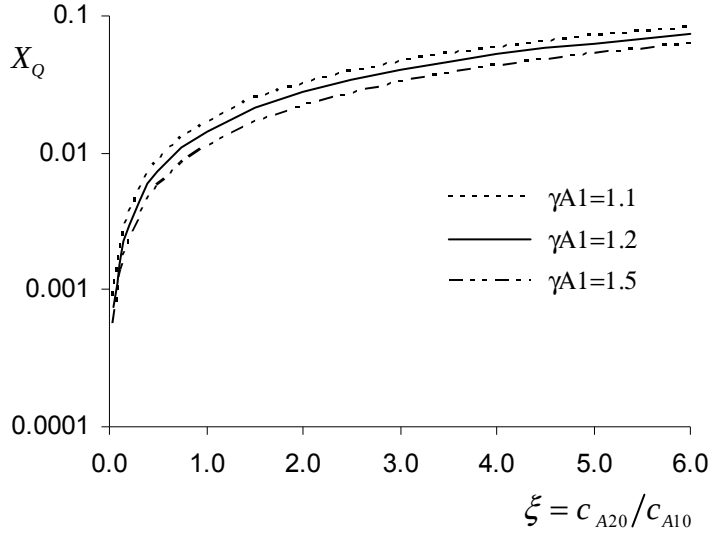

Figure 5.3 *Effect of stoichiometric ratios* $\gamma_{A1} = c_{A10}/c_{B0}$ *and* c_{A20}/c_{A10} *on* X_Q *in a PFR under slow regime,* $k_1/k_3 = 142.7$.

For a CSTR the resulting equation from the mass balances is given by:

$$\xi(1-w) - \frac{1}{1-\frac{k_1}{k_3}\left(1-\frac{1}{w}\right)} + 1 - \frac{1}{\gamma_{A_1}} = 0 \qquad (5.13)$$

The conclusions about the effects of the variables ξ and γ_{A_1} on X_Q are the same as for the PFR case, however, for the same conditions the curves of CSTR are always above the respective curves for PFR.

5.2.2.2 Instantaneous Regime

As it was already described, in this regime the reactions are instantaneous when compared with the time required for mixing. The fluids elements containing the naphthols and the diazotized sulfanilic acid remains poorly mixed, so that the intermediate R is practically all converted to the product S whilst A_2 is partially converted to Q (see Figure 5.1b). The original three equations are reduced to the following two:

$$A_1 + 2B \xrightarrow{k_1} S \qquad (5.14)$$

$$A_2 + B \xrightarrow{k_3} Q \qquad (4.5)$$

The rates of these reactions are independent of the respective rate constants and proportional to the concentrations of the reagents (Baldyga and Bourne, 1990), hence:

$$\frac{dc_{A_1}}{dc_{A_2}} = \frac{c_{A_1}}{c_{A_2}} \Rightarrow \int_{c_{A_{10}}}^{c_{A_1}} \frac{dc_{A_1}}{c_{A_1}} = \int_{c_{A_{20}}}^{c_{A_2}} \frac{dc_{A_2}}{c_{A_2}} \Leftrightarrow c_{A2} = \xi\, c_{A1} \tag{5.15}$$

In this regime it was assumed that when the limiting reagent is fully consumed, $c_R = 0$ and naturally $c_B = 0$. The mass balance of B results in:

$$x = 1 - \frac{1}{\gamma_{A_1}(2+\xi)} \tag{5.16}$$

where $x = c_{\mathrm{A2}}/c_{\mathrm{A20}}$, which is the fraction of 2-naphthol unreacted.

Finally X_Q and $X_S^{'}$ in the instantaneous regime is given by:

$$X_Q = \frac{\xi}{(\xi+2)} \tag{5.17}$$

and

$$X_S^{'} = \frac{2}{(\xi+2)} = 1 - X_Q \tag{5.18}$$

Using the last two equations it can be concluded that both segregation indexes are only dependent on the initial naphthols ratio (see Figure 5.4) and independent of $\gamma_{\mathrm{A1}} = c_{\mathrm{A10}}/c_{\mathrm{B0}}$.

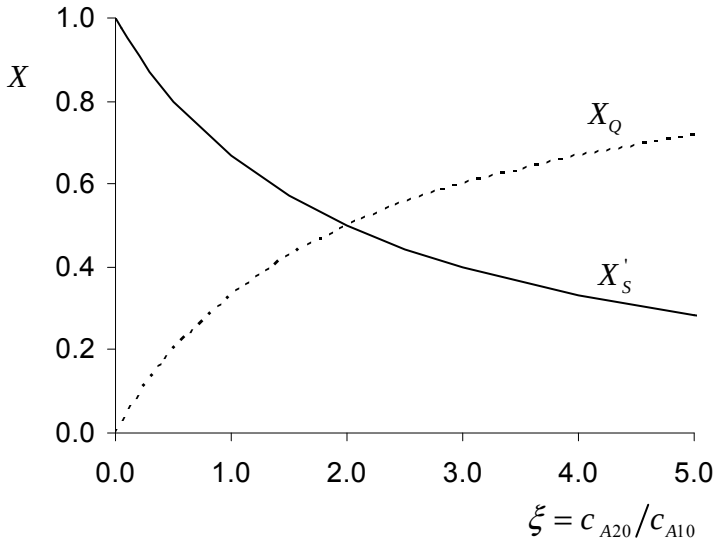

Figure 5.4 Influence of $\xi = c_{A_{20}}/c_{A_{10}}$ on $X_S^{'}$ and X_Q under instantaneous regime.

In this regime, the quantity of B initially used determines the conversion of A_1 and A_2 but not their relative rate or product distribution. Here, the problems with the analytical errors are usually inexistent, but problems arise with the formation of byproducts for which S is consumed. It is unknown the instability and degradation problems with the product Q and thus X_Q has no upper limit.

This regime as well as the slow regime should be avoided in any micromixing study, because $X_S^{'}$ and X_Q are independent of the mixing quality. For these studies the fast regime is recommendable.

5.2.2.3 Applicability of the Extended Test System

The simple calculations and simplifications made to predict the product distribution in slow and instantaneous regimes are not possible to do for the fast regime. In that case, a detailed analysis of the product distribution demands for model relating mixing and reaction.

Bourne and co-workers (1992a) used the engulfment micromixing model to predict $X_S^{'}$ and X_Q curves (against Damkhöler number) over the three regimes. They found asymptotic curves for higher energy dissipation rates ($>10^5$ $\mathrm{W \cdot kg^{-1}}$) and for low ones. Between the two extremes both curves have a sudden change, corresponding to the fast regime, where the maximum sensitivity to the mixing intensity is attained. Thus, in agreement with the mixing device to investigate, the experimental conditions must be suitably selected in order to work under fast regime. The initial concentrations and relative volume ratios, etc. of the three reagents are the variables to adjust. The naphthols are generally used in large excess in order to ensure that the reaction goes to completion in the mixer.

5.2.3 Comparison between Simplified and Extended Test System

Both simplified and extended test systems have a product distribution dependent upon mixing intensity (also expressed through the rate of dissipation of the kinetic energy of turbulent velocity fluctuations, $\varepsilon_{\mathrm{turb}}$) over a specific range of $\varepsilon_{\mathrm{turb}}$. Each test system has its own range (see Table 5.1), where the characteristic reaction time is on the order of, or smaller than that of the mixing process, thus mixing-controlled regime.

Higher $\varepsilon_{\text{turb}}$ values correspond to the slow regime, where product distribution is determined by the reaction kinetics, whereas in the instantaneous regime the product distribution no longer responds to changes in mixing intensity, occurring only when $\varepsilon_{\text{turb}}$ is below the useful range.

The useful range of the simplified test system is $0.04 \le X_S \le 0.4$ or in terms of energy dissipation rates $10^{-4} \le \varepsilon_{\text{turb}} \le 400\ \text{W} \cdot \text{kg}^{-1}$ (Baldyga and Bourne, 1999). The addition of a third fast reaction to this test system enabled to enlarge the applicability to intensive mixing rates upon $10^5\ \text{W} \cdot \text{kg}^{-1}$. This upper limit is established by the increasing analytical errors of the spectrophotometry technique for low X_Q values. On the other side, there is no upper limit for X_Q because Q is known as a stable product but it should be avoided $X_S^{'}$ can be in excess of $0.2 - 0.3$ because of the limited stability of S.

Table 5.1 Resume of the useful ranges of application of simplified and extended test systems.

	Slow regime	**Fast regime**	**Instantaneous regime**
Simplified test system	• Independent of $\varepsilon_{\text{turb}}$	• High-dependent of $\varepsilon_{\text{turb}}$ • Useful range: $0.04 \le X_S \le 0.4$ or $10^{-4} \le \varepsilon_{\text{turb}} \le 400\ \text{W} \cdot \text{kg}^{-1}$	• Independent of $\varepsilon_{\text{turb}}$
Extended test system	• Independent of $\varepsilon_{\text{turb}}$	• High-dependent of $\varepsilon_{\text{turb}}$ • Useful range: $\begin{cases} 0.03 \le X_S^{'} \le 0.3 \\ X_Q > 0.03 \end{cases}$ or $10^{-4} \le \varepsilon_{\text{turb}} \le 10^5\ \text{W} \cdot \text{kg}^{-1}$	• Independent of $\varepsilon_{\text{turb}}$

In short, the extended test system is used in this work to offer a faster chemical reaction needed to characterize some high-intensity mixers, for which the simplified test system cannot adequately be used.

Independently of the test system used, in any mixing investigation experiment, the limiting reagent B should be fully consumed. However, when the residence time in the mixer is very short (in comparison with the characteristic reaction time) or the viscosity is high, unreacted B can be present in the collected sample for analysis and then it is difficult or impossible to use and discuss the results. Thus, whenever possible, this occurrence should be avoided.

During the experimental planning of a micromixing assessment in a specific mixing device, it is desirable the know of the energy dissipation rate values practiced on that mixer in order to choose the suitable test reaction system as well as the experimental conditions such as: initial concentration reagents ratios and volumes reagents ratios. If this information is not previously available, the alternative way is start to do the experiments by the trial and error method. This was the case of both static mixers investigated in the present work: NETmix® and T-mixer from a RIM machine, presented in Section 5.3 and 5.4 respectively.

On the NETmix® it was successfully implemented the simplified test system in aqueous non-viscous medium and on the RIM machine it was used the extended test system in aqueous viscous medium. In both reactors it was investigated the influence of Reynolds number in the product distribution.

5.3 NETmix® Static Mixer

The NETmix® static mixer was developed by a research team from LSRE/FEUP (Lopes et al., 2005a; Laranjeira, 2006). It consists of a network of chambers interconnected by channels enabling the spatial control of micromixing quality and intensity along the reactor.

The adjacent technology of this static mixer enables the conduction of chemical reactions in pre-determined paths in order to obtain specific products with high selectivity, such as organic synthesis of pharmaceutical products. It can also be implemented in strongly exothermic reactions or explosives because it is possible and easier to control the dynamic temperature control along the reactor. Other applications can be the production of nanomaterials (Lopes et al., 2006), emulsions and chemicals of high added value.

The NETmix® technology is particularly suitable for reactions where mixing quality and intensity are critical. Its main advantages are: (i) the possibility of a controllable maximization of the reaction selectivity; (ii) the versatility of the operation layout by an easy implementation of different pre-mixing reagent feed schemes; (iii) the ability to control the

mean residence time of the reagents and the mixing intensity, (iv) the inclusion of temperature, pressure and concentration controls without dynamics modification and (v) inexistence of scale-up problems, since two or more NETmix® static mixers can be easily associated in parallel or in series.

Section 5.3.1 presents the major features of this technology and describes the pilot NETmix® used in this work. The study of the reaction patterns by visualization experiments is presented in Section 5.3.2, which was useful for the planning and for the interpretation of the results obtained in the micromixing studies shown in Section 5.3.3. In Section 5.3.4 it shown a simulation study about the effects in the X_S of feed schemes and the network geometry.

5.3.1 The NETmix® Reactor

The NETmix® reactor comprises a network structure that combines in an organized manner two different types of elements – chambers and channels – which are interconnected creating zones of complete mixing and of complete segregation, as it is shown in Laranjeira (2006) and Silva et al. (2008).

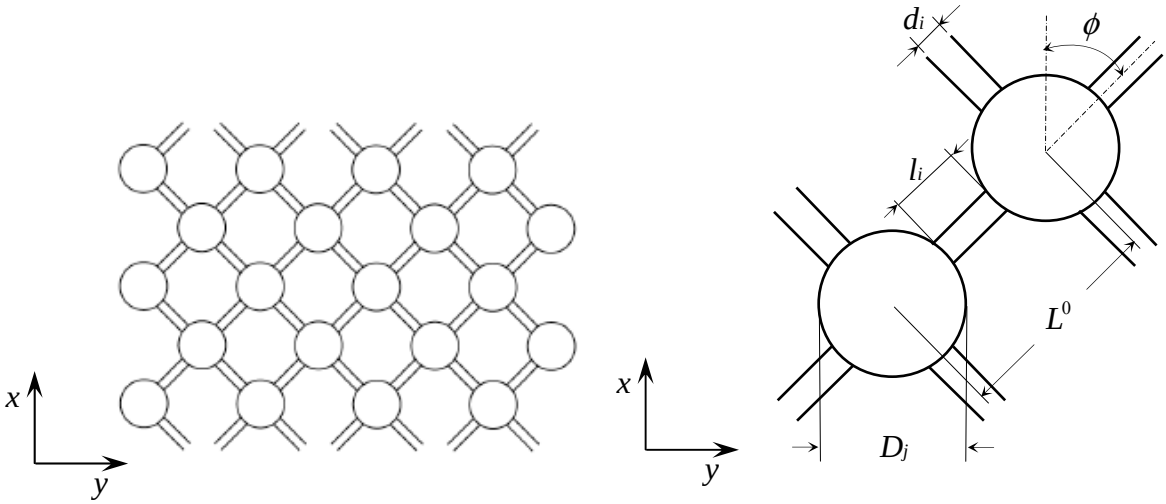

Figure 5.5 Example of a NETmix® static mixer network geometry: (a) global view (adapted from Laranjeira (2006)); (b) details of two adjacent chambers and respective connecting channels.

According to the set coordinate system of Figure 5.5a it was assumed that the direction of the flow is the x –axis. The NETmix® static mixer network size is specified by the number of chambers in the x and y directions, i.e. the number of rows and number of columns, n_x and n_y, respectively. As shown in Figure 5.5b, the chambers have a spherical geometry with diameter D_j. The channels are cylinders with diameter d_i and length l_i and they connect two

adjacent chambers that form an angle of ϕ. The oblique distance between those two chamber centers is L^0 (see Figure 5.5b). Figure 5.6 shows the technical drawings of the pilot NETmix® static mixer used in this work. It consists of $n_x = 49$ rows and 30 channels (inlet or outlet) per row. In each row the number of chambers alternates between 15 and 16, starting the first row with 15 chambers, called *inlet chambers* and ending the last row with 15 chambers denominated *outlet chambers*. With the exception of the boundary network chambers, each chamber is connected to four channels: two *inlet channels* and two *outlet channels*. In this configuration of the pilot NETmix® the chambers and channels dimensions are $D_j = 7$ mm, $d_i = 1.5$ mm, $l_i = 3$ mm, $\phi = 45°$ and $L^0 = 10$ mm, resulting in a total void volume of 1.439×10^{-4} m^3 with $\psi = V_{\text{channels}}/V_{\text{NETmix}}$ equal to 0.056. This last volume ratio is referred to as the segregation parameter (Laranjeira, 2006) and represents the segregation volume fraction existing in the static mixer and having influence in the product distribution (see Section 5.3.4.2).

Figure 5.7 is a photo of the pilot NETmix® unit and overall experimental setup used in this work. The equipment is composed of the following parts: four independent feeding reservoirs, two pump systems, a Plexiglas® static mixer (described previously), one discharging reservoir and accessories (pipes and fittings). NETmix® reactor is the core of the unit and the remaining equipment is used for the delivery of fluid with a controlled flow rate. Each *inlet chamber* has two feeding pipes: one in the front side and the other in the back side. The highest feed control was attained by feeding each front and back side of the static mixer with a single pump system (Ismatec® MCP), ensuring in this way an equal flow rate in all the 15 feeding pipes on the same side. The flow rate is manually controlled through the driver speed controller of each pump system, ranging from $1 - 240$ rpm, with a resolution of 0.1 rpm, corresponding to a flow rate of $3.15 - 750.15$ mL$\cdot$min^{-1} per pipe, at $20°$C. The maximum differential pressure that can be developed by the pump systems is 1.0 bar. The static mixer discharge is made, at atmospheric pressure, by only one of the two available discharging pipes per outlet chamber. The 15 discharging pipes are at same level in order to avoid preferential flow induced by pressure gradients (Laranjeira, 2006).

The flowing fluids used in the experiments were water or aqueous non-viscous solutions at atmospheric pressure and temperature of $20 \pm 0.5°$C, controlled by an air-conditioning equipment.

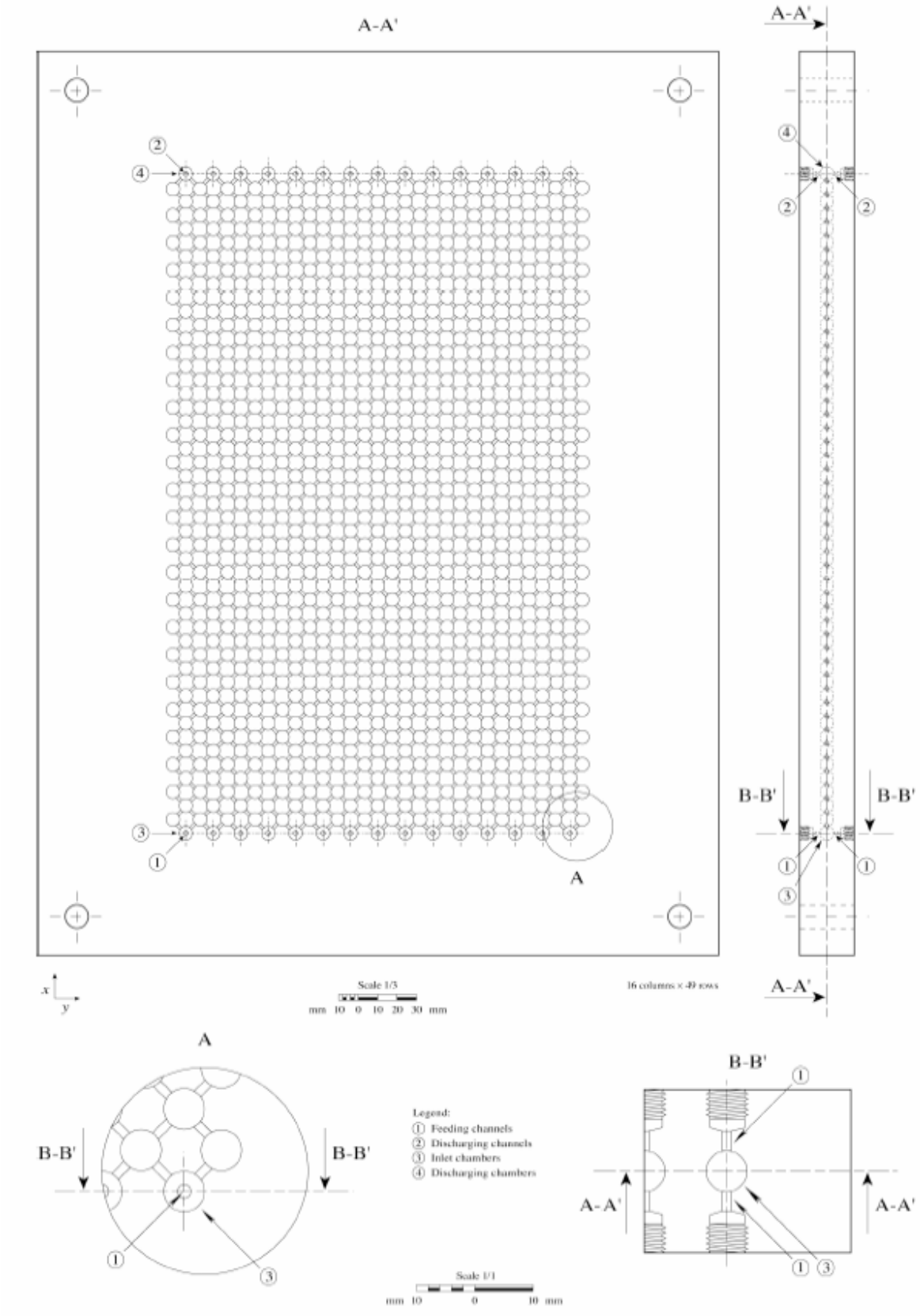

Figure 5.6 NETmix® static mixer technical drawings (Laranjeira, 2006).

Figure 5.7 Photos of the pilot NETmix® unit (adapted from Laranjeira (2006)).

5.3.2 Reaction Pattern Visualization

The NETmix® network structure determines the overall flow patterns along the reactor and consequently the residence time distribution (RTD), i.e., macromixing. Laranjeira (2006) identified two mechanisms of macromixing in the NETmix® static mixer: mixing inside the chambers and flow division. Through the first mechanism, the fluids coming from different adjacent chambers are repeatedly homogenized. The flow division occurs between successive rows of chambers since each chamber possesses two outlet channels. Moreover, the mixing phenomena are restricted to the chambers since the channels behave as plug-flow reactors (PFR), i.e, zones of total segregation. Thus, the segregation parameter introduced in Section 5.3.1 constitutes a key parameter related to mixing (Silva et al., 2008).

Both experimental and numerical macromixing assessment of this pilot NETmix® is reported in (Laranjeira, 2006). The experimental part of this work was restricted to the mixing at molecular scale characterization, by using the simplified test reaction system. In addition, mixing mechanisms existing on the NETmix® static mixer are further understood from flow pattern visualization studies. This can also be achieved by using the test system studied in the present work, since the products are colored. Since the product formation only occurs when reagents are in contact at the molecular level, it is possible to identify contact regions of both inlet streams in each chamber through the color development. For this purpose, it was carried out a set of experiments with Reynolds number in the range $50 \leq \mathrm{Re} \leq 700$. The Reynolds number is a dimensionless number defined as the ratio between the inertial and the viscous forces:

$$\mathrm{Re} = \frac{\rho\, \vartheta\, d}{\mu} \tag{5.19}$$

and, for the present static mixer experiments, Re numbers were calculated for flow on the channels.

In the tracer experiments of Laranjeira (2006), perturbations in the flow in the first three bottom chambers rows induced by pump systems were observed. However, it was also verified that this perturbation is shortly damped afterwards, vanishing in the fourth chamber row. This phenomenon was taken into account in the selection of the reagent feeding inlets for flow pattern visualization, i.e., the localization of the feeding inlets was set in such a way that contact between the reagents occurs first in the fourth chamber row from inlet. Figure 5.8

shows the selected feed scheme for flow visualization by using the test reaction system, where it can be seen that the reagents 1-naphthol, A_1, and diazotized sulfanilic acid, B, were fed separately ($c_A^{feed}/c_B^{feed} = 1.2$) in the 6th and 10th inlet chamber, respectively. The remaining inlet chambers were fed with water.

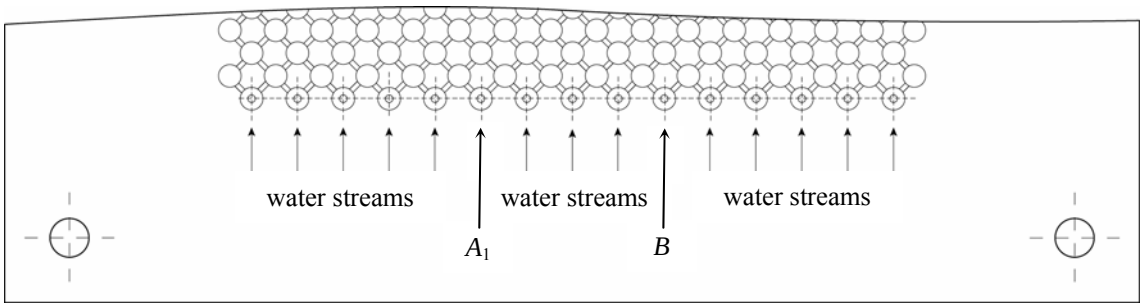

Figure 5.8 Test reaction system visualization experiments feed scheme (adapted from Laranjeira (2006)).

By both CFD simulations and tracer dynamic imaging, Laranjeira (2006) identified two types of flow field structures inside the chambers of the NETmix® static mixer: jets and vortices. He also observed the beginning of the mixing mechanisms inside each chamber (flow regime transition) at the critical Reynolds number $\mathrm{Re} = 50$, where the flow field presented a self-sustained oscillatory behavior. From $\mathrm{Re} = 50$ up to $\mathrm{Re} = 200$ the oscillation frequencies increased, i.e., the mixing intensity increased. For Re greater than 200 no improvement in mixing dynamic was observed. Consequently, the range of $\mathrm{Re} < 50$ was not studied in these visualization experiments, due to the mixing lack inside the chamber, which promotes the segregation of reagents A_1 and B along the NETmix® static mixer.

The reagents solutions were prepared in order to have $I = 444.4\ \mathrm{mol \cdot m^{-3}}$, $\mathrm{pH} = 9.9$ and $\mu = 1\ \mathrm{mPa \cdot s}$ after mixing.

Photos were taken in a steady-state flow and in the plane containing the channels and chambers centers, as shown in Figure 5.9 and Figure 5.10.

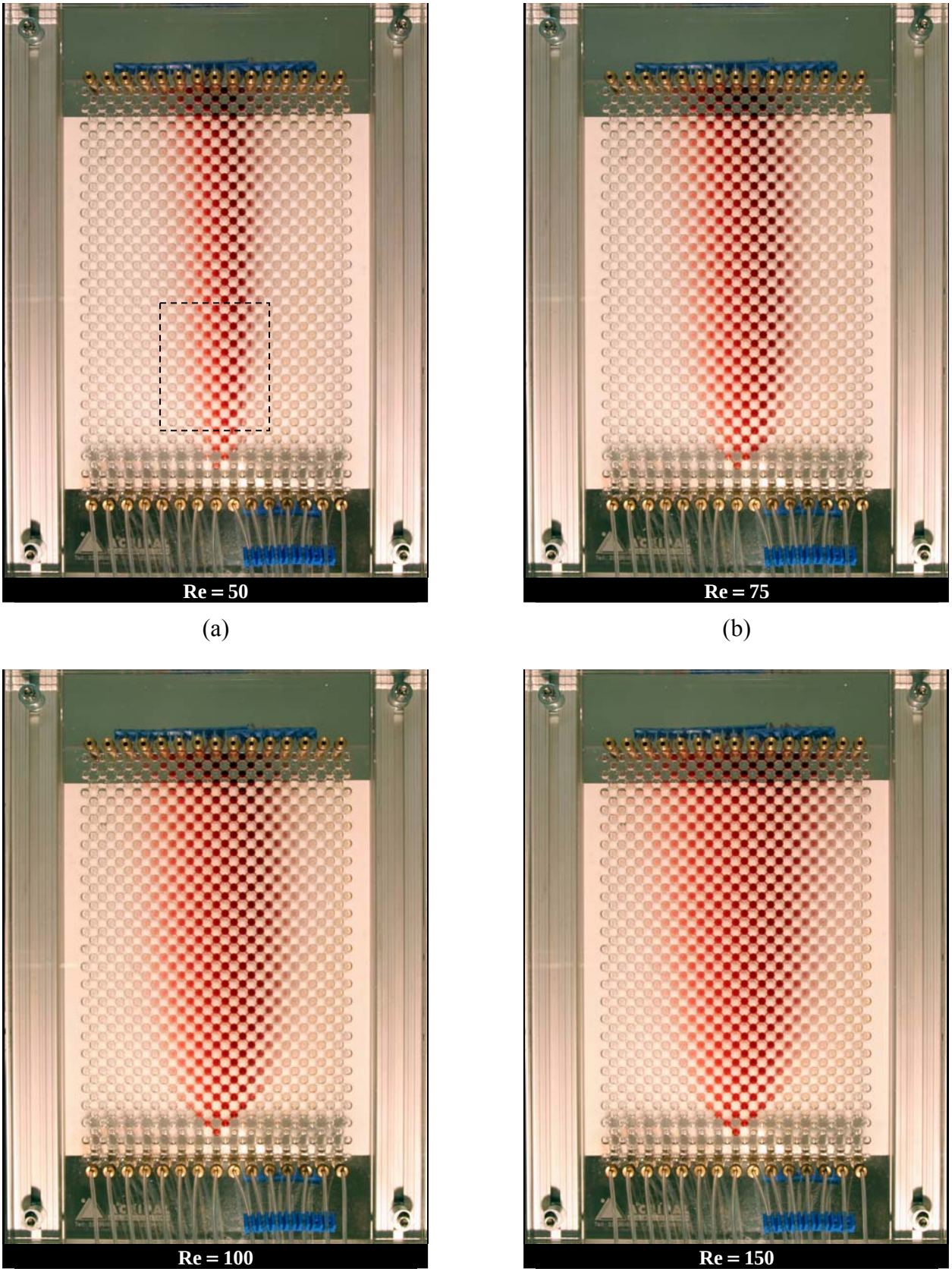

Figure 5.9 *Test system visualization experiments for Reynolds numbers ranging from $Re = 50$ to $Re = 150$: photos of the NETmix® static mixer in steady- state (Laranjeira, 2006).*

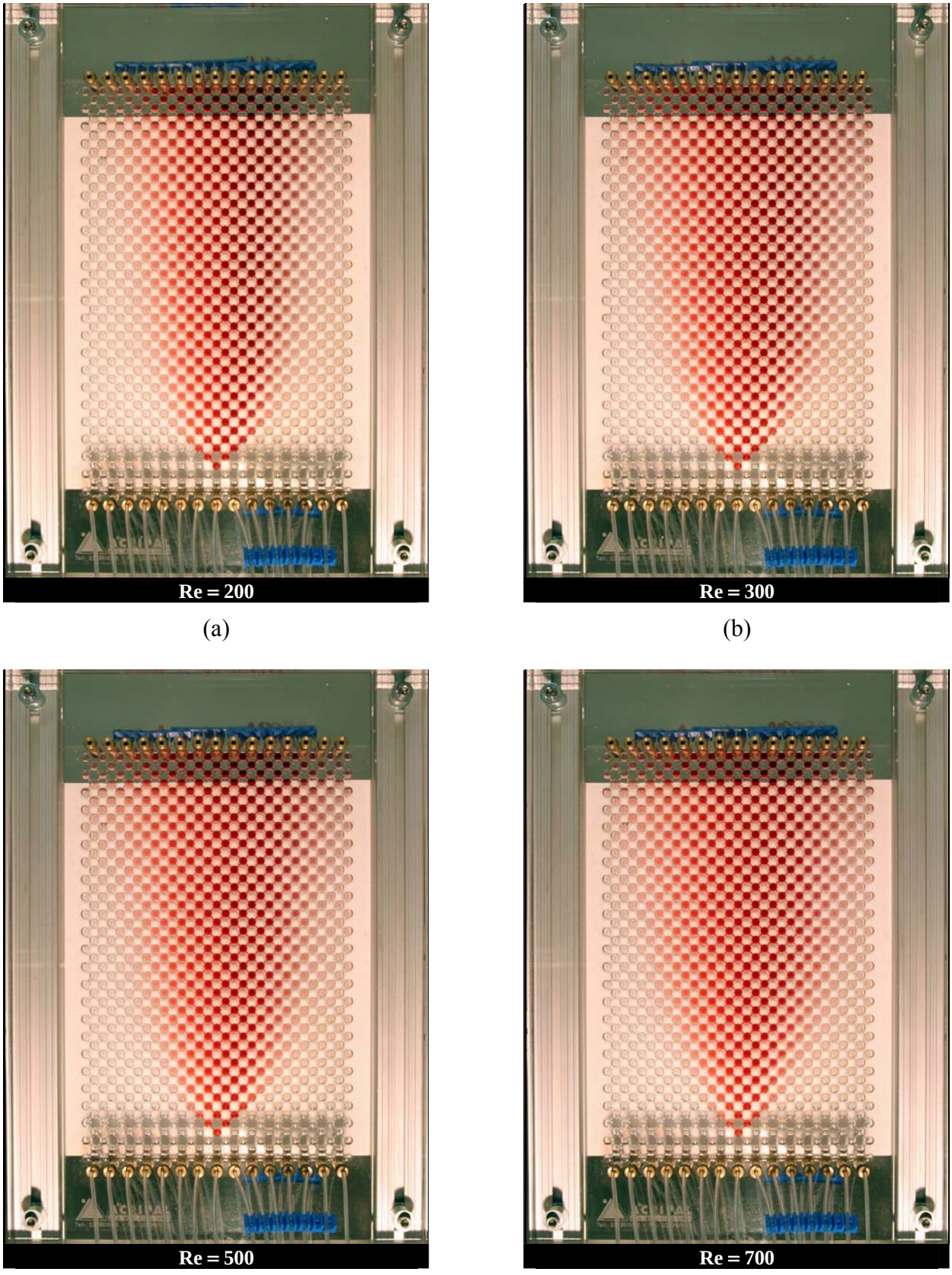

Figure 5.10 Test system visualization experiments for Reynolds numbers ranging from $Re = 200$ to $Re = 700$: photos of the NETmix® static mixer in steady-state (Laranjeira, 2006).

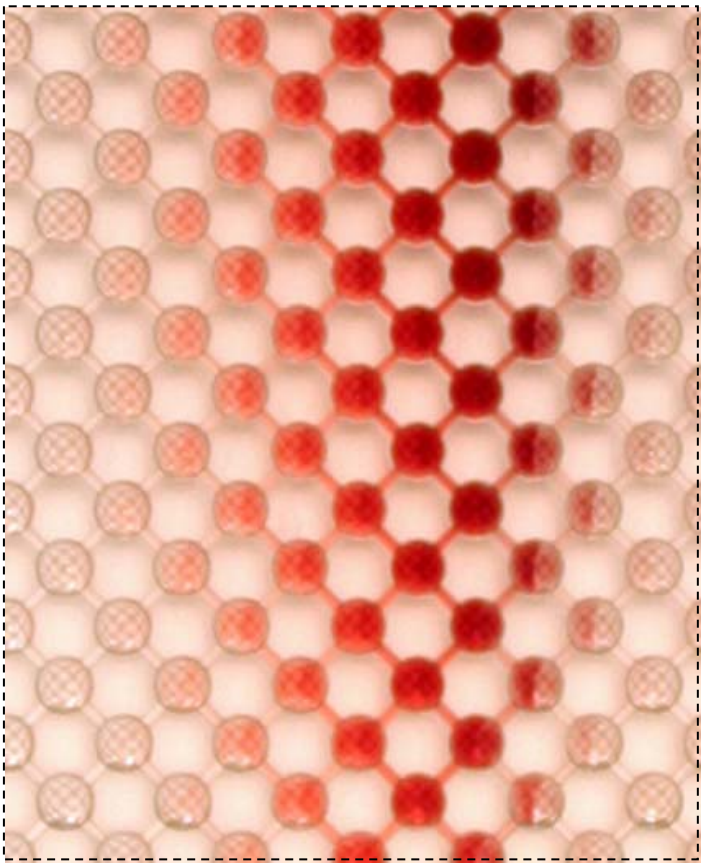

Figure 5.11 Amplification of a central region of the plume for $\mathrm{Re} = 50$.

As it was explained in Sections 4.3.1-4.3.3, the reaction between 1-naphthol, A_1, and diazotized sulfanilic acid, B, has three products: $o-R$, $p-R$ and S, whose distribution depends on the mixing quality. At $\mathrm{pH} = 9.9$, the $o-R$ and $p-R$ monoazo isomers have a red color and are impossible to be differentiated. Thus, for a simplicity, in this text they are denoted only by R. The product S has a maroon color and its formation is an evidence of poor micromixing intensity.

From the images collected, it is possible to identify the extent of the reaction zones through the color development, i.e., it is possible to do a qualitative estimation of local and global spatial product distribution.

Since reagents A_1 and B are fed separately, its first contact is visible in a single chamber of the fifth row from inlet, where the red color is exhibited, indicating the formation of R. To the upwards rows the color development appears in a larger number of chambers per row, forming a kind of plume. For lower Reynolds numbers the plume is narrow towards the exit of the NETmix®, showing that the reaction zone is limited to the central region of the mixer (see Figure 5.9a and Figure 5.9b). With increasing of Re the reaction zone is enlarged which

is visible through the continuous increasing of plume aperture, up to the physical limit of 45^{o} (see Figure 5.9 and Figure 5.10a). For $\mathrm{Re} \geq 200$ any alteration of the plume width is practically indistinguishable in photos.

Each plume reveals a color gradient throughout both main flow and normal flow directions, resulting from the asymmetric R and S spatial distribution. The reagent feed scheme used in this visualization experiments (see Figure 5.8) generates a concentration gradient along the normal flow direction for both A_1 and B. So, on the left side of the mixer it is observed only the red color, which can be explained by the greater predominance of A_1 and all B injected is immediately consumed to produce R, S being formed in residual quantities controlled by the kinetics. Further, in the present set of experimental conditions, $A_1 + B \rightarrow R$ is the unique possible reaction that can occur on the left side of the static mixer. This can be well visualized by the amplification of a central region of Figure 5.9 for $\mathrm{Re} = 50$, which is depicted in Figure 5.11. In this figure it is clearly visible the formation of R on the centre of the plume, however, its red color vanishes for the left side due to the dilution by the fluids (water and A_1) of neighboring chambers. Conversely, on the right side of the plume, B is in large excess and considerable quantities of this reagent remains unreacted even after ful consumption of A_1 into R. Thus, R has opportunity to encounter B and the maroon dye, S, is formed, which is more obvious for lower Reynolds numbers.

The occurrence of side-reactions on this side of the plume must be considered, because S flows to chambers where B is present or vice-versa (see Section 4.2.5.3). In the chambers where S is degraded the maroon color faded to give a yellowish color, which becomes very faint with time. Thus, the dilution phenomenon is not the only factor responsible for the color gradient observed from the centre to the right side of the plume, but the degradation of S should also be expected.

The product distribution (revealed by color gradient) over the static mixer and its evolution with Re allows inferring about macro and micromixing quality. Hence, the continuous decrease of S formation, over certain spatial regions with increasing Re, is an indicative of both increasingly greater spread of reagents A_1 and B through the static mixer and the increasingly reduction of local segregation, i.e., macromixing and micromixing, respectively. Besides the qualitative information obtained from these imaging experiments, they also show a general increase of both macro and micromixing, with Reynolds number. After these

experiments, the investigation proceeded to the quantitative micromixing studies, as it will be presented in the next section.

5.3.3 Micromixing Studies

Micromixing quantification is now introduced and applied to the set of experiments presented in Section 5.3.4.1. The reaction between 1-naphthol and diazotized sulfanilic acid was the test system option to perform these studies. Since it revealed to be suitable on the micromixing assessment of NETmix® static mixer, it was the unique being used.

It was previously known that static mixers are suitable characteristics for reactions needing fast mixing to obtain high product selectivity since these mixers develop high rates of energy dissipation and have short residence times (Bourne et al., 1992b). However, the energy dissipation rates values practiced in this specific static mixer were previously (to the current work) unknown.

The range of applicability of both test systems discussed in Section 5.2 recommends the extended test system employment in these investigation studies, where the energy dissipation rates are high. In spite of all that reasons, the simplified test system was the first choice to be implemented just by merely trial and error base.

As it was already seen, this simplified test system is composed by fast consecutive competitive reactions, described by Equations 4.1 to 4.4. First azo coupling reactions (4.1 and 4.2) are instantaneous and the other two are fast which characteristic time can be similar to micromixing time ($10-1000\,\text{ms}$), depending on the experimental conditions set. Hence, this test system has product distributions strongly depending upon the mixing intensity, i.e., upon the Reynolds number, and as a result, its segregation index, X_S, becomes an appropriate parameter for micromixing assessment.

The micromixing studies, shown in Section 5.2, should be performed under mixing-controlled regime. The experimental conditions were carefully chosen and/or tested in order to achieve that regime. In Section 5.3.4.1 the several experimental conditions selected to the micromixing study of NETmix® static mixer are presented, as well as the analytical method adopted.

5.3.3.1 Experimental Conditions and Analytical Method

One of the characteristics of the NETmix® static mixer is the possibility of using different reagents feed schemes as a key factor to control and attain different reaction selectivities. The reagents feed distribution configurations are numerous. In the present work, the micromixing study was limited to the pre-mixed feed scheme, shown in Figure 5.12, where the earliness of mixing is promoted.

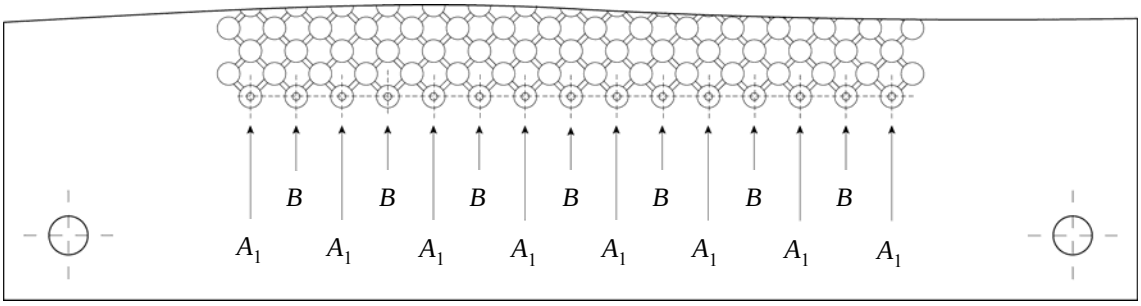

Figure 5.12 Pre-mixed feed scheme for micromixing experiments (adapted from Laranjeira (2006)).

The pre-mixed scheme consists in feed the reagents 1-naphthol (buffered), A_1, and diazotized sulfanilic acid, B, in alternating feeding chambers, so that 8 chambers are reserved to A_1 and the remaining 7 are to B. By assuming an initial complete mixing of both reagents, their concentrations were selected in order to have a initial stoichiometric ratio, c_{A10}/c_{B0}, of 1.37 (after mixing).

All experiments were carried out in aqueous non-viscous medium at: $T = 20 \pm 0.5^{\circ}\mathrm{C}$, $I = 444.4\ \mathrm{molm}^{-3}$, $\mathrm{pH} = 9.9$ and $\mu = 1\ \mathrm{mPa \cdot s}$.

The reagent concentration solutions employed to feed static mixer are listed in the Table 5.2 and were prepared as described in Sections 4.2.1.1 and 4.2.2.1 and their concentrations checked. To help the reader, it was introduced a column with the respective concentrations after mixing, i.e., assuming that the reagents are completely mixed on the first mixing chamber rows. The selection of successive lower reagent concentrations had as reason to perform experiments with increasing characteristic reaction time.

To verify the results reproducibility, two experiments were performed for each pair of concentration values, with the Reynolds number in the range $5 \le \mathrm{Re} \le 700$. Since it is supposed that reactions takes place completely within NETmix® and no concentration profile at the discharging pipes was expected to occur in this reagents feed scheme, all outlet streams

for each run were collected in a reservoir. At steady-state flow, the two samples were collected by transferring the discharging pipes from that reservoir to a sample container.

Table 5.2 List of reagents 1-naphthol and diazotized sulfanilic acid solutions for the micromixing experiments.

	Concentrations of A_1 and B in the feed	Concentrations of A_1 and B after mixing (inlet)
Pre-mixed feed scheme (see Figure 5.12)	$c_{A1}^{\text{feed}} = 0.720\ \text{mol}\cdot\text{m}^{-3}$	$c_{A10} = 0.384\ \text{mol}\cdot\text{m}^{-3}$
	$c_{B}^{\text{feed}} = 0.600\ \text{mol}\cdot\text{m}^{-3}$	$c_{B0} = 0.280\ \text{mol}\cdot\text{m}^{-3}$
	$c_{A1}^{\text{feed}} = 0.480\ \text{mol}\cdot\text{m}^{-3}$	$c_{A10} = 0.256\ \text{mol}\cdot\text{m}^{-3}$
	$c_{B}^{\text{feed}} = 0.400\ \text{mol}\cdot\text{m}^{-3}$	$c_{B0} = 0.187\ \text{mol}\cdot\text{m}^{-3}$
	$c_{A1}^{\text{feed}} = 0.240\ \text{mol}\cdot\text{m}^{-3}$	$c_{A10} = 0.128\ \text{mol}\cdot\text{m}^{-3}$
	$c_{B}^{\text{feed}} = 0.200\ \text{mol}\cdot\text{m}^{-3}$	$c_{B0} = 0.093\ \text{mol}\cdot\text{m}^{-3}$

The two samples served two purposes: (i) to ensure the sampling method reproducibility and (ii) to verify if all chemical reactions stopped at the static mixer outlet (due to the fully consumption of the limiting reagent), providing by this way a quantification of mixing only inside the NETmix® static mixer.

At the end of sampling stage, all samples were analyzed by absorbance measurements in the stopped-flow apparatus spectrophotometer (see Chapter 3) in wavelength range of $250-700\,\text{nm}$ with intervals of $10\,\text{nm}$. From these measurements, it is obtained an experimental curve, Abs_{exp}, for each sample.

5.3.3.2 Results

The methodology adopted to estimate the concentrations of the dyes, c_R and c_S, in the outlet mixture, was very similar to the described in Section 4.3.1.3. Hence, assuming that the Lambert-Beer law is valid and that the dyes in solution absorb light independently, the absorbance at a given wavelength over a optical pathlength, δ, can be estimated by:

$$Abs_{\text{calc}_\lambda} = \varepsilon_{R_\lambda}\, c_R\, \delta + \varepsilon_{S_\lambda}\, c_S\, \delta \tag{5.20}$$

where $\varepsilon_{R_\lambda} = 0.06\varepsilon_{o-R_\lambda} + 0.94\varepsilon_{p-R_\lambda}$ and ε_S are respectively the molar extinction coefficients of R and S at the same experimental conditions. ε_{R_λ} can be easily calculated from Figures 4.11 and 4.14 and ε_S is obtained from Figure 4.18.

From Equation 5.20 an absorbance curve, Abs_{calc}, can be calculated, based on reasonable estimations of both products concentrations c_R and c_S. Then, by using the Excel® Solver tool, that curve can be fitted to the experimental curve Abs_{exp}, where the fitting variables are c_R and c_S. This is done through the minimization of the deviation function

$$D^2 = \sum_{400\,\text{nm}}^{600\,\text{nm}} \left(Abs_{\text{exp}_\lambda} - Abs_{\text{calc}\,\lambda} \right)^2 \tag{5.21}$$

over the wavelengths range of $400 - 600\,\text{nm}$. Finally, the product distribution, X_S, was calculated using Equation 5.1.

In any micromixing experiment it is a requirement that at the moment of sample collection the limiting reagent, B, is fully consumed ($c_B = 0$). More, for each sample, the mass balance should be always checked:

$$\text{MB} = \frac{c_R + 2c_S}{c_{B0}} \times 100 \tag{5.22}$$

The next three tables (Table 5.3, Table 5.4 and Table 5.5) report, for each experiment, the mass balance (MB), the concentrations of R and S and X_S measured at the NETmix® static mixer outlet, in the range of Reynolds number $5 \le \text{Re} \le 700$, for the B feed concentration of: 0.6, 0.4 and $0.2\,\text{mol}\cdot\text{m}^{-3}$.

Table 5.3 NETmix® static mixer outlet product distribution in the pre-mixed feed scheme. $c_{A10} = 0.384\ \mathrm{mol \cdot m^{-3}}$ *and* $c_{B0} = 0.280\ \mathrm{mol \cdot m^{-3}}$.

Re	Experiment	MB	c_R [mol·m^{-3}]	c_S [mol·m^{-3}]	$X_S \pm$ stdev
5	Exp # 1	15.67%	0.122	0.057	0.486 ± 0.002
	Exp # 2	13.71%	0.124	0.059	
12.5	Exp # 1	4.80%	0.149	0.059	0.431 ± 0.016
	Exp # 2	5.37%	0.153	0.056	
25	Exp # 1	1.09%	0.181	0.048	0.356 ± 0.011
	Exp # 2	2.84%	0.184	0.052	
37.5	Exp # 1	1.84%	0.193	0.041	0.307 ± 0.009
	Exp # 2	0.59%	0.194	0.044	
50	Exp # 1	0.33%	0.209	0.036	0.255 ± 0.001
	Exp # 2	1.15%	0.207	0.035	
75	Exp # 1	1.37%	0.214	0.031	0.228 ± 0.003
	Exp # 2	3.43%	0.224	0.033	
100	Exp # 1	1.41%	0.224	0.026	0.188 ± 0.004
	Exp # 2	1.34%	0.224	0.026	
125	Exp # 1	0.95%	0.231	0.023	0.163 ± 0.003
	Exp # 2	0.46%	0.235	0.023	
150	Exp # 1	2.52%	0.233	0.020	0.145 ± 0.002
	Exp # 2	0.80%	0.238	0.020	
200	Exp # 1	1.89%	0.239	0.018	0.129 ± 0.001
	Exp # 2	1.38%	0.240	0.018	
250	Exp # 1	0.89%	0.246	0.018	0.125 ± 0.002
	Exp # 2	2.85%	0.238	0.017	
300	Exp # 1	0.16%	0.248	0.016	0.116 ± 0.002
	Exp # 2	0.27%	0.247	0.016	
400	Exp # 1	0.31%	0.253	0.013	0.096 ± 0.001
	Exp # 2	1.16%	0.251	0.013	
500	Exp # 1	0.39%	0.259	0.010	0.075 ± 0.001
	Exp # 2	1.18%	0.255	0.011	
700	Exp # 1	0.48%	0.259	0.010	0.075 ± 0.003
	Exp # 2	1.34%	0.254	0.011	

Table 5.4 *NETmix® static mixer outlet product distribution in the pre-mixed feed scheme.* $c_{A10} = 0.256\ \mathrm{mol \cdot m^{-3}}$ *and* $c_{B0} = 0.187\ \mathrm{mol \cdot m^{-3}}$.

Re	Experiment	MB	c_R [mol·m^{-3}]	c_S [mol·m^{-3}]	$X_S \pm$ stdev
12.5	Exp # 1	14.74%	0.106	0.027	0.340 ± 0.004
	Exp # 2	16.45%	0.103	0.027	
25	Exp # 1	10.16%	0.122	0.023	0.265 ± 0.007
	Exp # 2	4.29%	0.132	0.023	
37.5	Exp # 1	6.62%	0.139	0.018	0.200 ± 0.005
	Exp # 2	1.56%	0.148	0.018	
50	Exp # 1	3.23%	0.156	0.012	0.133 ± 0.008
	Exp # 2	2.62%	0.159	0.012	
75	Exp # 1	0.67%	0.169	0.009	0.089 ± 0.014
	Exp # 2	0.12%	0.172	0.007	
100	Exp # 1	2.99%	0.182	0.005	0.047 ± 0.009
	Exp # 2	0.28%	0.180	0.004	
125	Exp # 1	0.06%	0.183	0.002	0.024 ± 0.005
	Exp # 2	1.50%	0.184	0.003	
150	Exp # 1	1.56%	0.177	0.003	0.044 ± 0.013
	Exp # 2	2.68%	0.182	0.005	
200	Exp # 1	0.44%	0.182	0.003	0.023 ± 0.011
	Exp # 2	1.20%	0.182	0.001	
250	Exp # 1	0.64%	0.188	0.000	0.000
	Exp # 2	1.84%	0.190	0.000	
300	Exp # 1	-1.47%	0.189	0.000	0.000
	Exp # 2	0.68%	0.185	0.000	
400	Exp # 1	0.69%	0.188	0.000	0.000
	Exp # 2	0.38%	0.186	0.000	
500	Exp # 1	1.35%	0.189	0.000	0.000
	Exp # 2	0.12%	0.186	0.000	
700	Exp # 1	0.06%	0.187	0.000	0.000
	Exp # 2	2.06%	0.191	0.000	

Table 5.5 *NETmix® static mixer outlet product distribution in the pre-mixed feed scheme.* $c_{A10} = 0.128\ \mathrm{mol \cdot m^{-3}}$ *and* $c_{B0} = 0.093\ \mathrm{mol \cdot m^{-3}}$.

Re	Experiment	MB	c_R [$\mathrm{mol \cdot m^{-3}}$]	c_S [$\mathrm{mol \cdot m^{-3}}$]	$X_S \pm$ stdev
5	Exp # 1	17.63%	0.052	0.012	0.320 ± 0.001
	Exp # 2	19.02%	0.051	0.012	
12.5	Exp # 1	11.45%	0.063	0.010	0.240 ± 0.001
	Exp # 2	13.69%	0.061	0.010	
25	Exp # 1	3.95%	0.075	0.007	0.170 ± 0.005
	Exp # 2	2.29%	0.075	0.008	
37.5	Exp # 1	0.07%	0.082	0.006	0.119 ± 0.004
	Exp # 2	0.50%	0.082	0.005	
50	Exp # 1	0.88%	0.088	0.003	0.073 ± 0.009
	Exp # 2	2.86%	0.088	0.004	
75	Exp # 1	1.72%	0.093	0.001	0.026 ± 0.011
	Exp # 2	5.98%	0.096	0.002	
100	Exp # 1	1.21%	0.094	0.000	0.006 ± 0.008
	Exp # 2	6.51%	0.098	0.001	
125	Exp # 1	4.46%	0.097	0.000	0.010 ± 0.005
	Exp # 2	3.41%	0.095	0.001	
150	Exp # 1	3.66%	0.097	0.000	0.000
	Exp # 2	0.71%	0.094	0.000	
200	Exp # 1	1.29%	0.095	0.000	0.000
	Exp # 2	4.69%	0.098	0.000	
250	Exp # 1	4.49%	0.098	0.000	0.000
	Exp # 2	1.16%	0.094	0.000	
300	Exp # 1	1.09%	0.094	0.000	0.000
	Exp # 2	14.37%	0.097	0.000	
400	Exp # 1	4.71%	0.098	0.000	0.000
	Exp # 2	3.16%	0.096	0.000	
500	Exp # 1	2.25%	0.095	0.000	0.000
	Exp # 2	3.43%	0.097	0.000	
700	Exp # 1	0.05%	0.093	0.000	0.000
	Exp # 2	3.61%	0.097	0.000	

For the three set of experiments, the curves of the product distribution, X_S, against the Reynolds numbers are shown in Figure 5.13, where the horizontal lines represent the range of applicability of the simplified test system ($0.04 \le X_S \le 0.4$) presented in Section 5.2.1.

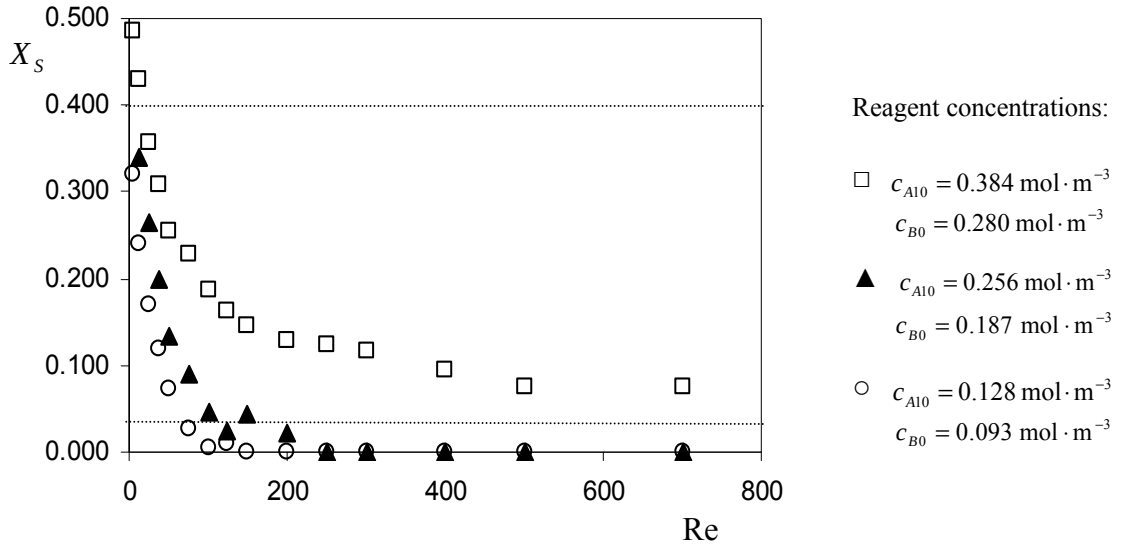

Figure 5.13 Effect of Reynolds number in the product distribution at discharging pipes of the NETmix® static mixer. Pre-mixed feed scheme, $c_{A10}/c_{B0} = 1.37$, $T = 20^{\circ}\text{C}$, $I = 444.4\ \text{mol}\cdot\text{m}^{-3}$, $\text{pH} = 9.9$ *and* $\mu = 1\ \text{mPa}\cdot\text{s}$.

According to the discussion in the previous section about the beginning of mixing mechanisms in the NETmix® static mixer, it has been expected some failure for the experiments carried out below critical Reynolds number ($\text{Re} = 50$). Low mixing intensity or even lack of mixing means segregation. Thus, the consequences of that in the static mixer are visible in both unclosed mass balance, MB, and in high product distribution X_S. For lower values of Re, in most of the experiments the MB ranges in the interval $5-15\%$, which is naturally unsatisfactory, and X_S attains values beyond the upper limit 0.4 in two cases. The experiments where these problems occurred should be discarded or interpreted just in a qualitative way.

For the remaining Reynolds numbers the mass balance check closes within $\pm 2\%$ in most of the experiments for three set experimental conditions. The limit of uncertainty on X_S was rarely greater than ±0.005.

Figure 5.13 shows product distribution, X_S, as a function of Reynolds number for all three set of experimental conditions with different reaction times. As Re increases, the value of X_S

decreases sharply, to the asymptotic value of zero, where X_S no longer depends upon Re, i.e. the chemical regime (or slow regime) is attained. Furthermore, the results show that as concentrations increase, a higher Re is necessary to obtain $X_S = 0$ or, in other words, higher mixing rates are needed by faster reactions before the slow regime is asymptotically attained.

The experimental data series, where the reaction times are higher ($c_{B0} = 0.093\ \mathrm{mol \cdot m^{-3}}$ and $c_{B0} = 0.187\ \mathrm{mol \cdot m^{-3}}$), reach the low limit of applicability of the test system, $X_S = 0.04$, rendering impossible to assess the mixing by quantitative way for higher Reynolds numbers.

These results suggest that the series $c_{B0} = 0.280\ \mathrm{mol \cdot m^{-3}}$ is more suitable for this study, because the whole range above the critical Reynolds number of the NETmix® static mixer is possible to be assessed. The characteristic reaction time for this experiment is $\cong 1\ \mathrm{s}$, which is 1.5 and 3 times lower than that obtained for the experiment where $c_{B0} = 0.187\ \mathrm{mol \cdot m^{-3}}$ and $c_{B0} = 0.093\ \mathrm{mol \cdot m^{-3}}$, respectively.

The series $c_{B0} = 0.280\ \mathrm{mol \cdot m^{-3}}$ shows a remarkable increasing mixing efficiency as Re increases up to $\mathrm{Re} = 200$. For higher Reynolds numbers the process mixing efficiency increases only slightly, i.e., the effects of Re in the mixing intensity are not so evident and the curve tends to become flat. The same effect is observed by the other two series but due to the low analytical accuracy the results for $\mathrm{Re} > 100$ can not be used.

From the visualization experiments (Section 5.3.3), no differences in mixing efficiency were registered for $\mathrm{Re} > 200$. However, this study reveals that mixing still increases in that range, though less and less, until the product distribution is no longer in a mixing controlled regime. Therefore, the slow regime achieved in the series $c_{B0} = 0.093\ \mathrm{mol \cdot m^{-3}}$ and $c_{B0} = 0.187\ \mathrm{mol \cdot m^{-3}}$ has $X_S^{\mathrm{NETmix\_exp}} = 0$. The achievement of the slow regime in the series $c_{B0} = 0.280\ \mathrm{mol \cdot m^{-3}}$ is not evident, however, the curve seems to tend to $X_S^{\mathrm{NETmix\_exp}} = 7.50 \times 10^{-2}$. The value of the product distribution X_S predicted by simulation of NETmix® network (see more details in Section 5.3.4) was $X_S^{\mathrm{NETmix\_sim}} = 1.78 \times 10^{-3}$ and for CSTR and PFR reactors design (by Figure 5.2) were $X_S^{\mathrm{CSTR}} = 1.01 \times 10^{-3}$ and $X_S^{\mathrm{PFR}} = 2.98 \times 10^{-4}$, respectively. In addition, assuming a complete mixed feed in the first

mixing chambers rows, the results of the simulation for $c_{A10}/c_{B0} = 1.37$ and $100 \leq \mathrm{Re} \leq 700$ are $1.85\times10^{-3} \leq X_S^{\mathrm{NETmix\_sim}} \leq 1.78\times10^{-3}$.

All predicted values are lower than the experimental value. However, those values can never be experimentally reached because they are out of the range of applicability of the test system.

Although Laranjeira (2006) reported the absence of inertial-convective processes (macromixing) for below the critical Reynolds number, all experimental series in the present work show a mixing evolution in a consistent manner in that range. Very likely, the instantaneous regime is attained (where $X_S \rightarrow 1$) for mixing intensity rates below the critical Reynolds number but cannot be identified by using this test system due to its own limitations, as it was mentioned in Section 5.2.1.

The pre-mixed feed scheme is not the only workable option of the NETmix® static mixer. Depending on the desired selectivity for a specific reaction, the feed scheme can adopt other configurations, generally called *segregated feed schemes*. Comparatively to these, in the pre-mixed feed scheme of NETmix® static mixer it is expected the lower X_S (or higher selectivity in R), for a given hydrodynamic operating condition, seeing that the feed configuration used aims at accelerating mixing. This feed configuration was the only experimentally investigated in the current work. However, in next section other segregated schemes are studied by macromixing simulation of the NETmix® network.

5.3.4 NETmix® Macromixing Simulation

The macromixing modeling of NETmix® static mixer presented in this work was made by using the NETmix® network model similar to the developed by Laranjeira (2006). This model considers that the chambers and the connecting channels behave as two different ideal continuous-flow reactors: (i) channels behave as plug-flow reactors (PFR), zones of total segregation and (ii) chambers behave as perfectly mixed continuous stirred tank reactors (CSTR), zones of complete mixing. The matrix of association of these reactors is the same represented in Figure 5.6. More, the model developed by Laranjeira (2006) uses an analogy to a pure resistive electrical circuit to simulate the distribution of flow rates inside any regular or irregular network. Since the present pilot NETmix® network is regular (all chambers have dimension $D_j = 7$ mm and all channels have dimensions $d_i = 1.5$ mm and $l_i = 3$ mm), in the model developed in this work (and based in the previous model) the flow rates inside the pilot

NETmix® network were assumed to be equal for all channels. Thus, the chambers flow rate is to the double of the channels flow rate, with the exception of the boundary network chambers that is equal to one channels flow rate.

In short, this kind of models is typically used to represent the residence time distribution (RTD), where nothing is specified about micromixing, because this does not influence RTD. It is a model of the bulk flow pattern and macromixing.

The NETmix® model is used to simulate the reactive mixing of initially separate feed streams of reagents A_1 and B, with different feed schemes (see Section 5.3.4.1). It is assumed that the reagents of the different feeds are mixed completely when they enter the network. For a micromixing modeling it would be necessary to use a micromixing model to describe how the separate feeds interact, but this was not done here.

The micromixing studies stated in Section 5.3.3 were performed using a pre-mixed feed scheme, where the reagents A_1 and B are fed in alternate feeding pipes. However, as it was reported before, the NETmix® static mixer is a device that gives other feed options in order to attain for instance different product distributions. The feed scheme or the network geometry can be used as operational conditions to obtain the desirable reaction selectivity, favoring for example one secondary product.

The purpose of the next two sections is to investigate the influence in the product distribution, X_S, of: (i) four different feed schemes (Section 5.3.4.1) and (ii) three network geometries, where the macromixing is evaluated theoretically in terms of the dimensionless number RTD and product distribution for different reagents feed schemes (Section 5.3.4.2). The reactions used correspond to the simplified test system, which are a representative of the group of competitive-consecutive reactions that can be used in this reactor. The rate constants used in the simulations are referent to: $T = 20^{\circ}\mathrm{C}$, $I = 444.4\ \mathrm{mol \cdot m^{-3}}$, $\mathrm{pH} = 9.9$ and $\mu = 1\ \mathrm{mPa \cdot s}$.

5.3.4.1 Influence of the Feed Scheme in the Product Distribution

The investigated feed schemes were: (i) one *pre-mixed* (previously used in micromixing experiments, see Figure 5.12) and (ii) three denominated *segregated feed schemes*, shown schematically in Figure 5.14.

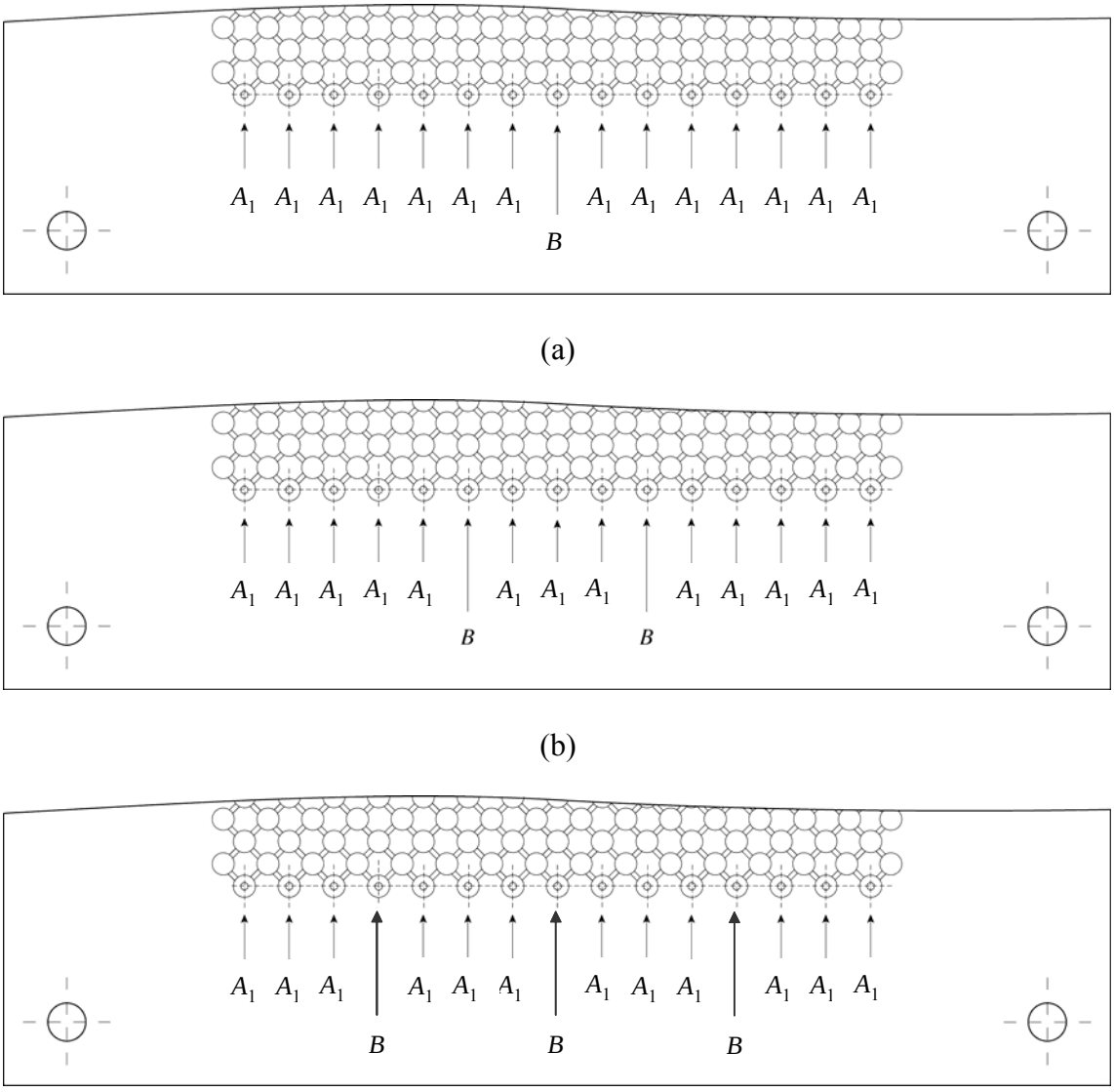

Figure 5.14 Segregation feed schemes: (a) Scheme 1; (b) Scheme 2 and (c) Scheme 3 (adapted from Laranjeira (2006)).

The concentration of each reagent A_1 and B used in the simulations are summarized in Table 5.6 for feed schemes simulated. The feed concentrations were selected so as to have inlet concentrations ($c_{A10} = 0.24\ \text{mol}\cdot\text{m}^{-3}$ and $c_{B0} = 0.20\ \text{mol}\cdot\text{m}^{-3}$ given a reagent ratio of $c_{A10}/c_{B0} = 1.20$) equal in all cases, if mixing of the 15 feed streams was virtually possible to attain in any scheme.

Table 5.6 List of reagents 1-naphthol and diazotized sulfanilic acid solutions for the different feed schemes in the NETmix® macromixing simulation.

	Number feed inlets		Feed concentrations [mol·m^{-3}]		Inlet concentrations [mol·m^{-3}]	
Feed scheme	A_1	B	c_{A1}^{feed}	c_B^{feed}	c_{A10}	c_{B0}
Pre-mixed scheme	8	7	0.450	0.429	0.240	0.200
Segregated scheme 1	14	1	0.257	3.000	0.240	0.200
Segregated scheme 2	13	2	0.277	1.500	0.240	0.200
Segregated scheme 3	12	3	0.300	1.000	0.240	0.200

Simulations were carried out at Reynolds numbers ranging from 100 to 700. The values of X_S were calculated for each NETmix® outlet and the results obtained for $\text{Re} = 100$ and $\text{Re} = 700$ are shown in Figure 5.15. Note that, despite for $\text{Re} = 100$ the flow inside the network NETmix® is not yet completely developed (see Section 5.3.2), it was studied just to have an example of segregation state to compare with a mixing state case: $\text{Re} = 700$.

Concerning the pre-mixed scheme, the values of X_S obtained are near zero (ca. 10^{-3}) and the reason for that is that this scheme promotes the initial state of effectiveness of mixing of the reagents A_1 and B before significant reaction occurs. Since k_1 is much higher than k_2, R is mainly formed and B is fully consumed. In this way S has no chance to be produced.

Figure 5.15 shows that the use of segregated feed schemes leads to higher X_S than the pre-mixed feed scheme. For a given Re, increasing from 1 to 3 B-feed inlets decreases X_S. The reason is that the local B/A_1 concentration ratio near the entrance to NETmix®, where most of the reaction occurs, is lower when more B-feed inlets are present. So, B is not in such a high excess and less R is converted to S. This decrease in the local B/A_1 ratio implies that B spreads more normal to the flow direction when more feed inlets are used.

Note that the concentration gradient normal to the direction of flow is steepest for 1 B-feed feed and the gradient is almost zero for 3 B-feed inlets.

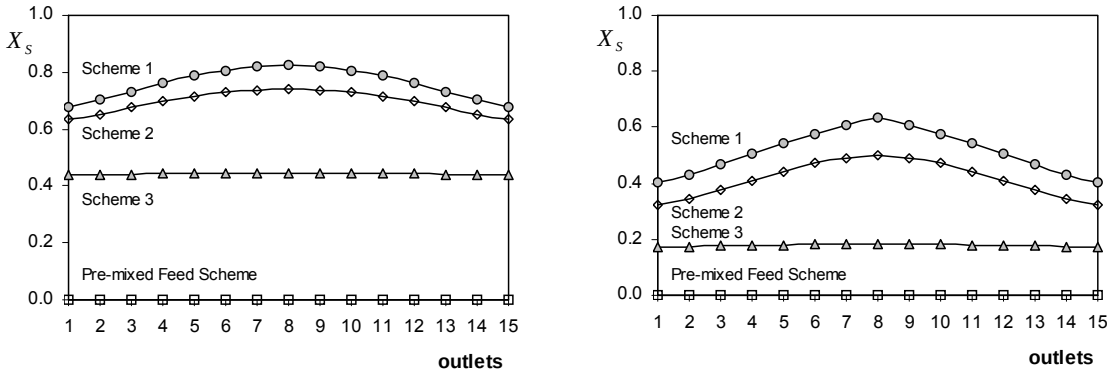

Figure 5.15 X_S *obtained at the several NETmix® outlets for the three segregated feed schemes and the pre-mixed feed scheme for: (a)* $\mathrm{Re} = 100$ *and (b)* $\mathrm{Re} = 700$.

In any of feed schemes an increase of Re decreases X_S. In fact, increasing Re causes faster exchange/macroflow in direction normal to the main flow and this promotes faster mixing between A_1 and B. Consequently, the formation of S is reduced and of R increased.

For a given feed scheme it is observed a concentration gradient steepen with increase of Re, which is more obvious in Scheme 1 and 2. The network residence time decreases with the increasing of Re, consequently slowest reaction occurs spatially far from network inlet, i.e., in the onwards network rows. More, in segregated feed schemes with few and central B-feed inlets, the secondary product is mainly formed in the central region of the network. Thus, S has few rows up to outlet to spread over the normal flow direction.

The average values of X_S at NETmix® outlet are summarized in Table 5.7 for the four feed schemes simulated as well as the values obtained for CSTR and PFR (from Figure 5.2), where reagents are completed mixed at the entrance of reactors and the slow regime is present. The higher X_S value corresponds to segregated Scheme 1 for $\mathrm{Re} = 100$ and the lower values were obtained in the pre-mixed scheme for $\mathrm{Re} = 700$. These two cases in Table 5.7 correspond to the weakest and strongest mixing of two reagents streams. The values of X_S obtained in the pre-mixed scheme are between the values obtained for CSTR and PFR, but is of the same order of magnitude of the values for CSTR. This means that this network configuration of NETmix® under the best mixing operational conditions behaves closest a CSTR than PFR.

Table 5.7 Average outlet values of product distribution, X_S, obtained by in the NETmix® macromixing simulation for the different feed schemes and for CSTR and PFR.

	X_S	
Feed scheme	Re = 100	Re = 700
Pre-mixed scheme	1.82×10^{-3}	1.62×10^{-3}
Segregated scheme 1	7.59×10^{-1}	5.15×10^{-1}
Segregated scheme 2	6.95×10^{-1}	4.14×10^{-1}
Segregated scheme 3	4.42×10^{-1}	1.78×10^{-1}
CSTR	1.87×10^{-3}	
PFR	4.33×10^{-4}	

These simulations of the macromixing in NETmix® static mixer allow inferring about a hypothetical experimental micromixing study using the simplified test system. The values of X_S obtained in the most of the simulation sets for the segregated feed schemes exceed the upper limit of applicability of this test system (see Table 5.1). The occurrence of side reactions can happen which makes unfeasible the implementation of the simplified test system in micromixing studies in this mixing device when these feed schemes are practiced. However, the extended test system seems to be more suitable since the parallel reaction ($A_2 + B \rightarrow Q$) of this system is faster than $R + B \rightarrow S$, avoiding the occurrence of side reactions of S degradation.

In addition, this numerical study permit to conclude that the use of segregated feed schemes in the NETmix® static mixer is well appropriate to favour the production of a secondary product of competitive-consecutive reactions. Besides the feed schemes, the versatility of this mixer allows manipulating other operational parameters in order to attain that goal. For instance, it is possible to change the network geometry in its: (i) number of rows and columns, (ii) dimensions of chamber, channel, angle ϕ (see Figure 5.5b) and (iii) number of channels per chamber.

In this work it is evaluated the influence of three network geometries in the product distribution, X_S. The study is presented following.

5.3.4.2 *Influence of the Configuration of NETmix® Network in the Product Distribution*

The macromixing for a given network can be characterized by its Residence Time Distribution – RTD. In the NETmix® model, the network structure determines the overall flow patterns and thus the RTDs. Laranjeira (2006) defined the NETmix® dimensionless RTD function, $E(\Theta)$, as

$$E(\Theta) = \frac{n_x}{(1-\psi)(n_x-1)!}\left[\frac{n_x(\Theta-\psi)}{1-\psi}\right]^{n_x-1} e^{-\frac{n_x(\Theta-\psi)}{1-\psi}} H(\Theta-\psi) \qquad (5.23)$$

where Θ is the dimensionless residence time $\Theta = t/\tau$, τ is the network mean residence time, ψ the segregation parameter defined previously as $\psi = V_{\text{channels}}/V_{\text{NETmix}}$ and $H(\Theta-\psi)$ is the Heaviside function defined as $H(\Theta-\psi) = \begin{cases} 0 & \Theta < \psi \\ 1 & \Theta \geq \psi \end{cases}$.

Several markedly different network geometries can display similar RTDs, but different product distributions. Therefore, three different network geometries with the same network volume were considered for investigation (see Table 5.8). Their denomination is: *Prototype*, *Design 1* and *Design 2*.

Table 5.8 Geometric parameters of various NETmix® networks.

Network	D_j [mm]	d_i [mm]	L^0 [mm]	ϕ	n_x	n_y	ψ
Prototype	7.0	1.5	10	45°	49	15	0.056
Design 1	6.0	1.5	16	45°	63	15	0.229
Design 2	5.9	1.0	10	45°	83	15	0.056

The Prototype geometry corresponds to the pilot NETmix® mixer studied in the previously sections. Design 1 has higher value of segregation parameter ψ and it exhibits a RTD with the smaller variance (see for example Fogler (1999)) than those of the Prototype (see Figure 5.16a). Finally, the network Design 2 has the same value of segregation parameter ψ of the Prototype and exhibits a RTD with the similar variance to the one of the Design 1 (see Figure 5.16a). More, all geometries have the same number of inlet chambers, 15, and four connecting channels per chamber.

The simulations were carried out at $\mathrm{Re} = 600$ for the three segregated feed schemes of Figure 5.14 and for the three network geometries. The inlet reagent concentrations used were the same stated in Table 5.6. The results are shown in (see Figure 5.16b).

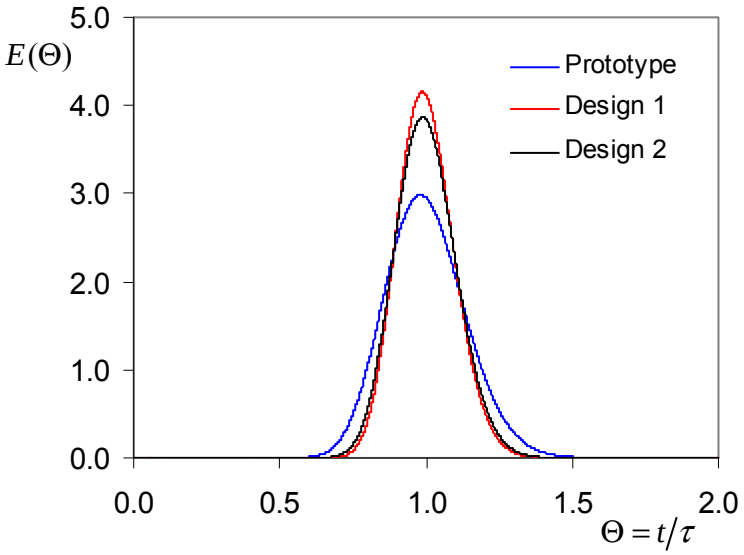

(a)

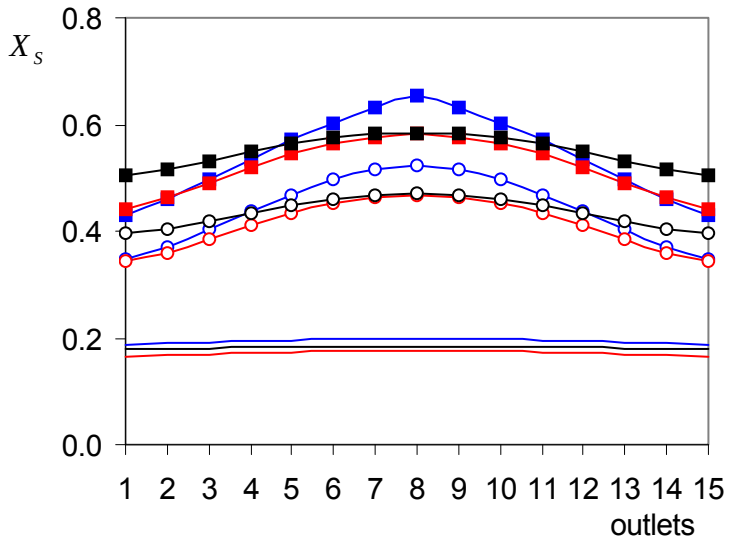

(b)

Figure 5.16 *Comparison of the performance of three NETmix® networks geometries: Prototype (blue lines), Design 1 (red lines) and Design 2 (black lines) (a) RTDs (b) Product distribution, at* $\mathrm{Re} = 600$*, for three segregated feed schemes: Scheme 1 (full squares), Scheme 2 (white circles) and Scheme 3 (lines).*

As the number of B-feed inlets increases, the feed concentration of B decreases. Very soon after B enters NETmix® there exist some regions where locally $c_B >> c_{A1}$, causing excessive production of S. This effect is smaller the lower the feed concentration of B and therefore as more B-feed inlets are used. This effect can be observed in Figure 5.16 by comparing the three groups of lines: full squares (Scheme 1), white circles (Scheme 2) and simple lines (Scheme 3). The segregated feed schemes 1 and 2 still clearly present concentration gradients in both "new" geometries (Design 1 and 2), however the gradient steepness tend to flat by increasing the segregation parameter, ψ, or by decreasing the variance of the curve RTD.

From the three network geometries, the Design 2 is the more suitable to produce the secondary product because it meets both high X_S and uniform composition of the outlets streams. However, this conclusion is valid for the ratio k_1/k_2 simulated.

In Figure 5.16 it also is visible that the average product distribution X_S is always the highest for the Prototype and the lowest for the Design 1. Comparing Design 1 and 2 it can be concluded that increasing the segregation parameter promotes mixing by flow division while reducing the proportion of mixing chambers and interestingly this slightly reduces X_S and improves mixing. There is scope to explore alternative designs in future CFD and experimental studies.

In the next section it is presented an application of the extended test system, in aqueous viscous medium, in the micromixing assessment of a mixing chamber of Reaction Injection Molding (RIM) machine.

5.4 Mixing Chamber of a RIM Machine

In recent years, the production of plastic products having performance properties (chemical, mechanical, electrical, optical, etc.) has emerged. This has claimed for greater control of the polymerization units, which yield the base polymer and for the development of novel processing methods to produce the final plastic products. The industry disposes of a variety of methods for plastic production, such as extrusion, injection molding and blow molding. However, it has been estimated that about one quarter of all articles made from polymer materials are manufactured using reactive processes, i.e. methods which involve polymerization directly in the production cycle (Edwards, 1984). Reaction Injection Molding, RIM, is one of these reacting processing methods and was developed to circumvent some of the problems (e.g. heat transference rate, clamping forces for the moulds, filling of complex geometry moulds) found during the production of larger pieces by traditional injection molding of thermoplastics and thermosetting plastics.

The RIM was originally developed at Bayer AG in 1964 (Santos, 2003) and consists of the impingement of two reactive monomer jets in a confined cylindrical chamber − mixing chamber − from where they flow to the mold. The residence time in the mixing chamber is very low so no significant polymerization reaction occurs until the mixture is supplied to the mould. The purpose of the mixing chamber is to bring reagents into sufficiently close contact reducing their scale of segregation up to molecular level (micromixing), avoiding by this way that the inherently fast polymerization reaction is not slow down by inadequate premixing reagents. Therefore, the RIM is an important process critically dependent upon mixing, where poor mixing results in poor polymeric parts (Kolodziej et al., 1982), i.e, micromixing ultimately controls the morphology, and consequently the performance properties, of the end product.

In spite of commercial success of the RIM, the heart of the process − impingement mixing of the jets in the mixing chamber − is poorly known. There are few quantitative information about this mixing device in the open literature, and the engineering design of this process has often largely involved trial and error procedures, with no firm understanding of the underlying principles (Frey and Denson, 1988; Kusch et al., 1989).

As it was previously referred, this work belongs to a research project of investigation about the mixing of reacting monomers inside the mixing chamber. Some studies were already

made, namely concerning flow field characterization by Laser Doppler Velocimetry (LDV), Laser Doppler Anemometry (LDA) and Particles Image Velocimetry (PIV) techniques (Santos et al., 2005; Teixeira et al., 2005). The investigation allowed to patent a control scheme the RIMcop® technology (Lopes et al., 2005b), based on the static pressure measurements in the injectors' feed lines to monitor the flow field regime (Erkoç et al., 2007).

The current work intends to contribute to the knowledge of mixing quality attained in the mixing chamber through a micromixing assessment study. Previous researchers have quantified the mixing under varying conditions using adiabatic temperature rise (Lee et al., 1980), polymerized tracer material (Tucker III and Suh, 1980; Kolodziej et al., 1982) and test reaction systems in aqueous non-viscous medium (Kusch et al., 1989). However, in this work the micromixing characterization is made by using the extended test system (discussed in Chapter 4) in aqueous solutions with viscosity of $20\,\mathrm{mPa\cdot s}$. Thus, the pilot RIM machine where this study was performed is briefly described in Section 5.4.1; a photographic study of flow pattern that assisted the micromixing experiments is shown in Section 5.4.2 and finally the quantification of mixing quality through the product distribution of the test system is presented in Section 5.4.3.

5.4.1 Pilot RIM Machine

The experimental RIM machine setup is illustrated in Figure 5.17 and Figure 5.18 and was previously described by Teixeira (2000) and Santos (2003). It consists of a cylindrical transparent mixing chamber with the same dimensions and geometric configuration of those used in the industry: internal diameter $D = 10.00\,\mathrm{mm}$ and height $H = 50.0\,\mathrm{mm}$, with two opposed injectors. The mixing chamber is constructed from acrylic − Plexiglas® −to permit visualization of flow patterns during mixing experiments. The injectors are located at $5.00\,\mathrm{mm}$ from the flat back wall of the mixing chamber, each having an internal diameter $d = 1.50\,\mathrm{mm}$ and $60.0\,\mathrm{mm}$ long in order to ensure a fully developed Poiseuille flow of the jets at the mixing chamber inlet. Each injector is fed from stainless steel tanks using a positive displacement pump (see Figure 5.18). The fluid from the mixing chamber flows into a mould and then leaves it through a discharging pipe that is connected to a storage "waste" tank. The fluid level into all three tanks is monitored through pressure transducers.

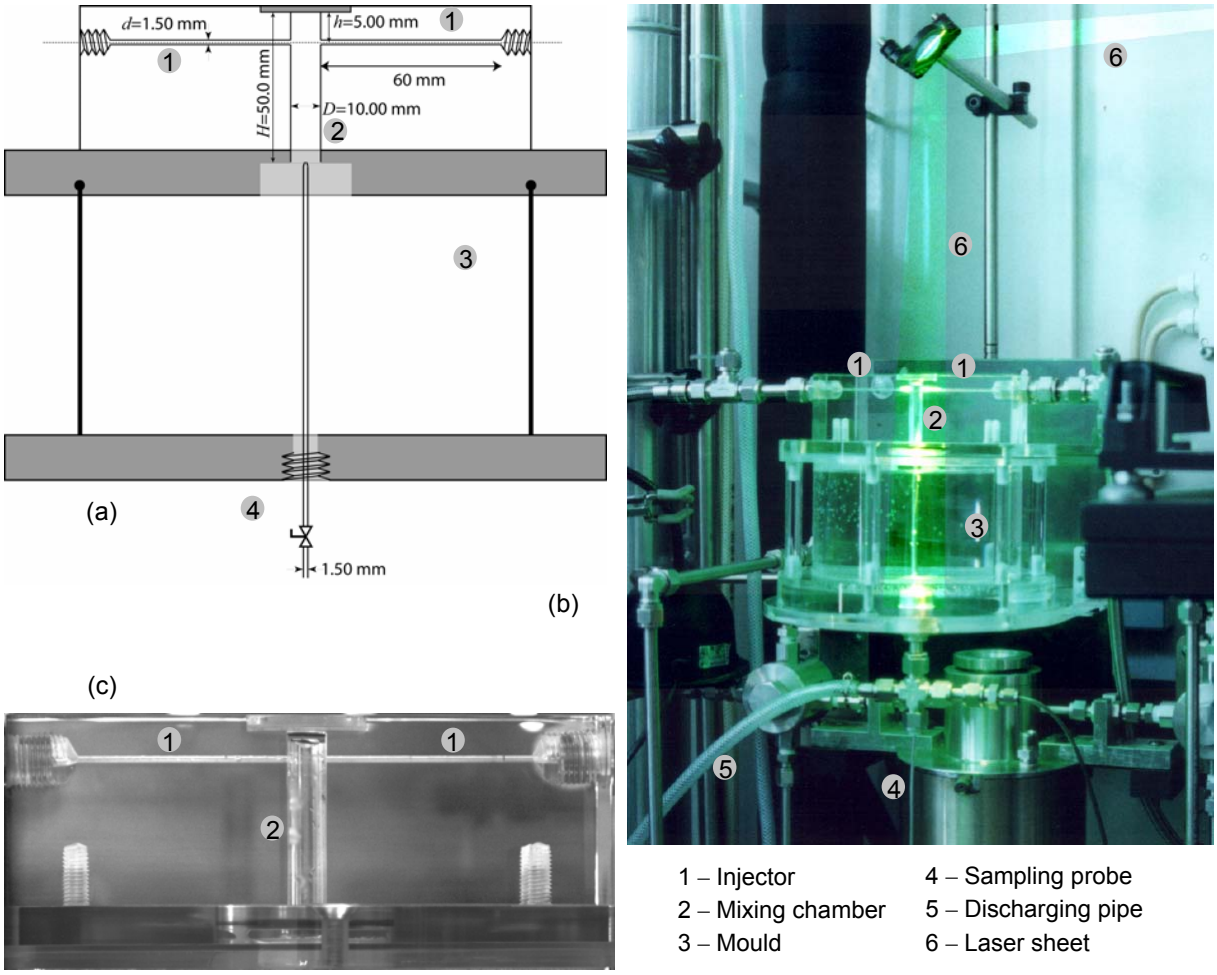

Figure 5.17 RIM machine: (a) Technical drawing of the mixing chamber and mould; (b) Photo of RIM overview; (c) Photo of mixing chamber and injectors detail (adapted from Santos (2003)).

All the instrumentation is controlled by a program developed on LabView which graphic interface is shown in Figure 5.19. The main feature of this program is the control of the injectors Reynolds number, which is based on the viscosity and density versus fluid composition and temperature curves. Therefore, a re-calibration of the control system is required if any of those properties of the flowing fluid changes, by the determination of the calibration curve function, for both pumps and pressure transducers. Moreover, it is possible and frequently made (see next section) finer adjustments of the pumps flow rate ratio by an entry field that allows the input of a positive or a negative small increments to the input signal in one of the pumps (Santos, 2003).

1 – Storage and feeding tanks

2 – Mixing chamber and mould

3 – Pressure transducers

4 – Positive displacement pumps

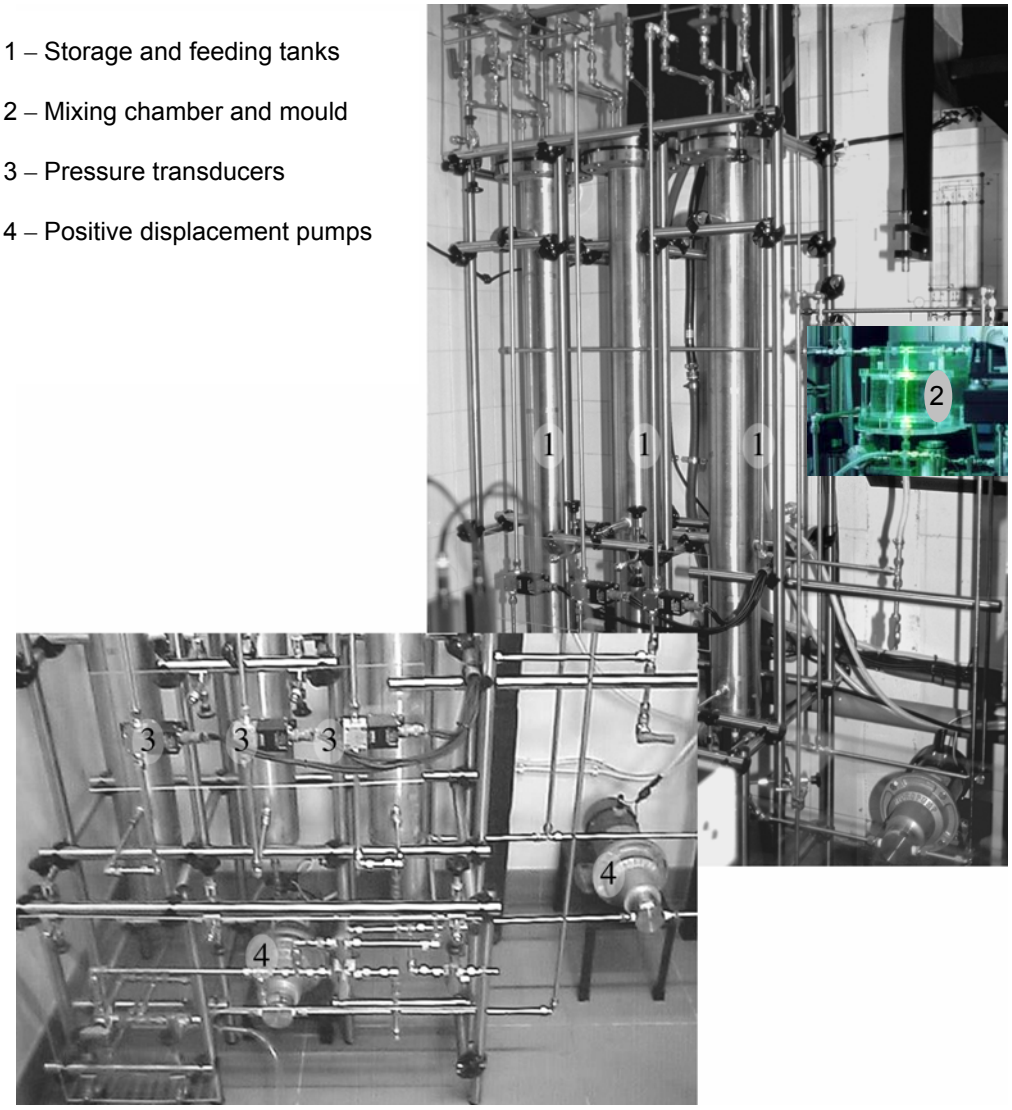

Figure 5.18 RIM machine setup (adapted from Santos (2003)).

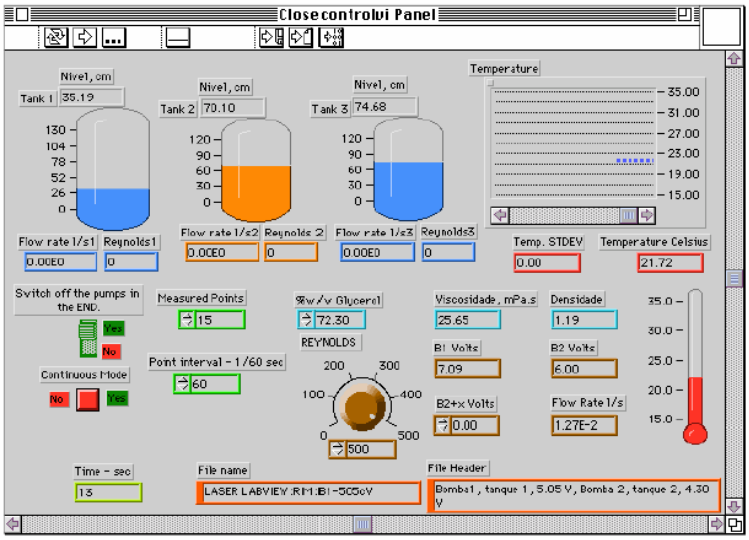

Figure 5.19 Graphic interface for the RIM machine control program (Santos, 2003).

The Reynolds number in the RIM mixing chamber is defined as $\mathrm{Re} = \rho \vartheta_{inj} d / \mu$, where ρ is the fluid density, d the injector diameter, ϑ_{inj} the superficial fluid velocity at the injector and μ the fluid viscosity.

The fluids are delivered through the injectors at high velocities ($1-8\ \mathrm{m \cdot s^{-1}}$, in this work). However, seeing that their viscosities can go up to $0.5\ \mathrm{Pa \cdot s}$, the typical operational Re falls in the range of $100-500$ (Coates and Johnson, 1997). At this low Re there is no turbulence generation in the mixing chamber and mixing can only be driven from complex chaotic flow patterns. This operational parameter is critical for mixing in the RIM process as well as the *momentum ratio* between the jets, defined (Santos, 2003) by:

$$R_M = \frac{\rho_1 \vartheta_{inj1}^2 d_1^2}{\rho_2 \vartheta_{inj2}^2 d_2^2} \tag{5.24}$$

where the indices 1 and 2 refer to each one of the injectors. When the fluid is the same in both injectors, such as in the present work, the momentum ratio is defined as

$$R_M = \frac{\vartheta_{inj1}^2 d_1^2}{\vartheta_{inj2}^2 d_2^2} \tag{5.25}$$

The momentum ratio must be one. Otherwise, lead/lag effects will be present in the mixing chamber, i.e., injection of one reagent prior to the other, compromising the mixing quality and subsequent polymeric product quality. Thus, the point of jets impingement should be located at the center of the mixing chamber.

The mixing assessment study performed in this work was limited to the mixing chamber and to the influence of the Reynolds number in the mixing efficiency. A sampling probe in the mixing chamber outlet under isokinetic conditions was installed, in order to disturb the main flow as little as possible, as shown in Figure 5.17a. Reagents 1 and 2-naphthols were fed in one injector and the diazotized sulfanilic acid on the other injector. The resulting mixture was sampled by the sample probe, as it will be described in more detail in Section 5.4.3.1.

The control of momentum ratio is important to achieve during these experiments. When the jets momentum were not equal (*non iso-momentum*), only the reagent from the higher momentum jet could be sampled at the outlet chamber. This fact indicates complete segregation or absence of mixture. So, all experiments should be done under the

iso-momentum condition, which is not achieved only by ensuring equal jets Reynolds number. Similarly to the observed by the authors Teixeira (2000) and Santos (2003), in this work it was noticed that in same cases even with equal injectors Re, it was necessary to make small adjustments on the input signal of one of the pumps in order to achieve the impingement point located at the centre of the mixing chamber. This control was helped by the flow visualization using a laser sheet and a PIV camera, which instruments setup is following briefly described and depicted in Figure 5.20.

The laser source is a double Nd:Yag laser from New Wave Research (model MiniLase – 15). The laser emits a wavelength of $530\ \mathrm{nm}$ beam with a diameter of $2.5\ \mathrm{mm}$, which is then converted into a sheet through a combination of one cylindrical and one spherical lens. This set of lenses yield a sheet of $17.5\ \mathrm{mm}$ height and $50.9\ \mu\mathrm{m}$ thickness at a distance of $20\ \mathrm{mm}$ from the lenses. The sheet is aligned to pass through the chamber and injectors axis by the positioning robot and by a mirror (Santos, 2003).

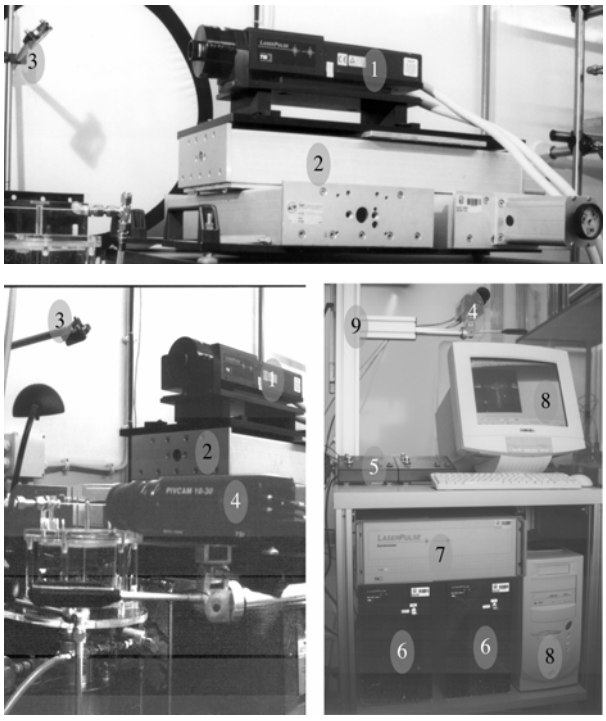

1 – Yag laser
2 – Positioning robot
3 – Mirror
4 – PIV camera
5 – Laser manual controller
6 – Laser power supply
7 – Synchroniser
8 – Computer
9 – Camera positioning arm

Figure 5.20 Photos of the instruments setup for the PIV (adapted from Santos (2003)).

The PIV camera model is PIVCAM 10-30 from TSI, with 1016 ×1024 pixels CCD and a frame rate of 30 Hz. The frames captured are transferred to the computer through a card.

Before the study of the mixing assessment in the mixing chamber using the extended test system, the pumps were calibrated for the used flowing fluid: aqueous solution of Rheolate 255 with viscosity of $20\,\mathrm{mPa}\cdot\mathrm{s}$. After the calibration curves determination (pump voltage versus Reynolds number) the flow field was imaged and recorded for several Reynolds numbers, in order to verify the impingement point location. The simplest technique used consists in the injection of a colored tracer in one of the injectors with the simultaneous capture of images of the formed patterns inside the mixing chamber. This visualization experiments is discussed in next section and some results are presented.

5.4.2 Flow Visualization Experiments with Colored Inert Tracer

The present experiments have no pretension to study the mixing mechanisms that take part in impinging jets of the mixing chamber. This investigation was previously done by others authors, including Teixeira (2000) and Santos (2003) by using different visualization techniques, as it was referred above. From those studies it is known that there are two distinct flow regimes:

- for $\mathrm{Re} < 100$ the fluid from each jet flows in its own side of the mixing chamber without further mixing mechanisms. This corresponds to the complete segregation case, where the reaction zone is confined to the interface of the flowing fluids.

- for larger Reynolds numbers the flow field is characterized by the formation of vortices immediately downstream of the opposed jets entrance. These vortices detach from the jets and evolve throughout the mixing chamber towards the outlet, promoting the engulfment of fluid fed from the opposed injectors in a self-sustainable chaotic flow regime. This mixing mechanisms leads to an enormous enhancement of the mass transfer and the reaction occurs in all the mixing chamber volume.

The transition between the two regimes occurs within a narrow interval of Reynolds numbers known as the critical Reynolds number, which was set at 120. More, it was observed that the flow regime depends mainly on the Re number and jets momentum ratio (Santos, 2003; Erkoç et al., 2007).

The main goal of this visualization experiments was to verify the impingement point location of the jets into the mixing chamber after the calibration of the pumps or, in other words, to evaluate if some deviations from momentum ratio unitary being observed at different Reynolds number in the range of $100-500$.

The chemical Orange I (Sigma&Aldrich 75360) described in Section 4.2.3 was chosen as the tracer for the flow visualization experiments. When buffered with $Na_2CO_3/NaHCO_3$ at $pH=10.0$, in Rheolate 255 aqueous solution with $20\,mPa\cdot s$, it presents a maximum absorbance at $516\,nm$, which is very near to the wavelength laser beam ($530\,nm$) used.

A buffered aqueous viscous solution (of $20\,mPa\cdot s$) of this tracer with $0.6\,mol\cdot m^{-3}$ was prepared and transferred for one of the feeding tanks shown in Figure 5.18. The other feeding tank was filled with a similar solution but without tracer.

Each experiment started by setting the operational Reynolds number in the interface shown in Figure 5.19. Then, the previous solutions were delivered separately to the mixing chamber through the two different injectors. Simultaneously the laser sheet, positioned in the plane containing the chamber axis and injectors centre (see Figure 5.17b), was emitted and the images acquisition was done by using the PIV camera. It was collected 100 frames per experiment (Re), with an interval of $500\,\mu s$. However, only four frames are shown in Figure 5.21. These photos show the characteristic flow pattern for Re and do not represent any temporal sequence.

A global appreciation of these experiments is that the impingement point was generally located at the centre of the mixing chamber. However in a few cases it was needed to make small adjustments on the signal input in one of the pumps, in order to attain the iso-momentum state. This means that the previous calibration pumps procedure was successful.

The observation of the several photos allows the visualization the different flow patterns possible to occur during an experiment at constant Re, together with the effect of this parameter in the mixing intensity and respective mechanisms.

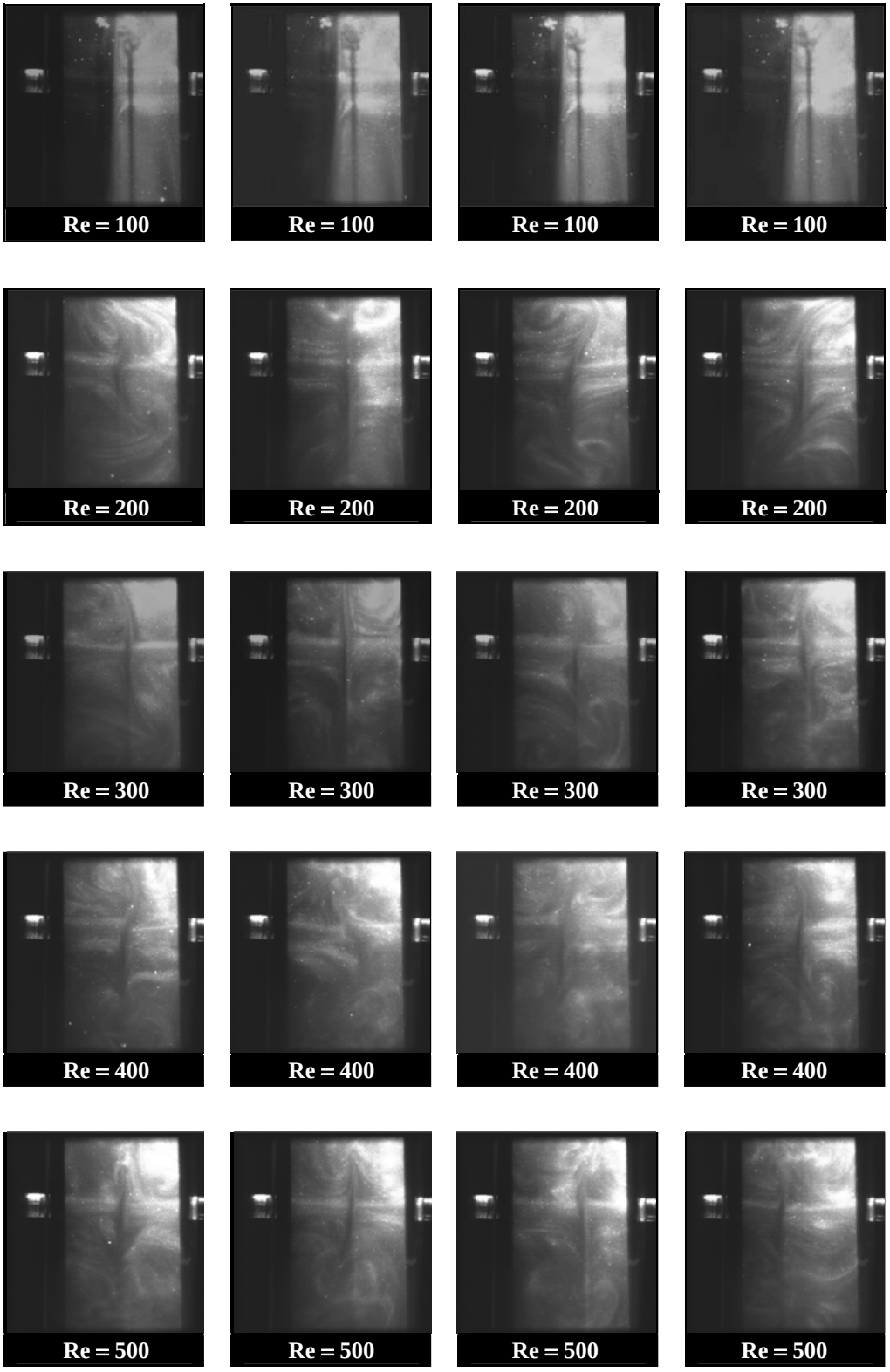

Figure 5.21 Example of different time frames for jets impinging alignment during the inert trace experiments for $100 \leq \mathrm{Re} \leq 500$.

It was observed that for $\mathrm{Re} < 50$ the jets do not impinge. They just bend and flow towards the outlet of mixing chamber. Consequently, the range of $\mathrm{Re} < 50$ will not be used in the micromixing experiments.

For $50 < \mathrm{Re} < 100$ the jets impinge at the mixing chamber axis in a pattern similar to images for $\mathrm{Re} = 100$ of Figure 5.21. In this Re range, two smaller nearly imperceptible upper vortices in the mixing chamber are observed. However, the overall behavior of the flow promoted a very weak mixing between both streams, because the oscillations of their interface do not present amplitude enough to promote the mixing of fluid between both halves of the mixing chamber.

From $\mathrm{Re} = 100$ to $\mathrm{Re} = 200$, the flow regime changes considerably. It is observed the formation of circular vortices downstream the injectors, which simultaneously break the jets interface symmetry and promote the engulfment of those jets with the surrounding fluid. The upper vortices are now well identified in the photos and change both in shape and rotation orientation. Between these two Reynolds numbers, it is evident that one passes from a complete segregation state to others where the mixing mechanisms start and results in self-sustainable chaotic flow. So, these experiments confirm that the critical Reynolds number should be here located.

From $\mathrm{Re} > 200$ the differences between the flow patterns are scarcely perceptible in the images of Figure 5.21. However, a common observation for the various studied Reynolds numbers is that, as the Reynolds number increases, the interface of the jets becomes increasingly unstable. It is observed eddies formation with different rotations and there is oscillatory motion on the interface of the impinging jets. Besides, the impingement point is located at the mixing chamber axis, oscillating around it, as can be clear seen in Figure 5.21 for $\mathrm{Re} = 500$.

The existence of an equal momentum of the two jets is one of the essential conditions for the mixing occurrence inside the mixing chamber. Besides, when the iso-momentum state is ensured, the impingement point of the jets is located at the centre of the mixing chamber or oscillating around it (Santos, 2003).

These visualization experiments revealed that, even after the calibration of the pumps, sometimes it was necessary to make small adjustments on the signal input of the pumps to attain the iso-momentum state. Figure 5.22 shows an example of this event, for $\mathrm{Re} = 200$.

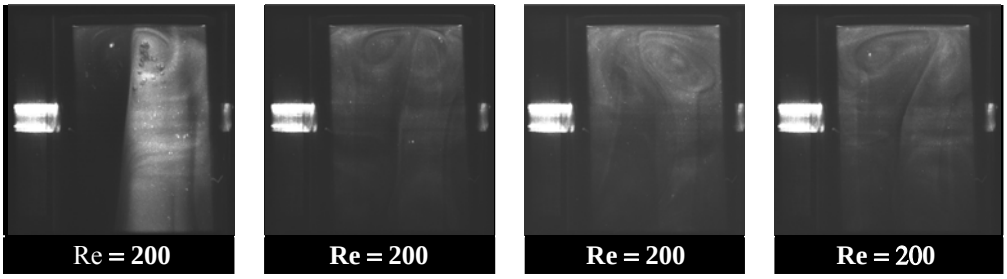

Figure 5.22 Effect of (non) iso-momentum in the self-sustained oscillation jet collision for $\mathrm{Re} = 200$.

At the beginning (Figure 5.22a), both jets impinge flowing side by side without mixing downward mixing chamber. A decrease of $0.06\ \mathrm{V}$ on the signal input of one of the pumps was sufficient to induce the mixing mechanisms previously referred and attaining a self-sustainable chaotic flow (Figure 5.22b-d).

The perception of this fact was previously observed by in both LDA and PIV experiments. (Santos, 2003) reported that deviations from the state of momentum balance between the jets changes dramatically the dynamics of the flowing fluid inside the mixing chamber, even above the critical Reynolds number.

In this way, for a successful operation of a RIM machine, the momentum ratio of the jets should be one. To attain this condition a close monitoring of the mixing chamber should be made. Consequently, during the experiments done in this work, for micromixing characterization in the mixing chamber (see Section 5.4.3), the jets impingement point was always located and eventually set using the same technique used in these tracer experiments. In addition, this procedure was extended to each Reynolds number studied.

In short, this visualization study allowed simultaneously: (i) to conclude about the success on the pumps calibration, since in the most of the Reynolds numbers the jets impinges at the mixing chamber axis and (ii) to observe the several flow patterns that can occur for different hydrodynamics flow conditions. Thus, under this panorama, the work could proceed with the micromixing studies presenting in the next section.

5.4.3 Micromixing Studies

The current section is reserved to the micromixing quantification in the mixing chamber of RIM machine when it is used flowing fluids with viscosity of $20\,\text{mPa}\cdot\text{s}$ in the Reynolds numbers range of $75-600$. The experimental plan for the set of experiments carried out is present in Section 5.4.3.1 and the respective results in Section 5.4.3.2.

The previous knowledge about the short mean residence times ($0.13-1\,\text{s}$) and the suspicion of high energy dissipation rates characteristics of this mixing device were the preponderant criteria for the selection of the test reaction system to be employed in this study. Thus, the reaction between 1 and 2-naphthol and diazotized sulfanilic acid was selected as the test system because it can give lower characteristic reaction times.

This test system was called, in Section 5.2.2, the extended test system and has two variables for the micromixing quantification: $X_S^{'}$ and X_Q, defined by the Equation 5.7 and 5.8, respectively. These variables have many designations, such as: segregation indexes, product distributions, product yields and selectivity.

As it was already referred, the micromixing studies should be performed under mixing-controlled regime and to attain this regime, the experimental conditions must be carefully chosen. The next section summarizes the set of experiments performed and the analytical method used.

5.4.3.1 Experimental Conditions and Analytical Method

The RIM machine studied in this work has two equal injectors (see Figure 5.17), which feed the mixing chamber. All experiments here presented were performed in aqueous viscous medium at: $20\pm0.5^{\circ}\text{C}$, $I = 222.2\ \text{mol}\cdot\text{m}^{-3}$, $\text{pH} = 9.9$ and $\mu = 20\,\text{mPa}\cdot\text{s}$. More, the fluids that flowed through the injectors had the same viscosity, density and flow rate; in one of the injectors delivered to the mixing chamber the diazotized sulfanilic acid, B, with the concentration of c_B^{feed} and the other injector delivered the solution of both 1 and 2-naphthols with concentrations c_{A1}^{feed} and c_{A2}^{feed}, respectively. Under these conditions the concentrations of the three reagents will be reduced by half in the mixing chamber and they are here designated as: c_{B0}, c_{A10} and c_{A20}.

Ensuring that B is always the limiting reagent, the combinations of the reagent ratio: $\gamma_{A1} = c_{A10}/c_{B0}$ and $\xi = c_{A20}/c_{A10}$ susceptible to be used in micromixing studies are vast. However, as was shown by Bourne et al. (1992a), the sensitivity of the parameters X_Q and $X_S^{'}$ to the mixing intensity is dependent of that reagent combination ratio. In this way, Table 5.9 summarizes the experimental plan that was elaborated by offering several combinations, in order to find the best sensitivity to the mixing degree.

Table 5.9 List of reagents 1- and 2 -naphthols and diazotized sulfanilic acid solutions for the micromixing experiments in the mixing chamber of RIM machine.

Experiment	Concentrations of A_1, A_2 and B in the feed	ξ	γ_{A1}
Exp # 1 & Exp # 2	$c_{A1}^{feed} = 1.100\ \text{mol}\cdot\text{m}^{-3}$ $c_{A2}^{feed} = 6.600\ \text{mol}\cdot\text{m}^{-3}$ $c_{B}^{feed} = 1.000\ \text{mol}\cdot\text{m}^{-3}$	6	1.1
Exp # 3	$c_{A1}^{feed} = 1.100\ \text{mol}\cdot\text{m}^{-3}$ $c_{A2}^{feed} = 3.300\ \text{mol}\cdot\text{m}^{-3}$ $c_{B}^{feed} = 1.000\ \text{mol}\cdot\text{m}^{-3}$	3	
Exp # 4	$c_{A1}^{feed} = 1.100\ \text{mol}\cdot\text{m}^{-3}$ $c_{A2}^{feed} = 1.100\ \text{mol}\cdot\text{m}^{-3}$ $c_{B}^{feed} = 1.000\ \text{mol}\cdot\text{m}^{-3}$	1	
Exp # 5	$c_{A1}^{feed} = 0.240\ \text{mol}\cdot\text{m}^{-3}$ $c_{A2}^{feed} = 1.440\ \text{mol}\cdot\text{m}^{-3}$ $c_{B}^{feed} = 0.200\ \text{mol}\cdot\text{m}^{-3}$	6	1.2
Exp # 6	$c_{A1}^{feed} = 0.240\ \text{mol}\cdot\text{m}^{-3}$ $c_{A2}^{feed} = 0.720\ \text{mol}\cdot\text{m}^{-3}$ $c_{B}^{feed} = 0.200\ \text{mol}\cdot\text{m}^{-3}$	3	
Exp # 7	$c_{A1}^{feed} = 0.240\ \text{mol}\cdot\text{m}^{-3}$ $c_{A2}^{feed} = 0.240\ \text{mol}\cdot\text{m}^{-3}$ $c_{B}^{feed} = 0.200\ \text{mol}\cdot\text{m}^{-3}$	1	
Exp # 8	$c_{A1}^{feed} = 0.300\ \text{mol}\cdot\text{m}^{-3}$ $c_{A2}^{feed} = 1.800\ \text{mol}\cdot\text{m}^{-3}$ $c_{B}^{feed} = 0.200\ \text{mol}\cdot\text{m}^{-3}$	6	1.5

Experiments 1 and 2 assisted to evaluate the experimental reproducibility. The group of the experiments 1 to 4, where the A_1 and B concentrations were kept constant, intended to evaluate the c_{A20} influence on the mixing sensitivity of the test system. The same can be said

of the group composed by experiments 5 to 7. Between these two groups of experiments the characteristic reaction time differs five fold and the parameter γ_{Al} was changed in order to evaluate its effect in the test system sensitivity to the mixing efficiency. Experiment 8 was planned to compare its results with the experiment 5, allowing appraising the effect of both naphthols concentrations in the referred sensitivity.

The make up of reagents solutions was started half-day before the experiments in the mixing chamber. It was prepared two reservoirs with 10 liters/each: one for diazotized sulfanilic acid and the other for the 1- and 2-naphthols. In each reservoir, the thickener − Rheolate 255 − was dissolved in stirred distilled water in a quantity of 3.8%, in order to attain a final solution viscosity with $20\ \text{mPa}\cdot\text{s}$. The solution of the reservoir reserved to $A_1 + A_2$ was also buffered with $Na_2CO_3 / NaHCO_3$ (given a $I = 222.2\ \text{mol}\cdot\text{m}^{-3}$ at the final solution. See Section 4.4.2.2) and the other acidified with HCl (see Section 4.4.2.1). Both solutions were left to rest overnight at $20 \pm 0.5^{\circ}\text{C}$.

Few moments before the beginning of the experiments, the reagents were added to the respective reservoirs and their rheograms determined in order to determine the viscosity value. Their concentrations were also checked by spectrophotometry:

- Directly for the $A_1 + A_2$ solution. Although the shift between their spectra is relatively small (see Figure 4.36), a two-component analysis allowed initial concentrations of A_1 and A_2 to be checked.

- Indirectly for B solution. This solution was injected in the stopped flow reaction analyzer (see Chapter 3) with an aqueous viscous solution of A_2 with known concentration (in excess), specially prepared to this test.

After these tests, the solutions were transferred to the respective feeding tanks (Figure 5.18) and the experiments proceeded in the Reynolds number range of $75 - 600$. The next step was to check the iso-momentum of the jets by the visualization of the impingement point, and to make some signal input adjustments if it was necessary (always ensuring B as the limiting reagent). Since the products of the reactions involved in the test system absorbs light in the wavelength of the laser beam, the technique used was similar to the described in Section 5.4.2 and some acquired frames are shown in Figure 5.23 for $\text{Re} = 75$ and $\text{Re} = 250$.

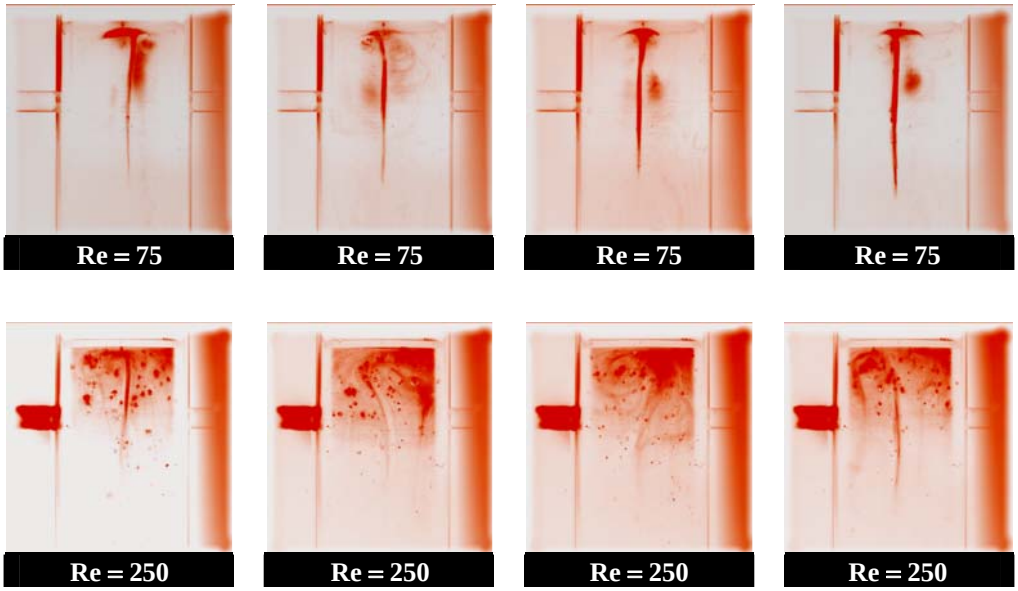

Figure 5.23 Different time frames of jets impinging alignment during the micromixing experiments for $\mathrm{Re} = 75$ *and* $\mathrm{Re} = 250$.

To enhance impingement point visualization, the images of Figure 5.23 were post-processed by indexing each gray level to a color level ranging from white to orange (the predominant color observed). The frames clearly allow seeing the impingement point of the jets, where the formation of the products is more intense consequently exhibiting a more intense orange color.

For $\mathrm{Re} = 75$, where the segregation state is always present, the reagent streams flow parallel and the reaction zone is limited to the interface of both streams. This phenomenon is undoubtedly visible in the frames by the orange filament.

In order to see more clearly the impingement point the image treatment led to loss of some information towards to the mixing chamber outlet, for $\mathrm{Re} = 250$. Thus, it is only visible the regions where the product concentration is higher, i.e., in the interface of impingement and in the two typical vortices existents in the top of the camera, where probably there are some product accumulation.

It should be noticed that for higher Reynolds numbers ($\mathrm{Re} \geq 400$) and in some experiments where the products concentrations were higher, the visualization of the impingement point of the jets revealed to be a hard task and sometimes impossible to do.

After the verification of the iso-momentum of the jets, three samples of the solution at the outlet mixing chamber were collected for further analysis, through the sample probe shown in

Figure 5.17a. However, to ensure a steady state, each sample was obtained after about five residence times of the mixing chamber had elapsed.

The collection of three samples had two objectives: (i) to ensure the sampling method reproducibility and (ii) to verify if the limiting reagent was fully consumed at the mixing chamber outlet, so that mixing assessment and quantification is done only inside this reactor.

The samples were kept in an iced bath until the end of the experiment, i.e., after all Reynolds numbers were tested. Then, they were analyzed in the spectrophotometer in a wavelength range $250-700\,\text{nm}$ with a step of $1\,\text{nm}$, obtaining by this way an experimental curve, Abs_{exp}, for each sample.

The subsequent data treatment was similar to the described in Section 5.3.3.2. However, from the analytical point of view, the current case presents two differences: (i) there is one more dye in solution, product Q and (ii) the percentage of $o-R$ and $p-R$ are respectively 10% and 90%, in agreement to the exposed in Section 4.4.4.1. Thus, assuming that the Lambert-Beer law is valid and that all dyes in solution absorb light independently, the absorbance at a given wavelength over a optical pathlength, δ, can be estimated by extending Equation 5.20 to include product Q:

$$Abs_{\text{calc}_\lambda} = \varepsilon_{R_\lambda}\, c_R\, \delta + \varepsilon_{S_\lambda}\, c_S\, \delta + \varepsilon_{Q_\lambda}\, c_Q\, \delta \tag{5.26}$$

where $\varepsilon_{R_\lambda} = 0.10\,\varepsilon_{o-R_\lambda} + 0.90\,\varepsilon_{p-R_\lambda}$, ε_{S_λ} and ε_{Q_λ} are respectively the molar extinction coefficients of R, S and Q at the same experimental conditions. The extinction coefficients, ε, for all dyes are obtained from Figure 4.36.

From Equation 5.24 an absorbance curve, Abs_{calc}, can be calculated, based on reasonable estimations of both products concentrations c_R, c_S and c_Q. Then, by using the Excel® Solver tool, that curve can be fitted to the experimental curve Abs_{exp}, where the fitting variables are c_R, c_S and c_Q. This is done through the minimization of the deviation function given by Equation 5.21 over the wavelengths range of $400-600\,\text{nm}$. Finally, the product distribution $X_S^{'}$ and X_Q were calculated using Equations 5.7 and 5.8.

B is the limiting reagent and should be fully consumed until the moment of the sample collection. Its mass balance was always checked, by using the Equation 5.27, obtained from an adaptation of Equation 5.22 in order to include the Q product.

$$\mathrm{MB} = \frac{c_R + 2c_S + c_Q}{c_{B0}} \times 100 \tag{5.27}$$

Finally, the results obtained in all experiments of the experimental plan of Table 5.9 are presented in Section 5.4.3.2.

In Section 4.2.1 it was verified that aqueous solutions of Rheolate 255 with $\mu = 20\ \mathrm{mPa \cdot s}$ have a Newtonian behavior up to shear rate $\dot{\gamma} = 3000\ \mathrm{s^{-1}}$. Previously to implementing solutions of this additive in the mixing chamber of RIM machine it is advisable to have an estimate of the shear rate values practiced in this mixing device, in order to ensure the Newtonian flow behavior in the flowing fluid. Barnes et al. (1997) refer that "the approximate shear rate involved in any operation can be estimated by dividing the average velocity of the flowing liquid by a characteristic dimension of the geometry in which it is flowing (e.g. radius of a tube or the thickness of a sheared layer)". Thus, the higher shear rate that can occur in the mixing chamber is for the higher Reynolds number (which is $\mathrm{Re} = 600$ in this work). Under this condition, the calculated shear rate is of the order of magnitude of 10, ensuring the Newtonian behavior in the experiments carried out in this work.

5.4.3.2 Results

As described earlier, the reaction scheme will be sensitive to the micromixing effects in the mixing chamber only if the value of the characteristic reaction time, $t_r = 1/k_3 c_{B0}$, is of the magnitude of the micromixing time constant, t_{mixing}. The first set of experiments was made with $c_{B0} = 0.5\ \mathrm{mol \cdot m^{-3}}$, which corresponds to $t_r \cong 21\ \mathrm{ms}$. The reproducibility of the micromixing experiments carried out in the mixing chamber was evaluated using exp#1 and exp#2, which results are depicted in Figure 5.24.

Note: due to the large number of data obtained in this study, it was decided to show them only in a graphic way, being the table representation suppressed.

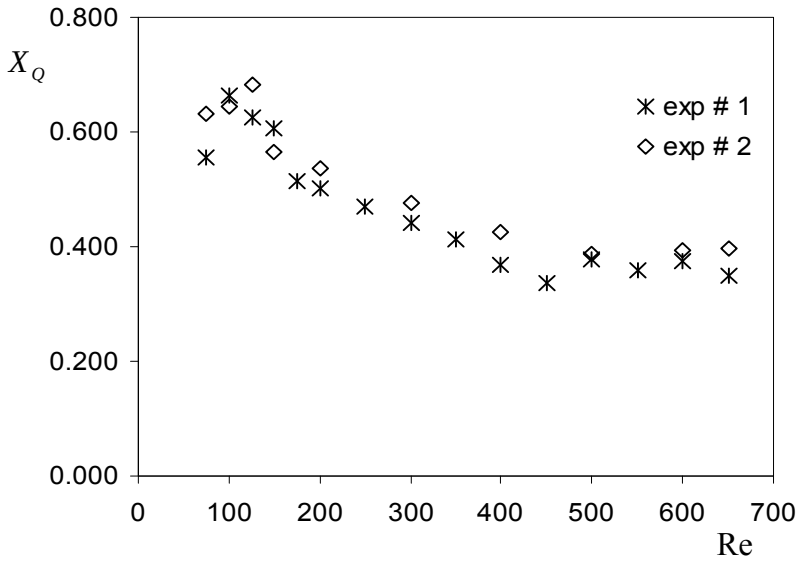

Figure 5.24 *Evaluation of the experiments reproducibility in the mixing chamber outlet of the RIM machine.* $c_{B0} = 0.5\ \text{mol}\cdot\text{m}^{-3}$, $\gamma_{Al} = 1.1$, $\xi = 6$, $T = 20^{\circ}\text{C}$, $I = 222.2\ \text{mol}\cdot\text{m}^{-3}$, $\text{pH} = 9.9$ *and* $\mu = 20\ \text{mPa}\cdot\text{s}$

This figure shows a good agreement between both experiments, except for Reynolds number near or lower than 100. The spread of X_Q values registered in this range of Re can be explained by the already known complete segregation regime, observed in Figure 5.21 and Figure 5.23.

The average curve obtained from the two experiments was used to compare with the other experiments belonging to the group of experiments with $\gamma_{Al} = 1.1$ (see Figure 5.25).

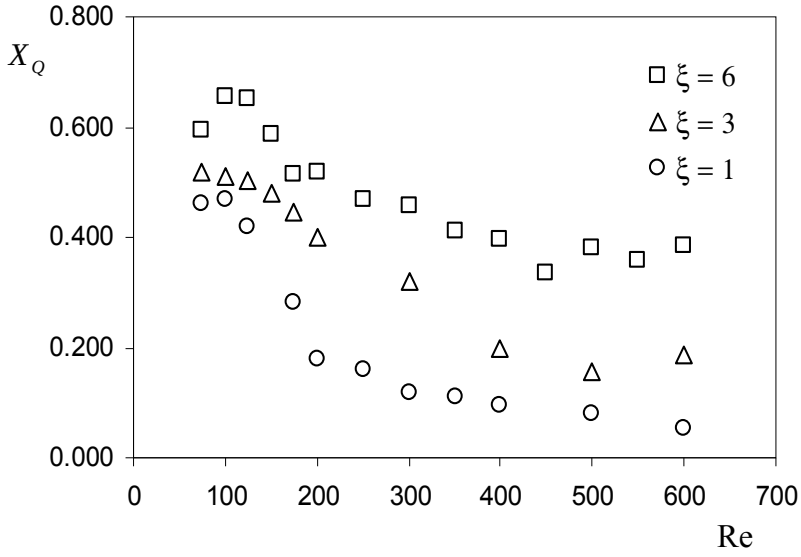

Figure 5.25 *Effect of Reynolds number in the product distribution at the mixing chamber outlet of the RIM machine.* $c_{B0} = 0.5\ \text{mol}\cdot\text{m}^{-3}$, $\gamma_{Al} = 1.1$, $T = 20^{\circ}\text{C}$, $I = 222.2\ \text{mol}\cdot\text{m}^{-3}$, $\text{pH} = 9.9$ *and* $\mu = 20\ \text{mPa}\cdot\text{s}$

A general comment to the three curves shown in Figure 5.25 is that the value of X_Q decreases with the increase of the Reynolds number, indicating the expected improvement of (macro and micro) mixing intensity. The highest difference on the value of X_Q is observed in the interval $100 < \mathrm{Re} < 175$. This could be an indicator of the Reynolds number range where the mixing transition occurs. The experimental curves fall within the region of two asymptotes:

- One for low values of Re ($\mathrm{Re} \leq 100$) indicating the instantaneous regime region. The predicted values obtained using Equation 5.17 (as can also be seen in Figure 5.4) are shown in the Table 5.10. The experimental curve obtained when $\xi = 1$ seems to be the unique that is more deviated from the predictable value. However, the remaining curves are in good agreement with the expected values.
- One for higher values of Re ($\mathrm{Re} \geq 500$) indicating the slow regime region. The predicted values for a PFR and CSTR reactor design, based in Equations 5.12 and 5.13, are summarized in the Table 5.10. The experimental values seem to tend for CSTR values, indicating some backmixing/recirculation in the macroscopic flow pattern, but for the Re range studied they are still above those values.

Table 5.10 X_Q *predictable values for slow and instantaneous regimes at* $T = 20^{\circ}\mathrm{C}$, $I = 222.2\ \mathrm{mol \cdot m^{-3}}$, $\mathrm{pH} = 9.9$ *and* $\mu = 20\ \mathrm{mPa \cdot s}$.

	Slow regime				
	$\gamma_{Al} = 1.1$		$\gamma_{Al} = 1.2$		Instantaneous regime
ξ	PFR	CSTR	PFR	CSTR	
6	0.083	0.152	0.074	0.130	0.750
3	0.046	0.101	0.040	0.081	0.600
1	0.017	0.048	0.014	0.034	0.333

In some cases, the trendlines between the data sets are not clear and the data within each set are scattered. One possible reason for that is the difficulty found in the visualization of the impingement point of the jets, due to the high intense color developed by the reaction products (higher reagent concentrations). This problem occurred often for $\mathrm{Re} \geq 400$. There was generally more scatter in Figure 5.25 than in corresponding graphs of X_S vs. Re for NETmix® (see Figure 5.13). Its flow is constrained by its mixing elements but in RIM the flow is only weakly constrained by the chamber walls and is less reproducible than in the NETmix® static mixer.

On one hand, the decreasing of reagents concentrations in the second group of experiments (exp#5, exp#6 and exp#7) increased the quality on the visualization of the impingement point, because the color developed was less intense than the previous set of experiments. However, on the other hand, the reaction time increased to $105\ \text{ms}$, which revealed to be closer to the mixing time in the mixing chamber, at least the results obtained present less spread and more consistent to each other (see Figure 5.26). Clearly, the three curves fall between two asymptotic values: (i) one for $\text{Re} \leq 100$, corresponding to fully-mixing regime (see Section 5.2) where the product distribution is controlled by mixing degree and (ii) the chemical-regime, where the product distribution is kinetically controlled. In these experiments the chemical or slow regime seems to be attained for $\text{Re} \geq 500$. In this Reynolds number range, the curves $\xi = 6$ and $\xi = 3$ tend to values between the predicted for PFR and CSTR (see Table 5.10). Conversely, the $\xi = 1$ curve tends to a value near zero, below that predicted for any of those reactors design. However, the analytical errors can be more significant in the determination of very low X_Q values. More, Figure 5.26 clearly shows a transition regime in the range $100 < \text{Re} \leq 125$. The visualization experiments have indicated no significant changes in the flow patterns for $\text{Re} > 200$ (Figure 5.21), meaning that mixing mechanisms at macro-scale do not change in this Re range. However, the mixing quality can still be improved considering that X_Q still decreases and the mechanisms responsible for that belong to the micro-scale.

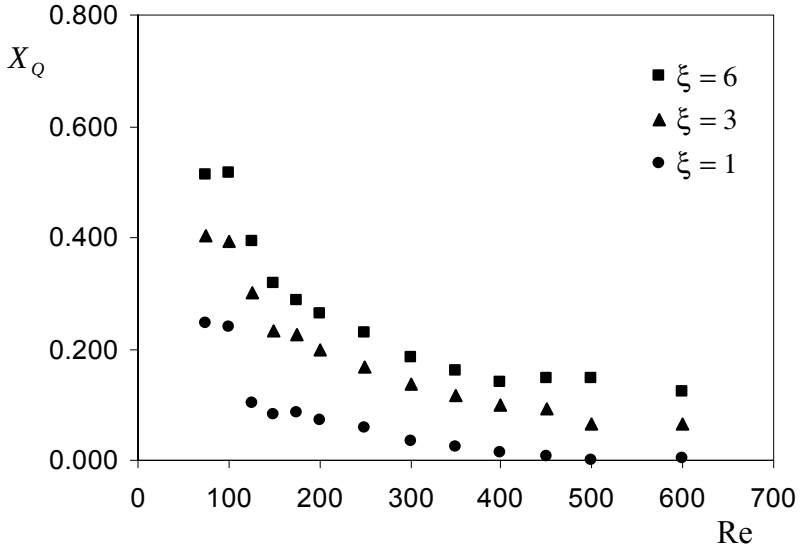

Figure 5.26 Effect of Reynolds number in the product distribution at the mixing chamber outlet of the RIM machine. $c_{B0} = 0.1\ \text{mol} \cdot \text{m}^{-3}$, $\gamma_{Al} = 1.2$, $T = 20^{\circ}\text{C}$, $I = 222.2\ \text{mol} \cdot \text{m}^{-3}$, $\text{pH} = 9.9$ *and* $\mu = 20\ \text{mPa} \cdot \text{s}$

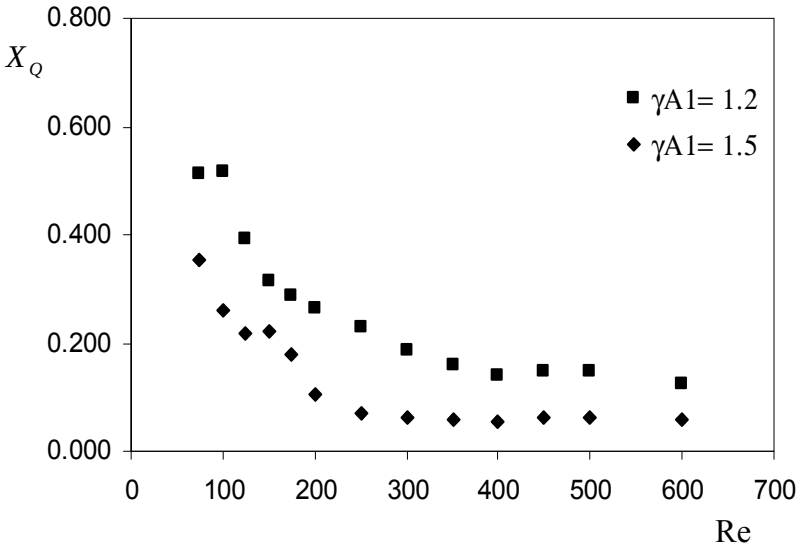

Figure 5.27 Effect of Reynolds number in the product distribution at the mixing chamber outlet of the RIM machine. $c_{B0} = 0.1\,\mathrm{mol \cdot m^{-3}}$, $\xi = 6$, $T = 20^{\circ}\mathrm{C}$, $I = 222.2\ \mathrm{mol \cdot m^{-3}}$, $\mathrm{pH} = 9.9$ *and* $\mu = 20\ \mathrm{mPa \cdot s}$.

Experiment 8 was carried out in order to verify the effect of the parameter γ_{Al}, keeping constants ξ and c_{B0}, relatively to the experiment 5. The results are shown in Figure 5.27 for comparison. This last experiment does not give much additional information, because it is observed that X_Q decreases comparatively to the curve for $\gamma_{Al} = 1.2$, as it was expected. However, in this curve the transition regime between in the range $100 < \mathrm{Re} \leq 125$ is not evident. Moreover, the slow regime is here attained earlier, i.e., for inferior Reynolds number ($\mathrm{Re} \geq 300$).

From these micromixing studies, the main remarks and conclusions that can be draw are:

- In the left-hand of all figures, X_Q curve shows an asymptotic value when segregation is complete and on the right-hand another asymptote when mixing is perfect. The experimental results fall within the region between these two asymptotes.
- The complete segregation regime was already identified, by visualization experiments shown in Section 5.4.2, to be for values of $\mathrm{Re} \leq 100$. The experiments performed during this work confirmed that conclusion. In addition, when the segregation is complete, it can not be ensure that reagent B is fully consumed inside the mixing chamber up to the sample collection. The consequences of this fact and observed in this work was that the mass balance of B (Equation 5.25) often did not close and a data spread among the three samples collected in each run was observed.

- In some cases, even for $\mathrm{Re} > 100$, the trend between the data sets are not clear and the data within each set are scattered. This fact was also observed by Kusch et al. (1989) in a similar study, but using the simplified test system in aqueous non-viscous medium. These authors imputed the data scatter to the complex time-varying mixing patterns existent inside the mixing chamber and consequently the samples obtained from different mixing experiments (at the same Reynolds number) could give different results. However, in this work another reason is suggested as responsible for the data scatter; considering that the mixing experiments were followed by the flow visualization technique (as described in Section 5.4.2) and that in some cases the iso-momentum ratio was difficult to ensure. Thus, it was considered that this is the main reason for data spread observed in some experiments, i.e., the chamber was fed by different flow rates of each injector, which means a reagents stoichiometric ratio different from the planned for that run. The mass balance of Equation 5.27 is a proof of this suggestion, because it did not close in these cases.

- For experiments with $\mathrm{Re} > 100$, where the iso-momentum state was verified, the mass balance closed within $\pm 5\%$.

- For experiments with $\mathrm{Re} \leq 100$, the product distribution $X_S^{'}$ presented values scattered in the interval $0.000 - 0.200$. When mixing is good, but not necessarily perfect, $X_S^{'}$ for the extended reaction system should be almost zero (Bourne et al., 1992a). At low Re unreacted B flows close to chamber walls and reaches the exit before it reacts in a region of low mixing intensity, allowing S to be formed.

- For the remaining Reynolds number range, $X_S^{'}$ falls to zero in all experiments, except in some runs where the iso-momentum of the jets was not ensured and the mass balance also did not close.

- The experimental conditions set of experiments 5 and 6 seems to be more suitable in the micromixing characterization in this mixing device, since the results spread is practically inexistent and the transition region (from segregated to mixing) is well identified between $100 < \mathrm{Re} \leq 125$. This result corroborates with the previous one obtained by other authors using visualization techniques, for which it was identify the $\mathrm{Re} = 120$ as the Reynolds number of transition. The results obtained in this work only allow the definition of an interval of Reynolds numbers corresponding to the transition region, instead of a unique value of Re. Since, in this RIM machine, the calibration error for Reynolds number is around 10% (Santos, 2003), in these experiments the small step of Re investigated was 25.

5.5 Conclusions

The mixing studies give important information regarding the effect of some important parameters in the mixing degree attained in a system. The Reynolds number was the parameter studied in the micromixing assessment of the two mixing devices investigated in this chapter. The test reaction systems are an important tool in this kind of studies, but they often present limitations and ranges of application. Furthermore, it is a requirement that the experiments must be performed under the mixing-controlled regime, where $t_{\text{mixing}} \approx t_{\text{reaction}}$. Seeing that the characteristic mixing times were unknown in both devices investigated, the experiments were carried out in a trial and error base. From the several set of experimental conditions used, it was identified one which seems to be more suitable for each mixer. This way, the simplified and the extended test systems here used revealed to be suitable in each case where they were implemented.

The results obtained for the mixing characterization study in the NETmix® static mixer allowed to conclude that the Reynolds number have a great influence in the mixing degree, being this influence more relevant upon $\text{Re} = 200$. In the RIM machine, the Reynolds number exerts a similar influence in the mixing intensity inside the mixing chamber, where it was identified a transition regime ($100 < \text{Re} \leq 125$), from segregated to mixing state. In addition, there was more scattering in RIM machine results than for that obtained in the NETmix® static mixer. These can mean that the flow pattern in the impinging jets is less reproducible than in the NETmix® static mixer. The elements of the NETmix® probably guide and channel the flow. Conversely, in RIM machine the jets possibly do not collide in exactly the same way and do not show exactly the same flow pattern in each run.

The visualization experiments were an important support to the studies performed in this chapter, once they assisted the results interpretation and/or their attainment by ensuring the better mixing conditions.

Concerning the NETmix® macromixing simulation study, it allowed to evaluate the viability of using different reagents feed schemes and network geometries to control and attain different product distributions. The results obtained incite to explore alternative designs and operational conditions. The versatility and the quality of mixing attainable are important key characteristics that could make promising this static mixer in the mixing field.

In short, the NETmix® static mixer is a novel mixing device recently patented (Lopes et al., 2005a) and naturally this study gave an important contribute for the micromixing assessment at its outlet.

The mixing chamber of the RIM machine has been an object of investigation for some years. But, there are few published studies about the mixing quality achieved inside it, by using test reaction systems, especially for viscous flowing fluids. Thus, when compared with other works (e.g. Kusch et al., 1989), the current investigation was performed using conditions closer to these used in the important industrial processes.

6. Final Remarks

6.1 Introduction

In the present work a deeper knowledge about a test system for microximing assessment is provided. Its application in the micromixing investigation of two promising reactors: NETmix® and mixing chamber of RIM machine confirmed the results of some of other complementary physical techniques for the mixing dynamics characterization.

At the end of each chapter, specific conclusions directly related with the chapter subject can be found. The present chapter summarizes the main results and conclusions derived from this work in Section 6.2 and it also provides a list of recommendations for future work in Section 6.3.

6.2 General Conclusions

A review on the state-of-the-art in the field of (micro) mixing was provided in Chapter2. From this review it is clear the importance of mixing at molecular scale in the processes where mixing and chemical reactions can occur simultaneously. The existence of methods for its characterization is indispensable. Among physical and chemical methods, the last one is the most appropriate for this task, since reactions are “perfect molecular probes”, and their occurrence demands for an intimate contact between the reagents at that fine scale.

Besides the quantification of the mixing quality, test systems are important tools for the micromixing models validation. More, without this validation, the models run the risk to become unrealistic and consequently useless. These models together with the test systems help engineers to design efficient operations and eventually to solve problems in reactive mixing processes of the industry.

Ideally, a test system should fulfill a list of requirements already stated, such as: rapid, irreversible, second-order kinetics with few products and no side reactions; reaction mechanisms easily to identify and to investigate the effects of the different physicochemical parameters; cheaper and accurate instrumental analytical method; low hazards and low cost of reagents. However, in practice there is no ideal test system but rather systems that draw near to the ideality.

The azo coupling reaction between 1-naphthol and diazotized sulfanilic acid – simplified test system – as well as the simultaneous coupling of 1- and 2-naphthols and diazotized sulfanilic acid – extended test system – are examples of those systems. The kinetics of these reactions must be well known under the same physicochemical conditions of their succeeding applications in the micromixing characterization. Seeing that they are fast reactions, suitable equipment is demanded for their kinetic studies.

In Chapter 3 the stopped-flow equipment is introduced as well as the determination of its intrinsic limitations. Limitations are due to the sensitivity of the spectrophtometric method and to the time response of the instrument. It was shown that the concentration profiles inside the optical cell can condition the performance of the equipment in the study of very fast reactions as well as the dead time, t_d, and the stoppage time, t_0. In order to minimize this problem, an innovative and simple data treatment procedure was proposed which takes into account those concentration gradients and time constants. Contrarily to the conventional data treatment, where the concentration profiles are neglected as well as the stoppage time, the proposed method showed consistent results between the measurements performed at both optional optical pathlength ($2\,\text{mm}$ and $10\,\text{mm}$). The developed methodology can now be extended, with the appropriate changes to the mathematical equations to the study of other reactions with different kinetics performed in this kind of equipment.

The reactions to be studied by using the SX.18MV stopped-flow spectrometer, with a $20\ \mu L$ optical cell, should have characteristic reaction time greater than $1\ ms$ and absorbance measurements lower than 0.01 are inadvisable.

The values obtained for t_d and t_0 depended on the viscosity of the fluids. For aqueous non-viscous medium $t_d = 1.3\ ms$ and $t_0 = 1.6\ ms$ and for aqueous viscous solutions with $20\ mPa \cdot s$, $t_d = 2.2\ ms$ and $t_0 = 1.8\ ms$. The increase of viscosity with a shift in Reynolds number in the direction of laminar flow was the assumed cause for the increase of both time constants.

The main contributions of kinetic studies stated in Chapter 4 are: (i) a clarification of some controversy around the spectrum of the product S found in the literature, by confirming the spectrum published by Bourne and co-workers (1990); (ii) to corroborate some rate constants in aqueous non-viscous medium, already published, and to actualize the ratio of k_{1o} and k_{1p} and (iii) enlarge the range of applicability of the test system for more viscous fluids ($20\ mPa \cdot s$). This last item provides an important and useful tool to characterize the mixing intensity in some industrial mixing devices or reactors, where the viscosities of solutions are frequently high, such as in the food and polymer industries.

The selection of the additive to raise the viscosity of the aqueous solutions revealed to be a hard task mainly due to two requisites: Newtonian behavior and chemically inertness. From the several investigated additives, Rheolate 255 was the best from the rheological and chemical point of views, i.e. for solutions having a Rheolate 255 mass percentage of $3.8\ wt.\%$, the Newtonian behavior is ensured up to shear rates of $3000\ s^{-1}$ and the stability of the diazotized sulfanilic acid solutions could be guaranteed up to 2 hours.

The rate constants in the viscous medium (containing the additive) differed from those in the simply aqueous medium. The chemical interference of the additive with reactions and also mixing limitations in the mixing chamber of stopped-flow equipment are two possible reasons for that.

After the study of the reactions kinetics in both referred media, the test systems were used for micromixing assessment in the NETmix® static mixer and the mixing chamber of a RIM machine. These studies are reported in Chapter 5 and the results obtained enable to conclude about the mixing effect of the Reynolds number.

Micromixing studies performed in NETmix® static mixer were done in aqueous non-viscous medium by using the simplified test system. It was only investigated one option of injection scheme – pre-mixed – in the Reynolds number range $5 \leq \mathrm{Re} \leq 700$. The results obtained clearly show an increasing mixing efficiency as Re increases up to $\mathrm{Re} = 200$. However, for higher Re the improvement of the mixing efficiency was not evident. Due to self limitations of the simplified test system, the critical Reynolds number could not be identified in the mixing experiments. This critical Re corresponds to a flow regime transition, where the mixing mechanisms inside each chamber start. CFD simulations and tracer dynamic imaging, (Laranjeira, 2005) pointed the critical value to be $\mathrm{Re} = 50$.

The macromixing simulation study demonstrated the versatility of the static mixer in the mixing field. They encouraged exploring alternative operational conditions (e.g. feed schemes and network designs) in order to attain and control the product distribution of reaction systems involving more than one reaction. The CFD and the experimental studies can help in those purposes.

In the industrial RIM process, the monomers are injected into the chamber to be mixed. It is simultaneously desirable a good intensity of micromixing and a low reaction polymerization yield at chamber outlet. Depending on the yield, the viscosity of flowing fluids can reaches values up to $0.5\,\mathrm{Pa \cdot s}$ (Coates and Johnson, 1997). The higher viscosities values can compromise the subsequent mold filling, especially in the strait zones. Thus, the mixing chamber has a narrow operation window, where the high mixing degree and low polymerization reaction yield should be reconciled.

The relation between the inertial and the body forces is given by the Froude number ($\mathrm{Fr} = v_{inj}^2 / g\,d$, where v_{inj} injectors linear velocity, g gravity and d injector diameter). Teixeira (2000) and Santos (2003) simulated the influence of this parameter (ca. 10 and ca. 10^3) on the dynamic of the flow in the mixing chamber. The fluid viscosity and the injector velocities were the studied parameters. The authors concluded that the Froude number was a critical parameter in the RIM process since for low values (keeping constant the value of Re) an increasingly stability of the flow up to the point where the system dynamic damped, was observed. The CFD simulation results obtained by the authors also enable to conclude that the use of lower viscosity fluids (ca. 1) in the RIM machines is an invalid option.

The experiments performed in this work in the mixing chamber of RIM machine were carried out for fluids with viscosity $20\,\mathrm{mPa\cdot s}$. Thus, for the Reynolds numbers investigated ($75-600$) the Froude number was ca. of 10^2. During the experiments the impingement of the jets was always observed.

The flow visualization experiments revealed the existence of two flow regimes: (i) complete segregated regime, for $\mathrm{Re}\le 100$, where a strong preferential flow through the chamber axis segregates its two halves and (ii) mixing regime, for $\mathrm{Re}>100$, occurring under a chaotic flow pattern, where the mixing mechanisms are present through the formation of downstream vortices which engulf the fluid from both streams and evolving towards to the chamber outlet.

Micromixing studies confirmed these results, but, they gave additional information about the mixing regime through the observed formation of red dyes (due to micromixing and reaction) and the segregation index, X_Q, values obtained for the several Reynolds number investigated.

Thus, the transition between the two regimes stated above occurs at the so-called *critical Reynolds number*, identified by Santos (2003) has being 120. However, the performed micromixing experiments just allow to point out a range for the flow transition: $100<\mathrm{Re}\le 150$. In this range the mixing mechanisms inside the mixing chamber start to occur, having as a consequence a significant enhancement on the mixing intensity.

For higher Reynolds number ($\mathrm{Re}\ge 500$) the experimental values of X_Q seems to tend to values predicted for an ideal continuous complete mixed reactor, indicating some backmixing/recirculation in the macroscopic flow pattern inside the mixing chamber.

The vortices generation (shown in Section 5.4.2) is responsible for the fluid recirculation and for the increasing of the mean residence time. Santos (2003) observed by CFD simulation that even in this flow state (chaotic) the fluid from the injectors do not decelerate, keeping higher velocities in the chamber without any shortcut towards the outlet. More, according to Unger and co-workers (1998), the chaotic flows are the only effective way to destroy segregation rapidly in viscous mixing.

In order to attain a self-sustainable chaotic state in the mixing chamber, a unitary momentum ratio of the jets must be ensured. In this work, this was achieved by making small adjustments on the signal of one of the pumps, always ensuring that the reagent B was the limiting in the mixing chamber. Although small, these adjustments implied different flow rates between the

jets. Therefore, the intended initial reagents ratio $\gamma_{A1} = c_{A10}/c_{B0}$ value for a certain experiment could not be practiced, which resulted in reagents mass balance which closes with values above the desirable ones. The different jets flow rate could also justify the scatter observed in several set of experiments. For the same Reynolds number, the diversity of flow patterns can also contribute for the scattering, since the sample is collected in a restricted zone of the mixing chamber outlet.

Comparing the spread of the results obtained in both investigated mixers, the NETmix® static mixer present less spread than the mixing chamber of RIM machine. These can mean that the flow pattern in the NETmix® static mixer is more reproducible than in the impinging jets. The elements (connecting channels and mixing chambers) of the NETmix® probably guide and channel the flow. In opposition, in the RIM machine the jets possibly do not collide in exactly the same way and do not show exactly the same flow pattern in each run.

Both NETmix® static mixer and mixing chamber of RIM machine are promising static mixers for the actual industry where reactive mixing processes are present. This work contributes for the knowledge about their mixing performances. Due to the NETmix® and RIM potentialities, more research should be pursued in order to improve their actual features and to develop new applications. In next section it is suggested some research topics.

6.3 Future Work

The background acquired in the course of present work helped to identify several important research subjects in the micromixing field. These subjects are in both experimental and simulation areas. Specific suggestions are listed below.

- The search of an “ideal” additive to raise the viscosity of the solutions to higher values than those practiced in the present work must be continued.

- Kinetic studies for very fast reactions are recommended to be performed in a stopped-flow equipment with shorter dead time and stoppage time. The existence of a diodo-array accessory could prove to be a useful addition to the stopped-flow equipment.

- Micromixing assessment in the NETmix® static mixer involving multiphase flow, fluids with different viscosities should also be considered as well as others schemes of feeding.

- Other geometries of NETmix® static mixer should be studied to identify likely mixing enhancing network structures. The effect of the network structure on the critical Reynolds number must be systematically considered.

- The technique to ensure the iso-momentum ratio of the jets of the mixing chamber of the RIM machine must be changed or improved. The option to use different injectors diameters suggested by Santos (2003) can be considered.

- Other geometries mixing chamber of RIM machine should be investigated.

- Mixing studies give important information regarding the effect of each parameter in the system but they lack the insight into the mechanisms of the process. The values of the segregation indexes (X_S, $X_S^{'}$ and X_Q) give a quantitative description of the degree of micromixing, however it is more valuable for reactor design to have a physically meaningful parameter – for example flow rate, viscosity, power input, mixer size – related to those parameters. This can be done by using a micromixing model which includes local rates of convective mixing by fluid deformation in both laminar and the turbulent flow regimes. Thus, it is recommended to articulate a micromixing model with a CFD code in order to simulate the reactive flows (using the test systems) in the reactors investigated in this work.

References

Angst, W., Bourne, J. R. and Sharma, R. N. (1982). Mixing and Fast Chemical Reaction-IV The Dimensions of the Reaction Zone. *Chemical Engineering Science*, **37**, 585-590.

Aoun, M., Plasari, E., David, R. and Villermaux, J. (1996). Are Barium Sulphate Kinetics Sufficiently Known for Testing Precipitation Reactor Models? *Chemical Engineering Science*, **51**, 2449-2458.

Assirellia, M., Bujalskia, W., Eagleshamb, A. and Nienowa, A. (2008). Macro- and Micromixing Studies in an Unbaffled Vessel Agitated by a Rushton Turbine. *Chemical Engineering Science*, **63**, 35-46.

Baldyga, J. and Bourne, J. R. (1989). Simplification of Micromixing Calculations. I. Derivation and Application of New Model. *Chemical Engineering Journal*, **42**, 83-92.

Baldyga, J. and Bourne, J. R. (1990). The Effect of Micromixing on Parallel Reactions. *Chemical Engineering Science*, **45**, 907-916.

Baldyga, J. and Bourne, J. R. (1992). Interactions Between Mixing on Various Scales in Stirred Tank Reactors. *Chemical Engineering Science*, **47**, 1839-1848.

Baldyga, J., Bourne, J. R. and Gholap, R. V. (1995). The Influence of Viscosity on Mixing in Jet Reactors. *Chemical Engineering Science*, **50**, 1877-1880.

Baldyga, J., Bourne, J. R. and Walker, B. (1998). Non-Isothermal Micromixing in Turbulent Liquids: Theory and Experiment. *Canadian Journal of Chemical Engineering*, **76**, 641-649.

Baldyga, J. and Bourne, J. R. (1999). *Turbulent Mixing and Chemical Reaction*. John Wiley & Sons, New York.

Barnes, H. A., Hutton, J. F. and Walters, K. (1997). *An Introduction to Rheology*. Elsevier Science B. V., Amsterdam.

Barresi, A. A., Pipino, M. and Baldi, G. (1992). A Three-Stage Micromixing Model for very Fast Reactions in Tubular Reactors. *Chemical Engineering Science*, **47**, 2831-2836.

Belevi, H., Bourne, J. R. and Rys, P. (1981). Chemical Selectivities Disguised by Mass Diffusion.VIII.Influence of pH-Gradients on the Product Distribution in Mixing-Disguised Azo Coupling Reactions. *Helvetica Chimica Acta*, **64**, 1618-1629.

Bourne, J. R., Crivelli, E. and Rys, P. (1977). Chemical Selectivities Disguised by Mass Diffusion.V.Mixing-Disguised Azo Coupling Reactions. *Helvetica Chimica Acta*, **60**, 2944-2957.

Bourne, J. R. and Kozicki, F. (1977). Mixing Effects During the Bromination of 1,3,5-trimethoxybenzene. *Chemical Engineering Science*, **32**, 1538-1539.

Bourne, J. R., Kozicki, F. and Rys, P. (1981). Mixing and Fast Chemical Reaction - I Test Reactions to Determine Segregation. *Chemical Engineering Science*, **36**, 1643-1648.

Bourne, J. R. and Rohani, S. (1983). Micro-mixing and the Selective Iodination of I-Tyrosine. *Chemical Engineering Research & Design*, **61**, 297-302.

Bourne, J. R. (1984). Micromixing Revisited. *IChemE Symposium Series 87 (ISCRE 8)*, 797-813.

Bourne, J. R. and Garcia-Rosas, J. (1985). Laminar Shear Mixing in Reaction Injection Molding. *Polymer Engineering and Science*, **25**, 1-5.

Bourne, J. R., Hilbert, C. and Tovstiga, G. (1985). Kinetics of the Azo Coupling Reactions between 1-Naphthol and Diazotised Sulfanilic Acid. *Chemical Engineering Communications*, **37**, 293-314.

Bourne, J. R. and Tovstiga, G. (1985). Measurement of the Diffusivity of 1-Naftol in Water With a Rotating Disc. *Chemical Engineering Communications*, **36**, 67-71.

Bourne, J. R., Gablinger, H. and Ravindranath, K. (1988). Local pH Gradients and the Selectivity of Fast Reactions.I:Mathematical Model of Micromixing. *Chemical Engineering Science*, **43**, 1941-1948.

Bourne, J. R., Hilber, C. P. and Petrozzi, S. (1989). The Influence of Viscosity on Micromixing in Turbulent Flows. *Chemical Engineering and Processing*, **25**, 133-139.

Bourne, J. R., Kut, O. M., Lenzner, J. and Maire, H. (1990). Kinetics of the Diazo Coupling between 1-Naftol and Diazotized Sulfanilic Acid. *Industrial & Engineering Chemistry Research*, **29**, 1761-1765.

Bourne, J. R. and Maire, H. (1991). Micromixing and Fast Chemicals Reactions in Static Mixers. *Chemical Engineering and Processing*, **30**, 23-30.

Bourne, J. R., Kut, O. M. and Lenzner, J. (1992a). An Improved Reaction System to Investigate Micromixing in High-Intensity Mixers. *Industrial & Engineering Chemistry Research*, **31**, 949-958.

Bourne, J. R., Lenzner, J. and Petrozzi, S. (1992b). Micromixing in Static Mixers: An Experimental Study. *Industrial & Engineering Chemistry Research*, **31**, 1216-1222.

Bourne, J. R. (1993). What Does the Modelling of Reactive Flows Ask of CFD. *Revue de l'Institute Français du Pétrole*, **48**, 615-630.

Bourne, J. R. and Yu, S. (1994). Investigation of Micromixing in Stirred Tank Reactors Using Parallel Reactions. *Industrial & Engineering Chemistry Research*, **33**, 41-55.

Bourne, J. R., Gholap, R. V. and Rewatkar, V. B. (1995). The Influence of Viscosity on Micromixing on Product Distribution of Fast Parallel Reactions. *Chemical Engineering Journal*, **58**, 15-20.

Bradley, J. N. (1975). *Fast Reactions*. Oxford University Press.

Buchmann, M. and Mewes, D. (1998). Measurement on the Local Intensities of Segregation with the Tomographical Dual Wavelength Photometry. *Canadian Journal of Chemical Engineering*, **76**, 626-630.

Buchmann, M. and Mewes, D. (2000). Tomographic Measurements of Micro-and Macromixing Using the Dual Wavelength Photometry. *Chemical Engineering Journal*, **77**, 3-9.

Caldin, E. F. (1964). Fast Reaction in Solution.

Cassiani, M., Radicchi, A. and Albertson, J. D. (2007). Modelling of Concentration Fluctuations in Canopy Turbulence. *Boundary-Layer Meteorol*, **122**, 655-681.

Chance, B. (1974). *Rapid Flow Methods*. Techniques of Chemistry. John Wiley & Sons, New York.

Chang, P. C., Mou, C. Y. and Lee, D. J. (1999). Micromixing and Macromixing Effects in Unsteady Chemical Reaction System. *Journal of Physical Chemistry A*, **103**, 5485-5489.

Chen, J., Chen, B. and Chen, G. (1993). Visualization of Meso- and Micro-mixing Status in Flow System by High Speed Stroboscopic Microscopic Photography. *Canadian Journal of Chemical Engineering*, **71**, 967-970.

Chen, M. S. K. (1971). The Theory of Micromixing for Unsteady State Flow Reactors. *Chemical Engineering Science*, **26**, 17-28.

Chua, G.-W., Songa, Y.-H., Yang, H.-J., Chena, J.-M., Chenb, H. and Chen, J.-F. (2007). Micromixing Efficiency of a Novel Rotor–Stator Reactor. *Chemical Engineering Journal*, **128**, 191-196.

Coates, P. D. and Johnson, F. A. (1997). *Reaction Injection Processing of Polymers. Thermosetting Plastics*. Addison Wesley Longman, London.

Danckwerts, P. V. (1953a). The Definition and Measurement of Some Characteristics of Mixtures. *Applied Scientific Research*, **A3**, 279-296.

Danckwerts, P. V. (1953b). Continuous Flow Systems. Distribution of Residence Time. *Chemical Engineering Science*, **2**, 1-13.

Danckwerts, P. V. (1958). The Effect of Incomplete Mixing on Homogeneous Reactions. *Chemical Engineering Science*, **8**, 93-102.

David, R. and Villermaux, J. (1987). Interpretation of Micromixing Effects on Fast Consecutive-Competing Reactions in Semi-Batch Stirred Tanks by a Simple Interaction Model. *Chemical Engineering Communications*, **54**, 333-352.

Demyanovich, R. J. and Bourne, J. R. (1989). Rapid Micromixing by the Impingement of Thin Liquid Sheets. 2. Mixing Study. *Industrial & Engineering Chemistry Research*, **28**, 830-839.

Dickson, P. N. and Margerum, W. (1986). Extension of Accessible First-Order Rate Constants and Accurate Dead-Time Determinations for Stopped-Flow Spectroscopy. *Analytical Chemistry*, **58**, 3153-3158.

Dunn, B. C., Meagher, D. E. and Rorabacher, D. B. (1996). Resolution of Stopped-Flow Kinetic Data for Second-Order Reactions with Rate Constants up to 108 M-1 s-1 Involving Large Concentrations Gradients. Experimental Comparison Using Three Independent Approaches. *Journal of Physical Chemistry*, **100**, 16925-16933.

Edwards, M. F. (1984). Chemical Reaction Engineering of Polymer Processing: Reaction Injection Moulding. *IChemE Symposium Series 87 (ISCRE 8)*, 783-796.

Ekambara, K., Dhotre, M. T. and Joshi, J. B. (2006). CFD Simulation of Homogeneous Reactions in Turbulent Pipe Flows - Tubular Non-Catalytic Reactors. *Chemical Engineering Journal*, **117**, 23-29.

Erkoç, E., Santos, R. J., Nunes, M. I., Dias, M. M. Q. and Lopes, J. C. B. (2007). Mixing Dynamics Control in RIM Machines. *Chemical Engineering Science*, **62**, 5276 – 5281.

Ferrouillat, S., Tochon , P. and Peerhossaini, H. (2006). Micromixing Enhancement by Turbulence: Application to Multifunctional Heat Exchangers. *Chemical Engineering and Processing*, **45**, 633-640.

Fogler, H. S. (1999). *Elements of Chemical Reaction Engineering*. Prentice-Hall, New Jersey.

Forney, L. J. and Gray, G. E. (1990). Optimum Design of a Tee Mixer for Fast Reactions. *AIChE Journal*, **36**, 1773-1776.

Fournier, M.-C. (1994). *Caractérisation de L'Efficacité de Micromélange par une Nouvelle Réaction Chimique Test*. Ph.D. Thesis, L'Instute National Polythechnique de Lorraine, France.

Fournier, M.-C., Falk, L. and Villermaux, J. (1996a). A New Parallel Competing Reaction System for Assessing Micromixing Efficiency-Determination of Micromixing Time by a Simple Mixing Model. *Chemical Engineering Science*, **51**, 5187-5192.

Fournier, M.-C., Falk, L. and Villermaux, J. (1996b). A New Parallel Competing Reaction System for Assessing Micromixing Efficiency-Experimental Approach. *Chemical Engineering Science*, **51**, 5053-5064.

Fox, R. O. (1998). On the Relationship between Lagrangian Micromixing Models and Computational Fluid Dynamics. *Chemical Engineering and Processing*, **37**, 521-535.

Frey, J. and Denson, C. D. (1988). Imidization Reaction Parameters in Inert Molten Polymers for Micromixing Tracer Studies. *Chemical Engineering Science*, **43**, 1967-1973.

Gholap, R. V., Petrozzi, S. and Bourne, J. R. (1994). Influence of Viscosity on Product Distribution of Fast Competitive Chemical Reactions. *Chemical Engineering & Technology*, **17**, 102-107.

Guichardon, P. (1996). *Caractérisation Chimique du Micromélange par la Réaction Iodure-Iodate. Application aux Milieux Visqueux et aux Suspensions Liquide-Solide*. Ph.D. Thesis, L'Instute National Polythechnique de Lorraine, France.

Guichardon, P. and Falk, L. (2000). Characterization of Micromixing Efficiency by the Iodide-Iodate Reaction System. Part I: Experimental Procedure. *Chemical Engineering Science*, **55**, 4233-4243.

Guichardon, P., Falk, L. and Villermaux, J. (2000). Characterization of Micromixing Efficiency by the Iodide-Iodate Reaction System. Part II: Kinetic Procedure. *Chemical Engineering Science*, **55**, 4245-4253.

Heeb, T. G. and Brodkey, R. S. (1990). Turbulent Mixing with Multiple Second-Order Chemical Reactions. *AIChE Journal*, **36**, 1457-1470.

Hjertager, L. K., Hjertager, B. H. and Solberg, T. (2002). CFD Modelling of Fast Chemical Reactions in Turbulent Liquid Flows. *Computers & Chemical Engineering*, **26**, 507-515.

Johnson, B. K. and Prud'homme, R. K. (2003). Chemical Processing and Micromixing in Confined Impinging Jets. *AIChE Journal*, **49**, 2264-2282.

Kaminsky, V. A., Rabinovich, A. B. and Fedorov, A. Y. A. (1996). Modelling of Turbulent Micromixing for Two Independent Variables. *Chemical Engineering Science*, **51**, 2613-2617.

Kirk-Othmer (1982). *Encyclopedia of Chemical Technology*. Wiley, New York.

Kolodziej, P., Macosko, C. W. and Ranz, W. E. (1982). The Influence of Impingement Mixing on Striation Thickness Distribution and Properties in Fast Polyurethane Polymerization. *Polymer Engineering and Science*, **22**, 388-392.

Kresta, S. M. and Brodkey, R. S. (2004). *Mixing and Chemical Reactions*. Handbook of Industrial Mixing Science and Pratice. John Wiley & Sons, New Jersey.

Kusch, H. A., Ottino, J. M. and Shannon, D. M. (1989). Analysis of Impingement Mixing-Reaction Data: Use of a Lamelar Model to Generate Fluid Mixing Information. *Industrial & Engineering Chemistry Research*, **28**, 302-315.

Laranjeira, P. E. M. S. C. (2006). *NETMIXER Static Mixer - Modelling, CFD Simulation and Experimental Characterisation*. Ph.D. Thesis, Faculdade de Engenharia da Universidade do Porto, Porto.

Lee, L. J., Ottino, J. M., Ranz, W. E. and Macosko, C. W. (1980). Impingement Mixing in Reaction Injection Molding. *Polymer Engineering and Science*, **20**, 868-874.

Lenzner, J. (1991). *Der Einsatz rascher, kompetitiver Reaktionen zur Untersuchung von Mischeinrichtungen*. Ph.D. Thesis, Dipl. Chem. Ing. ETH, Switzerland.

Lopes, J. C. B., Laranjeira, P. E. M. S. C., Dias, M. M. Q. and Martins, A. A. A. (2005a). *Network Mixer and Related Mixing Process*. PCT WO 2005/077508 A1.

Lopes, J. C. B., Santos, R. J., Teixeira, A. M. and Costa, M. R. P. F. N. (2005b). *Production Process of Plastic Parts by Reaction Injection Moulding, and Related Head Device*. PCT WO 2005/097477 A1.

Lopes, J. C. B., Dias, M. M. Q., Silva, V. M. T. M., Santos, P. A. Q. O., Monteiro, F. J. M., Gomes, P. J. C. and Mateus, A. Y. P. (2006). *Método de Produção de Nanopartículas de Fosfatos de Cálcio com Elevada Pureza e Respectiva Utilização*. Patent 103528 (pending).

Mahajan, A. J. and Kirwan, D. J. (1996). Micromixing Effects in a Two-Impinging-Jets Precipitator. *AIChE Journal*, **42**, 1801-1814.

Mao, K. W. and Toor, H. L. (1970). A Diffusion Model for Reactions with Turbulent Mixing. *AIChE Journal*, **16**, 49-52.

Marchisio, D. L. and Barresi, A. A. (2003). CFD Simulation of Mixing and Reaction: the Relevance of the Micro-mixing Model. *Chemical Engineering Journal*, **58**, 3579-3587.

Matsumura, K., Enoki, Y. and Kohzuki, H. (1990). A Simple Procedure for Determination of the Dead Time of a Stopped-Flow Instrument. *Japanese Journal of Physiology*, **40**, 567-571.

McCarthy, E. D., Dunk, W. A. E. and Boodhoo, K. V. K. (2007). Application of an Intensified Narrow Channel Reactor to the Aqueous Phase Precipitation of Barium Sulphate. *Journal of Colloid and Interface Science*, **305**, 72-87.

Meagher, N. E. and Rorabacher, D. B. (1994). Mathematical Treatment for Very Rapid Second-Order Reversible Kinetics as Measured by Stopped-Flow Spectrophotometry with Corrections for the Cell Concentrations Gradient. *Journal of Physical Chemistry*, **98**, 12590-12593.

Morrison, R. and Boyd, R. (1983). *Química Orgânica*. Fundação Calouste Gulbenkian,

Muhr, H., Leclerc, J.-P. and Plasari, E. (1997). A Rapid Method for the Determination of Growth Rate Kinetic Constants: Application to the Precipitation of Aluminum Trihydroxide. *Ind. Eng. Chem. Res.*, **36**, 675-681.

Nabholz, F. and Rys, P. (1977). Chemical Selectivities Disguised by Mass Diffusion. IV. Mixing-Disguised Nitrations of Aromatic Compounds with Nitronium Salts. *Helvetica Chimica Acta*, **60**, 2937-2943.

Nadeau, P., Berk, D. and Munz, R. J. (1996). Measurement of Residence Time Distribution by Laser Absorption Spectroscopy. *Chemical Engineering Science*, **1996**, 2607-2612.

Nauman, E. B. (1975). The Droplet Diffusion Model for Micromixing. *Chemical Engineering Science*, **30**, 1135-1140.

Nienow, A. W., Drain, S. M. and Boyes, A. P. (1997). An Experimental Study to Characteriza Imperfect Macromixing in a Stirred Sembatch Reactor. *Industrial & Engineering Chemistry Research*, **36**, 2984-2989.

Nishimura, Y. and Matsubara, M. (1970). Micromixing Theory Via the Two-Environment Model. *Chemical Engineering Science*, **25**, 1785-1797.

Nunes, M. I. (1996). *Reacções Teste para a Caracterização da Micromistura em Reactores Químicos*. M.Sc. Thesis, Faculdade de Engenharia da Universidade do Porto, Porto.

Nunes, M. I., Dias, M. M. Q. and Lopes, J. C. B. (2001). Kinetic Study of Fast Reactions in Viscous Media. *CHEMPOR'2001 8th International Chemical Engineering Conference*, Aveiro, Portugal.

Ottino, J. M., Ranz, W. E. and Macosko, C. W. (1979). A Lamellar Model for Analysis of Liquid-Liquid Mixing. *Chemical Engineering Science*, **34**, 877-890.

Ottino, J. M. (1980). Lamellar Mixing Models for Structured Chemical Reactions and Their Relationship to Statistical Models: Macro- and Micromixing and the problem of Averages. *Chemical Engineering Science*, **35**, 1377-1391.

Partin, L. R. (1995). Opportunities in PC and MAC Numerical Software for Process Engineering. *AIChE Symposium Series*, **91**, 340-343.

Patterson, G. K. (1981). Application of Turbulence Fundamentals to Reactor Modelling and Scale-Up. *Chemical Engineering Communications*, **8**, 25-32.

Patterson, G. K., Paul, E. L., Kresta, S. M. and Etchells III, A. W. (2004). *Mixing and Chemical Reactions*. Handbook of Industrial Mixing Science and Pratice. John Wiley & Sons, New Jersey.

Paul, E. L. and Treybal, R. E. (1971). Mixing and Product Distribution for a Liquid-Phase, Second-Order, Competitive-Consecutive Reaction. *AIChE Journal*, **17**, 718-724.

Paul, E. L., Mahadevan, H. and Foster, J. (1992). The Effect of Mixing on Scale of a Parallel Reaction System. *Chemical Engineering Science*, **47**, 2837-2840.

Paul, E. L., Atiemo-Obeng, V. A. and Kresta, S. M. (2004). *Handbook of Industrial Mixing Science and Practice*. John Wiley & Sons, New Jersey.

Ranade, V. V. (1992). Decoupling of Micro- and Macromixing in Turbulent Reacting Flow. *AIChE Journal*, **38**, 466-470.

Robinson, B. H. (1986). *Rapid Flow Methods*. Techniques of Chemistry. John Wiley & Sons, New York.

Santos, R. J. (2003). *Mixing Mechanisms in Reaction Injection Moulding-RIM. An LDA/PIV Experimental Study and CFD Simulation*. Ph.D. Thesis, Faculdade de Engenharia da Universidade do Porto, Porto.

Santos, R. J., Teixeira, A. M. and Lopes, J. C. B. (2005). Study of Mixing and Chemical Reaction in RIM. *Chemical Engineering Science*, **60**, 2381 – 2398.

Saunders, K. H. and Allen, R. L. M. (1985). *Aromatic Diazo Compounds*. Edward Arnold.

Schaer, E., Guichardon, P., Falk, L. and Plasari, E. (1999). Determination of Local Energy Dissipation Rates in Impinging Jets by a Chemical Reaction Method. *Chemical Engineering Journal*, **72**, 125-138.

Sheikh, F. and Vigil, R. D. (1998). Simulation of Imperfect Micromixing for First-Order Adiabatic Reactions: the Coalescence-Dispersion Model. *Chemical Engineering Science*, **53**, 2137-2142.

Silva, V. M. T. M., Quadros, P. A., Laranjeira, P. E. M. S. C., Dias, M. M. and Lopes, J. C. B. (2008). A Novel Continuous Industrial Process for Producing Hydroxyapatite Nanoparticles. *J Dispersion Science Technology*. (in press)

Soleymani, A., Kolehmainen, E. and Turunen, I. (2008). Numerical and Experimental Investigations of Liquid Mixing in T-type Micromixers. *Chemical Engineering Journal*, **135S**, S219-S228.

Spencer, J. L., Lunt, R. R. and Leshaw, S. (1980). Identification of Micromixing Mechanisms in Flow Reactors: Transient Inputs of Reactive Tracers. *Industrial & Engineering Chemistry Fundamentals*, **19**, 135-141.

Sykes, P. (1977). *Guidebook to Mechanism in Organic Chemistry*. Longman, London.

Teixeira, A. M. (2000). *Escoamento na Cabeça de Mistura de uma Máquina RIM*. Ph.D. Thesis, Faculdade de Engenharia da Universidade do Porto, Porto.

Teixeira, A. M., Santos, R. J., Costa, M. R. P. F. N. and Lopes, J. C. B. (2005). Hydrodynamics of the Mixing Head in RIM: LDA Flow-Field Characterization. *AIChE Journal*, **51**, 1608-1619.

Tonomura, B. I., Nakatani, H. and Ohnishi, M. (1978). Test Reactions for a Stopped-Flow Apparatus. Reduction of 2,6-Dichlorophenolindophenol and Potassium Ferricyanide by L-Ascorbic Acid. *Analytical Biochemistry*, **84**, 370-383.

Trambouze, P. (1996). CFD Applied to Process Engineering - An Introduction. *Revue de l'Institute Français du Pétrole*, **51**, 199-203.

Treleaven, C. R. and Tobgy, A. H. (1971). Conversion in Reactors having Separate Reactant Feed Streams. The State of Maximum Mixedness. *Chemical Engineering Science*, **26**, 1259-1269.

Treleaven, C. R. and Tobgy, A. H. (1973). Residence Times, Micromixing and Convertion in an Un-Premixed Feed Reactor-II. Chemical Reaction Measurements. *Chemical Engineering Science*, **28**, 413-425.

Tsai, K. and Fox, R. O. (1998). The BMC/GIEM Model for Micromixing in Non-Premixed Turbulent Reacting Flows. *Industrial & Engineering Chemistry Research*, **37**, 2131-2141.

Tucker III, C. L. and Suh, N. P. (1980). Mixing for Reaction Injection Molding. I. Impingement Mixing of Liquids. *Polymer Engineering and Science*, **20**, 875-886.

Unger, D. R., Muzzio, F. J. and Brodkey, R. S. (1998). Experimental and Numerical Characterization of Viscous Flow and Mixing in an Impinging Jet Contactor. *Canadian Journal of Chemical Engineering*, **76**, 546-555.

van Krevelen, D. W. (1958). Micro- and Macro-Kinetics. *Chemical Engineering Science*, **8**, 5-17.

Villermaux, J. (1983). Mixing in Chemical Reactors. *ACS Symposium Series*, **226**, 135-186.

Villermaux, J., Falk, L. and Fournier, M.-C. (1992). Use of Parallel Competing Reactions to Characterize Micromixing Efficiency. *AIChE Symposium Series*, **88**, 6-10.

Villermaux, J. and Falk, L. (1996). Recent Advances in Modeling Micromixing and Chemical Reaction. *Revue de l'Institute Français du Pétrole*, **51**, 205-213.

Vogel, A. I. (1964). *Pratical Organic Chemistry. Including Qualitative Organic Analysis*.

Weinstein, H. and Adler, R. J. (1967). Micromixing Effects in Continuous Chemical Reactors. *Chemical Engineering Science*, **22**, 65-75.

Wenger, K. S., Dunlop, E. H. and MacGilp, I. D. (1992). Investigation of the Chemistry of a Diazo Micromixing Test Reaction. *AIChE Journal*, **38**, 1105-1114.

Wenger, K. S., Dunlop, E. H. and Kedar, T. (1993). Micromixing in a Tubular Flow Reactor Under Simulated Microgravity. *AIChE Journal*, **39**, 1569-1573.

Wu, G., Zhou, H. and Zhu, S. (2007). Precipitation of Barium Sulfate Nanoparticles via Impinging Streams. *Materials Letters*, **61**, 168-170.

Zauner, R. and Jones, A. G. (2000a). Mixing Effects on Product Particle Characteristics from Semi-Batch Crystal Precipitation. *Transactions of the Institution of Chemical Engineers, Part A*, **78**, 894-902.

Zauner, R. and Jones, A. G. (2000b). Scale-Up of Continuous and Semibatch Precipitation Processes. *Industrial & Engineering Chemistry Research*, **39**, 2392-2403.

Zollinger, H. (1961). *Azo and Diazo Chemistry. Aliphatic and Aromatic Compounds*. Intercience Publishers, New York.

Zwietering, T. N. (1959). The Degree of Mixing in Continuous Flow Systems. *Chemical Engineering Science*, **11**, 1-15.

A. Chemicals Hazards

A.1 Sulfanilic Acid

Table A.1 Sulfanilic acid hazards (ACROS)

Emergency overview	Irritating to eyes and skin. May cause sensitization by skin contact.
Potential Health Effects	Eye: Causes eye irritation. Contact may cause transient eye irritation. Skin: Causes skin irritation. Ingestion: Expected to be a low ingestion hazard. Inhalation: May cause respiratory tract irritation. The toxicological properties of this substance have not been fully investigated.
Carcinogenicity	Not listed as a carcinogen by ACGIH, IARC, NTP, or CA Prop 65

A.2 Orange II

Table A.2 Orange II hazards (ACROS)

Emergency overview	Irritating to eyes, respiratory system and skin. May cause sensitization by skin contact.
Potential Health Effects	Eye: Causes eye irritation. Skin: Causes skin irritation. May be harmful if absorbed through the skin. Ingestion: May cause irritation of the digestive tract. May be harmful if swallowed. Inhalation: May cause respiratory tract irritation. May be harmful if inhaled.
Carcinogenicity	Not listed as a carcinogen by ACGIH, IARC, NTP, or CA Prop 65

A.3 1- and 2-Naphthols

Table A.3 1 and 2-naphthol hazards (ACROS)

	1-Naphthol	2-Naphthol
Emergency overview	Harmful in contact with skin and if swallowed. Irritating to respiratory system and skin. Risk of serious damage to eyes.	Harmful by inhalation and if swallowed
Potential Health Effects	Eye: May cause eye injury. Skin: Causes skin irritation. Harmful if absorbed through the skin. Ingestion: Harmful if swallowed. Causes gastrointestinal irritation with nausea, vomiting and diarrhea. May cause burns to the digestive tract. Inhalation: Harmful if inhaled. May cause severe irritation of the upper respiratory tract with pain, burns, and inflammation. Chronic: May cause liver and kidney damage. May cause anemia and other blood cell abnormalities. Chronic inhalation, skin absorption or ingestion of naphthalene have caused severe hemolytic anemia.	Eye: Causes moderate eye irritation. Skin: Causes mild skin irritation. May be harmful if absorbed through the skin. Ingestion: Harmful if swallowed. May cause irritation of the digestive tract. Inhalation: May be fatal if inhaled. Harmful if inhaled. May cause respiratory tract irritation. Chronic: Prolonged or repeated exposure may cause permanent eye damage.
Carcinogenicity	Not listed as a carcinogen by ACGIH, IARC, NTP, or CA Prop 65	Not listed as a carcinogen by ACGIH, IARC, NTP, or CA Prop 65.